

Characterisation of the BCAT1 CXXC motif in Acute Myeloid Leukaemia

J Hillier

A thesis submitted for the fulfilment of the degree of
Doctor of Philosophy in Biological Sciences

2020

University of Worcester

Acknowledgments

I would like to thank the people who have supported me along the way. Firstly, thank you to Dr. Steven Coles for giving me this opportunity and always having an open door. Thank you to Dr. Amy Cherry for many useful and pragmatic conversations regarding this work, and for giving me my first opportunity to do research at Worcester. Thank you to the Sir Halley Stewart Trust and University of Worcester for funding this project. A big thank you to all my colleagues at the ISE for their help over the years and particularly to Dr. Anne Sinnott for her part in setting up the lab and keeping it running so efficiently. Thank you to Mark Cook for showing me the ropes in the early days and his support and friendship throughout our time at Worcester together. A special thank you to Sarah for always being there for me. Finally, I would like to thank my father for his support throughout my education, without whose help this would not have been possible.

Contents

ACKNOWLEDGMENTS	2
FIGURES AND TABLES	1
ABBREVIATIONS	7
ABSTRACT	13
CHAPTER 1: INTRODUCTION	15
1.1 Leukaemia	15
1.1.1 Haematopoiesis	15
1.1.2 Subtypes of Leukaemia	20
1.2 Acute Myeloid Leukaemia	21
1.2.1 AML Classification	23
1.2.2 AML Cytogenetics	26
1.2.3 Metabolic mutations	27
1.2.3 Metabolic mutations	31
1.3 BCAT1	33
1.3.1 Enzyme kinetics	33
1.3.2 Expression and survival	37
1.3.3 BCAT1 metabolic role in Cancer	40
1.3.4 The CXXC motif	44
1.4. ROS	50
	3

1.4.1 Sources of ROS	50
1.4.2 Antioxidant networks	53
1.5 Oxidative Stress in cancer	57
1.5.1 Genomic integrity	57
1.5.2 Redox signalling	58
1.5.3 Nrf2 antioxidant response	63
1.6 Hypothesis	65
PROJECT AIMS	66
CHAPTER 2: MATERIALS AND METHODS	68
2.1. Antibodies	68
2.2 Cell Lines	68
2.3 Plasmids and Constructs	68
2.4 Primers	69
2.5 Transformation of E.coli with pCMV6-BCAT1	70
2.6 Site-directed Mutagenesis of the CXXC Motif	71
2.7 Subcloning pLenti-BCAT1 Vector	72
2.8 Colony PCR	73
2.9 Subcloning pET28a-BCAT1	74
2.10 Recombinant BCAT1 Protein Overexpression	75
2.11 Recombinant BCAT1 Protein Extraction and Purification	75
2.12 Recombinant BCAT1 Protein Quantification	77
2.13 SDS-PAGE	77
2.14 Western Blot Detection of Purified BCAT1 Protein	78
2.15 Spectrophotometric Analysis of Reduced Cysteine Thiol Groups	78
2.16 Generation of Lentiviral Particles	79

2.17 Viral Titre	80
2.18 Transcription Analysis of BCAT1 Expression	81
2.19 Puromycin Cytotoxicity Assay	81
2.20 Lentiviral Transduction	82
2.21 qPCR of BCAT1 Transcript	82
2.22 Western Blot Detection of BCAT1 in Transgenic and Control U937 Cells	84
2.23 Cell Culture of U937 BCAT1 Transgenic and Control Cells	85
2.24 Trypan Blue Cell Viability Staining	86
2.25 U937 Transgenic and Control Cell Growth Curves	86
2.26 Cell Cycle Analysis of Transgenic and Control U937 Cells	86
2.27 Measuring Intracellular ROS in Transgenic and Control U937 Cells Using the DCFDA Flow Cytometric Assay	87
2.28 Measuring Mitochondrial Membrane Potential in Transgenic and Control U937 Cells Using the DiOC2(3) Assay	88
2.29 Measuring the Intracellular Redox Environment in Transgenic and Control U937 cells Using the Glutathione Assay	89
2.30 Evaluating the Effects of Serum Starvation on Transgenic and Control U937 Cells	90
2.31 Evaluating the Effect of Mitochondria ROS in Transgenic and Control U937 Cells	90
2.32 Differentiation of Transgenic and Control U937 Cells Using PMA	91
2.33. Evaluating the Pharmacological Effect of Chemotherapeutic Agents on Transgenic and Control U937 Cells	92
2.34 Data Handling and Interpretation	92
CHAPTER 3: SITE-DIRECTED MUTAGENESIS OF BCAT1 CXXC MOTIF	93
3.1 INTRODUCTION	93
	100

3.2 AIMS	101
3.2.1 Objectives	102
3.3 METHODS	104
3.3.1 Site-directed Mutagenesis of the CXXC motif	104
3.3.2 Subcloning pET28a-BCAT1	104
3.3.3 BCAT1 overexpression, purification and verification by Western blot	105
3.3.4 Spectrophotometric analysis of reduced cysteine thiol groups	105
3.4 RESULTS	106
3.4.1 Site directed mutagenesis of pCMV6-BCAT1	106
3.4.2 Subcloning BCAT1 and CXXC motif mutants to pET28a expression vector.	108
3.4.3 Expression and purification of BCAT1 and CXXC mutants	111
3.4.4 Assessment of purified BCAT1(WT) and BCAT1 CXXC mutated protein cysteine thiol groups	116
3.5 DISCUSSION	118
CHAPTER 4: LENTIVIRAL TRANSDUCTION AND OVEREXPRESSION OF BCAT1(WT) AND BCAT1 CXXC MOTIF MUTANTS IN THE MYELOID CELL LINE U937	121
4.1 INTRODUCTION	121
4.2 AIMS AND OBJECTIVES	128
4.2.1 Objectives	129
4.3 METHODS	130
4.3.1 Subcloning pLenti-BCAT1 vector	130

4.3.2	<i>Transcription analysis of BCAT1 expression</i>	130
4.3.3	<i>Stable Transduction of BCAT1(WT) and CXXC Motif Mutant U937 Cells</i>	131
4.4	RESULTS	132
4.4.1	<i>Subcloning BCAT1(WT) and respective CXXC motif mutant clones to pLenti vector</i>	132
4.4.2	<i>Transcription analysis of BCAT1 expression</i>	132
4.3.2	<i>Lentiviral titre quantification</i>	137
4.5	DISCUSSION	153
CHAPTER 5: THE ANTIOXIDANT ROLE OF THE BCAT1-CXXC MOTIF IN OXIDATIVE STRESS INDUCED DIFFERENTIATION AND APOPTOSIS IN U937		158
5.1	INTRODUCTION	158
5.2	AIMS & OBJECTIVES	162
5.2.1	Objectives	163
5.3	METHODS	164
5.3.1	Characterisation of BCAT1(WT) and CXXC Motif Mutant Transgenic Cells.	164
5.3.2.	Evaluation of the BCAT1 CXXC Motif in Myeloid Differentiation	165
5.4	RESULTS	166
5.4.1	Growth characterisation: Cell growth and density	166
5.4.2	Growth characterisation: Cell cycle analysis	168

5.4.3	Growth characterisation: Cell viability	170
5.4.4	Growth characterisation: Intracellular redox environment	172
5.4.5	The Antioxidant Effect of the CXXC Motif on Serum Starved Transgenic U937 cells	176
5.4.6	The effect of the BCAT1 CXXC motif on PMA mediated cellular differentiation	182
5.4 DISCUSSION		188
CHAPTER 6: THE EFFECT OF BCAT1 CXXC MOTIF ON TREATMENT WITH CYTARABINE AND THE PRO-OXIDANT ROTENONE IN U937 CELLS.		199
6.1 INTRODUCTION		199
6.2 AIMS AND OBJECTIVES		203
6.2.1	Objectives	204
6.3 METHODS		205
6.3.1.	Dose Response Curves	205
6.3.2	Rotenone Generated ROS by DCFDA Assay	205
6.4 RESULTS		206
6.4.1.	Cytarabine Dose Response	206
6.4.2.	Gabapentin Dose Response	208
6.4.3.	Rapamycin Dose Response	210
6.4.4.	Rotenone Dose Response	212
6.5 DISCUSSION		215
CHAPTER 7. FINAL DISCUSSION AND FUTURE WORK		221

7.1 Final Discussion	221
7.2 Future Work	227
PUBLICATIONS	230
REFERENCES	231
APPENDICES	262

Figures and Tables

Chapter 1

Figure 1.1	Haematopoiesis	17
Table 1.1	FAB classification of Acute Myeloid	25
Table 1.2	WHO classification of Acute Myeloid leukaemia	26
Figure 1.2	Ten-year survival rates for cytogenetic abnormalities	28
Figure 1.3	Common myeloid leukaemia cytogenetic lesions	29
Table 1.3	Comparison of <i>in vitro</i> enzyme kinetics for BCAT1/ BCAT2	34
Figure 1.4	Branched Chain Amino Acid Metabolism	35
Figure 1.5	Expression of BCAT1 and BCAT2	38
Figure 1.6	Five-year survival of patients displaying differential expression of BCAT1 and BCAT2	39
Figure 1.7	Metabolic Reprogramming in AML.	41
Figure 1.8	Redox activity of the BCAT1 and BCAT2 CXXC motifs.	46
Figure 1.9	Redox control of cellular processes.	49
Figure 1.10	The glutaredoxin and thioredoxin redox cycle.	56
Figure 1.11	Protein thiol oxidation/reduction reaction via glutathione/ NADPH redox couple	59

Figure 1.12	Receptor Tyrosine Kinase (RTK) signalling	62
Chapter 3		
Figure 3.1	Cysteine to serine site directed mutagenesis pCMV6- <i>BCAT1</i>	94
Figure 3.2	DTNB modification of reactive cysteine thiol/ate(s)	97
Figure 3.3	Redox reactions of the wild-type <i>BCAT1</i> CXXC motif and C-terminal CXXS mutant	100
Figure 3.4	Site directed mutagenesis of <i>BCAT1</i> CXXC motif in pCMV6 vector	107
Figure 3.5	Subcloning <i>BCAT1</i> (WT) and <i>BCAT1</i> CXXC motif mutants from pCMV6-Entry vector to pET28a expression vector	109
Figure 3.6	Sequence alignment of pCMV6-Entry, pET28a and pLenti constructs containing <i>BCAT1</i> and CXXC motif mutants	110
Fig 3.7	SDS-PAGE gel displaying protein expression of <i>BCAT1</i> (WT) and CXXC mutants in BL21 (DE3) cells	112
Figure 3.8	Chromatogram profiles displaying <i>BCAT1</i> (WT) and <i>BCAT1</i> CXXC mutant proteins purified by ion exchange	113
Fig 3.9	SDS-PAGE displaying purification of <i>BCAT1</i> (WT) and <i>BCAT1</i> CXXC mutant proteins	114
Figure 3.10	Detection of <i>BCAT1</i> (WT) and <i>BCAT1</i> CXXC motif mutants by western blot analysis	115

Figure 3.11	DTNB cysteine thiol titration of BCAT1(WT) and BCAT1 CXXC mutant protein	117
-------------	--------------------------------------------------------------------------	-----

Chapter 4

Figure 4.1	Production of Lentivirus using the third-generation system	124
Figure 4.2	pLenti plasmid system for cellular transduction	127
Figure 4.3	Subcloning <i>BCAT1</i> WT and CXXC motif mutants from pCMV6-Entry vector to pLenti destination vector	134
Figure 4.4	Sequence alignment of pCMV6-Entry and pLenti constructs containing <i>BCAT1</i> (WT) and CXXC motif mutants	135
Figure 4.5	<i>BCAT1</i> transcript expression in immortalised leukaemia cell lines	136
Table 4.1	Transducing units (TU) lentiviral titre calculated from p24 ELISA	137
Figure 4.6	Generation and quantification of Lentivirus	139
Figure 4.7	Antibiotic selection of transgenic cell lines	140
Table 4.2	Fold-change in <i>BCAT1</i> mRNA following transgenic overexpression	142
Figure 4.8	Analysis of RNA integrity extracted from U937 cell	144
Figure 4.9	qPCR primer pair optimisation	146
Figure 4.10	Optimisation of qPCR cycling parameters	146
Figure 4.11	Calibration curves of <i>BCAT1</i> and β 2M primers	147
Figure 4.12	qPCR amplification curves and melt-curve analysis	148

Figure 4.13	Fold expression change of BCAT1(WT) and CXXC motif mutants in transgenic U937 cells	149
Figure 4.14	Anti-Myc/DDK (FLAG) mAb titration by Western Blot analysis	151
Figure 4.15	Protein expression validation of BCAT1(WT) and respective CXXC motif mutants in transgenic U937 cells	152
Chapter 5		
Figure 5.1	Growth profile of BCAT1 overexpressing and control U937 cells in culture	167
Figure 5.2	Effect of BCAT1(WT) and BCAT1(C338S) overexpression on cell cycle in U937 cells	169
Figure 5.3	Viability profile of BCAT1 overexpressing and control U937 cells	171
Figure 5.4	Effect of BCAT1(WT) and BCAT1(C338S) overexpression on mitochondrial membrane potential ($\Delta\Psi_m$)	173
Figure 5.5	Effect of BCAT1(WT) and BCAT1(C338S) overexpression on Reactive Oxygen Species (ROS)	174
Figure 5.6	Effect of BCAT1(WT) and BCAT1(C338S) overexpression on intracellular glutathione and redox potential	175
Figure 5.7	Effect of BCAT1(WT) and BCAT1(C338S) overexpression on intracellular ROS following serum starvation	178

Figure 5.8	Effect of BCAT1(WT) and BCAT1(C338S) overexpression on 7AAD/Annexin in U937 cells following serum starvation	179
Table 5.1	Cell viability determined by 7AAD/ Annexin V staining following serum starvation summarised	180
Figure 5.9	The effect of BCAT1(WT) and BCAT1(C338S) overexpression on cellular proliferation following serum starvation	181
Figure 5.10	The effect of BCAT1(WT) and BCAT1(C338S) overexpression on cellular morphology	183
Figure 5.11	The effect of BCAT1(WT) and BCAT1(C338S) overexpression on Phorbol 12-myristate 13-acetate (PMA) induced ROS	184
Figure 5.12	The effect of PMA treatment on the markers of myeloid differentiation CD36 and CD11b	187
Chapter 6		
Figure 6.1.	Cellular density and viability in response to Ara-C treatment	207
Figure 6.2	Cellular density and viability in response to Gabapentin treatment	209
Table 6.1	Mean (\pm SEM) IC50 values for therapeutics across all cell lines	210
Figure 6.3	Cellular density and viability in response to Rapamycin treatment	211
Figure 6.4	Cellular density and viability in response to Rotenone treatment	213
Figure 6.5	The effect of BCAT1overexpression on intracellular ROS following Rotenone treatment	214

Appendix A	NCBI Blast vector sequence alignments	262
Appendix B	Densitometric analysis of RNA agarose gels. 28S:18S rRNA ratio ≥ 2 indicates intact RNA suitable for downstream analysis	285
Appendix C	Melt-curve analysis of qPCR calibration curves	286
Appendix D	Differential aggregation of U937 transgenic cells following addition of PMA	287

Abbreviations

AML	Acute Myeloid Leukaemia
AMPK	AMP-activated Protein Kinase
ALL	Acute Lymphocytic Leukaemia
APL	Acute promyelocytic leukaemia
ATP	Adenosine Triphosphate
Ara-C	Cytarabine
ATRA	All-Trans Retinoic Acid
BCAT1/2	Branched Chain Aminotransferase 1 + 2
BCA	Bicinchoninic Acid Assay
BCAA	Branched Chain Amino Acids
BCKA	Branched chain-keto acid
BSA	Bovine Serum Albumin
β 2M	Beta-2 Microglobulin
CEBPA	CCAAT/Enhancer Binding Protein α
CLL	Chronic Lymphocytic Leukaemia
CML	Chronic Myeloid Leukaemia
CML	Common Myeloid Progenitor

CMV	Cytomegalovirus
CoA	Coenzyme A
Cp	Crossing point
Cys	Cysteine
DCFDA	2',7' –dichlorofluorescein diacetate
DiOC2(3)	3,3'-diethyloxacarbocyanine Iodide
DMEM	Dulbecco's Modified Eagle Media
DNA	Deoxyribonucleic acid
DTNB	5,5'-dithio-bis-2-nitrobenzoic acid
DTT	Dithiothreitol
EDTA	Ethylenediaminetetraacetic acid
EGF	Epidermal Growth Factor
ELISA	Enzyme-linked immunosorbent assay
ETC	Electron Transport Chain
EV	Empty Vector
FCS	Fetal Calf Serum
FLT3	FMS-Like Tyrosine Kinase-3
FSC	Forward Scatter

GAC	Glutaminase C
GDH	Glutamate Dehydrogenase
GDP/GTP	Guanosine Diphosphate/Guanosine Triphosphate
GFP	Green Fluorescent Protein
GLS	Glutaminase
GMP	Granulocyte/Macrophage Progenitor
GPx	Glutathione Peroxidase
Grx	Glutaredoxin
GSH	Glutathione
GSSG	Glutathione disulfide
HIF-1 α	Hypoxia Inducible Factor-1 alpha
HIV-1	Human immunodeficiency virus -1
HSC	Haematopoietic Stem Cell
IC ₅₀	Half-maximal inhibitory concentration
IDH1/2	Isocitrate Dehydrogenases 1 + 2
IPTG	Isopropyl β -D-1-thiogalactopyranoside
KIC	α -ketoisocaproate
KIV	α -ketoisovalerate (KIV)

KMV	α -ketomethylvalerate
α -KG	α -ketoglutarate
LB	Luria-Bertani
LDL	Low Density Lipoprotein
LEDGF	Lens Epithelium Derived Growth Factor
LSC	Leukemic Stem Cell
LTR	Long Terminal Repeat
MOI	Multiplicity of Infection
mTOR	Mammalian Target of Rapamycin
NAC	<i>N</i> -acetyl-L-cysteine
NADH	Nicotinamide Adenine Dinucleotide
NADPH	Nicotinamide Adenine Dinucleotide Phosphate
NPM1	Nucleolar Phosphoprotein B23
RNA	Ribonucleic acid
RNS	Reactive Nitrogen Species
ROS	Reactive Oxygen Species
S6K1	S6 Kinase 1
TCA	The Citric Acid Cycle

TPM	Transcripts per million
Trx	Thioredoxin
TrxR	Thioredoxin Reductase
TSC	Tuberous Sclerosis Complex
TSP-1	Thrombospondin-1
PBS	Phosphate Buffered Saline
PCR	Polymerase Chain Reaction
PHD2	Prolyl Hydroxylase Domain-containing Protein 2
PI	Propidium Iodide
PIC	Pre-integration Complex
PKC	Protein Kinase C
PMA	Phorbol 12-myristate 13-acetate
<i>PML</i>	Promyelocytic Leukaemia Protein
PRDX	Peroxiredoxin
PTP	Protein Tyrosine Phosphatases
RTK	Receptor Tyrosine Kinases
RAR α	Retinoic Acid Receptor alpha
RUNX1	Runt-related Transcription Factor 1

SDS-PAGE	Sodium dodecyl sulphate polyacrylamide gel electrophoresis
SSC	Side Scatter
VSV-G	Vesicular Stomatitis Virus
WCL	Whole Cell Lysate
WHO	World Health Organisation
WT	Wild type

Abstract

Acute Myeloid Leukaemia (AML) is the most common acute white blood cell cancer in adults, with a U.K. incidence of 3,100 new cases/year approximately 30% of all leukaemia. Survival remains below 15% for patients over the age of 60 diagnosed with AML, who respond poorly to standard non-specific chemotherapy treatment, therefore there is a need for new targeted therapies .

Recently, expression of cytosolic isoform of Branched Chain Aminotransferase (*BCAT1*) has been correlated with shorter overall survival in AML. Current research has focussed on the *BCAT1* metabolites α -ketoglutarate (α -KG) , glutamate and leucine, however *BCAT1* contains a redox active CXXC motif, a feature of antioxidant enzymes such as Thioredoxin, suggesting *BCAT1* may have a novel antioxidant role.

Overproduction of Reactive Oxygen Species (ROS) in AML is extremely well characterised and contributes to the pathogenesis of the disease. Targeting leukaemia cells with pro-oxidants to overwhelm the antioxidant capacity of the cell is recognised as an attractive strategy, particularly in respect to leukemic stem cells which are a major cause of therapy resistance and relapse. Therefore, in this study, the potential antioxidant effect of the *BCAT1* CXXC motif was investigated with respect to well documented redox mediated processes dysregulated in AML. These redox mediated processes included cellular proliferation, differentiation and apoptosis. To evaluate this a myeloid leukaemia cell line, U937 (ATCC CRL 1293.2) was engineered to stably overexpress wild-type *BCAT1* protein and CXXC motif mutant *BCAT1*.

The key findings of the study showed that the BCAT1 CXXC motif provides a protective effect against ROS mediated apoptosis induced by serum starvation in U937 cells. Moreover the CXXC motif reduced intracellular ROS and CD36⁺ cells, a marker of macrophage differentiation following addition of Phorbol 12-myristate 13-acetate (PMA) which has been demonstrated to induce differentiation of U937 cells using H₂O₂, a biologically relevant ROS species, as a secondary messenger. Finally, the feasibility of targeting BCAT1 with standard chemotherapy, metabolic inhibitors and pro-oxidants therapy has been explored with a view to developing a treatment strategy for patients with BCAT1^{high} and BCAT1^{low} levels of expression. For the first time this study demonstrated that the BCAT1 CXXC motif reduces intracellular ROS and provides protection against apoptosis in response to treatment with pro-oxidant Rotenone whilst BCAT1 increases sensitivity to standard chemotherapeutic Cytarabine (Ara-C).

Overall, the findings in this study indicate that the BCAT1 CXXC motif acts as a novel antioxidant in AML impacting redox mediated cellular differentiation and apoptosis through ROS modulation. Similarly, the BCAT1 and the antioxidant capacity of the CXXC motif can protect against pro-oxidant therapy, an important finding that could inform treatment strategies in future.

Chapter 1: Introduction

1.1 Leukaemia

1.1.1 Haematopoiesis

Haematopoiesis is the process by which pluripotent haematopoietic stem cells (HSCs) residing in the bone marrow differentiate along several well-defined pathways producing the full complement of differentiated blood tissue. In mammals, hematopoietic development occurs in two main stages throughout embryogenesis called primitive and definitive haematopoiesis (Ivanovs *et al.*, 2017). These stages occur in several different locations in the early embryo as it develops and are sometimes referred to as waves, representing their overlapping nature. In murine models, primitive haematopoiesis takes place in a region called the Yolk sac at embryonic day 7. It is marked by a relatively simple model of cellular differentiation, producing endothelial cells and primitive red blood cells, with embryonic haemoglobin that supply blood to the developing embryo. This is followed by the emergence of HSCs, which develop in the aorta-gonad-mesonephros (AGM) region several days later (Ivanovs *et al.*, 2017). HSCs are capable of self-renewal and functionally defined as being able to reconstitute the hematopoietic system following transplantation into irradiated bone marrow (Mikkola and Orkin, 2006; Boulais and Frenette, 2015). Following development of the vasculature around day 12, HSCs migrate to the liver where they proliferate and finally to the bone marrow by day 17-18 (Jagannathan-Bogdan and Zon, 2013). Population of the bone marrow marks the transition from primitive to definitive haematopoiesis, which is maintained throughout adult life. In the definitive hematopoietic model, the lineage

repertoire is expanded to include the full complement of blood tissue. This includes the leukocytes of the immune system, of which there are two primary branches, the 'lymphoid lineage' and 'the myeloid lineage' (Figure 1.1). The lymphoid lineage produces the lymphocytes of the adaptive immune system, which consists of Natural Killer cells, T-cells and B-cells, whilst the myeloid lineage matures into cells of the innate immune system including, neutrophils, basophils, macrophages, dendritic cells, thrombocytes and erythrocytes (Weiskopf *et al.*, 2016).

Self-renewing long-term HSCs sit at the top of this developmental hierarchy, existing in a stable quiescent state, which provides a lifelong pool of HSCs (Figure 1.1). Maintenance of the HSC pool and mechanisms that drive self-renewal are still poorly understood, given the structural complexity of the bone marrow niche and the difficulty of analysing cells *in situ* (Morrison and Scadden, 2014). Initial experiments pointed towards HSCs direct association with Osteoblasts that line the inner bone marrow or endosteal bone surface mediated by N-Cadherin (Zhang *et al.*, 2003). However, this direct interaction through N-Cadherin has been subject to debate, as knockout of N-Cadherin in HSCs and Osteoblasts did not change HSC numbers (Bromberg *et al.*, 2012). Other studies suggest that quiescence is maintained through thrombopoietin and angiopoietin-1 produced by activated Osteoblasts (Arai *et al.*, 2004; Yoshihara *et al.*, 2007).

Another pivotal study using cell surface markers CD150, CD48 and CD244 to differentiate between multipotent and pluripotent progenitors, located most HSCs next to the sinusoidal endothelium, a type of capillary within the bone marrow termed the vascular niche (Kiel *et al.*, 2005). Exactly how and under what circumstances the HSCs in

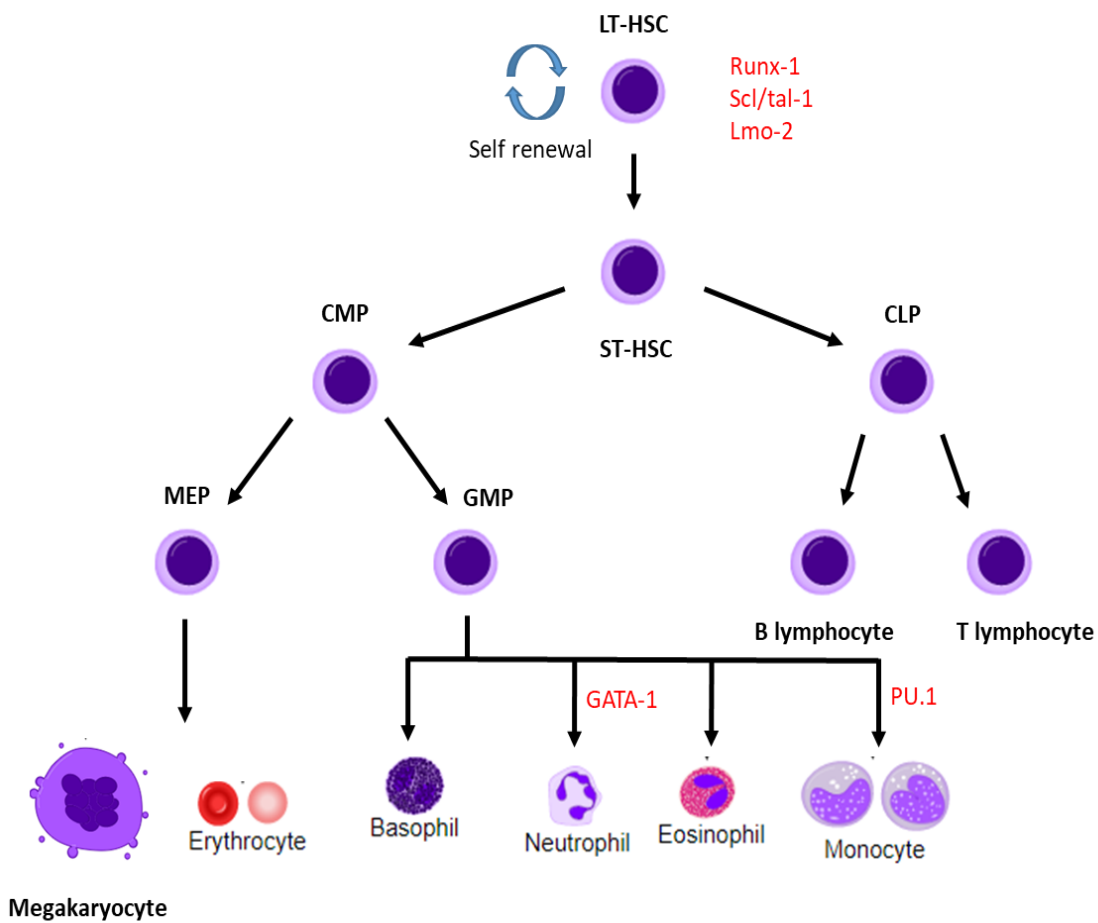


Figure 1.1 Haematopoiesis. In myeloid development generation of self-renewing Long-term Haematopoietic Stem Cells (LT-HSC) residing in the bone marrow requires expression of transcription factors Runx-1, Scl/tal-1 and Lmo-2. Short-term Haematopoietic Stem Cells (ST-HSC) differentiate into the common myeloid progenitor (CMP) which further differentiates the granulocyte/ macrophage progenitor (GMP). This is the last common precursor of the granulocytic and monocytic lineages of cells from which myeloid leukaemia arises development of which is directed by GATA-1 and PU.1 respectively. In normal development these immature blasts cells mature into terminally differentiated leukocytes of the innate immune system. Adapted from [https://commons.wikimedia.org/wiki/File:Hematopoiesis_\(human\)_diagram.png](https://commons.wikimedia.org/wiki/File:Hematopoiesis_(human)_diagram.png).

the osteoblastic and vascular niches interact or migrate between the two remains uncertain. One major factor to be elucidated in HSC maintenance is the production of chemoattractant CXC chemokine ligand (CXCL) 12 by CXCL12-abundant reticular (CAR) cells, that are localised to the vascular niche. High CXCL12 expression by CAR cells resulted in contact with increased numbers of HSCs, whilst deletion of its corresponding receptor (CXCR4) in HSCs resulted in a severe reduction in HSC numbers, suggesting CXCL12 may modulate movement to the vasculature (Sugiyama *et al.*, 2006). Subsequently CXCL12 was shown to be expressed primarily by perivascular stromal cells and at lower levels by endothelial cells, osteoblasts and HSCs. Deletion of CXCL12 from vascular niche cells including endothelial and stromal cells depleted HSCs whilst deletion of CXCL12 from osteoblasts did not deplete HSCs, highlighting the importance of the vascular niche in HSC (Ding and Morrison, 2013; Greenbaum *et al.*, 2013; Morrison and Scadden, 2014).

It was believed that HSCs regulate quiescence vs proliferation in the bone marrow microenvironment because the Osteoblastic niche provides a hypoxic environment for maintaining quiescence, whilst the vascular niche is more oxygenated allowing HSCs to proliferate and differentiate (Suda, Takubo and Semenza, 2011). This view is supported by data demonstrating areas of regional hypoxia associated with the endosteum (Spencer *et al.*, 2014), and the HSCs within this niche stabilise hypoxia inducible factor-1 alpha (HIF-1 α), allowing cells to shift to anaerobic metabolism and survive in low oxygen conditions (Suda, Takubo and Semenza, 2011). However more recent reports conflict with this interpretation by demonstrating that oxygen tension was lowest around vascular sinusoids and highest near the endosteum, moreover the bone marrow

hypoxic niche was lost when haematopoiesis was nullified by cytotoxic drugs, indicating that oxygen consumption during haematopoiesis renders the marrow hypoxic (Morrison and Scadden, 2014; Spencer *et al.*, 2014).

Perhaps better understood is how HSCs direct differentiation by expression of lineage specific transcription factors. One of the best studied examples are PU.1 and GATA-1 which are essential for the development of myeloid and erythroid lineages respectively (Burda, Laslo and Stopka, 2010). PU.1 has been shown to direct macrophage differentiation where continuous overexpression of PU.1 in multipotent progenitors directed a strong bias toward macrophage differentiation over granulocytes and eliminated erythroid differentiation (McIvor *et al.*, 2003). Supporting this, PU.1 knockout mice displaying an 80% reduction in PU.1 expression developed AML whilst viral overexpression rescued myeloid differentiation (Rosenbauer *et al.*, 2004). Importantly PU.1 and GATA-1 have been demonstrated to act antagonistically, where inhibition occurs in a dose dependent manner and is mediated by direct physical interaction (Nerlov *et al.*, 2000). PU.1 binds to GATA-1 on DNA where PU.1 recruits transcriptional corepressor pRB and histone H3K9 methyltransferases that creates a repressed chromatin structure and silencing GATA-1 directed gene expression (Rekhtman *et al.*, 2003; Burda, Laslo and Stopka, 2010). Conversely, GATA inhibits binding of PU.1 to c-Jun, a critical coactivator of PU.1 (Zhang *et al.*, 1999). Further evidence to support this antagonistic mechanism has been demonstrated in an *in vivo* Zebrafish model, where loss of GATA-1 directs to a monocytic fate whilst the converse is true of PU.1 (Orkin and Zon, 2008; Galloway *et al.*, 2005; Rhodes *et al.*, 2005).

The relationship between hematopoietic transcription factor dysregulation and leukemic malignancy has been extensively studied. Several transcription factors found to be essential to the production of HSCs by gene knockout experiments in mouse models include RUNX-1, SCL1/TAL1 and LMO-2. These were first discovered through the analysis of chromosomal translocations in human leukaemia underlining, the importance of genetic control of differentiation the pathogenesis of blood cancers (Shivdasani, Mayer and Orkin, 1995; Rabbits, 1998; Lacaud *et al.*, 2002).

1.1.2 Subtypes of Leukaemia

Leukaemia is a cancer of the blood, which is characterised by proliferation of abnormal immature white blood cells or leukocytes, known as blast cells (Hoffbrand, Moss and Pettit, 2016). Leukaemias have an incidence of approximately 10 100 cases per year in the UK, which accounts for 3% of all new cancer cases (*Leukaemia | Cancer Research UK, 2017*). Incidence rates for leukaemia have risen by 16% in the UK over the last ten years, reflecting an aging population where leukaemia incidence and mortality rates remains the highest amongst people aged 85-89. Incidence rates are expected to rise a further 5% to 19 cases per 100 000 by 2035. Despite this, mortality rates have fallen in the last ten years by 7% and are projected to fall by a further 18% to 8 deaths per 100 000 people by 2035. This increased survival reflects decades of research and advances in leukaemia treatment since the 1970s, which has increased the 10 year survival rate nearly 10-fold from approximately 5% to 46% (2010-11) (*Leukaemia (all subtypes combined) statistics | Cancer Research UK, 2017*). For Acute Myeloid Leukaemia specifically, data from the Medical Research Council trials collected between 1988–

2012, shows an increased overall survival rate from just 4% to 22% for patients ages >60 years old only, highlighting the challenge in treating older patients (Burnett A.K., 2012).

Despite an overall progress in treatment outcome, leukaemia remains a heterogeneous disease, with large variations in incidence and prognostic outlook, depending on the subtype and age. Broadly leukaemia is categorised based on four criteria; whether a leukaemia is chronic or acute and whether it originates from the myeloid or lymphoid lineage of white blood cells (*Leukaemia | Cancer Research UK, 2020*). This gives rise to 4 main types of leukaemia: Acute Myeloid Leukaemia (AML), Chronic Myeloid Leukaemia (CML), Acute Lymphocytic Leukaemia (ALL) and Chronic Lymphocytic Leukaemia (CLL). Chronic leukaemias proliferate more slowly and are generally made up of more mature leukocytes meaning symptoms can take years to manifest, whilst acute forms can progress extremely quickly and without immediate treatment survival can be measured in months (Hoffbrand, Moss and Pettit, 2016). This is reflected in overall survival rates in the USA from 2007-2013 for CML (68.7%), CLL (86.8%), ALL (71.6%) and AML (28.1%) (*Leukemia and Lymphoma Society, 2020*).

1.2 Acute Myeloid Leukaemia

AML is blood cell cancer of the myeloid lineage of white blood cells (leukocytes) and it is the most common acute white blood cell cancer in adults, with a U.K. incidence of around 3,100 new cases/year approximately 30% of all leukaemia (*Leukaemia | Cancer Research UK, 2020*). AML is characterised by a block in cellular differentiation and rapid proliferation of immature leukocytes, the block in differentiation and clonal expansion of these immature progenitors or 'myeloblasts' causes an abnormal accumulation in the

bone compromising normal haematopoiesis, consequently patients suffer from a range of cytopenias (a reduction in the number of mature blood cells), including red blood cells (anaemia), neutrophils (neutropenia) and platelets (thrombocytopenia). These cytopenias manifest as a range of symptoms, including, bone and joint pain, lethargy, increased susceptibility to infection and bleeding (Döhner, Weisdorf and Bloomfield, 2015). As blast-crisis progresses, myeloblast cells can infiltrate peripheral blood and migrate to the spleen and liver enlarging these organs, eventually the disease may progress and metastasise to the central nervous. If left untreated, death can typically occur within 3-6 months due to bone marrow failure. (Oran and Weisdorf, 2012).

Traditional treatment of AML involves an initial course of chemotherapy known as the induction stage. At this stage patients are assessed to determine their fitness for high dose or low dose chemotherapy as non-specific chemotherapeutic agents target both healthy and malignant cells and the presence pre-existing health conditions results in poorer treatment outcomes (Østgård *et al.*, 2015). For example, the chemotherapeutic agent Cytarabine (*1β-arabinofuranosylcytosine*) is a nucleoside analogue of the nucleic acid cytosine where the ribose sugar of the sugar phosphate backbone for arabinose is substituted producing cytosine arabinose. Cytarabine is randomly incorporated into DNA during semiconservative replication in S-phase interrupting daughter strand synthesis, thus inhibiting all cell growth (Mompalmer, 2013).

Following induction therapy, patients that are in remission are progressed to the consolidation phase, where additional rounds of chemotherapy aim to eliminate any residual malignant cells. Patients that do not respond to induction therapy may undergo

radiotherapy which is used to irradiate the bone marrow before haematopoietic stem cell transplantation that may reconstitute the bone marrow and restore normal haematopoiesis (*Acute myeloid leukaemia - NHS, 2020*). The physical demands of non-specific therapies contribute to the relatively poor survival data for AML compared to other leukaemia subtypes, where older patients are placed on lower dose chemotherapy regimens that result in more refractory outcomes i.e. residual blast cells remaining following the first round of intensive treatment (Löwenberg *et al.*, 2011). For these reasons AML survival in patients younger than 15 years is 68.8% (*Leukemia and Lymphoma Society, 2020*) whilst survival remains around 22% for patients over the age of 60 (Burnett, 2013). Therefore, there has been a drive over the last 20 years to understand the underlying cytogenetic and biochemical characteristics of AML, so that new-targeted therapies may be established.

1.2.1 AML Classification

AML was first comprehensively classified by a French-American-British co-operative group of haematologists in 1976 (Bennett *et al.*, 1976). Commonly known as the FAB system, AML subtypes were based on morphological differences of peripheral blood and bone marrow when Romanowsky stained (a precursor of the modern Giemsa stain) and examined under a light microscope. Cells were separated based on two criteria, 1) the direction of differentiation along cell lineages and 2) the degree of maturation. This defined 8 sub-groups M0-M7, beginning with M0 which represents the most undifferentiated i.e. most 'stem-cell like' acute myeloblastic leukaemia. Types M1-M3 are predominantly granulocytic in nature, but differ in terms of their level of maturation and therefore were termed 'Myeloblastic leukaemia without maturation' (M1),

'Myeloblastic leukaemia with maturation' (M2), and 'Hypergranular promyelocytic leukaemia' (M3) now called Acute promyelocytic leukaemia (APL) accordingly. M4 displays both monocytic and granulocytic differentiation and was therefore was labelled 'Myelomonocytic leukaemia' with a later further division of 'Acute myelomonocytic leukaemia with eosinophilia' (M4 eos). M5, M6 and M7 are predominantly monocytic, erythroid and megakaryoblastic differentiation and were termed 'Acute monocytic leukaemia', 'Acute erythroid' and 'Acute megakaryoblastic leukaemia' respectively (Table 1.1) (Bennett *et al.*, 1976). Although the FAB system proved a useful initial framework, it failed to take into account many of the underlying genetic factors that affected patient survival called prognosis. This informed a new classification system implemented by the World Health Organisation (WHO), that organised leukaemia by a combination of immunophenotypic, morphologic, genetic and prognostic factors (Table 1.2). Since it's inauguration in 2001 it has been updated in 2008 and most recently in 2016, chiefly to incorporate the increased understanding of AML pathogenesis provided by advances in sequencing technology (Arber *et al.*, 2016).

There are currently over 25 clinically distinct classifications of AML, which are primarily divided by gross cytogenetic alterations such as chromosomal translocations, inversions and deletions that the WHO classifies as 'AML with recurrent genetic abnormalities'. Other categories include 'AML with myelodysplasia related changes', 'Therapy related myeloid neoplasms', 'Myeloid sarcoma' and 'AML not otherwise specified (NOS)'. Chromosomal abnormalities have been particularly useful for clinicians, as they can be identified by karyotype analysis under a light microscope

allowing prognostic stratification and targeted treatment of certain AML subtypes (Degos *et al.*, 1995; Mrózek, Heerema and Bloomfield, 2004).

Table 1.1 FAB classification of Acute Myeloid Leukaemia (adapted from Bennett *et al.*, 1976).

FAB subtype	Name
M0	Undifferentiated acute myeloblastic leukemia
M1	Acute myeloblastic leukemia with minimal maturation
M2	Acute myeloblastic leukemia with maturation
M3	Acute promyelocytic leukemia (APL)
M4	Acute myelomonocytic leukemia
M4 eos	Acute myelomonocytic leukemia with eosinophilia
M5	Acute monocytic leukemia
M6	Acute erythroid leukemia
M7	Acute megakaryoblastic leukemia

Table 1.2 WHO classification of Acute Myeloid leukaemia. (Arber *et al.*, 2016)

Acute myeloid leukemia (AML) and related neoplasms

AML with recurrent genetic abnormalities
AML with t(8;21)(q22;q22.1); <i>RUNX1-RUNX1T1</i>
AML with inv(16)(p13.1q22) or t(16;16)(p13.1;q22); <i>CBFB-MYH11</i>
APL with <i>PML-RARA</i>
AML with t(9;11)(p21.3;q23.3); <i>MLLT3-KMT2A</i>
AML with t(6;9)(p23;q34.1); <i>DEK-NUP214</i>
AML with inv(3)(q21.3q26.2) or t(3;3)(q21.3;q26.2); <i>GATA2, MECOM</i>
AML (megakaryoblastic) with t(1;22)(p13.3;q13.3); <i>RBM15-MKL1</i>
<i>Provisional entity: AML with BCR-ABL1</i>
AML with mutated <i>NPM1</i>
AML with biallelic mutations of <i>CEBPA</i>
<i>Provisional entity: AML with mutated RUNX1</i>
AML with myelodysplasia-related changes
Therapy-related myeloid neoplasms
AML, NOS
AML with minimal differentiation
AML without maturation
AML with maturation
Acute myelomonocytic leukemia
Acute monoblastic/monocytic leukemia
Pure erythroid leukemia
Acute megakaryoblastic leukemia
Acute basophilic leukemia
Acute panmyelosis with myelofibrosis
Myeloid sarcoma
Myeloid proliferations related to Down syndrome
Transient abnormal myelopoiesis (TAM)
Myeloid leukemia associated with Down syndrome

1.2.2 AML Cytogenetics

There are currently six recognised recurrent gross cytogenetic alterations that are associated with prognostic outlook, broadly separated into favourable and unfavourable abnormalities, however 10 year survival rates vary significantly between these abnormalities (Figure 1.2) (Grimwade *et al.*, 2010).

For example, the chromosomal translocation t(15;17) (*PML-RAR α*), which fuses the tumour suppressor Promyelocytic Leukaemia Protein (*PML*) gene to the Retinoic acid receptor alpha(*RAR α*) gene, results in loss of function of *PML*, culminating in a block in myeloid cell differentiation and the development of APL mediated by the *PML-RAR α* fusion protein (Olsson *et al.*, 2009). Patients with the *PML-RAR α* fusion protein have a complete remission rate of >80%, due to the treatment with all-trans retinoic acid (*ATRA*), which targets *PML-RAR α* and lifts the block in myeloid differentiation (Figure 1.3) (Coombs, Tavakkoli and Tallman, 2015).

Similarly, chromosomal translocation t(8;21) (*RUNX1-RUNX1T1*), which fuses the Runt-related transcription factor 1 (*RUNX1*) with the zinc finger protein '*ETO*', resulting in transcriptional repression and a block in differentiation, has a ten year survival rate of >60% (Figure 1.3) (Mrozek and Bloomfield, 2008). Conversely, the t6;9 chromosomal translocation and inversions of chromosome 3 *inv(3)/ t(3;3)* result in subtypes that are highly therapy resistant, and survival rates remain extremely poor at 11% and 3% respectively (Grimwade *et al.*, 2010). These various chromosomal translocations (karyotypes) highlight to some degree the heterogeneity of AML

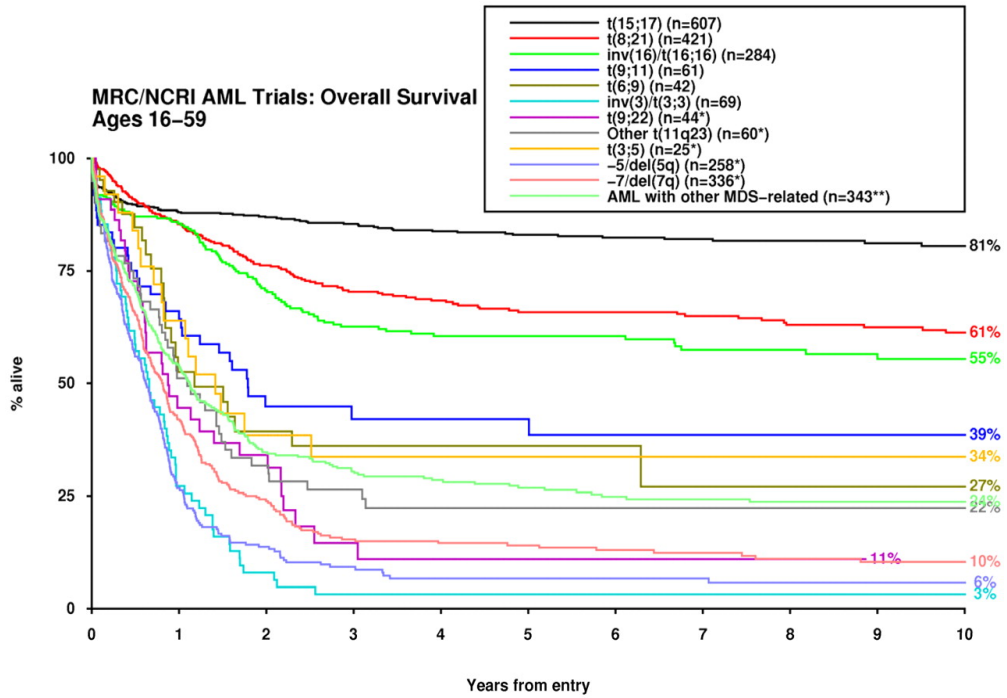


Figure 1.2 Ten year survival rates for cytogenetic abnormalities recognised in the 2008 WHO classification (Grimwade *et al.*, 2010).

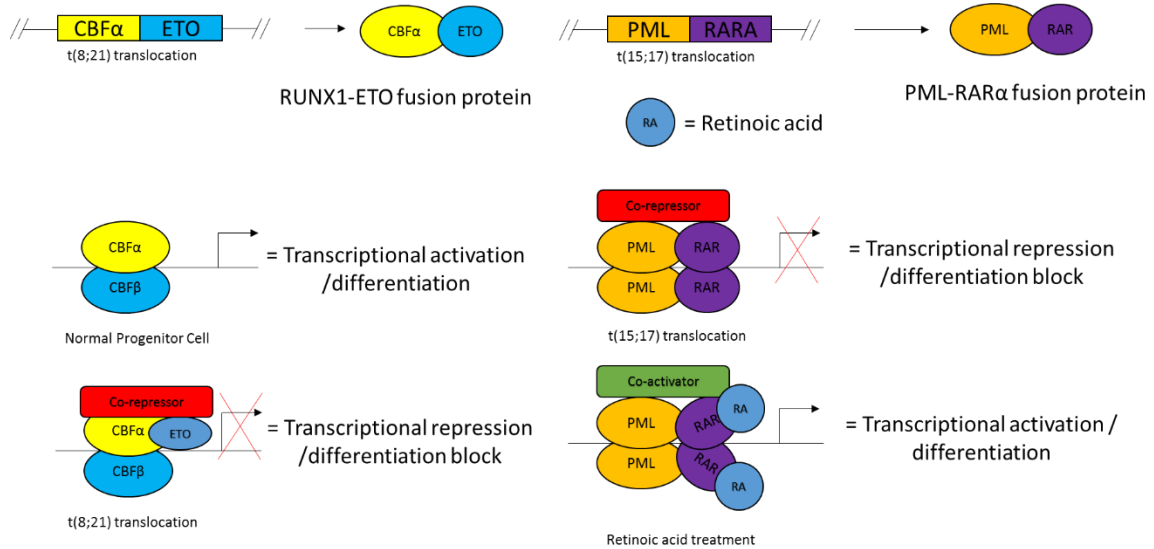


Figure 1.3 Common myeloid leukaemia cytogenetic lesions. Translocations t(15;17) (PML-RAR) and t(8;21) (*RUNX1-RUNX1T1*) both produce transcription factor fusion proteins that result in transcriptional repression and blocks in differentiation. Categorized as prognostically favourable treatment with Retinoic acid initiates transcriptional activation and cellular differentiation. Adapted from (Downing, 2003)

Diagnosis by karyotype analysis has proved a powerful prognostic indicator in AML, providing an invaluable tool that informs treatment strategies. However it is estimated that 40-50 % of patients are cytogenetically normal i.e. have no gross chromosomal translocations / inversions (Schlenk *et al.*, 2008). Advances in gene expression analysis coupled with survival data, has identified several somatic gene mutations e.g. nucleolar phosphoprotein B23 (*NPM1*) and CCAAT/enhancer binding protein α (*CEBPA*) that are associated with altered outcomes (Suzuki, 2014). In last 10 years mutations in *NPM1*, *CEBPA* and *RUNX1* have been incorporated into the latest WHO classification of haematological malignancies (Arber *et al.*, 2016). *RUNX1* and *CEBPA* are transcription factors involved in hematopoietic development, whilst *NPM1* is a multifunctional protein involved in ribosome biogenesis and modulation of the p53 stress response.(Verhaak *et al.*, 2005)

There are additional gene mutations not currently recognised as clinically distinct but contribute to prognostic outlook. Typically, these mutations have resulted in changes to key proliferative signalling cascades that result in a change of gene expression. For example, transmembrane receptor tyrosine kinases; FMS-Like Tyrosine Kinase-3 (*FLT3*) and c-KIT are two of the most common accompanying mutations, occurring in approximately 25% and 8% of AMLs, resulting in the activation the PI3K-AKT-mTOR, RAS-RAF-MEK-ERK and JAK-STAT signalling cascades that mediate growth and survival(Gilliland and Griffin, 2002; Cairoli *et al.*, 2006). Both kinases are central to normal haematopoiesis and promote blood progenitor cell proliferation, however mutations in AML promote leukemic cell division (Escribano *et al.*, 1998; Gilliland and Griffin, 2002)

1.2.3 *Metabolic mutations*

Recently mutations in metabolic genes that alter or reprogram metabolic pathways have become a focus of research, highlighting the leukaemogenic importance of cellular processes outside of the typical growth and survival signalling pathways. (Feng *et al.*, 2012)

Proliferating cells have markedly different metabolic requirements to quiescent cells, which express basal levels of metabolic enzymes for repair and maintenance, since transformed cells e.g. AML cells, must accumulate sufficient pools of macromolecules such as lipids and nucleotides for cell division (Ward and Thompson, 2012). Additionally, they exist in highly variable microenvironments that are generally characterised by poor nutrient availability and hypoxias such transformed cells display a reprogrammed metabolism that allows them to adapt to these conditions (Vander Heiden, Cantley and Thompson, 2009). Altered cancer metabolism was first observed by Otto Warburg who noted cancer cells favour relatively inefficient glycolysis to oxidative phosphorylation, even in aerobic conditions, hence it was termed aerobic glycolysis or the Warburg effect (Potter, Newport and Morten, 2016). As glycolysis is much less efficient at producing Adenosine triphosphate (ATP) than oxidative phosphorylation Warburg, assumed cancer cells had defective mitochondria, however we now understand cells redirect glucose carbon for nucleotide, lipid and protein synthesis (Liberti and Locasale, 2016). The emerging importance of metabolic reprogramming is reflected by the addition of deregulation of cellular energetics to Hanahan and Weinberg's 'Hallmarks of Cancer' in 2011 (Hanahan and Weinberg, 2011).

Important metabolic genes mutated / deregulated in AML are Isocitrate Dehydrogenases 1 and 2 (*IDH1/IDH2*). Both isoforms of this metabolic enzyme have been extensively studied in AML (Medeiros *et al.*, 2017). The IDH isoenzymes are mutated in ~20% AML cases, these mutations are associated with worse patient outcomes (Feng *et al.*, 2012). The IDH1/2 isoenzymes are the cytosolic and mitochondrial isoforms respectively, that catalyse the oxidative decarboxylation of isocitrate, to alpha-keto glutarate (α -KG) in the Citric Acid Cycle. (Medeiros *et al.*, 2017).

The Citric Acid Cycle (TCA) is a central metabolic nexus linking key processes including ATP generation through oxidative phosphorylation, lipid biosynthesis and regeneration of reducing equivalents for cellular redox reactions. *IDH1/2* mutations result in a loss of normal catalytic activity, rendering the proteins unable to produce α -KG. Instead mutant IDH enzymes have neomorphic activity catalysing the reduction of α -KG to a structurally similar oncometabolite 2-hydroxyglutarate, which competitively inhibits α -KG-dependant enzymes, leading to enhanced proliferation and blocked differentiation of HSCs. (Xu *et al.*, 2011) IDH1 targeted therapies are currently under clinical investigation (Medeiros *et al.*, 2017). However, 80% of AML patients have functional copies of IDH1, therefore identifying potential gene targets in this population is therefore of great importance. In recent years interest has increased in other metabolic enzymes that feed into the same pathway as IDH1 (Altman, Stine and Dang, 2016).

In the last 5 years, cytosolic Branched Chain Aminotransferase (BCAT1) overexpression has been associated with metastasis, cell proliferation and altered metabolism in various types of cancer (Zheng *et al.*, 2016; Hattori *et al.*, 2017; Zhang and

Han, 2017; Wang *et al.*, 2019). The BCAT1 metabolite α -KG feeds into the same metabolic pathways mediated by IDH1, albeit at a different entry level (Figure 1.4). Interestingly, in AML BCAT1 over-expression has been shown to decrease intracellular levels of α -KG in a similar manner to mutant IDH1 and is linked with shorter patient survival (Raffel *et al.*, 2017). Furthermore, a recent study in a glioma model demonstrated expression of BCAT1 was dependant on IDH1 mutational status, where knockdown of BCAT1 in cells with 'wild-type' IDH1 (IDH1^{wt}) was sufficient to reduce the growth of the cancer, making BCAT1 an attractive potential target for patients with IDH^{wt} status (Tönjes *et al.*, 2013).

Beyond IDH more recent research has highlighted the metabolic role of BCAT1 in macrophage differentiation by modulation of the TCA. These studies demonstrated that, following lipopolysaccharide stimulation, inhibition of BCAT1 supresses production of itaconate, an anti-inflammatory metabolite has been that has been implicated in the switching of macrophages from a pro to an anti-inflammatory state(Papathanassiu *et al.*, 2017; Yu *et al.*, 2018). Moreover, this was subsequently shown to activate Nrf2 and antioxidant responses suggesting BCAT1 has a role modulating the antioxidant response in activated macrophages by altering TCA metabolites(Ko *et al.*, 2020).

1.3 BCAT1

1.3.1 Enzyme kinetics

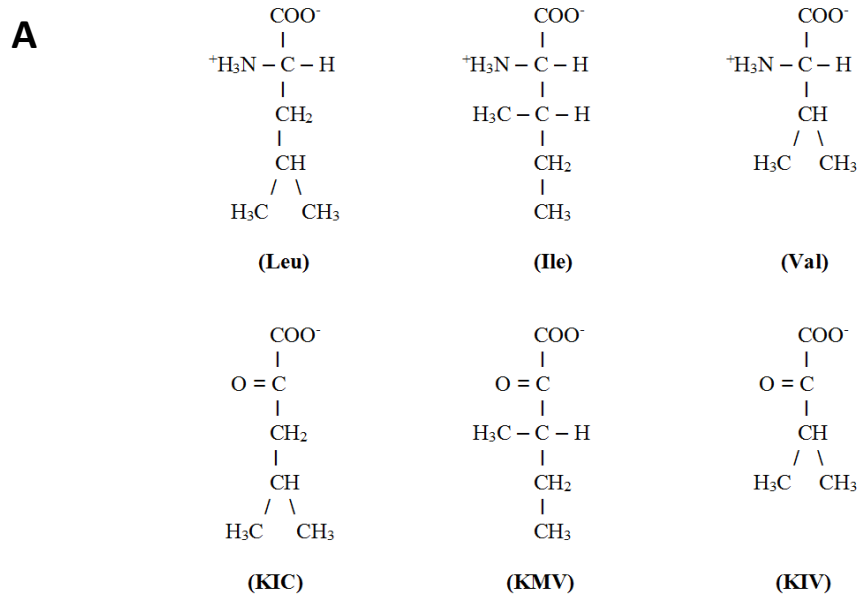
BCAT1 belongs to the fold-type IV class of pyridoxal 5'-phosphate (PLP)-dependent enzymes and catalyses the transamination of branched chain amino acids (BCAA) Leucine, Isoleucine and Valine (Figure 1.4, Panel A). In this reversible reaction an α -

amino group is transferred from the BCAAs to α -KG producing glutamate a branched chain-keto acid (BCKA); α -ketoisocaproate (KIC), α -ketomethylvalerate (KMV) and α -ketoisovalerate (KIV) respectively (Figure 1.4, Panel B) (Davoodi et al. 1998).

Like IDH, BCAT has two isoforms, the cytosolic isoform - BCAT1 and mitochondrial isoform - BCAT2. *In vitro* characterisation of both isoforms demonstrates that of the three BCKA substrates, KIC displays the lowest K_m value, the substrate concentration at which half maximal enzyme reaction rate is achieved (Davoodi *et al.* 1998, Conwy *at al* 2008). Moreover, the K_m values of BCAT1 and BCAT2 for KIC and glutamate are approximately an order of magnitude lower than for leucine and α -KG, concurrently the enzymatic turnover (K_{cat}) is also 2-3 times faster in the direction of alpha-KG formation for both isoforms. This demonstrates both BCAT1 and BCAT2 strongly favour glutamate and KIC as substrates, whilst the primary products are leucine and α -KG. (Table 1.3). Despite favouring the same enzymatic direction, BCAT1 and BCAT2 differ with respect to their kinetics. BCAT1 has an increased K_{cat} and lower K_m when metabolising KIC and Glutamate compared to BCAT2. This equates to an increased catalytic efficiency of $4905 \times 10^3 \text{ M}^{-1} \text{ S}^{-1}$ for BCAT1 compared to $1525 \times 10^3 \text{ M}^{-1} \text{ S}^{-1}$ for BCAT2, which is perhaps a reflection of the substrate concentrations in their respective subcellular locations (Davoodi *et al.* 1998)

Table 1.3 Comparison of *in vitro* enzyme kinetics for BCAT1 and BCAT2

Substrate	BCAT1			BCAT2		
	kcat (S ⁻¹)	Km (mM)	kcat/Km (x10 ³ M ⁻¹ S ⁻¹)	kcat (S ⁻¹)	Km (mM)	kcat/Km (x10 ³ M ⁻¹ S ⁻¹)
Leucine + α -KG	132	0.60	220	105	1.21	88
KIC + Glutamate	309	0.063	4905	244	0.16	1525



B)

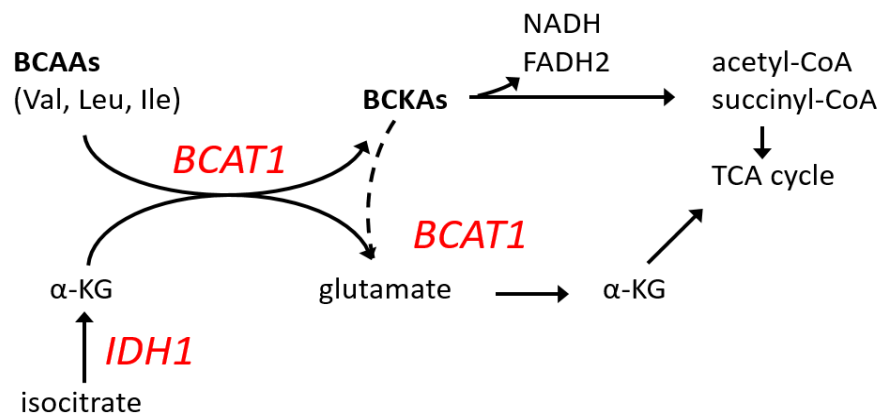


Figure 1.4 Branched Chain Amino Acid Metabolism. **A)** BCAT1 catalyses transamination between branched-chain amino acids (BCAA) Leucine (Leu), Iso-Leucine (Ile) and Valine (Val) and their ketoacid counterparts ; α -ketoisocaproate (KIC), α -ketomethylvalerate (KMV) and α -ketoisovalerate (KIV). **B)** IDH1 regenerates α -KG from isocitrate whereupon BCAT1 catalyses the transfer of NH₃ from the BCAA to α -ketoglutarate (α -KG) forming the respective branched-chain alpha-keto acid (BCKA) and glutamate. BCAT1 metabolites feed into the citric acid cycle and yield ATP. Where there is a build-up of BCKA, BCAT1 will favour the reverse reaction, generating BCAA. (Adapted from Tönjes *et al.*, 2013)

Despite the *in vitro* enzyme kinetics favouring BCAA anabolism, BCAT1 is commonly seen as the first step in BCAA catabolism (Tönjes *et al.*, 2013; Thewes *et al.*, 2017). In the canonical forward reaction, BCAT1 catalyses the transfer of NH_3 from the BCAA to α -KG forming the respective BCKA and glutamate. After transamination, BCKAs are further catabolised to Citric Acid Cycle intermediates acetyl coenzyme A (acetyl-CoA) and succinyl-CoA, providing macromolecule precursors and energy for mitochondrial ATP synthesis (Tönjes *et al.*, 2013).

Supporting this model, it was reported in glioblastoma cell lines that BCAT1 expression was upregulated by the addition of cell-permeable dimethyl α -KG and could be suppressed by mutant IDH1 overexpression, a primary source of α -KG, in immortalized human astrocytes (Tönjes *et al.*, 2013). Additionally, treatment with Gabapentin, a BCAT1 enzymatic inhibitor, resulted in an intracellular accumulation of BCAA and reduction in release of glutamate. These findings were replicated in AML cell lines, where normal expression of BCAT1 lead to a decrease in α -KG, whilst BCAT1 knockdown caused an accumulation of α -KG (Raffel *et al.*, 2017). Conversely BCAT1 expression was shown to increase BCAA in a mouse model of CML (Hattori *et al.*, 2017). In the Hattori study, BCAT1 expression in peripheral blood of patients was found to increase with disease progression from a chronic to acute phase and was associated with poorer survival. Interestingly, blocking BCAT1 metabolic activity with Gabapentin in the CML mouse model reduced intracellular BCAA concentrations and extended survival (Hattori 2017). Taken together, these studies indicate that the direction of BCAT1 catalysis in disease states is dynamic and may be context dependant on substrate

concentrations providing the cancer cell with the ability to respond to fluctuating nutrient concentrations.

1.3.2 Expression and survival

Recently BCAT1 expression has been associated with a poor prognostic outlook in numerous cancers. For example, BCAT1 expression correlated with significantly poorer prognosis in breast cancer, gastric cancer, hepatocellular and urothelial carcinoma (Chang *et al.*, 2016; Zheng *et al.*, 2016; Xu *et al.*, 2018a; Zou *et al.*, 2019; Song *et al.*, 2020). In AML studies examining BCAT1 expression converge on the importance of BCAT1 in HSCs. For example, it was reported that BCAT1 expression was significantly higher in CD34⁺ CD38⁻ leukemic stem cell populations and was significantly increased in relapsed AML samples (Raffel *et al.*, 2017). Additionally an another recent study demonstrated that blocking BCAT1 induced cellular differentiation (Hattori *et al.*, 2017), taken together these studies indicate a possible role for BCAT1 in cellular differentiation.

To support this notion, analysis of open source Affymetrix by the Coles Lab at the University of Worcester shows that BCAT1 expression levels are high in HSCs and low in differentiated healthy white blood cells. Moreover, in disease context, examination of 158 AML and 107 CLL patients at diagnosis for the expression level of BCAT1 revealed BCAT1 expression is highly dysregulated in AML and CLL blasts compared to healthy donor 'normal' bone marrow (Figure 1.5 Panel A). In contrast to BCAT1, BCAT2 expression is relatively stable, indicating it is not significant in leukaemia development (Figure 1.5 Panel B). Expression of BCAT1 in these patients with CLL was also associated with poorer patient survival which is consistent with previous findings (Figure 1.6) (Coles and Wadley, 2018).

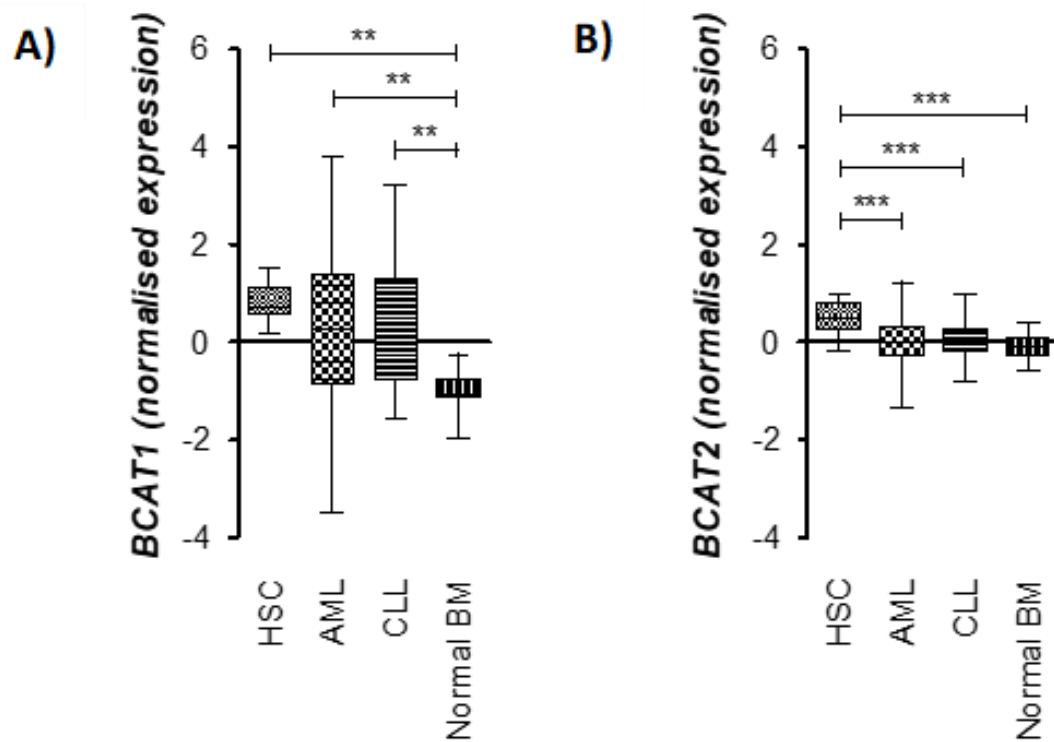


Figure 1.5 Expression of BCAT1 and BCAT2. **A)** Affymetrix (U133a_Plus_2.0) gene expression data of *BCAT1* expression in haematopoietic stem cells (HSC), acute myeloid leukaemia (AML; 157 patients), chronic lymphocytic leukaemia (CLL; 107 patients) and normal bone marrow tissue. **B)** Data compared with expression of *BCAT2*, a ubiquitously expressed mitochondrial analogue.

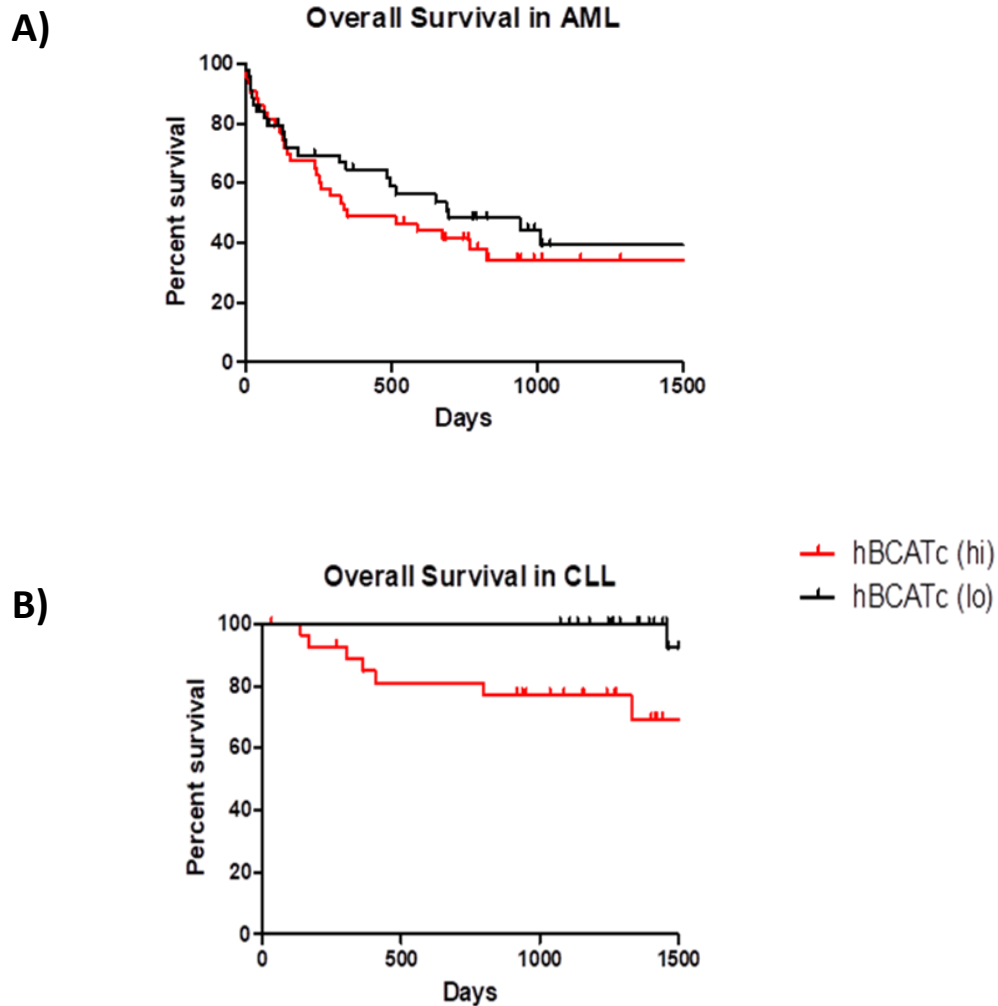


Figure 1.6 Five-year survival of patients displaying differential expression of BCAT1 and BCAT2. Kaplan Meier analysis displaying 5-year survival stratified for BCAT1 expression above (red line) or below (black line) the median for Acute Myeloid Leukaemia **A)**(AML; 157 patients) and chronic lymphocytic leukaemia. **B)** (CLL; 107 patients). Figure adapted from http://ologyjournals.com/cooaj/cooaj_00001.pdf

1.3.3 BCAT1 metabolic role in Cancer

Leucine and α -KG both play important roles in cellular metabolism and their dysregulation is part of the metabolic rewiring of the cancer cell. For example, AML displays increased aerobic glycolysis resulting in a decreased flux of metabolites to the TCA through the glycolytic pathway (Emadi, 2015). Transformed cells compensate for this by an increased dependency on glutamine metabolism, which is converted to α -KG to replenish the TCA - a process called anaplerosis. In this pathway glutamine is converted to glutamate by Glutaminase (GLS) and subsequently to α -KG by Glutamate Dehydrogenase (GDH) or aminotransferases i.e. BCAT1. (Figure 1.7). Whilst the by-product of GDH is the cytotoxic NH_4^+ , the by-product of BCAT1 is leucine, which interestingly is required for GDH activation (Oppliger *et al.*, 2012; Altman, Stine and Dang, 2016). Inhibition of the GLS isoform Glutaminase C (GAC), expressed in AML cell lines, negatively influences mitochondrial respiration, proliferation and survival, demonstrating the importance of glutamine and α -KG in AML cell metabolism (Jacque *et al.*, 2015).

α -KG is not only a BCAT1 metabolite, but is also a cofactor for more than 60 α -KG dependant dioxygenases enzymes, which have diverse roles including epigenetic regulation and the hypoxia response, both roles of which are dysregulated in AML (Drolle *et al.*, 2015; Wouters and Delwel, 2016). Raffel *et al.* reported that high expression levels of BCAT1 reduced intracellular α -KG and displayed a DNA hypermethylation phenotype similar to cases carrying a mutant IDH, in which epigenetic modifier TET2 is inhibited by the oncometabolite 2-hydroxyglutarate.

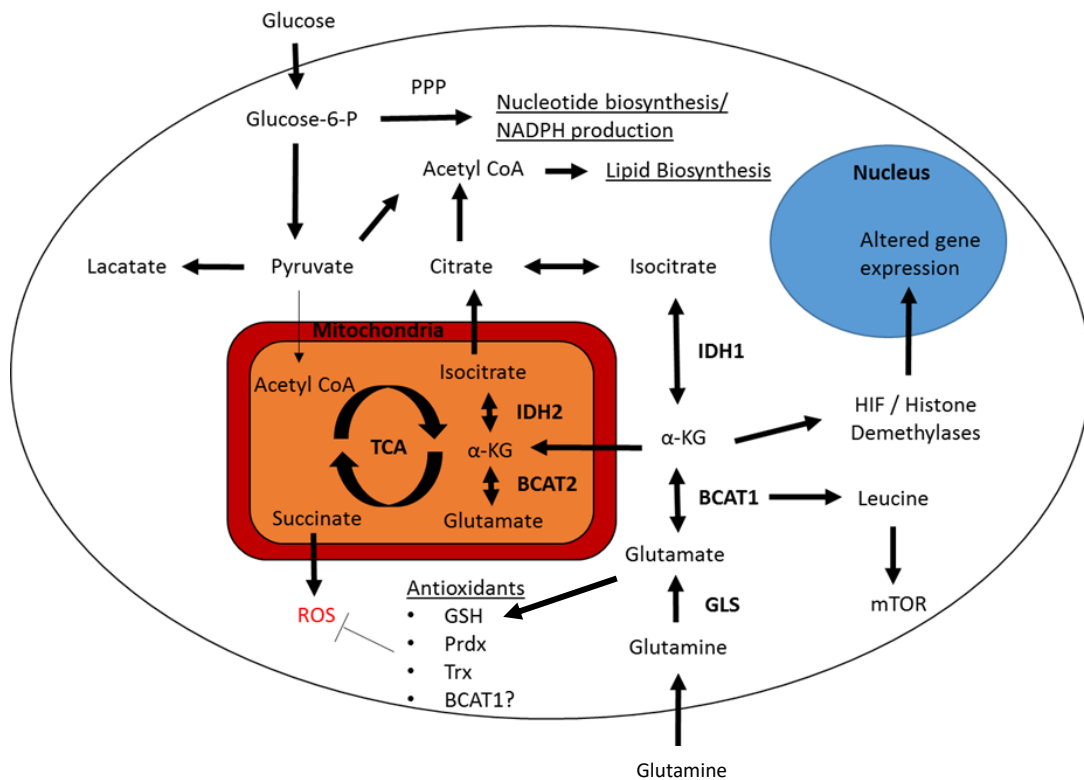


Figure 1.7 Metabolic Reprogramming in AML. Transformed cells displayed altered metabolism. An increase in aerobic glycolysis also known as the Warburg effect results increased lactate production and a decrease in mitochondrial Acetyl CoA shuttling. Glucose-6-P and Acetyl CoA are redirected for nucleotide and lipid biosynthesis respectively to fuel cell division. Concurrently an increase in glutamine results in increased α -KG levels that can anaplerotically replenish the depleted Citric Acid cycle (TCA) providing ATP and reducing equivalents. An increase in succinate derived mitochondrial ROS are metabolised by cellular antioxidants. Additionally, α -KG acts as a cofactor for histone demethylases that perform epigenetic alterations to the genome. Adapted from (Cairns and Mak, 2013)

Furthermore, Hypoxia Inducible Factor (HIF) transcription factors, which mediate primary transcriptional response to hypoxic stress, are regulated by α -KG dependent dioxygenases enzymes. Under normoxic conditions, HIF- α subunits are marked for the ubiquitin-proteasome degradation pathway through hydroxylation of proline by prolyl hydroxylase domain-containing protein 2 (PHD2), which is α -KG dependent (Deynoux *et al.*, 2016). Knockdown of BCAT1 in leukaemia cells caused accumulation of α -KG leading to PHD2 mediated HIF1 α protein degradation, conversely BCAT1 expression stabilised HIF1 α through a reduction in α -KG. Interestingly stabilisation of HIF- α has been shown to maintain HSC quiescence (Takubo *et al.*, 2010). Given most standard chemotherapy relies on targeting dividing cells, induction of the hypoxia response through α -KG regulated HIFs provides a mechanism for therapy resistance in AML by promotion of quiescence (Matsunaga *et al.*, 2012; Drolle *et al.*, 2015).

The other canonical forward reaction BCAT1 metabolic product, leucine, is an essential amino acid that cannot be manufactured *de novo* by the cell and plays an important role in nutrient sensing. Uptake of leucine is linked to glutamine through the LAT family of antiporters, which export glutamine in exchange for leucine (Altman, Stine and Dang, 2016). Additionally cells can scavenge intracellular or extracellular leucine through autophagy or macropinocytosis respectively, though these pathways are reported to be reduced in malignant hematopoietic progenitors (Sheen *et al.*, 2011).

Leucine is also obligatory for the activation of mammalian target of rapamycin complex 1 (mTORC1), a serine-threonine kinase multi-protein complex that has emerged as a signalling nexus that integrates upstream energy/nutrient availability, stress, oxygen sensing and exogenous signals from growth factors to effect downstream

changes in cell growth, metabolism and survival (Oppliger *et al.*, 2012; Jewell, Russell and Guan, 2013). Whilst the precise amino acid sensing mechanism is not known, leucine accumulates in the lysosome where it is required for the v-ATPase/Ragulator dependant guanine exchange of the Rag A/B and Rag C/D heterodimers. Activation of the pathway occurs with the guanosine diphosphate (GDP) to guanosine triphosphate (GTP) exchange of Rag A/B, which causes relocation of mTORC1 from an undefined cytoplasmic location to the lysosomal surface where it is activated by Rheb. Once activated, mTORC1 positively regulates protein biosynthesis through p70 ribosomal S6 kinase 1 (S6K1) which increases in mRNA biogenesis and translation of ribosomal protein S6 a component of the 40S ribosomal subunit (Oppliger *et al.*, 2012). As well as upregulating anabolic processes mTORC1 activation downregulates catabolic processes, such as autophagy, through the regulation of a protein complex composed of unc-51-like kinase 1 (Chan, 2009). Therefore, leucine availability is important for protein biosynthesis and cell survival.

Leucine is also obligatory for the allosteric activation of GDH, which as previously mentioned produces α -KG from glutamate, a vital step in the metabolism of glutamine. This pathway is upregulated in AML (Oppliger *et al.*, 2012; Jewell, Russell and Guan, 2013), the transamination of glutamate by BCAT1 provides a route to leucine production that does not require intracellular scavenging or export of glutamine, an important cellular resource. This may have important implications for mTORC1 activation which requires sufficient energy for activation as well as leucine availability.

Monitoring of cellular energetics occurs upstream of mTORC1 via the serine/threonine kinase AMP-activated protein kinase (AMPK) complex (Xu, Ji and Yan,

2012). Increases in the cellular ADP/ATP ratio through mitochondrial respiration activate AMPK which negatively regulates mTORC1 through tuberous sclerosis complex (TSC) 1/2 heterodimer. AMPK phosphorylates TSC2, which increases the GTPase activity of TSC2 catalysing the hydrolysis of active GTP bound Rheb to inactive GDP form (Inoki, Corradetti and Guan, 2005). Consequently, mTORC1 may remain inactive after leucine activated localisation to the lysosomal surface if there is insufficient generation of ATP. Thus, the BCAT1 metabolic pathway may provide both the energetic and nutrient sensing requirements for mTORC1 activation through the generation of leucine and α -KG respectively. Taken together, these studies highlight a central role for BCAT1 in AML metabolism, where the generation of leucine and α -KG by BCAT1 feed into multiple cellular processes that impact on AML cell survival, stemness and biosynthesis.

1.3.4 The CXXC motif

An important aspect of the BCAT isoenzymes is the presence of a surface CXXC motif, that is two cysteine amino acids (C) separated by two other amino acids (X), located 10 angstroms from the active site. In BCAT2 the CXXC motif (C315-X-X-C318) functions as a redox sensitive molecular switch modulating the catalytic activity of the enzyme (Myra E. Conway, Poole and Hutson, 2004). Mechanistically this is achieved through oxidation of the thiol (-SH) groups of the CXXC motif cysteines. Examination of the crystal structure revealed the N-terminal C315 exists as a thiolate anion (Cys-S⁻) at physiological pH, exposure to ROS intermediate hydrogen peroxide (H₂O₂) can oxidize the thiolate anion to sulfenic form (Cys-SOH) which can react with another Cys-SH forming a disulphide (Cys-S-S-Cys) and H₂O (Figure 1.8). Disulphide bond formation

elicits a conformational change that inactivates the enzymatic capacity, this process can be reversed by the addition of antioxidant dithiothreitol (DTT) which restores the active form of the enzyme (Conway 2002). Site directed mutagenesis of the BCAT2 CXXC motif substituting the C-terminal cysteine to alanine (C318A) demonstrated the N-terminal C315 becomes irreversibly oxidised to a sulfonic acid when exposed to H₂O₂, resulting in complete loss of catalytic activity. Substitution of C315 to alanine (C315A) on BCAT2 largely retained its enzymatic capacity whilst the ability to be regulated by H₂O₂ was lost, revealing that that C315 acts as a redox sensor whilst C318 is the 'resolving' cysteine that forms a disulphide bond with C315, protecting it from irreversible oxidation. (Conway 2004).

Amino acid sequence alignment analysis between the BCAT1 and BCAT2 shows 58% sequence homology, where the CXXC motif is conserved between the two isoforms, however the biochemical properties vary between the two (Goto et al. 2005). The midpoint redox potential, that is the electron potential at which the ratio of oxidised/reduced thiols, is -225mV for BCAT2 CXXC motif and -310Mv for BCAT1. This demonstrates BCAT1 is more readily oxidised than BCAT2, otherwise stated it is a more powerful antioxidant i.e. more reducing in nature (Coles, Hancock and Conway, 2012). Whilst upon oxidation BCAT2 forms a disulphide bond that inactivates the protein, it has been demonstrated that the BCAT1 N-terminal cysteine (C335) is glutathionylated protecting its catalytic activity (Figure 1.8) (Conway *et al.*, 2008). Conway *et al* demonstrated that the amount of CXXC motif S-glutathionylation increased as the redox

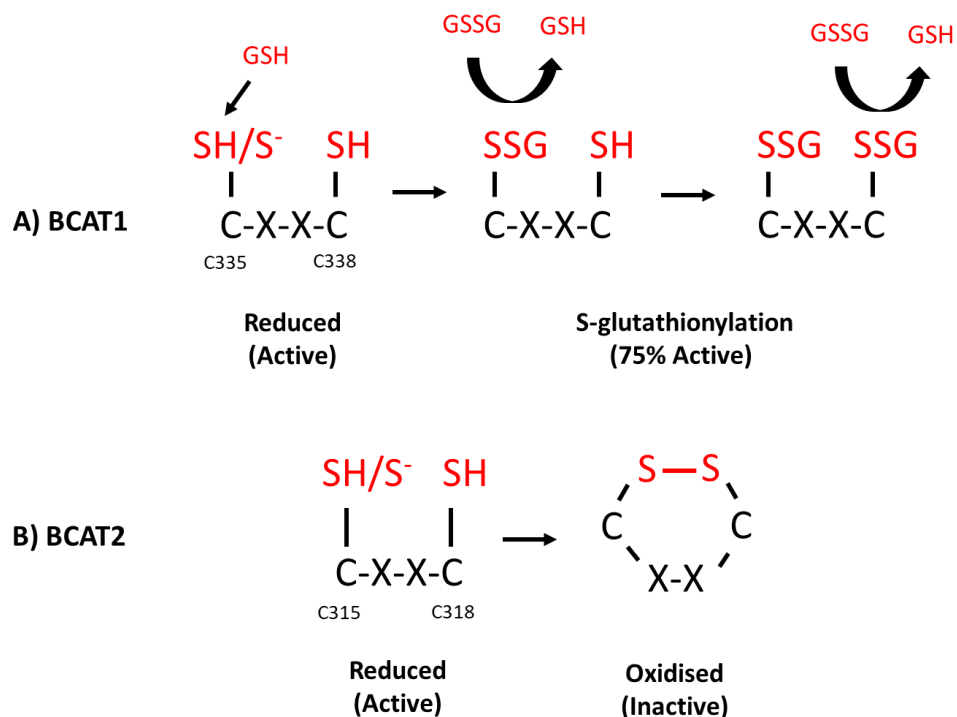


Figure 1.8 Redox activity of the BCAT1 and BCAT2 CXXC motifs. **A)** BCAT1 N-terminal Cys residue exists as a thiolate/thiol under reducing conditions cycling between the two using GSH as an electron donor. As the redox environment becomes more oxidised (2:1 GSH/GSSG ratio) the N-terminal cysteine becomes S-glutathionylated restoring GSH with a modest loss in enzymatic activity. Glutathionylation of the C-terminal cysteine occurs upon further oxidation (1:2.5 GSH/GSSG ratio) A similar reaction occurs upon H_2O_2 mediated oxidative stress perhaps through sulphenic or sulphinic acid intermediates. **B)** BCAT2 N-terminal cysteine residue is active at a redox potential of > -225 mV. Upon oxidation by mitochondrial free radicals it forms an inter subunit disulphide causing a conformational change which denatures the enzyme and inactivates it.

environment became more oxidised, which could be induced by the addition of H₂O₂. Importantly, this S-glutathionylation could be reversed by the GSH/glutaredoxin antioxidant couple, thus linking BCAT1 to a wider antioxidant network, a feature the BCAT2 isoform does not display.

In fact CXXC motifs, or at least the presence of a single surface cysteine, are a common feature of many anti-oxidant enzymes e.g. thioredoxin (Trx1) and peroxiredoxin (Prdx1), which utilise cysteine thiol groups as reducing agents to perform their oxidoreductase activities (E. S. Arnér and Holmgren, 2000; Rhee, 2016). This suggests that BCAT1 may function as a novel antioxidant given the highly reducing nature of the BCAT1 CXXC motif (Coles, Hancock and Conway, 2012). In support of this theory, the redox midpoint potential of BCAT1 (-260mV) is lower than Trx1 (-230mV) suggesting that BCAT1 is a more powerful antioxidant by comparison (Pohl, 2003) (Figure 1.9). However, BCAT1's role as an antioxidant is unknown.

Antioxidant proteins produce an equilibrium of reduced/ oxidised forms called a redox couple that buffer against cellular redox changes.(Fomenko and Gladyshev, 2003) Physiologically normative changes in cellular reduction potential are produced as a cell moves from a proliferative state through to differentiation. Although there is variation between cell types, in general proliferation occurs between a reduction potential of -260 to -210mV, differentiation -210 to -180mV and apoptosis -180 to -160 mV (F Q Schafer and Buettner, 2001). Interestingly, the AML cell line HL60 is in a proliferative state at -239 mV and apoptotic at -167mV a change of -72 mV (Figure 1.9) (F Q Schafer and Buettner, 2001). Therefore, it may be hypothesised that overexpression of antioxidant proteins may shift a cancer cell away from differentiation or cell death to a

more proliferative state. Indeed, leukaemia cells are known to upregulate antioxidant proteins in response to higher reactive oxygen species (ROS) production. For example, Trx1 is upregulated in relapsed AML patients and is correlated with higher ROS production and poorer patient prognosis (Chen et al 2010). Moreover, inhibition of Trx1 increases sensitivity to the pro-oxidant Arsenic Trioxide, suggesting Trx1 is protecting AML cells from ROS induced cell death. (Jiang et al 2014).

The relative contribution of the enzymatic and antioxidant activity of BCAT1 to the pathophysiology of AML has yet to be elucidated. The effect of BCAT1 expression on the metabolic and epigenetic mechanisms of oncogenesis remains the current research focus in the field. However, overproduction of ROS in AML is extremely well characterised and contributes to the pathogenesis of the disease. (Hole *et al.*, 2013; Testa *et al.*, 2016; Moloney *et al.*, 2017) Preliminary data demonstrates that BCAT1 can directly metabolise H₂O₂ *in vitro* (Unpublished Coles *et al*). Moreover, analysis of the redox potential BCAT1 CXXC motif suggests it has an antioxidant capacity that is comparable to major cellular antioxidant Trx1. Importantly BCAT1 CXXC motif S-glutathionylation demonstrates an ability to interact directly with the most abundant cellular redox couple reduced/oxidised glutathione (GSH/GSSG), suggesting BCAT1 could buffer these systems during periods of oxidative stress. This provides the rationale that overexpression of BCAT1 may be able to influence processes dysregulated in cancer including proliferation, differentiation and apoptosis by an antioxidant mechanism, namely the elimination of ROS and buffering the cellular antioxidant systems which are discussed in detail in section 1.4 below.

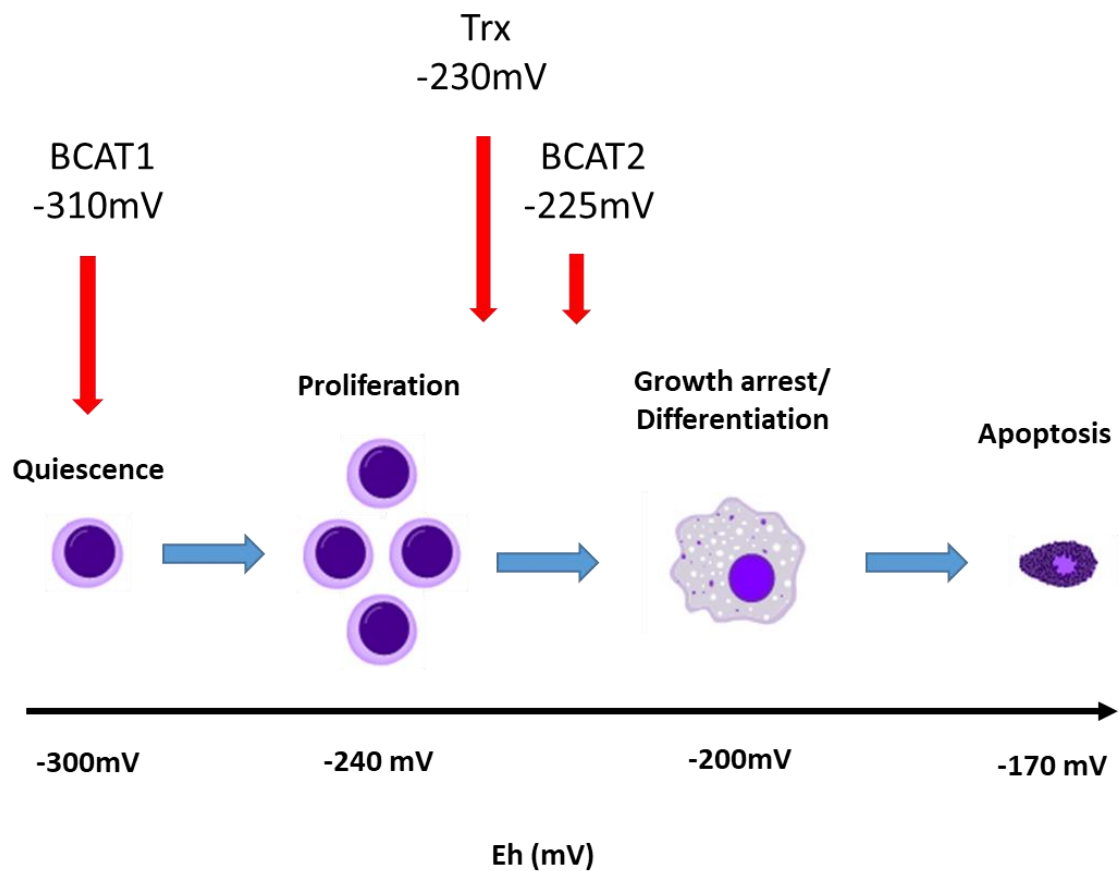


Figure 1.9 Redox control of cellular processes. Key cellular processes dysregulated in cancer including proliferation, differentiation and apoptosis are executed at different redox potentials. More negative/reductive environments favour quiescence and proliferation whilst a more positive/oxidative shift see cells arrest growth and differentiate, further oxidation may result in oxidative stress and apoptosis. Analysis of the CXXC motifs of BCAT1, BCAT2 and Thioredoxin reveal that BCAT1 is oxidised at a redox potential $\sim 80\text{-}85\text{mV}$ lower than either Trx or BCAT2. S-glutathionylation of the BCAT1 CXXC motif at a 'quiescent' redox potential ($-280\text{-} -310\text{mV}$) often associated with HSCs suggests it could buffer this environment maintaining leukemic stem cells.

1.4. ROS

1.4.1 Sources of ROS

Reactive Oxygen Species (ROS) are a number of chemically reactive species including the oxygen radicals such as the superoxide anion ($O_2^{\bullet-}$), the perhydroxyl radical ($^{\bullet}OOH$) the hydroxyl radical (OH^{\bullet}) and non-radicals oxidising agents such as hypochlorous acid (HOCl) and hydrogen peroxide (H_2O_2) that play an important role in cellular health and disease (Lushchak, 2014).

The majority of cellular ROS is generated endogenously by partial reduction of oxygen in the final stages of mitochondrial oxidative phosphorylation. Initially succinate and nicotinamide adenine dinucleotide + hydrogen (NADH) generated from the TCA are oxidised passing their electrons to a series of adjacent protein complexes embedded in the inner mitochondrial membrane space known as the electron transport chain (Murphy, 2009). The electrons are passed from one electron carrier to another from complex I to complex IV in a series of redox reactions that releases Gibbs free energy (ΔG) to power the transport of NADH derived H^+ ions from the mitochondrial matrix across the inner membrane to the intermembrane space. This creates an electrochemical proton gradient that is utilised by ATP synthase which acts as an ion channel allowing protons to re-enter the mitochondrial matrix catalysing the formation of ATP from ADP and Pi. In the final step electrons held by Cytochrome C are passed to molecular oxygen which functions as the final electron acceptor creating the superoxide anion $O_2^{\bullet-}$, which is reduced to H_2O_2 and finally H_2O by the action of superoxide dismutase. However, leakage of electrons from the electron transport chain (ETC) or an

insufficient pool of H^+ due to proton leakage leads to single electron reduction of O_2 and over-generation of $O_2^{\bullet-}$. (Brand et al 2011)

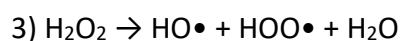
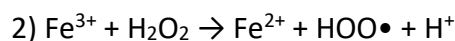
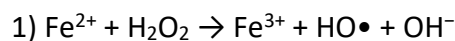
Another major source of cellular ROS comes from the nicotinamide adenine dinucleotide phosphate (NADPH) oxidase (NOX) family of proteins, which produce ROS not as a by-product as is the case with mitochondrial respiration, but as a primary function of the enzyme (Bedard and Krause, 2007). The NOX family of proteins, which consist of NOX1-5 as well as DUOX1/2, function as a membrane bound complexes that facilitate the import of electrons across the plasma membrane to molecular oxygen producing $O_2^{\bullet-}$. Although functionally similar, they vary significantly in their subcellular localisation, tissue distribution and physiological effects.

Perhaps the best understood remains NOX2, which was originally discovered as the source of neutrophilic respiratory bursts and has been extensively studied. It is from NOX2 that the model of NOX function is broadly derived (Panday *et al.*, 2015). NOX2 contains 2 transmembrane subunits gp91-phox (NOX2) and p22-phox, three cytosolic subunits (p47-phox, p67-phox, p40-phox), and the G-protein Rac. During NOX activation, stimuli induce Protein Kinase C (PKC) activation, which phosphorylates cytosolic p47/p67-phox dimer, eliciting a conformational change that exposes the p47-phox SH3 domain. This is followed by translocation of p47/p67-phox and p40-phox to the membrane, where the SH3 domains of p47-phox interacts with the proline rich region of p22-phox, whereupon Rac translocates to the complex to activate NOX2. NOX2 itself contains 6 transmembrane domains which contain 4 highly conserved heme binding histadines and a $-COOH$ terminal cytosolic domain which contains FAD and NADPH binding domains. Electrons derived from NADPH are transferred to FAD then to

the transmembrane heme and finally to oxygen in the luminal or extracellular space generating superoxide (Brandes, Weissmann and Schröder, 2014).

The significance of p47-phox and p22-phox interaction has been demonstrated clinically in a patient with Chronic granulomatous disease (CGD), an immune disorder characterised by the inability of phagocytes to generate superoxide through NOX resulting in the eponymous granulomas, a collection of macrophages that are unable to eliminate the infection. A single proline to glutamine substitution at residue 156 in the proline region of p22-phox results in impaired p47-phox translocation in cells stimulated with PMA which activates PKC (Leussen *et al.* 1994).

Whether it is generated through mitochondrial respiration or NOX, the superoxide anion ($O_2^{\bullet-}$) is highly reactive and if left unchecked can cause damage to DNA, lipids and proteins. Therefore it is normally rapidly eliminated by enzymatic dismutation to H_2O_2 via cytosolic superoxide dismutase (SOD1) (rate constant = $2 \times 10^9 M^{-1}s^{-1}$) (Fridovich, 1983). However, at this stage yet more ROS can be formed from H_2O_2 which can be broken down into the highly reactive hydroxyl (OH^{\bullet}) and perhydroxyl ($^{\bullet}OOH$) radicals via the iron catalysed Haber–Weiss and Fenton reactions or photolysis by UV light (Winterbourn, 1995):



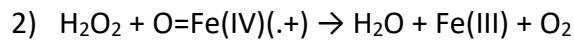
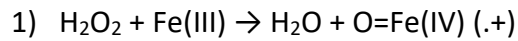
Finally, $O_2^{\bullet-}$ may interact with nitric oxide (NO^{\bullet}) leading to formation of a distinct family of pro-oxidant molecules collectively known as reactive nitrogen species (RNS), the primary species being peroxynitrite (ONO_2^{-}) (Martínez and Andriantsitohaina, 2009).

Like $O_2^{\bullet-}$ the majority these ROS and RNS radicals are short-lived before being neutralised by a network of enzymatic and non-enzymatic antioxidant defences which maintain redox homeostasis(Baran *et al.*, 2004).

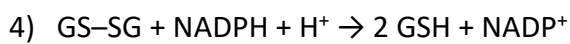
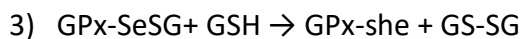
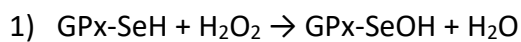
1.4.2 Antioxidant networks

Cellular defences against ROS are orchestrated by a network of antioxidant enzymes that actively remove ROS including, Catalase and Glutathione peroxidase (GPx) and Peroxiredoxins (Prx), as well a oxidoreductases such as Thioredoxin (TRx) and Glutaredoxin (Grx), and low molecular weight thiols, such as Glutathione (GSH). Collectively, these act as redox couples that eliminate ROS through a series of reduction-oxidation (Redox) reactions (Figure 1.10) (Li *et al.*, 2000; Forman, Zhang and Rinna, 2009; Marengo *et al.*, 2016). In this system, H_2O_2 generated from the dismutation of mitochondrial or NOX derived $O_2^{\bullet-}$ is metabolised by peroxidase enzymes which include Catalase, GPx and Prxs. Whilst functionally analogous mechanistically, Catalase is able to achieve reduction of H_2O_2 , independently whilst GPx and Prx require GSH and Trx respectively to act as electron donors and regenerate the enzymes to their reduced active form via oxidoreductase activity (Hanschmann *et al.*, 2013).

Catalase contains four identical subunits of 62 kDa, each subunit containing a prosthetic heme group, which is central to its enzymatic function. Reduction of H_2O_2 is a two-step process, initial oxidation of the iron containing heme complex by H_2O_2 leads to formation of an oxyferryl porphyrin cation radical represented in step one of the schematics as $O=Fe(IV)$. A second H_2O_2 then reacts with $O=Fe(IV)$ to reform $Fe(III)$ creating water and oxygen(Alfonso-Prieto *et al.*, 2009):



Like Catalase, GPx structure is tetrameric, however the catalytic redox mechanism relies on cysteine analogue selenocysteine that substitutes the thiol group (R-SH) with a selenium-containing selenol group (GPx-SeH) rather than iron-complexed haem (Battin and Brumaghim, 2009). In the first step, oxidation of the selenol group with H_2O_2 yields selenic acid (GPx-SeOH) and H_2O . Selenic acid reacts with GSH to form GPx-SeSG and an additional H_2O before finally GPx is reduced back to GPx-SeH by GSH forming Glutathione disulfide (GSSG):



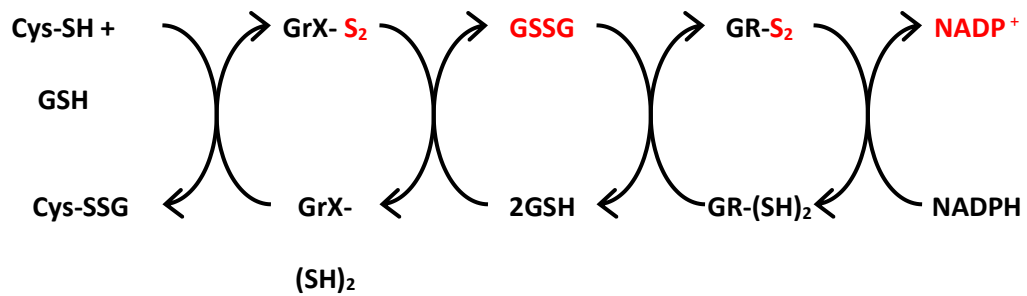
GSSG is regenerated to GSH by glutathione reductase using NADPH as a reducing equivalent creating NADP^+ , which in turn is restored by various oxidoreductase reactions of the TCA and pentose phosphate pathway (Jin and Zhou, 2019).

Peroxiredoxin utilises the cyclical oxidation-reduction of cysteine thiols in a manner mechanistically analogous to the BCAT1 CXXC motif, however the catalytic cysteine residues of Prx are located on different peptide chains forming inter-subunit disulphide bonds, this is in contrast to the contiguous arrangement of the CXXC motif which forms an intra-subunit bond. Typical 2-Cys Prx's including Prx1-4, contain a highly conserved redox active N-terminal peroxidatic cysteine (C_P) and a semi conserved resolving cysteine (C_R) the location of which varies amongst the Prx family (Rhee, 2016). During catalysis C_P is oxidised to a sulphenic acid (Prx-S-OH) intermediate by the

peroxide substrate releasing H₂O. The hydroxyl group of the sulphenic acid is liberated by the formation of the inter-subunit disulphide bond between the peroxidatic cysteine and the resolving cysteine releasing a second H₂O molecule (Woo *et al.*, 2010). Oxidised Prx disulphide bonds are reduced back to cysteine thiols by Trx, a 12kDa oxidoreductase that facilitates the reduction of oxidised proteins (E. S. J. Arnér and Holmgren, 2000).

Thioredoxin is characterised by a tertiary structural motif, the thioredoxin fold which consists of three α -helices surrounding a central core of a four-stranded β -sheet and a highly conserved CXXC motif active site. Like BCAT1, the CXXC motif consists of two vicinal cysteine residues separated by two variable amino acids, the N-terminal cysteine thiol has a low pK_a value and is deprotonated at physiological pH forming the thiolate anion (R-S⁻) (Arnér and Holmgren, 2000). Thiolate nucleophilic attack of a disulphide bond on another protein (substrate) results in Thx-substrate mixed disulphide linkage, that is resolved by the C-terminal cysteine thiol that breaks the mixed disulphide, yielding the reduced protein substrate and an oxidized Trx. Reduced Trx is regenerated by thioredoxin reductase (TrxR), which like glutathione reductase utilises NADPH as an electron source (E. S. Arnér and Holmgren, 2000).

A)



B)

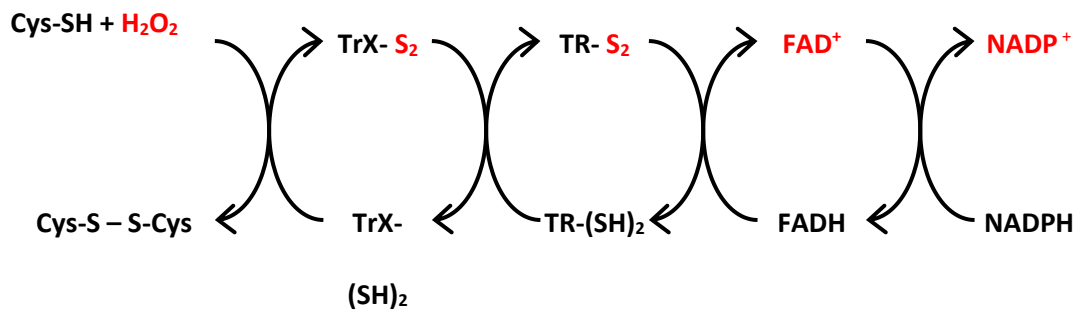


Figure 1.10 The glutaredoxin and thioredoxin redox cycle. Cysteine S-glutathionylation as seen in BCAT1 is removed by reduced GrX which is regenerated by GSH or NADPH, ultimately the electron source is NADPH regenerated by the pentose phosphate pathway (Panel A). H₂O₂ induced cysteine disulphide bond formation is reversed by Trx causing the CXXC motif of TrX to form an intramolecular disulphide bond. This is reduced again by the action of TrxR utilising reducing equivalents from a TrxR FADH domain and NADH (Panel B) (Adapted from Coles 2008)

1.5 Oxidative Stress in cancer

1.5.1 Genomic integrity

Excessive ROS production through endogenous or exogenous mechanisms or a decrease in cellular antioxidant defences, can cause cells to enter a state of biochemical imbalance known as oxidative stress. Unchecked ROS can cause oxidative damage DNA, lipids and proteins and alter redox signalling cascades (Ray, Huang and Tsuji, 2012).

Genomic insults to oncogenes or tumour suppressors mediated by ROS, can lead to malignant transformation, for example hydroxyl radicals cause double-strand breaks or oxidative base pair damage, that results in a range of derivatives (Cadet and Richard Wagner, 2013). Due to a high reduction potential, guanine is most frequently attacked by ROS, commonly resulting in the 8-oxo-7,8-dihydro-2'-deoxyguanosine (8-oxodG) DNA lesion (Radak and Boldogh, 2010). This represents approximately 1 in 20 of all DNA lesions and left unrepaired results in mutagenic mismatched pairing with adenine and the G:C to T:A transversion event. Base excision repair initiated by DNA glycosylase enzymes that cleave the N-glycosidic bond connecting nucleobases to the sugar phosphate backbone, results in the excision of 8-oxodG. Due to oxidised bases acting as poor substrates for enzymes involved in DNA synthesis, 8-oxodG is conveniently excreted in urine and therefore has frequently been used as a biomarker to assess oxidative DNA damage (Loft and Poulsen, 1996; Roszkowski *et al.*, 2011). Based on this method alone, even under steady state or normal physiological ROS production, DNA is oxidatively damaged at a rate of 10^5 residues per cell per day in rats and 10^4 in humans, perhaps reflecting the lower basal metabolic rate of human cells (Loft and Poulsen, 1998). Urinary excretion and leukocyte DNA levels of 8-oxodG were reported to increase

up to 50% in response to smoking tobacco, a source of exogenous ROS (Loft and Poulsen, 1998). Furthermore, similar increases in 8-oxodG have been observed in cancer patients exhibiting various malignant tumours compared to healthy individuals, underlining the role ROS plays in carcinogenesis (Loft and Poulsen, 1996; Roszkowski *et al.*, 2011). In healthy cells DNA damage initiates the ATM-p53 DNA damage response pathway, where in the cell cycle is arrested and the damage is either repaired or the damaged cell is eliminated through induction of apoptosis. Archetypal DNA damage response protein TP53 is mutated in approximately half of human cancers making it the most frequently mutated cancer gene further underlining the importance of maintaining genomic integrity (Reinhardt and Schumacher, 2012).

1.5.2 Redox signalling

As well as driving genomic mutation, defective control of ROS homeostasis can alter redox sensitive signalling cascades that impact cellular proliferation, differentiation and apoptosis (Ray, Huang and Tsuji, 2012). As with the BCAT CXXC motif, redox signalling is mediated, in part, by cysteine thiols that can undergo reversible H_2O_2 oxidation altering the activity of redox sensitive proteins. This oxidation may result in several oxidised thiol derivatives, including sulphenic acids (-SOH), which can undergo further oxidation to sulphinic (Cys- SO_2) and finally sulphonic acids (Cys- SO_3) (Miki and Funato, 2012). Sulphenic acids can be reduced by disulphide reductases, such as Trx and glutaredoxin (Grx), restoring protein function. In this way ROS can act as a secondary messenger relaying the redox status of the cell and modulating a cellular response (Figure 1.11) (Hanschmann *et al.*, 2013). However, sulphinic and sulphonic acid oxidation

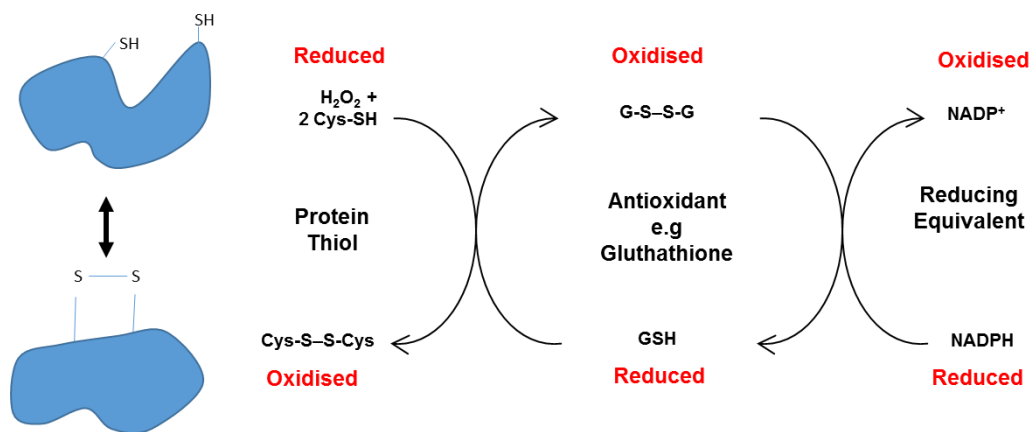


Figure 1.11 Protein thiol oxidation/ reduction reaction inducing conformational change and homeostatic regeneration via glutathione/ NADPH redox couple.

Protein thiols are oxidised to form intramolecular disulphide bridges that form part of the secondary structure of the protein. Formation or dissolution of disulphide bridges induce a conformational change that acts as a molecular nano switch modulating enzymatic activity. Proteins can regenerate by antioxidants such as glutathione which in turn are regenerated by NADPH/ NADP⁺. Adapted from (Dröge, 2002)

is largely irreversible and a manifestation of oxidative stress that can result in impaired redox signalling.

For example, receptor tyrosine kinases (RTK) such as epidermal growth factor (EGF) and platelet derived growth factor (PDGF), result in the activation of signal transduction pathways PI3-K-AKT. The activity of these RTKS are negatively regulated by protein-tyrosine phosphatases (PTP) such as PTEN, a gene frequently mutated in human cancer, which dephosphorylates PI3-K (Morotti *et al.*, 2015). PTPs are redox active and can be deactivated by ROS through the oxidation of cysteine residues to sulphenic acid intermediates, resulting in the activation of the PI3-K-AKT (Figure 1.12) (Leslie *et al.*, 2003). In fact, EGF and PDGF stimulation results in a transient oxidative burst generated from NOX proteins that are required for growth factor induced RTK phosphorylation. NOX derived H₂O₂ mediated oxidation and subsequent disulphide bond formation of between Cys¹²¹ and Cys⁷¹ inactivates PTEN, whilst reduction by Trx restores PTEN activity (Schieber and Chandel, 2014). Given NOX derived oxidative bursts could cause cellular damage or alter thiol signalling away from the site of generation, the cell exerts localised control via membrane associated antioxidant Prdx1. Prdx1 is inactivated upon growth factor stimulation causing localised accumulation of H₂O₂ and inhibition of PTP activity (Woo *et al.*, 2010).

High ROS levels are also a feature of AML, which displays defective control over RTK- NOX-PTP signalling (Sillar *et al.*, 2019). A greater than 10-fold increase in NOX derived ROS was reported in more than 60% of AML blasts causing increased proliferation (Hole *et al.*, 2013). A common ROS producing defect seen in ~30% of AML patients and associated with the poor prognosis is autophosphorylation of the FMS-like

Tyrosine Kinase (FLT3) receptor through the Internal Tandem Duplication (ITD) of the transmembrane domain, which increases ROS production via activation of AKT and stabilization of p22^{phox}, a regulatory subunit for NOX1-4 (Gilliland and Griffin, 2002b). Furthermore FLT3-ITD enhances NOX4 expression and ROS cysteine thiol inactivation of the PTP DEP-1, where inactivation of NOX4 restores DEP-1 attenuating cell transformation by FLT3-ITD in *in vitro* and *in vivo* models (Jayavelu *et al.*, 2016). Furthermore, Prdx1 expression suppresses FLT3-ITD signalling by restoring PTP activity and increasing survival in cell culture and mouse models (Godfrey *et al.*, 2012). Taken together, these studies demonstrate the importance of redox regulation in RTK–NOX–PTP signalling events in AML.

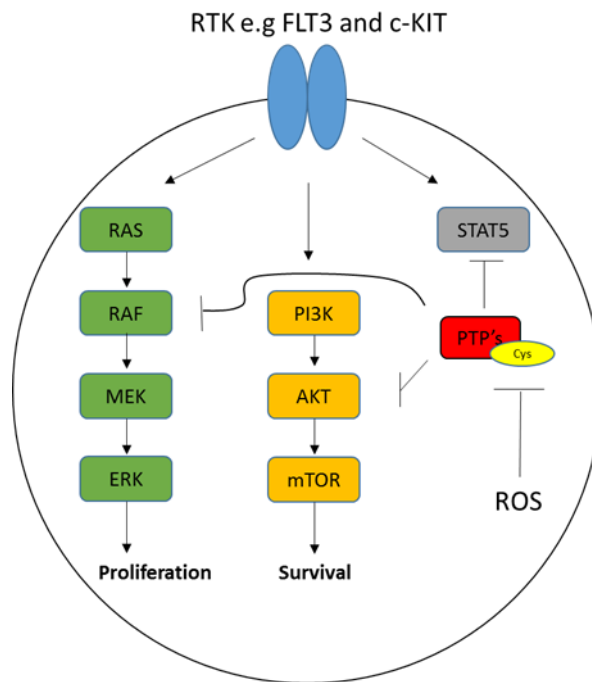


Figure 1.12 Receptor Tyrosine Kinase (RTK) signalling e.g. c-KIT and FLT3 Clinically distinct mutations in FLT3 and c-KIT RTK result in autonomous activation of growth and survival signalling cascades PI3K-AKT-mTOR, RAS-RAF-MEK-ERK and JAK-STAT. PTPs negatively regulate these signalling cascades. PTPs in turn are negatively regulated by ROS. Adapted from (Cauchy *et al.*, 2015)

1.5.3 Nrf2 antioxidant response

Due to high ROS levels, cancer cells are susceptible to oxidative stress induced cell death. In order to maintain a sublethal redox environment, high ROS production in cancer cells is matched by an equally high antioxidant activity, thus protecting the cancer cell from ROS-induced apoptosis (Gorrini, Harris and Mak, 2013). Antioxidant production is controlled through the activation of the redox sensitive transcription factor; nuclear factor erythroid 2-related factor 2 (NRF2), which activates the transcription of over 100 cytoprotective and antioxidant genes (Sporn and Liby, 2012). Under low ROS conditions cytoplasmic Nrf2 interacts with Kelch-like ECH-associated protein 1 (KEAP1), whereby ubiquitination of the Nrf2-KEAP1 complex leads to proteasomal degradation (Tonelli, Chio and Tuveson, 2018). Under oxidative stress, KEAP1 undergoes cysteine thiol oxidation and dissociation from Nrf2 which translocates to the nucleus. Nuclear relocated Nrf2 heterodimerizes with small musculoaponeurotic fibrosarcoma proteins binding antioxidant-response elements (AREs) located upstream of multiple antioxidant genes, initiating transcription of targets including the GSH and Trx antioxidant systems, as well NADPH regeneration and haem/iron metabolism (Tonelli, Chio and Tuveson, 2018). The Nrf2 pathway is negatively regulated by the transcriptional repressor Bach1, which competes with Nrf2 to bind the ARE enhancers following ROS induced nuclear relocalisation. Antioxidants are reported to delay nuclear accumulation of Bach1, reflecting its opposing role to Nrf2 in redox regulation (Dhakshinamoorthy *et al.*, 2005).

Nrf2 regulates GSH levels by controlling expression of glutamate-cysteine ligase (GCL), which catalyses the reaction of glutamate and cysteine, the rate-limiting step in the synthesis of GSH (Tonelli, Chio and Tuveson, 2018). In addition, Nrf2 upregulates

antioxidant enzymes such as Glutathione peroxidase 2 (Gpx2), Sulfiredoxin and Trx, as well as Thioredoxin reductase (TrxR) and NADPH reducing equivalents through increased transcription of key enzymes in NADPH generation including glucose-6-phosphate dehydrogenase (G6PD) and IDH1 (Singh *et al.*, 2006; Zhou *et al.*, 2015; Tonelli, Chio and Tuveson, 2018). As well as upregulating the antioxidant network, Nrf2 upregulates haem oxygenase, which catalyses the breakdown of heme molecules thus preventing the formation of haem derived Fe²⁺ which could participate in Fenton based production of hydroxyl radicals (Surh *et al.*, 2009). Furthermore, Nrf2 induces expression of the Ferritin light and heavy polypeptides of the 24 subunit ferritin complex that oxidises and sequesters Fe²⁺, making it unavailable for the Fenton chemistry (Pietsch *et al.*, 2003).

Induction of such a wide battery of cellular defences has led to the observation that the contribution of Nrf2 to carcinogenicity is context dependant, providing protection from transformative ROS insult in healthy cells, whilst preventing apoptosis in malignant cells. In AML, Nrf2 expression provides chemo-resistance to Ara-C and arsenic trioxide (ATO), where targeting Nrf2 with the inhibitor Brusatol, increased sensitivity to these agents, demonstrating the antioxidant network as an attractive therapeutic target (Olayanju *et al.*, 2015; Karathedath *et al.*, 2017). Disruption of downstream targets of Nrf2 has also proven effective, where inhibition of Trx leads to enhanced apoptosis and sensitivity to pro-oxidant treatment ATO in AML (Tan *et al.*, 2014). Thus, a similar strategy may be effective targeting the proposed antioxidant action of BCAT1.

1.6 Hypothesis

This study has been carried out to explore the antioxidant role of the BCAT1 CXXC motif in the development and treatment of AML. The rationale for this stems from the fact cysteine thiol redox reactions are part of the mechanism through which cellular antioxidant defences eliminate excessive ROS and prevent oxidative stress. Oxidative stress and upregulation of antioxidant proteins such as Thioredoxin (Trx), which contains a redox active CXXC motif, is a feature of AML. This has been speculated to contribute to malignant cell pathology by the dysregulation of redox controlled processes including differentiation and apoptosis. Previous studies have demonstrated the BCAT1 CXXC motif has a more negative reduction midpoint potential than the Trx CXXC motif suggesting it is a more powerful antioxidant. Moreover, overexpression of BCAT1 is associated with poorer prognosis, suggesting it is contributing to malignant processes in AML. To explore this possibility, here the CXXC motif has been mutated substituting the cysteine residues for serine, abolishing the putative cysteine thiol antioxidant activity. Overexpression of BCAT1 *wild-type* and CXXC motif mutant protein in immortalised monocytic AML cell line U937 will allow the effect of the effect of the CXXC motif to be elucidated with respect to ROS and the development and treatment of AML.

Project Aims

The principal aim of this project is to investigate the antioxidant role of the BCAT1 CXXC motif in the development and treatment of AML. To fulfil this aim, the specific objectives are as follows:

1. Site directed mutagenesis of the BCAT1 CXXC motif substituting amino acid cysteine (C) to serine (S) creating three constructs in pCMV6-Entry vector:
 - a. BCAT1(WT) → CXXC
 - b. BCAT1(C338S) → CXXC to CXXS
 - c. BCAT1(C335/8S) → CXXC to SXXS

This objective should abolish the potential antioxidant effect of the CXXC motif whilst retaining BCAT1 metabolic activity allowing the antioxidant capacity of the BCAT1 CXXC motif can be directly evaluated.

2. Lentiviral transduction and overexpression of BCAT1(WT) and CXXC motif mutants in U937 cells (ATCC CRL 1293.2)
3. Investigate the antioxidant effect of CXXC motif on redox environment of the cell and how this affects redox mediated processes in the development of AML including proliferation, apoptosis and differentiation in U937.
4. Investigate the effect of BCAT1 CXXC motif in the treatment of AML. Evaluation of transgenic cell lines will be carried out *in vitro* with respect to proliferation

and viability following incubation with standard chemotherapeutic compounds
and BCAT1 targeted metabolic and pro-oxidant therapies

Chapter 2: Materials and Methods

2.1. *Antibodies*

ECA39 (BCAT1) primary antibody (Santa Cruz SC-517185) and Rabbit anti-goat IgG-HRP secondary (Santa Cruz SC-2768) were obtained from Santacruz Biotechnology (Dallas, TX, USA). Anti-DDK (FLAG) monoclonal antibody was obtained from Origene (Clone OTI4C5). Recombinant Anti-Cyclophilin B HRP loading control (ab205875) was obtained from Abcam (Cambridge, UK).

2.2. *Cell Lines*

U937 human histiocytic lymphoma cell lines (ATCC® CRL-1593.2™) and HEK293T (ATCC® CRL-3216™) were obtained from Public Health England (Salisbury, UK.). *E. coli* BL21(DE3) and α -Select Gold Efficiency chemically competent cells were obtained from BioLine (London, UK.).

2.3. *Plasmids and Constructs*

Lyophilised pCMV6-Entry vector (catalog no. RC229972) containing human cDNA clone *BCAT1*, cytosolic transcript variant 5 (NM_01178094) and pLenti-C-Myc-DDK-IRES-Puro vector (catalog no. PS100069) were obtained from Origene (Rockville, Maryland, USA). pET-28a (catalog no. 69864) expression plasmid was obtained from Novogen (Cambridge, UK).

2.4 Primers

All primers used in this project were manufactured and supplied by Eurofins Scientific (Ebersberg, Germany).

BCAT1_424 5'-GCA GCT AGC ATG GAT TGC AGT AAC GGA-3'

BCAT1_1582 5'-GCA GCT GTC GAC TGA TCA GGA TAG CAC AAT TGT C-3'

C335 F 5'-GGC TCT GGT ACA GCC TCT GTT TGC CCA-3

C335 R 5'- TGG GCA AAC AGA GGC TGT ACC AGA GCC-3

C338 F 5'-GGT ACA GCC TGT GTT AGC CCA GTT TCT GAT ATA CTG-3'

C338 R 5'-CAG TAT ATC AGA AAC TGG GCT AAC ACA GGC TGT ACC-3'

C335/8 F 5'-GGT ACA GCC TCT GTT AGC CCA GTT TCT-3'

C335/8 R 5'- AGA AAC TGG GCT AAC AGA GGC TGT ACC- 3'

T7 F 5'- TAA TAC GAC TCA CTA TAG GG-3'

T7 R 5'- GCT AGT TAT TGC TCA GCG -3'

V2 5'- AGA GCT CGT TTA GTG AA-3'

LR-50 5'- CAG AGG TTG ATT ATC GAT AAG 3-3'

VP1.5 5'- GGA CTT TCC AAA ATG TCG-3'

XL-39 5' ATT AGG ACA AGG CTG GTG GG 3'

BCAT1-F 5'- TGG AGA ATG GTC CTA AGC TG -3'

BCAT1-R 5'- GCA CAA TTG TCC AGT CGC TC -3'

β2M-F 5'- ATG AGT ATG CCT GCC GTG TGA -3'

β2M-R 5'- GGC ATC TTC AAA CCT CCA TG-3'

2.5 Transformation of *E.coli* with pCMV6-BCAT1

pCMV6-BCAT1 and CXXC mutant constructs were transformed into α-Select Gold Efficiency chemically competent cells (Bioline BIO-85027) according to the manufacturer's instructions. Briefly, 25 μL of competent cells were mixed with 3-5 μL of construct DNA and incubated on ice for 30 min. The mixture was heat shocked at 42 °C for 40 sec using a block heater and returned to ice for 2 min. The transformation mixture was diluted by addition of 500 μL Luria-Bertani (LB) broth (1% tryptone, 0.5% yeast extract, 1% NaCl) and incubated on an orbital shaking platform at 50 rpm for 1 h at 37 °C followed by inoculation onto LB agar supplemented with 50 μg/mL kanamycin. Plate cultures were incubated overnight at 37 °C.

Single colonies were added to 10 mL LB broth supplemented with 50 μg/mL kanamycin and incubated overnight at 37 °C in an orbital shaker at 50 rpm. Cells were harvested by centrifugation at 4000 x *g* using a VWR MegaStar 1.6R centrifuge and plasmids were purified from cell pellets the Isolate II plasmid mini-prep kit (Bioline BIO-52056) according to instructions. Briefly cells were resuspended in 500 μL of resuspension buffer P1, following addition of 500 μL lysis buffer P2 the suspension was mixed by inversion and incubated at room temperature for 5 min. The lysis reaction was stopped by addition of 600 μL of neutralisation buffer P3 and lysate centrifuged at 11 000 x *g* for 5 min. Following centrifugation, the supernatant was removed, added to Isolate II plasmid mini spin column and bound by centrifugation as previously described

for 1 min. The column was washed by addition of 500 μ L of wash buffer P1 and centrifuged for 1 min. Following addition of 600 μ L of wash buffer P2 and centrifugation for 1 min the column was dried by centrifugation for 2 min and plasmids were eluted by addition of 50 μ L of elution buffer and centrifugation for 1 min as previously described. Concentration and purity of plasmid vector was determined by measuring absorbance at λ 260/280 nm using a Nanodrop 2000c spectrophotometer (Thermo-Fisher).

2.6 Site-directed Mutagenesis of the CXXC Motif

Mutagenesis of *BCAT1* CXXC motif cysteine residues C335 and C338 to serine was implemented in pCMV6-*BCAT1* vector using the Quikchange II Site-directed Mutagenesis Kit (Agilent technologies, catalog no. 200523) in accordance with the manufacturer's instructions. Three mutant constructs were generated as follows - pCMV6- *BCAT1*(C335S), pCMV6- *BCAT1*(C338S) and pCMV6- *BCAT1*(C335/8S) using the C335S, C338S and C335/8S primer pairs listed in section 2.4 and the following cycling parameters: Initial denaturation 95 °C for 2 min. 95 °C for 20 sec, 60 °C for 10 sec, 68 °C for 3 min 10 sec for 18 cycles. Final extension 68 °C for 5 min using a PCR thermocycler (Prime Techne). CXXC mutant constructs were transformed into competent *E.coli* α -Select Gold (Bioline BIO-85027) and purified as previously described in section 2.5. For long-term storage cultures containing all vectors were kept at -80 °C in 30% glycerol.

Mutation of *BCAT1* was confirmed by DNA sequence analysis. The chain termination reaction was carried out using the Big Dye Terminator V3.1 cycle sequencing kit (ThermoFisher 4337457) as per manufacturer's instructions using the VP1.5 and FTAG primer set and the following cycling parameters: Initial denaturation 95 °C for 5

min. 96 °C for 10 sec, 50 °C for 10 sec, 60 °C for 4 min for 25 cycles. Final extension 72 °C for 5 min. Capillary electrophoresis was performed by the Functional Genomics Facility at The University of Birmingham using an Applied Biosystems ABI 3730 sequencer. Sequence fidelity was analysed using Chromas Lite 2.0 software, NCBI's nucleotide BLAST and M-coffee alignment tools.

2.7 Subcloning pLenti-BCAT1 Vector

Wild-type (WT) *BCAT1* and CXXC mutants were subcloned from pCMV6-*BCAT1* to pLenti-C-Myc-DDK-IRES-Puro vector using Origene's precision shuttle system. Briefly, 5 µg of pCMV6-*BCAT1* and pLenti plasmids were each digested with 2 µL AsiSI (NEB R0630) and Mlul (NEB R0198) restriction endonucleases in 5 µL 10x NEBuffer 2.1 (NEB B7002S) made up to 50 µL with nuclease free water and incubated at 37 °C for 4-6 h. Following digestion, linearized *BCAT1*(WT), CXXC mutant cDNA and pLenti vector were separated by gel electrophoresis in a 1.2% agarose gel at 100 V for 1 h. Agarose gels were stained with GelRed (Biotium 41003) nucleic acid stain prior to visualisation on a UVP Model M-20 transilluminator (Sigma-Aldrich). Linearized pLenti and *BCAT1* cDNA fragments were identified as 7.6 kb and 1.1 kb fragments predicted *in silico* by the Serial Cloner software tool (http://serialbasics.free.fr/Serial_Cloner.html) . Following excision, fragments were gel purified using the Isolate II PCR and Gel kit (Bioline BIO-52059) according to the manufacturer's instructions. Briefly, 50 ng of pLenti vector was ligated at a 3:1 insert to vector molar ratio with 1 µL T4 DNA ligase (NEB M202) and 2 µL of x10 T4 DNA ligase buffer made up to a total volume 20 µL with nuclease free water and incubated overnight at 16 °C. The reaction was stopped by denaturation at 65 °C for 10

min and α -Select competent cells were transformed with the ligation mixture as previously described (section 2.5), followed by inoculation onto LB agar supplemented with 35 $\mu\text{g}/\text{mL}$ chloramphenicol and incubated overnight at 37°C. *BCAT1* positive colonies were discriminated from colonies containing uncut or re-circularised p-Lenti by Colony PCR (section 2.8) using the V2 and FTAG primers (section 2.4).

pLenti-*BCAT1* positive colonies were inoculated in 5mL LB broth supplemented with 34 $\mu\text{g}/\text{mL}$ chloramphenicol and incubated over night at 37 °C in an orbital shaker at 50 rpm. Plasmids were purified using the Isolate II plasmid mini-prep kit (Bioline BIO-52056), concentration and were purity determined by spectrophotometric analysis as previously described (section 2.5). pLenti-*BCAT1* sequence fidelity was confirmed by DNA sequence analysis as previously described using the V2 and FTAG sequencing primers.

2.8 Colony PCR

Single colonies were inoculated on to a new LB agar plate prior to suspension in 50 μL of dH_2O and heating to 95 °C for 15 min. 12.5 μL of boiled cell suspension was added to a PCR reaction mixture containing 12.5 μL of ReddyMix (Thermofisher AB-0575) with V2/LR50 primers for pCMV6 vector, VP1.5/XL39 for pLenti vector and *BCAT1_424/BCAT1_1582* for pET28a vector at a final concentration of 0.4 μM . The PCR mixture was amplified using the following cycling parameters: 95 °C for 30 sec, 50 °C for 30 sec and 70 °C for 1 min 40 sec for 25 cycles. PCR product was separated by gel electrophoresis on a 1.2% agarose gel. Images were captured using a gel doc transilluminator (SynGene).

2.9 Subcloning pET28a-BCAT1

NheI and Sall restriction sites flanking *BCAT1* cDNA in pCMV6 were introduced via PCR using the *BCAT1_424* and *BCAT1_1582* primer pair (section 2.4). 50 ng of pCMV6-*BCAT1* template DNA was incubated with 0.2 μ L Phusion DNA Polymerase (NEB M0530), 4 μ L 5X Phusion HF, 0.4 μ L 10mM dNTPs, 1 μ L 10 μ M *BCAT1_424* and 1 μ L 10 μ M *BCAT1_1582* (Final primer concentration 0.5 μ M) and made up to a final reaction volume of 20 μ L with nuclease free H₂O. The PCR reaction was performed using the following cycling parameters: 95 °C for 30 sec, 68.5 °C for 30 sec, 70 °C for 1 min 15 sec for 25 cycles. 5 μ g of PCR product and pET28a were digested with 2 μ L of NheI-HF (NEB R3131S) and Sall-HF (NEB R3138S) restriction endonucleases in 5 μ L x10 CutSmart buffer (NEB B7204S). The total reaction volume was made up to 50 μ L and incubated for 4-6 h at 37 °C. The digestion reaction was stopped by denaturing at 80 °C for 10 min. Linearised pET28a vector and *BCAT1* cDNA amplicons were separated by gel electrophoresis, gel purified, ligated and transformed into BL21(DE3) competent cells (Bioline C2527H) as previously described in section 2.5. Transformed cells were selected on LB Agar plates supplemented with 50 μ g/mL kanamycin and screened for the *BCAT1* insert via Colony PCR as described in section 2.8 using the *BCAT_424* and *BCAT1_1582* primer pair.

BCAT1 positive transformants were inoculated in 10mL LB broth supplemented with 50 μ g/mL kanamycin and incubated at 37 °C overnight with shaking. Cell suspensions were pelleted by centrifugation at 4000 x *g* and pET28-*BCAT1* plasmids were purified using the Isolate II plasmid miniprep kit (Bioline BIO-52056). Concentration and purity of plasmid was determined by spectrophotometric analysis as previously described (section 2.5). Full reading frame fidelity of the *BCAT1* insert was

confirmed by DNA sequence analysis as previously described (section 2.6) using the T7F and T7R primers (section 2.4).

2.10 *Recombinant BCAT1 Protein Overexpression*

Overexpression and purification of BCAT1 proteins are described in Davoodi *et al*, 1998 whose method was adopted here. Briefly, transformed *E. coli* BL21(DE3) cells from broth culture stores were inoculated into 100 mL of sterile LB broth adjusted to contain 50 µg/mL kanamycin and incubated overnight on orbital shaking platform at 37 °C and 50 rpm. This was transferred to 1L LB broth adjusted to contain 50 µg/mL kanamycin and incubated overnight at 30 °C at 50 rpm. The overexpression of BCAT1 protein was induced using 1 mM Isopropyl β-D-1-thiogalactopyranoside (IPTG) to an optical density of approximately 0.8 measured at λ600 nm with a spectrophotometer (libra S12, Biochrom, Cambridge. UK) and incubated at 37 °C and 50 rpm for 4 h. The cells were pelleted by centrifugation (4000 x *g*) at 4 °C for 5 min and stored at overnight at -80 °C.

2.11 *Recombinant BCAT1 Protein Extraction and Purification*

The over expressed BCAT1 proteins were extracted from 5-10 g of pelleted BL21 (DE3) cells. Pellets were suspended in 25mL extraction buffer (0.1 M K_iPO₄, pH 8.0, 0.01 M Tris-HCl, 0.035% v/v β-mercaptoethanol) prior to sonication (QSonica, model. Q125) on ice for 10 min at an amplitude of 35% with 15 sec intervals every 30 sec using a 6 mm probe. The sonicate was centrifuged at 4000 x *g* at 4 °C for 10 min using a Denley BR-401 refrigerated centrifuge (Denley). The supernatant was stored on ice, and the pellet

was re-suspended in a further 25mL of extraction buffer and subjected to repeat sonication and centrifugation. The supernatant was pooled and 8 mL of Ni-NTA agarose (Qiagen LTD, West Sussex) pre-equilibrated in extraction buffer was added. The mixture was agitated gently for 1 h at 4 °C prior to being transferred to a 20 mL glass column (Biorad) followed by 4 column volumes of extraction buffer. The column was subjected to sequential washes with buffer B (0.1 M K_2PO_4 , pH 7.4, 0.01 M Tris-HCL, 0.5 M NaCl, 20% w/v glycerol, 0.035% v/v β -mercaptoethanol), buffer C (0.1 M K_2PO_4 , pH 6.0, 0.01 M Tris-HCL, 1.5 M NaCl, 20% w/v glycerol, 0.035% v/v β -mercaptoethanol), and buffer C50 (0.1M K_2PO_4 , pH 6.0, 0.01 M Tris-HCL, 0.75 M NaCl, 0.075 M imidazole, 10% w/v glycerol, 0.035% v/v β -mercaptoethanol).

The BCAT1 protein was eluted from the column in 10-20 mL of elution buffer (0.1 M K_2PO_4 , pH 6.0, 0.01 M Tris-HCL, 0.75 M NaCl, 0.75 M imidazole, 20% w/v glycerol, and 0.035% v/v β -mercaptoethanol). The 6-x histidine affinity tag was cleaved from BCAT1 using (100 NIH units) thrombin in, 0.5 M Tris (pH 7.4), 0.15 M NaCl, for 1 h at 37 °C. Finally, ion-exchange chromatography was performed using a HiTrap™ Q HP strong anion column (GE Healthcare, Buckinghamshire), by means of a concentration gradient between 0 to 0.5 M NaCl in 0.1 M K_2PO_4 (pH 8.0), on ice at a flow rate of 1 mL min⁻¹ for 20 min. The purified BCAT1 protein was dialysed at 4 °C in storage buffer (0.05 M Tris-HCL pH 7.5, 0.15 M NaCl, 5 mM glucose, 1 mM EDTA, 1 mM KIC, 5 mM DTT), prior to the addition of 30% v/v glycerol and storing at -80 °C. To verify purity, BCAT1 protein extracts were resolved using SDS-PAGE, on a 12 % gel under reduced conditions (section 2.13).

2.12 Recombinant BCAT1 Protein Quantification

BCAT1 protein concentration was determined by the Bicinchoninic acid assay (BCA) as described by Smith *et al*, 1985. The BCA Working Reagent was prepared as described by the manufacturer's instruction (ThermoFisher 23225) mixing 8 mL of Reagent A (bicinchoninic acid, sodium carbonate, sodium tartrate, sodium bicarbonate in 0.1 N NaOH, pH 11.25) with 0.16 mL part of Reagent B (4% (w/v) copper(II) sulphate pentahydrate). Bovine serum albumin (BSA) standards were prepared at a concentration of 0, 0.2, 0.4, 0.6, 0.8 and 1 mg/mL in dH₂O. A 1:20 dilution BCAT1 protein extract was prepared from stock solutions in dH₂O, all samples were stored at 4 °C prior to loading. 10 µL of BSA standards and BCAT1 samples were added to a 96-well plate in triplicate followed by addition of 200 µL BCA working reagent. The plate was incubated for 30 min at room temperature. Absorbance at λ 562 nm was measured using a ThermoFisher Multiskan FC microplate photometer (ThermoFisher). BCAT1 protein concentrations were determined from the BSA standard curve.

2.13 SDS-PAGE

5-30µg of samples as determined by BCA assay were separated by SDS-PAGE on a 5% stacking gel (4% Bis-acrylamide, 0.13M Tris PH 6.8, 0.1% SDS, 0.1% APS, 0.001% v/v TEMED) electrophoresed at 100 mv / 70 mA for 15 min until the dye front had migrated to the 12% resolving gel (12% Bis-acrylamide, 0.37 M Tris PH 8.8, 0.1% SDS, 0.1% APS, 0.001% v/v TEMED), at which point the electrophoresis was increased to 180 mV / 70 mA for a further 60 min (Sambrook and Russell, 2006). Gels were stained overnight with Brilliant Blue G-Colloidal (Sigma, UK.) before destaining for 1 h in a solution containing

10% glacial acetic acid in 40% (v/v) methanol. Gel images were taken using a Syngene PXi-gel-doc-system (Syngene).

2.14 *Western Blot Detection of Purified BCAT1 Protein*

5-30 μ g of protein samples were separated by SDS-PAGE electrophoresis as previously described in section 2.13. Following electrophoretic separation, proteins were transferred to a nitrocellulose membrane by electroblotting in cold transfer buffer (25 mM Tris, 192 mM glycine, 20% v/v methanol, pH 8.3) for 1 h at 100V 350 mA with stirring. The membrane was washed in TBST (50 mM Tris-Cl, pH 7.5, 150 mM NaCl, 0.2% tween) and blocked overnight in 5% w/v dried milk in TBST. For detection of BCAT1 the membrane was incubated with 5% w/v dried milk supplemented with 1:2000 primary antibody ECA-39/BCAT1 (Santacruz SC-517185) and incubated at room temperature for 1hr. After washing with TBST the membrane was incubated with 1:2000 secondary antibody rabbit-anti goat-HRP (Santacruz SC-2768) for 1h at room temperature. The membrane was washed in TBST prior to elicitation of chemiluminescence using ECL Plus detection reagent (Amersham RPN 2132) as per manufacturer's instructions. Chemiluminescent signal was captured using Syngene PXi-gel-doc-system.

2.15 *Spectrophotometric Analysis of Reduced Cysteine Thiol Groups*

The number of reduced cysteine (C, Cys) thiol (-SH) groups in BCAT1(WT) and CXXC mutant protein cysteine thiol groups were measured using the 5,5'-dithio-bis-2-nitrobenzoic acid (DTNB) titration method as described by Conway *et al.* (2002). BCAT1 proteins were exchanged into thiol assay buffer (50 mM HEPES (pH 7.2), 1 mM EDTA) by

desalting using a PD10 column (GE Healthcare). The BCAT1 concentration was calculated after a spectrophotometric reading at λ 280 nm ($\epsilon = 86\,300\text{ M}^{-1}\text{cm}^{-1}$ per BCAT1 monomer) as reported by Davoodi *et al.*, 1998. A final concentration of 2 μM BCAT1 was incubated with 100-fold molar excess of DTNB in the dark for 20 min at room temperature. The absorbance changes at λ 412 nm, was monitored over the course of the titration. The final reduced cysteine thiol count per subunit was calculated stoichiometrically using $\epsilon = 14\,150\text{ M}^{-1}\text{cm}^{-1}$ for the TNB anion (Davoodi *et al.* 1998).

2.16 Generation of Lentiviral Particles

Lentiviral particles containing pLenti- BCAT1 vectors were generated using Origene's Lenti-vpak packaging system (Origene ref: TR30022). HEK293T (ATCC® CRL-3216™) cells were sub-cultured at 3×10^5 cells/mL in T75 flasks with 10mL Dulbecco's Modified Eagle Media (DMEM) supplemented with 10% FCS and 2 mM L-Glutamine. After 24 h incubation cultures reached approximately 50% confluency. The transfection mixture was prepared adding 6.5 μg of pLenti-BCAT1 vector, 7.5 μg of packaging plasmid and 55 μL of MegaTran transfection reagent to was added to 1.25mL of Opti-MEM reduced serum medium (TheroFisher, no. 31985062) . The mixture was incubated for 30 min at room temperature. The transfection mixture was added to the T75 flask containing the HEK293T cells and incubated overnight. After 24 h the culture medium containing viral particles was harvested and stored at 4°C. Following the addition of fresh culture medium viral supernatant was harvested and pooled with the initial batch at 48 and 72 h post transfection. 30 mL of supernatant centrifuged at $3000 \times g$ at 4 °C

and filtered using a 0.45µm filter to remove cellular debris. The viral supernatant was divided into 1mL aliquots and snap frozen and stored in liquid nitrogen.

2.17 Viral Titre

Viral titre was assessed by measuring lentiviral coat protein p24 by ELISA using QuickTiter™ Lentivirus Titer Kit (Cell-Bio Labs, no. VPK-107-T 3), in accordance with manufacturer's instruction. Briefly, Virus associated p24 was isolated from free p24 by pull down. 10 µL of ViraBind™ Lentivirus Reagent A was added to 1 mL of lentiviral sample followed by 10 µL of ViraBind™ Lentivirus Reagent B and mixed by inversion. Following incubation for 30 min at 37°C the mixture was centrifuged at 12 000 x *g* and the supernatant discarded. The pellet was resuspended in 250µl of sample diluent, vortexed and incubated at 37 °C to inactivate the virus.

100µL of lentiviral sample was added in duplicate to anti-p24 antibody coated plate and incubated overnight at 4°C. Sample wells were washed x3 with 250 µL of wash buffer and 100 µL of FITC-conjugated Antip24 Monoclonal Antibody was added to each well and incubated for 1 h at room temperature. Following incubation sample wells were washed as previously described with 250 µL wash buffer and 100 µL of HRP-Conjugated Anti-FITC Monoclonal Antibody was added to each well and incubated for 1h at room temperature with shaking. Following incubation, wells were washed with wash buffer before 100 µL of Substrate Solution was added to each well. The plate was incubated for 15 min at room temp before addition of 100 µL of stop solution and absorbance at was recorded at λ450 nm using a Microplate Spectrophotometer (Thermo Scientific™ Multiskan™ GO, Catalog no. 51119200)

2.18 Transcription Analysis of BCAT1 Expression

In order to select a cell line for appropriate overexpression of BCAT1, transcript levels in immortalised leukaemia cell lines were analysed in HL60 (ATCC® CCL-240), K562 (ATCC® CCL-243), U937 (ATCC® CRL-1593.2™) and THP1 (ATCC® TIB-202). Data was provided by <https://www.proteinatlas.org/cell>. U937 cells were selected based on their relatively low background of BCAT1 expression in combination with favourable growth characteristics compared to THP1.

2.19 Puromycin Cytotoxicity Assay

Prior to antibiotic selection of transduced cells sensitivity of the U937 (ATCC® CRL-1593.2™) cell line to puromycin was determined by cytotoxicity assay. U937 cells were suspended at a density of 5×10^5 cells/mL in complete Roswell Park Memorial Institute media (RPMI-1640; 2 mM L-glutamine, 200 U/mL penicillin, 200 µg/mL streptomycin, 10% Fetal Calf Serum) supplemented with 10, 5, 2 and 1 µg/mL Puromycin and added at a volume of 100 µL/per well to a 96-well plate in triplicate. After 72 h 50 µL of Phosphate Buffered Saline (PBS; 137 mM NaCl, 2.7 mM KCl, 10 mM Phosphate) and 50 µL of Viacount cell viability dye (Luminex Cat no.4000-0040) was added to each sample. The mixture was transferred to a 1.5 mL microcentrifuge tube and incubated in the dark at room temperature for 5 min prior to analysis. The viability of the cells was analysed by flow cytometry using a Guava EasyCyte platform (MerckMillipore) running the Guavasoft 3.1.1 Viacount module. 3000 events were captured for each sample and the number of viable cells per sample was determined by the EasyFit cluster analysis algorithm.

2.20 Lentiviral Transduction

Lentiviral aliquots stored in liquid nitrogen were thawed in a water bath for 10 min at 37 °C immediately before use. 2×10^5 U937 cells were resuspended in 1 mL of viral suspension by gentle aspiration. 'Spinoculation' of the transduction mixture was performed by centrifugation at $900 \times g$ for 2 h at 32 °C (adapted from O'Doherty, Swiggard and Malim, 2000), following transduction the lentiviral supernatant was discarded. Cells were resuspended in 1 mL of complete RPMI-1640 (Sigma-Aldrich) and transferred to a 24-well plate and returned to the tissue culture incubator for 48-72 h at 37 °C and 5% CO₂. In order to select successfully transduced cells after incubation, cells were exchanged into fresh complete RPMI-1640 supplemented with 0.5 µg/mL Puromycin and transferred to a 96-well plate in 100 µL aliquots and returned to the tissue incubator. Fresh media containing 0.5 µg/mL Puromycin was exchanged every 3-5 days until outgrowth of puromycin resistant clones was evident.

2.21 qPCR of BCAT1 Transcript

Puromycin resistant clones were assessed for expression of BCAT1 at the transcript level by relative qPCR. RNA was extracted using the Isolate II RNA mini kit (Bioline BIO-52072) following the manufacturer's instructions. RNA quality was assessed by spectrophotometric analysis with a 260/280 nm ratio >2 indicating pure RNA. RNA integrity was assessed measuring 28S:18S RNA subunit ratio by gel electrophoresis, relative peak intensity was measured using Genetools analysis software (Syngene) with a 2:1 ratio indicating intact RNA. Pure intact RNA was divided into 5 µL aliquots and stored at -80 °C for future use.

cDNA was synthesised according to the manufacturer's instructions using PCR biosystems cDNA synthesis kit (PCRBiosystems, no. PB.30 11-10). Briefly 400 ng of RNA was incubated with 4 μ L cDNA synthesis mix and 1 μ L of Reverse Transcriptase made up to a final volume of 20 μ L with dH₂O. Samples were incubated at 42 °C for 30 min and the reaction stopped by denaturing Reverse Transcriptase at 85 °C for 10 min, following cDNA synthesis samples were diluted with dH₂O to a final volume of 50 μ L in dH₂O.

cDNA samples were interrogated for BCAT1 and β 2-microglobulin (β 2M) expression using primers BCAT1-F/R and β 2M-F/R respectively (section 2.4). To eliminate amplification of non-specific products/ primer dimers, optimal annealing temperatures of each primer set was determined by gradient PCR. 2 μ L of forward and reverse primer at a final concentration 0.4 μ M without cDNA template were incubated with Reddymix (Thermofisher AB-0575) as previously described (section 2.7) with a gradient between 55-65°C. The optimal temperature for each primer was determined to be the lowest temperature without any non-specific PCR product present i.e. primer dimers.

To ensure amplification fidelity, cycling efficiency of each primer was determined by standard curve using a 1/10 serial dilution of cDNA template and the reaction conditions described below. The amplification efficiency (e) was calculated using the equation $e = 10^{-1/\text{slope}}$ where $1.8 \leq e \leq 2.2$ indicates an efficiency between 90-110% within acceptable limits (Schmittgen and Livak, 2008).

For each qPCR reaction forward primer and reverse primers at a final concentration of 0.4 μ M and 100 ng cDNA template was added to 10 μ L SybGreen Blue mix (PCR Biosystems PB20.17-01) in a final volume of 20 μ L dH₂O and kept on ice prior

to addition to 96-well PCR microplate (Axygen CR-96-LC480-W-BC). Negative controls containing no cDNA were performed for each reaction. Following this the qPCR reaction was carried out using a Roche 480 LightCycler, cycling parameters were as follows: 1) Initial denaturation: 95 °C for 10 sec 2) Annealing: 63 °C for 10 sec 3) Extension 72 °C for 20 sec for 35-40 cycles. A final melt-curve analysis was performed to assess the PCR product. Relative expression of BCAT1 to reference gene β 2M was calculated from Crossing Point (Cp) values using the $-2^{\Delta\Delta C_p}$ method where $-2^{\Delta\Delta C_p} = (C_p \text{ Gene of interest} - C_p \text{ Internal control}) \text{ Sample A} - (C_p \text{ Gene of interest} - C_p \text{ Internal control}) \text{ Sample B}$.

2.22 *Western Blot Detection of BCAT1 in Transgenic and Control U937 Cells*

For detection of BCAT1 in whole cell lysate samples approximately 5-10 x10⁶ U937 cells were pelleted by centrifugation at 2500 x g for 5 min prior to washing with sterile PBS. Cells were resuspended in 0.5-1 mL cold RIPA buffer (Sigma: R0278) supplemented with Proteinase Inhibitor Cocktail (Sigma P8340) at 25 μ L/mL and incubated on ice for 30 min with regular vortexing. Cells were pelleted by centrifugation at 14000 x g and the supernatant was transferred to a clean 1.5 mL microcentrifuge tube for BCA analysis as previously described in section 2.12.

Following protein quantification by BCA assay 30 μ g of whole cell lysate protein was processed by SDS-PAGE and western blot as previously described in 2.13 and 2.14 with the following alterations. For detection of transgenic BCAT1 subsequent to blocking overnight at 4 °C the membrane was incubated with 5% w/v dried milk supplemented with 1:2000 Anti-DDK (FLAG)-HRP mAb (Origene : TA50011-100) and incubated at room temperature for 1 h prior to detection. For detection of native background expression

of BCAT1 the membrane was incubated with 5% w/v dried milk supplemented with 1:2000 primary antibody ECA-39/BCAT1 (Santa Cruz SC-517185) as previously described (section 2.14). BCAT1 expression was normalised to Cyclophilin B loading control using Recombinant Anti-Cyclophilin B HRP Ab (Abcam EPR12703(B)). Following capture of BCAT1 chemiluminescent signal the membrane was washed in TBST before being stripped and re-blocked as per manufacturer's instructions using Restore Stripping Buffer (ThermoFisher 21059). For detection of Cyclophilin the membrane was incubated with 5% w/v dried milk TBST supplemented with 1:2000 Anti-Cyclophilin B HRP Ab and incubated at room temperature for 1 h prior to detection.

2.23 Cell Culture of U937 BCAT1 Transgenic and Control Cells

U937 cells were maintained in 10mL of complete RPMI-1640 in T75 flasks in a humidified cell culture incubator kept at 37 °C supplied with 95% air and 5% CO₂. Media was exchanged every 3-5 days keeping cells at a density of 0.1-1.5x10⁶ cells/mL.

Confluent flasks were used to create frozen stocks, 1mL aliquots were resuspended at a density of 1x10⁶ cells/mL in complete RPMI-1640 supplemented with 10% DMSO. Aliquots were transferred to a freezing container and stored at -80c overnight to achieve slow cooling of -1 °C/min before being transferred to liquid nitrogen. After multiple subcultures U937 cells can gradually differentiate, therefore cells were discontinued approximately every 2-3 months. Revived frozen aliquots were pelleted by centrifugation at 300 x g for 5 min and washed with complete RPMI-1640 before resuspension in complete RPMI supplemented with 20% FCS to facilitate recovery.

2.24 Trypan Blue Cell Viability Staining

For all assays seeded with a specified number of cells, trypan blue staining was used to determine viable cell numbers. Cells from a T75 flask were pelleted by centrifugation (300 x *g*) and resuspended in 1mL of complete RPMI-1640. 10-20 μL of this suspension was added to an equal volume of 0.4% trypan blue solution (Thermofisher 15250061) in a 1.5mL microcentrifuge tube and incubated for 5 min before counting with a haemocytometer.

2.25 U937 Transgenic and Control Cell Growth Curves

In order to assess the effect of BCAT1 overexpression on the growth dynamics of the U937 cell, T75 flasks were seeded at 2×10^5 cells/mL in a total volume 10 mL and incubated in a cell culture incubator (37°C, 5% CO₂) as previously described in section 2.23. Cell density and viability was measured using the Viacount module (section 2.19) at $t=0$ then at 24 h intervals from 0-96 h to capture exponential and stationary phase growth, followed by 168-192 h to capture death phase. At each time point 100 μL was removed and stained with 50 μL of Viacount reagent mixed with 150 μL PBS and incubated in the dark for 5 min prior to flow cytometric analysis as previously described (section 2.19).

2.26 Cell Cycle Analysis of Transgenic and Control U937 Cells

T75 flasks were seeded with transgenic or control U937 cells at a density of 2×10^5 cells/mL in a total volume 10 mL and incubated in a culture incubator (37°C, 5% CO₂) as previously described in section 2.23. 100 μL of sample was removed from each flask at

t=48, 72 and 96 h and transferred to a 1.5 mL microcentrifuge for analysis. Samples were pelleted by centrifugation at 400 x *g* for 5 min and washed in sterile cold PBS. To fix cells prior to staining cells were resuspended 0.5 mL ice cold 70% Ethanol and incubated at 4 °C for 30 min. To account for cell shrinkage during fixation cells were pelleted by centrifugation at 850 x *g* for 10 min and washed in PBS. Cells were resuspended in 0.2 mL of Propidium Iodide (50 µg/mL) and incubated for 5 min at room temperature in the dark before flow cytometric analysis. For each sample 10-20 000 events were captured using a GuavaCyte flow cytometer with Incyte software (Merck). Intact cells were separated from debris by relatively high Forward Scatter (FSC) / Side Scatter (SSC) gate. From this population a single parameter histogram was generated using the FL2 (Yellow/Blue) channel and cell populations containing 2n, S and 4n were distinguished by relative Median Fluorescence Intensity (MFI) peaks where 4n>S>2n, these peaks were gated and analysed as a percentage of total cell population.

2.27 Measuring Intracellular ROS in Transgenic and Control U937 Cells Using the DCFDA Flow Cytometric Assay

Cellular ROS was measured by 2',7' -dichlorofluorescein diacetate (DCFDA) staining using the DCFDA Assay kit, in accordance with manufacturer's instruction (Abcam 113815). Briefly, T75 flasks were seeded at a density of 2×10^5 U937 cells/mL in a total volume 10 mL and incubated in a culture incubator (37 °C 5% CO₂) as previously described in section 2.23. 100 µL of sample was removed at t= 48, 96 and 168h and transferred to a 1.5 mL microcentrifuge tube for analysis. 100 µL of 2 µM DCFDA was added directly to the sample and incubated for 30 min at 37 °C prior to flow cytometric

analysis. For each sample 10-20 000 events were captured using a GuavaCyte flow cytometer with Incyte software (Merck). Intact cells were separated from debris by relatively high Forward Scatter (FSC) / Side Scatter (SSC) gate. From this population a single parameter histogram was generated using the FL1 (Green/Blue) channel and DCFDA was measured by MFI.

2.28 Measuring Mitochondrial Membrane Potential in Transgenic and Control U937

Cells Using the DiOC2(3) Assay

Mitochondrial membrane potential (ψ_m) was measured using the 3,3'-Diethyloxacarbocyanine Iodide (DiOC2(3)) probe which accumulates in mitochondria with active membrane potentials at concentrations 100 nM and below (Bunting *et al.*, 1989). 100 μ L samples of transgenic or control U937 cells were removed from T75 cultures at t= 48, 96 and 168 h equating to $1-1.5 \times 10^5$ cells per sample. Cells were pelleted by centrifugation at x 300 g for 5 min and resuspended in 100 μ L PBS before addition of 1 μ L of 10 μ M DiOC2(3) to a final concentration of 100 nM DiOC2(3). Samples were incubated at 37°C, 5% CO₂ for 30 min prior to pelleting by centrifugation and resuspension in 300-500 μ L PBS. Samples were analysed by flow cytometry, for each sample 10-20 000 events were captured. using a GuavaCyte flow cytometer with Incyte software (Merck). Intact cells were separated from debris by relatively high Forward Scatter (FSC) / Side Scatter (SSC) gate. From this population a bivariate plot was generated using the FL1 (Green/Blue) and FL3 (Red/Blue) channels. Mitochondria associated DiOC2(3) was measured as the ratio of Red/Green MFI where a higher ratio indicates increased stacking in the inner membrane space.

2.29 Measuring the Intracellular Redox Environment in Transgenic and Control U937 cells Using the Glutathione Assay

Cellular glutathione was measured using the Glutathione Assay Kit (Sigma CS0260), in accordance with manufacturer's instruction, subject to adjustments to directly quantitate oxidised glutathione (GSSG). To measure total reduced glutathione (GSH) content cells were washed in twice in PBS and harvested by centrifugation at 600 $\times g$ for 5 min. In order to assess oxidised glutathione (GSSG) content cells were incubated with 50 mM N-Ethylmaleimide (NEM) for 20 min prior to washing with PBS and harvesting by centrifugation at 600 $\times g$ for 5 min. Cells were then resuspended in 150 μL 5% 5-Sulfosalicylic Acid (SSA) Solution to deproteinise the sample prior to freeze thawing twice in liquid nitrogen. Following freeze/thaw samples were incubated at 4 $^{\circ}\text{C}$ for 5 min samples were centrifuged at 10 000 $\times g$ for 10 min and the supernatant removed prior to analysis. The reduction of 5,5'-dithiobis (2-nitrobenzoic acid) (DTNB) to yellow product, 5-thio2-nitrobenzoic acid (TNB) by GSH reduction was measured spectrophotometrically at $\lambda 412$ nm. To determine the GSH concentration a standard curve from 50-3.125 μM was generated by a $\frac{1}{2}$ serial dilution with 5% SSA solution. 150 μL of working mixture containing 8 mL of 1 \times Assay Buffer, 228 μL of the diluted Enzyme Solution (6 units/mL) and 228 μL of DTNB Stock Solution (1.5 mg/mL) was added to 10 μL of sample in a 96-well plate. Following addition of 50 μL NADPH Solution (0.16 mg/mL) the reaction was incubated for 10 min at room temperature before reading absorbance at $\lambda 412$ nm. Cellular Redox potential (Eh) was calculated using the Nernst Equation where $E_h = E_m - (RT / nF) 2.303 \log [2\text{GSH}]/[\text{GSSG}]$ as previously described(Coles, Hancock and Conway, 2012).

2.30 Evaluating the Effects of Serum Starvation on Transgenic and Control U937 Cells

In order to simulate *in vitro* stationary/ death phase oxidative stress, U937 cells were cultured in serum starvation conditions i.e. complete RPMI-1640 without FCS supplementation (0% FCS). Cells were incubated at a density of 5×10^5 cells/ well in a 96-well plate in 100 μ L RPMI-1646 + 0%FCS for 48-72 h. Control wells contained complete RPMI-1640 +10% FCS. Following incubation, cellular ROS and viability were measured by DCFDA assay and Viacount staining respectively as previously described (sections 2.19 and 2.27). Cellular viability/apoptosis was confirmed by flow cytometric analysis using 7AAD/ Annexin V FITC staining. Cells were washed twice in 1 mL sterile cold PBS and resuspended in 0.5 mL cell staining buffer (Biolegend 420201). 3 μ L of 7AAD (Biolegend 420404) and Annexin V FITC (Biolegend 640945) were added and gently vortexed before incubation for 15 min at room temperature in the dark prior to flow cytometric analysis using a GuavaCyte flow cytometer with Incyte software (Merck). Intact cells were separated from debris by relatively high Forward Scatter (FSC) / Side Scatter (SSC) gate. Bivariate analysis in the FL1 (Blue/Green) and FL3 (Blue/Red) channels identified percentage populations of apoptotic/non-apoptotic and viable/non-viable cells.

2.31 Evaluating the Effect of Mitochondria ROS in Transgenic and Control U937 Cells

In order to generate mitochondrial ROS induced oxidative stress, transgenic or control U937 cells were treated with the complex I inhibitor Rotenone (Fato *et al.*, 2009). A Rotenone dose response curve was generated by a $\frac{1}{2}$ dilution series ranging from 0-1000 nM. Cells were incubated at a density of 5×10^5 cells/ well in a 96- well plate for t=72 h in a cell culture incubator (37°C, 5% CO₂) as previously described (section 2.23).

Following incubation, cellular ROS and viability were measured by DCFDA assay and viacount staining respectively as previously described (section 2.19 and 2.27).

2.32 Differentiation of Transgenic and Control U937 Cells Using PMA

In order to differentiate U937 cells from monocytes to macrophage, 1×10^6 cells/mL were incubated with complete RPMI-1640, supplemented with a final concentration of 10-100 nM phorbol 12-myristate 13-acetate (PMA, Sigma Aldrich P1585) in 24-well plates for 48 h in a cell culture incubator (37 °C 5% CO₂). PMA was dissolved in DMSO to create stocks concentration of 10-100 μM. 1 μL of PMA stock was added to 1 mL of media ensuring a final concentration of DMSO of 0.1% and final concentrations of PMA between 10-100 nM respectively. To control for the effect of DMSO on cellular differentiation, control wells were supplemented with 0.1% DMSO without PMA. In order to control for the metabolic contribution of BCAT1 to differentiation control, wells were supplemented with 20 mM Gabapentin, a competitive inhibitor of BCAT1 aminotransferase activity (Goto *et al.*, 2005). To control for the contribution of cellular ROS in differentiation, the reducing agent 10 mM *N*-acetyl-L-cysteine (NAC, Sigma Aldrich A7250) was added prior to incubation. NAC stocks were dissolved in complete RPMI-1640 at a concentration of 1M and stored at -20 °C before use.

Following incubations, a 100 μL sample was removed and analysed for ROS by DCFDA staining as previously described (section 2.27). For analysis of U937 cellular differentiation, 1×10^5 cells were harvested and subjected to centrifugation at 400 x *g* and washed twice in sterile cold PBS and once with flow stain buffer (PBS, 10% FCS),

before resuspension in 0.1 mL flow stain buffer. To examine cellular differentiation, samples were incubated at 4 °C for 5 min with 3 µL of anti-CD36 PE (Biolegend 336206) and anti-CD11b FITC (Biolegend 301330) prior to flow cytometric analysis using a GuavaCyte flow cytometer with Incyte software (Merck). Intact cells were separated from debris by relatively high Forward Scatter (FSC) / Side Scatter (SSC) gate. Bivariate analysis in the FL2(Yellow/Blue) and FL1 (Blue/Green) channels identified percentage populations of CD36 positive/negative and CD11b viable/non-viable cells respectively .

2.33. Evaluating the Pharmacological Effect of Chemotherapeutic Agents on Transgenic and Control U937 Cells

Dose Responses for Gabapentin, Cytarabine, Rapamycin and Rotenone were performed in a 96-well format at a cell density of 5×10^4 cells/ well. Transgenic or control U937 cells were incubated for 72 h in a cell culture incubator (37 °C 5 % CO²), in the presence of increasing drug concentration. Following incubation, the viability of the cells was analysed using Viacount reagent as previously described (section 2.19).

2.34 Data Handling and Interpretation

All data was analysed and in GraphPad prism version 5.01. Statistical averages were calculated as mean \pm standard error of the mean. Statistical differences between mean values were calculated using a one-way or two-way ANOVA and Bonferroni post-test. Dose response relationships were analysed by non-linear regression and LD₅₀ values compared using the extra sum of squares F-test. For all tests a p value of ≤ 0.05 was considered significant.

Chapter 3: Site-directed mutagenesis of BCAT1

CXXC motif

3.1 Introduction

The BCAT1 CXXC motif contains two redox active cysteine thiol groups (-SH), 1) an N-terminal at position C335 and 2) a C-terminal at position C338. These thiols can be oxidised through S-Glutathionylation, which can be reversed by the Glutaredoxin (Grx) and Glutathione (GSH) antioxidant couple, linking BCAT1 to the wider cellular antioxidant network (Conway *et al.*, 2008). Moreover, it has been demonstrated that the BCAT1 CXXC has a reduction midpoint potential analogous to the thioredoxin (Trx) family of oxidoreductases, suggesting BCAT1 may function as a novel antioxidant. To evaluate this possibility, mutational studies of the BCAT1 CXXC motif were carried out (Collet and Messens, 2010; Coles, Hancock and Conway, 2012).

Site directed mutagenesis of the *BCAT1* CXXC motif in pCMV6-Entry vector (Origene PS100001) altering the C335 codon from ACA to AGA and C338 codon from GCA codon to GCT results in a cysteine to serine amino acid substitution. Serine differs from cysteine by a single atom, replacing the Sulphur containing thiol (-SH) group with an Oxygen containing hydroxyl (-OH) group (Figure 3.1, panel A). Oxygen has a higher electronegativity value than Sulphur (3.44 compared to 2.58) on the Pauling scale (χ_r), which translates into an increased bond dissociation energy (BDE). For example, methanethiol (CH₃SH) has a BDE of 366 kJ/mol, compared with methanol (CH₃OH), which has a BDE of 440 kJ/mol (Ouellette and Rawn, 2018), consequently hydroxyl groups have a higher pKa value ($pK_a = \log_{10} [HA]/[A^-][H^+]$) than thiol groups where for

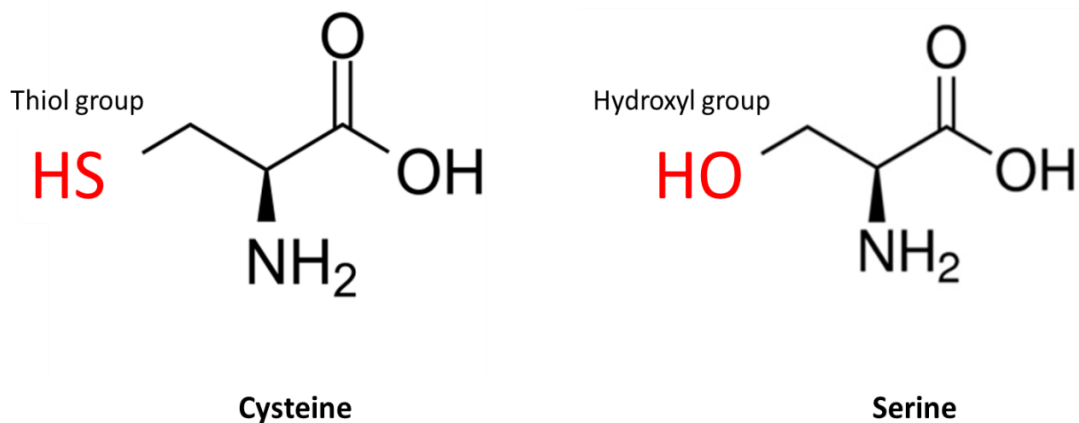
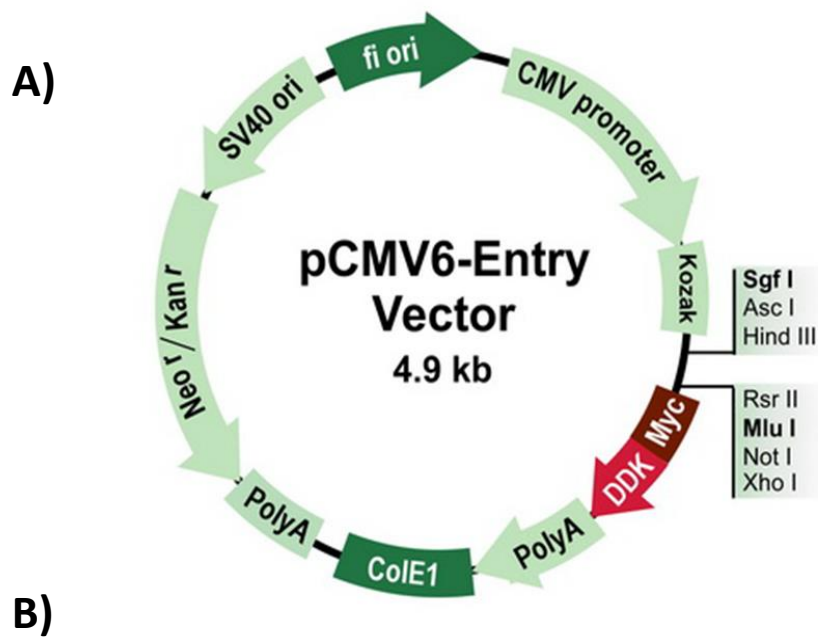


Figure 3.1 Cysteine to Serine site directed mutagenesis of the pCMV6-BCAT1 vector

Site directed mutagenesis the CXXC motif was performed in the pCMV6-Entry vector (OriGene cat no. PS100001). **A)** Alteration of the C335 codon ACA to AGA should result in a cysteine to serine amino acid substitution. Cysteine to serine modification of C338 is achieved by altering the GCA codon to GCT. **B)** Cysteine to serine substitution changes the amino acid functional group from a Sulphur containing thiol (-SH) group to an Oxygen containing hydroxyl (-OH) group.

example Methanol (CH_3OH) has a pKa of 15.3 compared with Methanethiol (CH_3SH) which has pKa of 10.3 (Serjeant & Dempsey, 1979). Thus, mutating the CXXC motif residues from cysteine to serine (CXXC \rightarrow SXXS) i.e. changing the 'thiol' functional group 'hydroxyl', thus reduces the capacity for deprotonation effectively eliminating the antioxidant capacity of the motif. Mutation of the CXXC motif in such a way is therefore essential to evaluate whether the BCAT1 CXXC motif has antioxidant capacity.

Previously the mechanistic details of the BCAT1 mitochondrial homologue - BCAT2 CXXC motif, have been explored by site directed mutagenic conversion of cysteine to serine and alanine (Myra E Conway, Poole and Hutson, 2004). This study demonstrated that mutation of the N-terminal cysteine residue (C315) resulted in a 26-33% reduction in the K_{cat} values compared to wild-type BCAT2, moreover the C315 mutants lost their sensitivity to redox regulation by H_2O_2 . However, by contrast the enzyme kinetics were largely unaffected by mutation of the C-terminal residue (C318), whilst reaction with H_2O_2 led to a complete loss of catalytic activity. Analysis of the N-terminal cysteine in the C318 single mutant revealed irreversible C315 thiol oxidation to sulfenic ($-\text{SO}_2\text{H}$) and sulfonic acids ($-\text{SO}_3\text{H}$). These results demonstrated that the N-terminal C315 cysteine residue acts as a redox sensor, that is initially oxidised to a sulfenic intermediate ($-\text{SOH}$) upon H_2O_2 oxidation before C318 acts as the 'resolving cysteine' reducing the C315 residue and forming a disulphide bond in the process. Site directed mutagenesis of the C318 residue to serine abolishes the capacity of the C-terminal amino acid to reduce the N-terminal cysteine and therefore the C315 residue becomes irreversibly oxidised.

Redox active cysteine thiols can be examined by titration with 5'5 –dithiobis (2-nitrobenzoic) acid (DTNB), which results in nucleophilic attack of a protein cysteine thiol/ate on the disulphide bond of DTNB, splitting the molecule and forming a mixed disulphide between the protein and TNB anion (Figure 3.2). Therefore, the number of cysteine thiol/ate(s) can be determined spectrophotometrically from the simultaneous liberation of the TNB anion, which absorbs light at λ_{412} nm, by using the molar extinction coefficient $\epsilon = 14\ 150\ \text{M}^{-1}\ \text{cm}^{-1}$ for TNB (Winther and Thorpe, 2014). Using this method, previous analysis has revealed that BCAT1 contains 6 reactive cysteine thiols including the 2 thiols of the CXXC motif at position 335 and 338 respectively (Davoodi et al. 1998).

Mutational studies of the BCAT1 CXXC motif revealed that mechanistically it functions in manner similar to BCAT2, i.e. the N-terminal C335 residue functions as the redox sensor whilst the C-terminal C338 residue acts as the resolving cysteine (Conway *et al.*, 2008). However, the BCAT1 CXXC motif has been demonstrated to have a lower overall reduction midpoint potential, that is the redox potential at which 50% of CXXC motif thiols are oxidised, compared to BCAT2 (Coles, Hancock and Conway, 2012). Analysis of CXXC motif thiols status by DTNB titration, found that CXXC motif has a redox midpoint potential of -310mV, which is significantly lower than the BCAT2 CXXC motif which has a midpoint potential of -225mV. This suggests a potential antioxidant role for the BCAT1 motif, since these values indicate that the BCAT1 CXXC motif may provide 'reducing power' at lower cellular redox potentials (Coles, Hancock and Conway, 2012). However, direct analysis of this antioxidant role for the BCAT1 CXXC motif has yet to be elucidated.

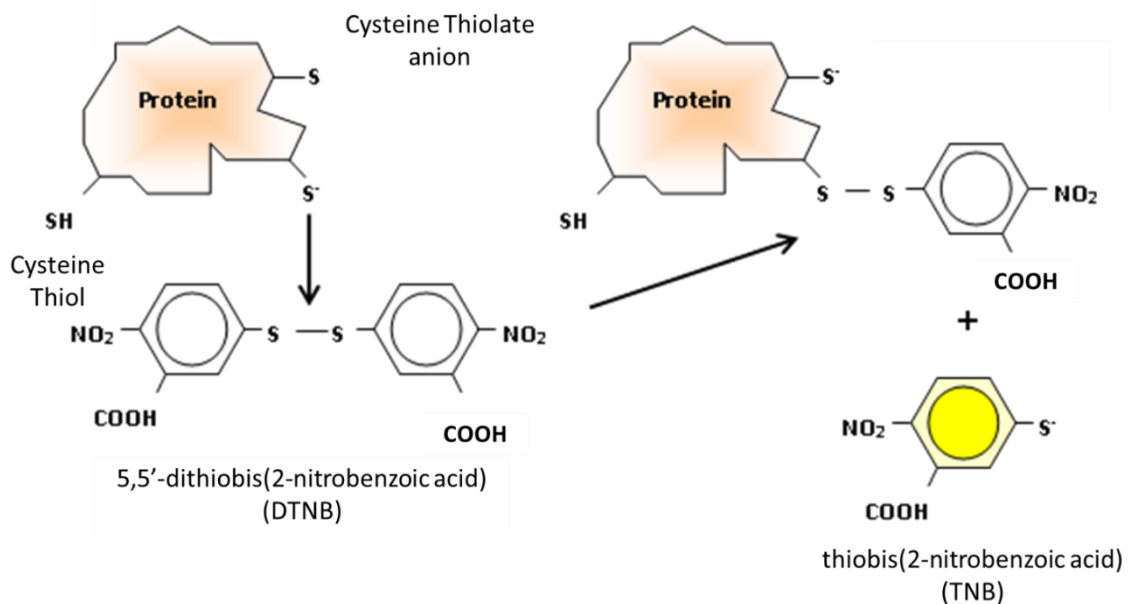


Figure 3.2 DTNB modification of reactive cysteine thiol/ate(s). A nucleophilic attack of a protein cysteine thiol/ate on the disulphide bond of the DTNB molecule results in a mixed disulphide bond between protein cysteine-TNB and liberation of the TNB anion which absorbs light at λ 412 nm. The number of cysteine thiol/ate(s) can be determined spectrophotometrically using $\epsilon = 14\ 150\ \text{M}^{-1}\ \text{cm}^{-1}$ for TNB. (Adapted with permission from Coles 2008)

Like BCAT2, the N-terminal cysteine (C335) of the BCAT1 CXXC motif, which primarily exists as a thiolate ($-S^-$) anion even under highly reduced conditions (around -320mV), is more sensitive to oxidation than the C-terminal cysteine (C338) (Goto *et al.*, 2005; Coles, Hancock and Conway, 2012). Relating this to the cell, at physiological redox potentials as determined by the reduced/oxidised glutathione ratio (GSH/GSSG) (Coles, Hancock and Conway, 2012), the binding of GSH (S-glutathionylation) to C335 of the BCAT1 CXXC motif occurs readily, where mutational studies have ascertained the C335 residue is S-glutathionylated first at -275mV followed by C338 between -260- -160mV (Coles, Hancock and Conway, 2012). In the HL60 AML cell line, this mV change denotes a shift from a proliferative state at -239 mV, through differentiation at -210mV, to apoptosis at -167mV (Freya Q. Schafer and Buettner, 2001).

Whilst the precise nature of this modification is unknown, it has been suggested the CXXC motifs may act as a GSH buffer during periods of oxidative stress (Grek *et al.*, 2013). Therefore it may be that the BCAT1 CXXC motif also plays a role in this process, whereby the redox sensor N-terminal cysteine at C335 may form mixed-disulphides with GSH (or other proteins with redox active cysteines) under periods of oxidative stress, thus providing a novel antioxidant role. Furthermore, in the GSH scenario, the C-terminal resolving cysteine of the BCAT1 CXXC motif at C338 can form an intra-subunit disulphide bond with C335 releasing free GSH back into the cellular environment. Subsequently once redox homeostasis has been restored this intramolecular disulphide bond of the BCAT1 CXXC motif can be reversed by the Grx or Trx oxidoreductases using NADPH as a cofactor (Figure 3.3)(Conway *et al.*, 2008). This process mediated by BCAT1 may therefore serve to maintain the cellular pool of GSH during periods of oxidative

stress, therefore placing BCAT1 in the centre of a wider antioxidant network. This hypothesis is explored in more detail through the work presented in this thesis, which could in theory impact on cellular growth and development (Ye *et al.*, 2015).

To explore the putative antioxidant role of the BCAT1 CXXC motif, the potential canonical metabolic effect mediated BCAT1 through the generation of α -KG, needs to be mitigated (section 1.3.1 and 1.3.3). Importantly in this regard, the wild-type BCAT1 and C338S single mutants retain remarkably similar enzymatic activity following the binding of GSH (S-glutathionylation) at 90 and 85 IU (IU= μ mol of valine formed per min), thus allowing a direct comparison of the CXXC motif between the two mutants (Conway *et al.*, 2008). Therefore, the CXXC motif may be mutated in a way that exclusively evaluates its role as a putative cellular antioxidant, whilst having very little impact on BCAT1 aminotransferase activity.

Previous studies by Conway and Coles support the rationale for site directed mutagenesis of the BCAT1 CXXC motif. Published data show that mutation of the C-terminal C338 residue from cysteine to serine results in the preservation of the BCAT1 metabolic aminotransferase activity, yet terminates the ability for the intramolecular CXXC motif to form, thereby preventing release of GSH (Conway *et al.*, 2008). Furthermore, if both C335 and C338 of the BCAT1 CXXC motif are mutated, almost complete abolition of the catalytic activity and the antioxidant capacity is observed (Conway *et al.*, 2008). Therefore, to explore the hypothesis that the BCAT1 CXXC motif may have an antioxidant role the analysis of wild-type BCAT1, C338S and C335/8S mutants is needed for separation of the metabolic effects of BCAT1 and antioxidant effects of the CXXC motif.

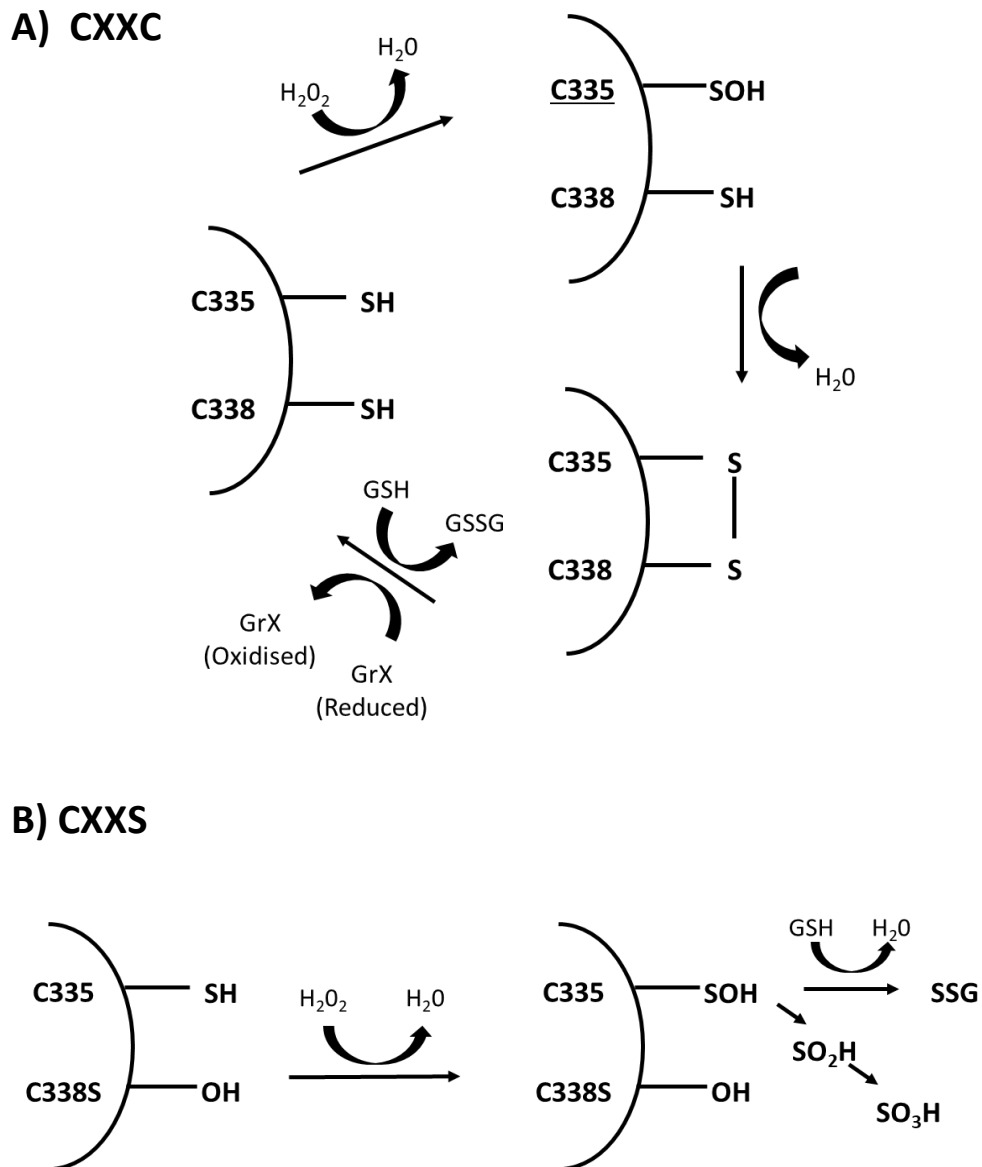


Figure 3.3 Redox reactions of the wild-type BCAT1 CXXC motif and C-terminal CXXS mutant. **A)** Following H_2O_2 oxidation the wild-type CXXC motif the N-terminal C335 is oxidised forming a sulfenic acid (-SOH) intermediate. The resolving C-terminal C338 residue forms an intramolecular disulphide which can be regenerated to the original reduced form by GrX/GSH. **B)** Substituting the C338 cysteine for serine abolishes the regenerative antioxidant properties of the resolving residue causing either irreversible oxidation to sulfinic(-SO₂) then sulphonic(-SO₂) acids or S-glutathionylation (adapted from Conway 2004).

3.2 Aims

The aim of this chapter is to abrogate the antioxidant capacity of the BCAT1 CXXC motif by site directed mutagenesis substituting amino acid cysteine (C) to serine (S) creating three constructs in PCMV6-Entry vector:

- 1) *BCAT1*(WT) → CXXC
- 2) *BCAT1*(C335S) → CXXC to SXXC
- 3) *BCAT1*(C338S) → CXXC to CXXS
- 4) *BCAT1*(C335/8S) → CXXC to SXXS

Substitution of CXXC motif amino acids C→S results in exchanging a redox active thiol (-SH) group for a hydroxyl group (-OH) eliminating the ability of the Hydrogen to act as an electron donor and therefore abolishing the antioxidant activity of the CXXC motif. These mutated *BCAT1* gene constructs will then be subcloned to pET28a protein expression vector to allow overexpression, purification and functional characterisation of mutated BCAT1 CXXC motif cysteine thiols at the protein level.

3.2.1 Objectives

The following objectives are required to fulfil this aim.

- C→S site-directed mutagenesis of the *BCAT1* CXXC motif in the pCMV6-Entry vector (Origene), creating three mutant constructs; *BCAT1*(C335S), *BCAT1*(C338S) and *BCAT1*(C335/8S). Successful mutagenesis at the genetic level will be confirmed by DNA sequence analysis.
- Subcloning *BCAT1*(WT) and CXXC motif mutants from pCMV6 to pET28a expression vector. Successful ligation into pET28a will be confirmed by digestion with pET28a specific endonucleases and fragment analysis by agarose DNA electrophoresis. Reading frame and *BCAT1* sequence fidelity will be confirmed by DNA sequence analysis.
- To verify that *BCAT1* protein is produced, overexpression and purification of *BCAT1*(WT) and CXXC motif mutants was carried out. pET28a-*BCAT1* constructs are overexpressed using the pET system (Novagen) in *E.coli* BL21(DE3) cells and purified using Ni-NTA and Hi-trap anion exchange chromatography using the AKTA platform. Verification of *BCAT1* protein will be confirmed by SDS-PAGE and western blotting.

- DTNB titration of BCAT1(WT) and CXXC motif mutant protein *in vitro*. To confirm C→S substitution at the protein level the number of reactive cysteine thiol groups for each purified BCAT1 protein was assessed by DTNB titration.

3.3 Methods

3.3.1 Site-directed Mutagenesis of the CXXC motif

Mutagenesis of *BCAT1* CXXC motif cysteine residues to serine was implemented in pCMV6-*BCAT1* vector using the Quikchange II Site-directed Mutagenesis Kit (Agilent). Three mutant constructs were generated pCMV6-*BCAT1*(C335S), pCMV6- *BCAT1*(C338S) and pCMV6- *BCAT1*(C335/8S) using the C335S, C338S and C335/8S primer pairs described in section 2.4 and the cycling parameters outlined in section 2.6. *BCAT1*(WT) and CXXC motif mutant constructs were transformed into competent *E.coli* α -Select Gold cells where plasmids were cloned, purified and mutation of *BCAT1* cDNA confirmed by DNA sequence analysis as previously described in section 2.5 and 2.6. Sequence fidelity was analysed using Chromas Lite 2.0 software, NCBI's nucleotide BLAST and M-coffee alignment tools.

3.3.2 Subcloning pET28a-*BCAT1*

For the subcloning of *BCAT1*(WT) and CXXC mutant cDNA from the pCMV6-*BCAT1* vector to pET28a expression vector, NheI and Sall restriction sites flanking *BCAT1* cDNA were introduced via PCR using the *BCAT1*_424 and *BCAT1*_1582 primer pair described in section 2.4 and the cycling parameters outlined in 2.9. pET28a vector and *BCAT1* cDNA amplicons were digested with NheI-HF and Sall-HF restriction endonucleases and separated by gel electrophoresis, gel purified, ligated and transformed into *E.coli* BL21(DE3) competent cells as previously described in section 2.5. Transformed cells were selected on LB Agar plates supplemented with 50 μ g/mL

kanamycin and screened for the *BCAT1* insert via Colony PCR as described in section 2.8 using the BCAT_424 and BCAT1_1582 primer pair. BCAT1 positive transformants containing pET28a-*BCAT1*(WT) and CXXC motif mutant plasmids were cloned, purified and verified for reading frame and sequence fidelity by DNA sequence analysis using the T7F and T7R primer pairs as previously described in section 2.9.

3.3.3 BCAT1 overexpression, purification and verification by Western blot

Overexpression and purification of BCAT1 proteins is described in section 2.10. To confirm the presence of pure BCAT1 and to assess detection limits 1, 2, 5 and 10 µg of BCAT1 protein was loaded onto a 12% SDS-PAGE and separated by electrophoresis as previously described in section 2.13. BCAT1 protein was visualised on the SDS-PAGE gel following Coomassie blue staining, where BCAT1 appears as an enriched 43 kDa band. To confirm enriched 43kDa band as BCAT1 western blotting was performed as described in section 2.14.

3.3.4 Spectrophotometric analysis of reduced cysteine thiol groups

To verify that the mutated gene translates to the mutation of cysteine at the protein level the number of reduced cysteine thiol (-SH) groups in BCAT1(WT) and CXXC mutant protein was measured using the 5,5'-dithio-bis-2-nitrobenzoic acid (DTNB) titration method as described in section 2.15. It was expected that BCAT1(WT) titrated 6 cysteine thiols, with BCAT1(CXXS) titrating 5 cysteine thiols and BCAT1(SXXS) titrating 4 cysteine thiols accordingly.

3.4 Results

3.4.1 Site directed mutagenesis of *pCMV6-BCAT1*

In order to exchange the N-terminal (C335) and C-terminal (C338) cysteine residues of the BCAT1 CXXC motif to serine, site-directed mutagenesis was employed using the C335S, C338S and C335/8S primer pairs (section 2.4) and cycling parameters previously described in section 2.6. This resulted in a single base pair substitution of the C335 cysteine codon from GCA to GCT and the C338 cysteine codon from ACA to AGA. Base pair substitutions were confirmed by DNA sequencing and analysed using the Chromas program. Chromatograms reveal successful substitution reaction at C335 and C338 codons creating three mutant constructs, which include - the N-terminal mutated *pCMV6-BCAT1(C335S)*, the C-terminal mutated *pCMV6-BCAT1(C338S)* and the N+C terminal mutated *pCMV6-BCAT1(C335/8S)* (Figure 3.4). Full reading frame analysis was performed using the NCBI-Blast webtool, alignment of sequenced *pCMV6-BCAT1* constructs with the full *pCMV6-BCAT1* sequence revealed no additional spontaneous base pair mutations and the correct reading frame position (Appendix A).

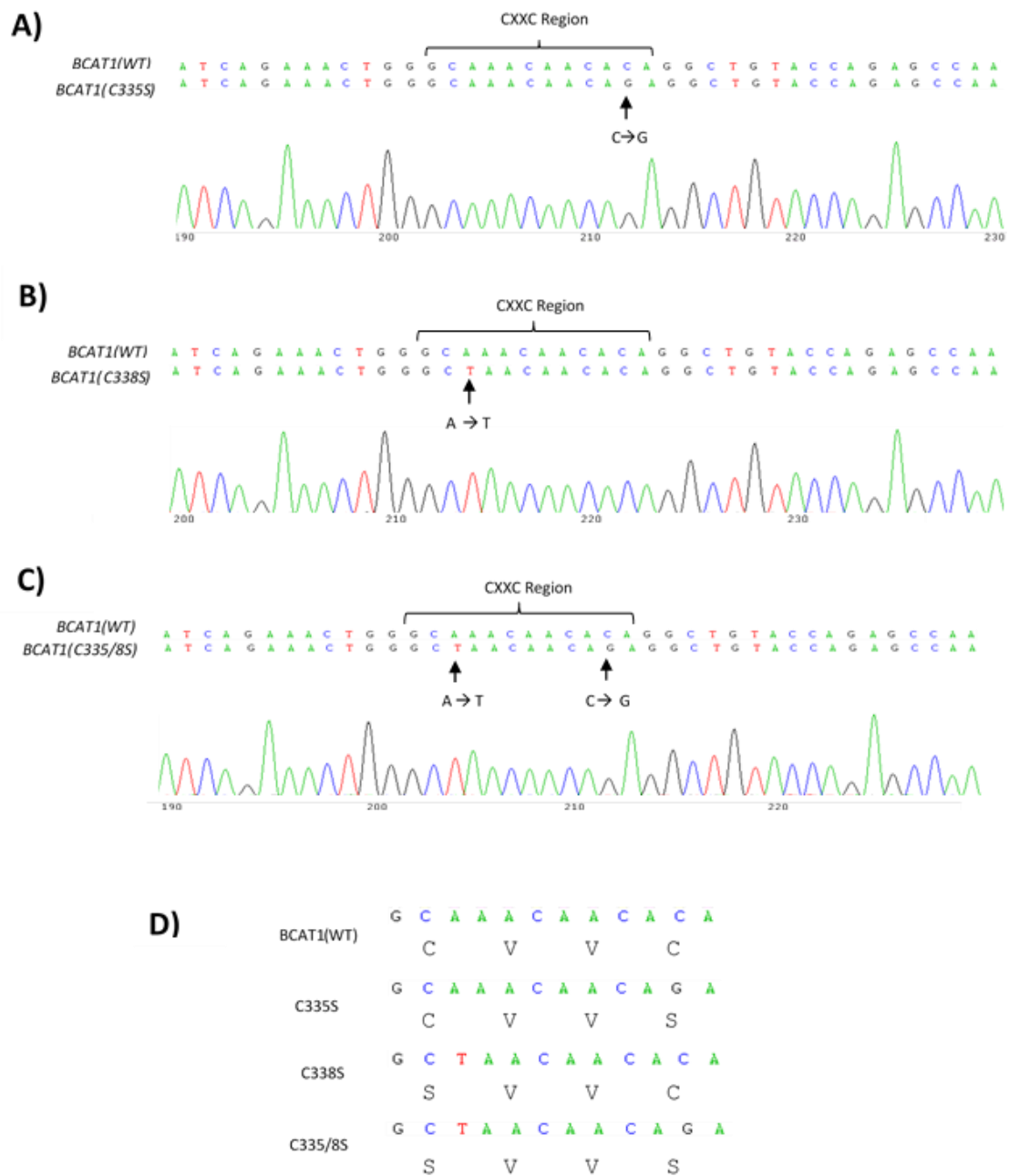


Figure 3.4 Site directed mutagenesis of *BCAT1* CXXC motif in pCMV6 vector. CXXC motif base pair substitutions of *BCAT1* cDNA (OriGene) in the pCMV6-Entry vector. Chromatograms illustrate the mutation sites of **A)** C335S, **B)** C338S and **C)** C335/8S mutants. Full reading frame analysis shows no additional mutations. (data not shown). **D).** Corresponding cysteine (C) to serine (S) amino acid changes flanking tandem valine (V) residues are shown BCAT1(WT), C335S, C338S and C335/8S mutants respectively

3.4.2 Subcloning *BCAT1* and CXXC motif mutants to pET28a expression vector.

To produce *BCAT1* containing pET28a expression vectors, *BCAT1*(WT) and *BCAT1* CXXC mutant cDNA was PCR amplified from the respective pCMV6- Entry vectors and isolated by gel electrophoresis (Figure 3.5 Panel A). Successful insertion of *BCAT1*(WT) and respective CXXC mutant cDNA into pET28a expression vectors was confirmed by the presence of 1.16 kb fragment isolated by agarose gel electrophoresis, following digestion with *NheI* and *Sall* (Fig.3.5 Panel B). Full *BCAT1*(WT) and respective *BCAT1* CXXC mutant cDNA sequence and reading frame fidelity was confirmed by DNA sequence analysis and NCBI-Blast alignment with pET28-*BCAT1* sequence generated *in silico* using the Serial Cloner (Serial Basics Version 2.6) program (Appendix A). The *BCAT1* CXXC mutant sequence variations were highlighted using the M-Coffee multiple sequence alignment tool (Fig 3.6).

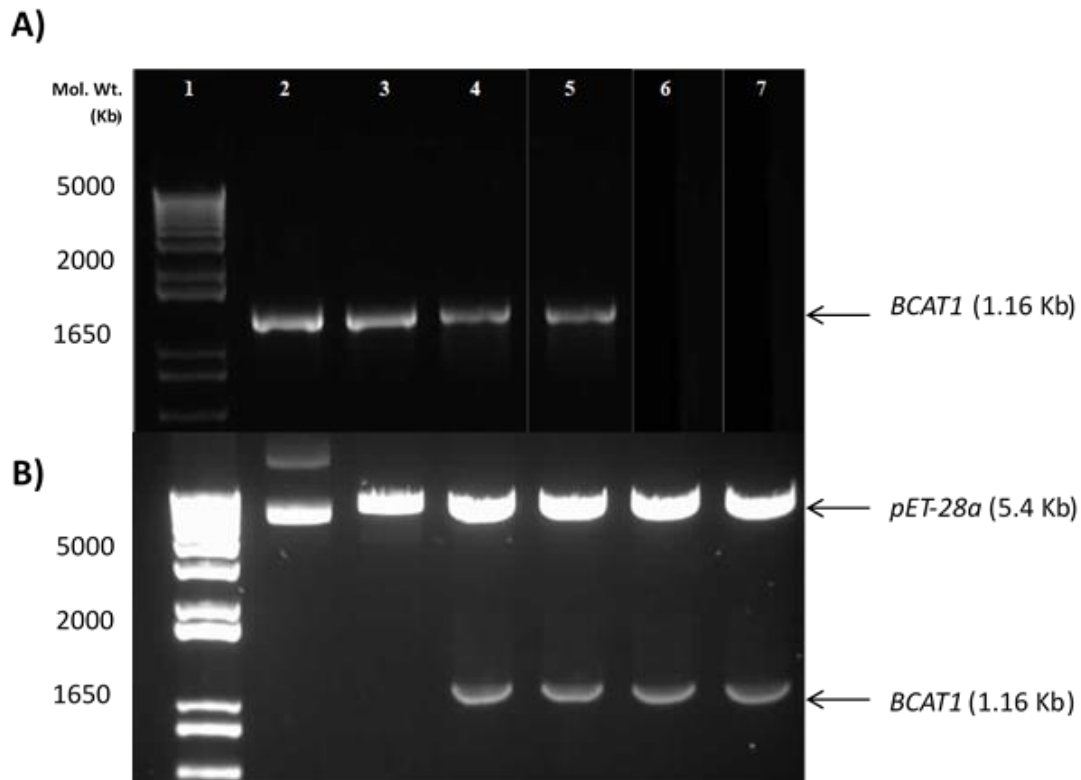


Figure 3.5 Subcloning *BCAT1*(WT) and *BCAT1* CXXC motif mutants from pCMV6-Entry vector to pET28a expression vector. A) *BCAT1*(WT) cDNA and respective *BCAT1* CXXC motif mutants (C335S, C338S, C335/8S) were PCR amplified from the pCMV6-Entry vector and separated by agarose gel electrophoresis prior to ligation. B) To verify successful *BCAT1*(WT) and *BCAT1* CXXC motif mutant subcloning into pET28a, the purified pET28a-*BCAT1* constructs were NheI/SalI restriction digested and analysed by agarose gel electrophoresis to confirm *BCAT1* insertion. Gel loading is as follows:

- A)** Lanes 2-5 20 μ l loads. **Lane 1:** 5 μ l 1 kb Plus DNA ladder. **Lane 2:** *BCAT1*(WT) amplicon **Lane 3:** *BCAT1*(C335S) amplicon **Lane 4:** *BCAT1*(C338S) amplicon and **Lane 5:** *BCAT1*(C335/8S) amplicon.
- B)** Lanes 2-7 100ng loads. **Lane 1:** 5 μ l 1 kb Plus DNA ladder. **Lane 2:** undigested pET28a vector control **Lane 3:** digested pET28a control **Lane 4:** digested pET28a-*BCAT1*(WT) construct **Lane 5:** digested pET28a-*BCAT1*(C335S) construct **Lane 6:** cut pET28a-*BCAT1*(C338S) construct **Lane 7:** digested pET28a-*BCAT1*(C335/8S) construct.

A)

PCMV6- <i>BCAT</i>	177	CTTTGTACAGTATATCAGAAACTGGGCA	AACAACAC	CAGGCTGTACCAGAGCCAAACATCT
C335S	177	CTTTGTACAGTATATCAGAAACTGGGCA	AACAACAC	CAGGCTGTACCAGAGCCAAACATCT
C338S	181	CTTTGTACAGTATATCAGAAACTGGGCT	AACAACAC	CAGGCTGTACCAGAGCCAAACATCT
C335/8S	176	CTTTGTACAGTATATCAGAAACTGGGCT	AACAACAC	CAGGCTGTACCAGAGCCAAACATCT

B)

pET28- <i>BCAT</i>	232	CAGAAACTGGGCA	AACAACAC	AGGCTGTACCAGAGCCAAACATCTCTCTCACTCTGTTCC
C335S	240	CAGAAACTGGGCA	AACAACAG	AGGCTGTACCAGAGCCAAACATCTCTCTCACTCTGTTCC
C338S	232	CAGAAACTGGGCT	AACAACAC	AGGCTGTACCAGAGCCAAACATCTCTCTCACTCTGTTCC
C335/S	233	CAGAAACTGGGCT	AACAACAG	AGGCTGTACCAGAGCCAAACATCTCTCTCACTCTGTTCC

Figure 3.6 Sequence alignment of pCMV6-Entry, pET28a and pLenti constructs containing *BCAT1* and CXXC motif mutants. *BCAT1*(*WT*) and CXXC motif mutants were

subcloned from **A)** pCMV6-Entry into expression vectors **B)** pET28a. Sequences were analysed using M-Coffee multiple sequence alignment tool. CXXC motif base substitutions are highlighted in white. Full reading frame analysis of each construct shows no additional mutations (Appendix A).

3.4.3 Expression and purification of BCAT1 and CXXC mutants

To overexpress BCAT1 and CXXC mutant protein, pET28-*BCAT1* and CXXC mutant constructs were transformed into *E.coli* BL21-DE3 cells and induced with IPTG. Uninduced and induced whole cell lysates were collected and analysed by SDS-PAGE. The expression of BCAT1 was denoted by the presence of a large band at 43KDa (Figure 3.7). Expressed protein was harvested and purified from bacterial cultures using Ni-NTA and Ion exchange chromatography on the AKTA platform. Successive stages of purification were analysed by SDS-PAGE, increasingly pure BCAT1 is displayed from left to right in Lanes 2-7 denoted by the gradual disappearance of extraneous banding (Figure 3.8). Elution of purified protein samples following Ion exchange chromatography was measured using the AKTA pure system (Figure 3.9) Purified BCAT1 protein was confirmed by western blot analysis. Increasing loads of pure BCAT1 protein was loaded from 1 μ g-10 μ g, to determine detection limits of the ECA39 Ab (Figure 3.10).

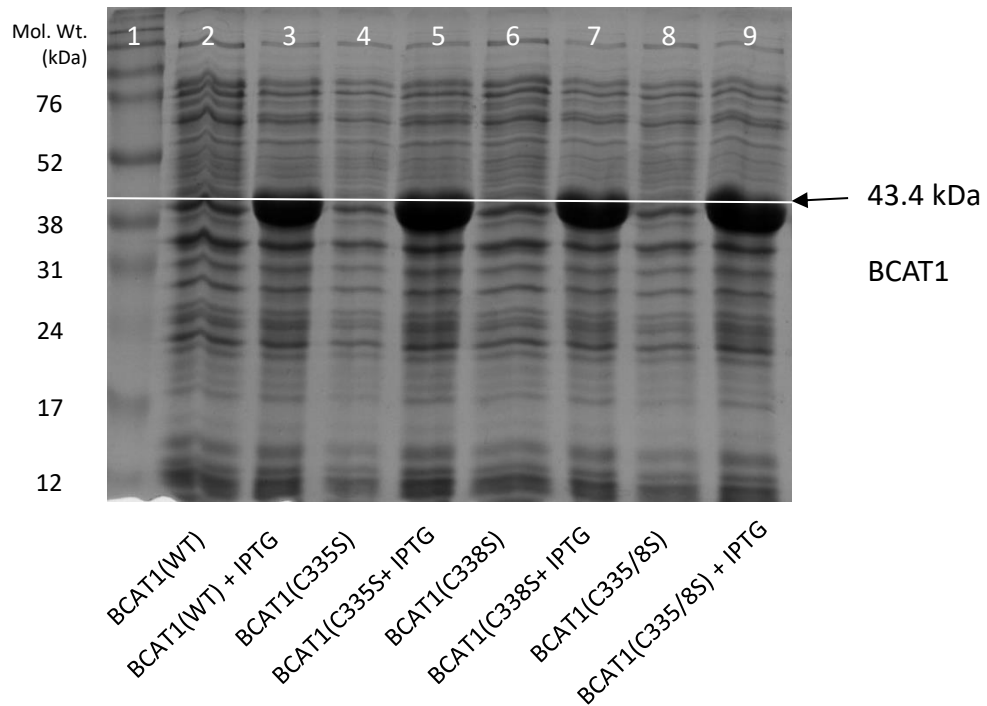


Fig 3.7 SDS-PAGE gel displaying protein expression of BCAT1(WT) and CXXC mutants in BL21 (DE3) cells. Following transformation into *E.coli* BL21(DE3) BCAT1(WT) and CXXC mutants were maintained in liquid cultures before induction with IPTG. Samples were harvested immediately pre-induction and 4 h post induction. Whole cell lysate loads were normalised to 0.15 OD₆₀₀ units. **Lane 1:** 5µl Full Range Rainbow Marker **Lane 2:** BCAT1(WT) **Lane 3:** BCAT1(WT) + IPTG **Lane 4:** BCAT1(C335S) **Lane 5:** BCAT1(C335S) + IPTG **Lane 6:** BCAT1(C338S) **Lane 7:** BCAT1(C338S) + IPTG **Lane 8:** BCAT1(C335/8S) **Lane 9:** BCAT1(C335/8S) + IPTG.

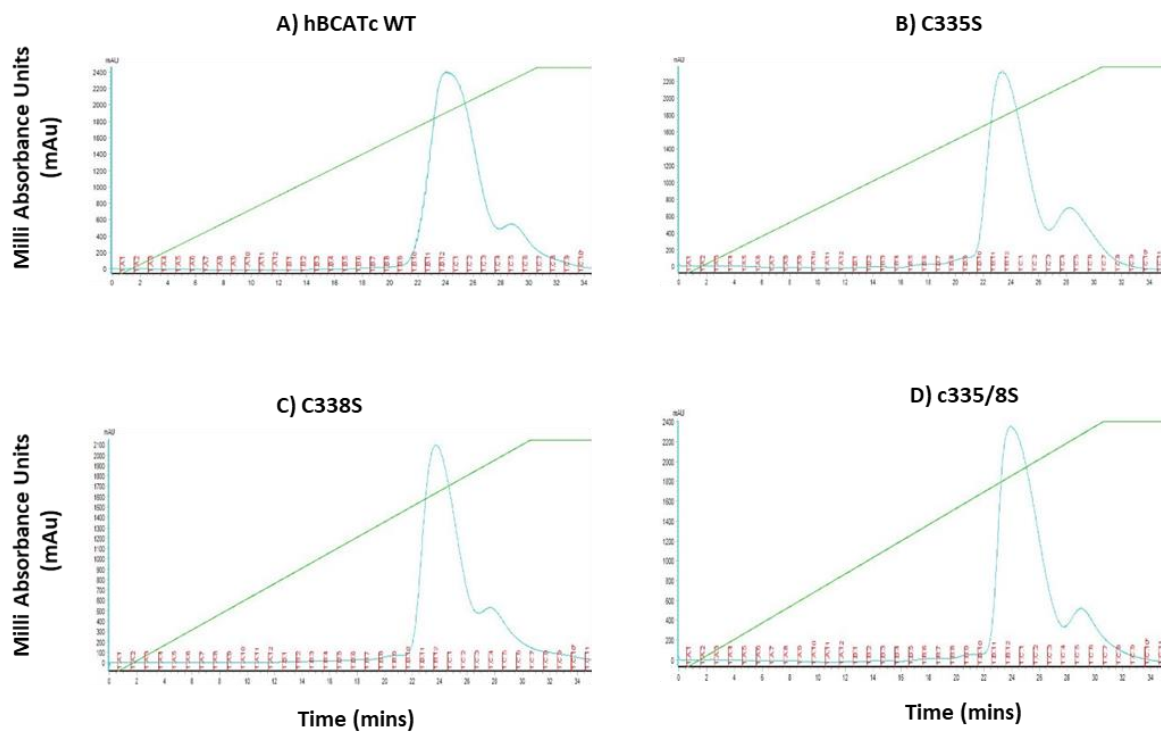


Figure 3.8 Chromatogram profiles displaying BCAT1(WT) and BCAT1 CXXC mutant proteins purified by ion exchange. Following Ni-NTA purification, BCAT1 proteins were purified using HiTrap™ Q HP strong anion columns using the AKTA pure protein purification system. Samples were eluted by 0-0.5M NaCl concentration gradient (green line) and pooled for future analysis by SDS-PAGE and western blot. Blue peaks represent purified protein elution: **A)** BCAT1(WT) **B)** BCAT1(C335S), **C)** BCAT1(C338S) and **D)** BCAT1(C335/8S). Red divisors displayed along the x-axis represent eluted fractions.

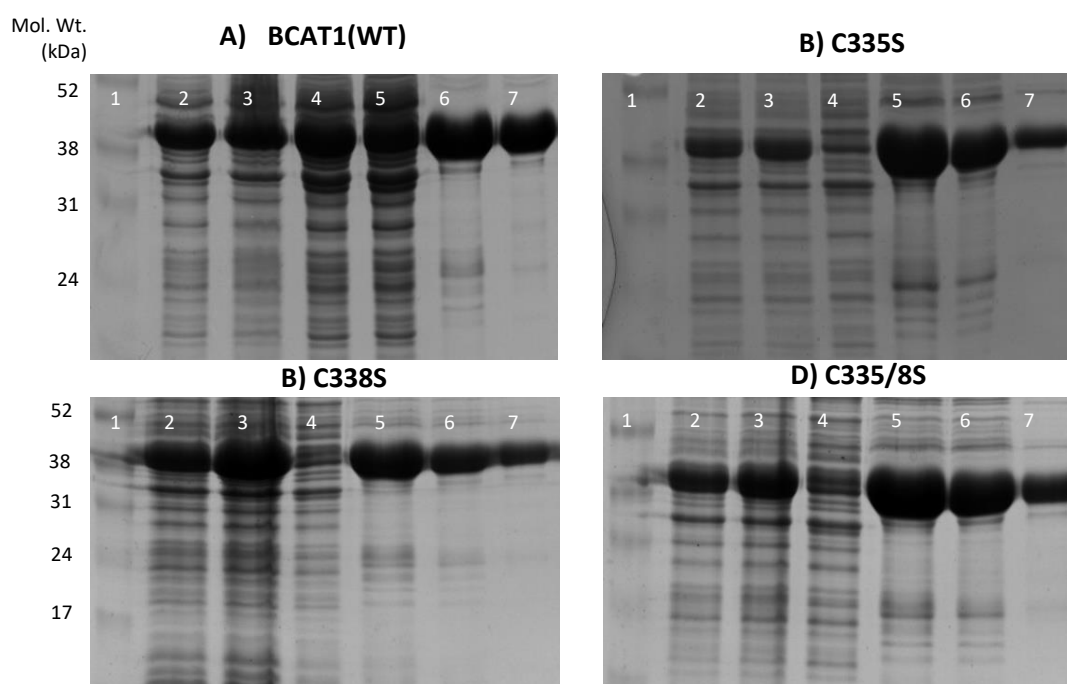


Fig 3.9 SDS-PAGE displaying purification of BCAT1(WT) and BCAT1 CXXC mutant proteins. BCAT1(WT) and BCAT1 CXXC mutants were purified from 2-5 g *E.coli* BL21(DE3) cell pellets following sonication by Ni-NTA affinity chromatography and Ion Exchange chromatography. Whole cell lysates were (WCL) normalised to 0.15 OD₆₀₀ units prior to loading. **Lane 1:** 5µl Full Range Rainbow Marker **Lane 2:** WCL BCAT1 **Lane 3:** WCL Induced BCAT1 **Lane 4:** Ni-NTA unbound flow through **Lane 5 :** Ni-NTA purified BCAT1 **Lane 6:** Thrombin cleaved BCAT1 **Lane 7:** Ion Exchange Chromatography purified BCAT1.

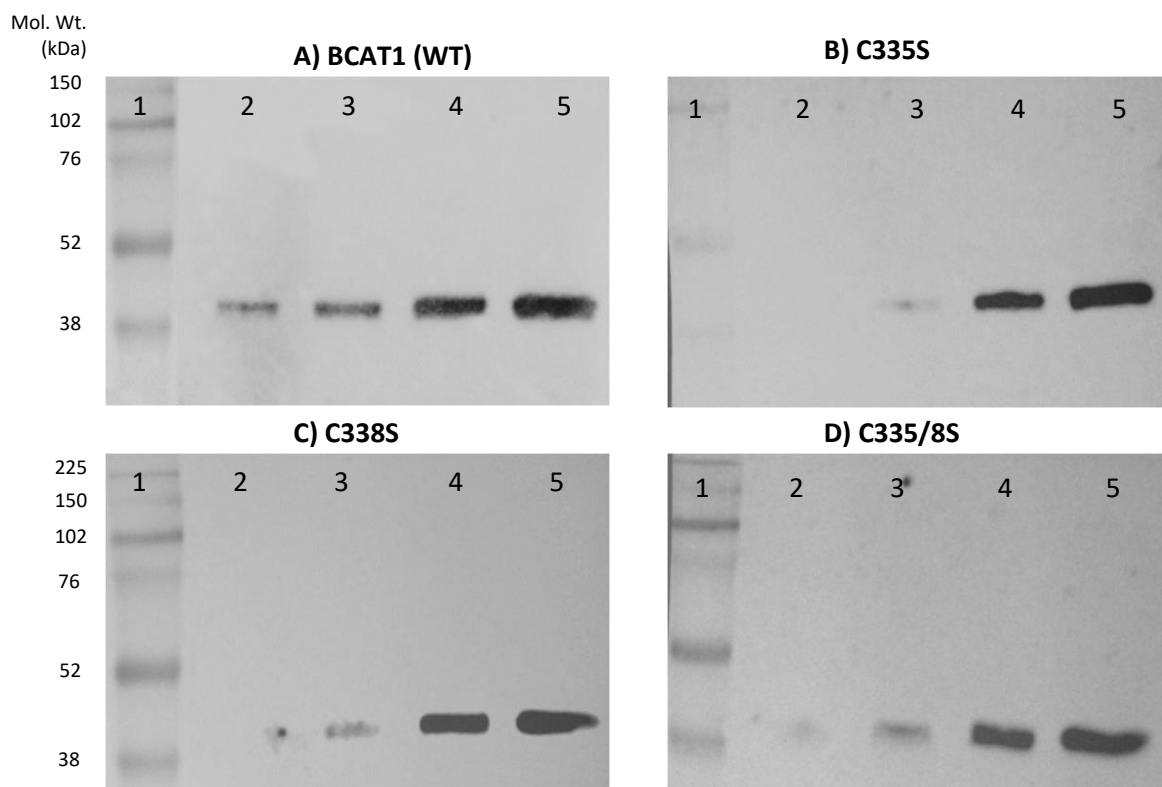


Figure 3.10 Detection of BCAT1(WT) and BCAT1 CXXC motif mutants by western blot analysis. BCAT1(WT) and BCAT1 CXXC motif mutant purified proteins were validated by western blot analysis. In order to define detection parameters, increasing loads of BCAT1(WT) and respective CXXC motif mutants were incubated with (1:2000) ECA39 polyclonal primary Ab. **Lane 1:** 5 μ l Full Range Rainbow Marker **Lane 2:** 1 μ g BCAT1 **Lane 3:** 2 μ g BCAT **Lane 4:** 5 μ g BCAT and **Lane 5 :** 10 μ g BCAT.

3.4.4 Assessment of purified BCAT1(WT) and BCAT1 CXXC mutated protein cysteine thiol groups

To confirm mutation of the BCAT1 CXXC motif was displayed at the protein level, assessment of the number free solvent accessible cysteine thiol groups was performed by DTNB titration. Initial reaction rates varied between the proteins, after 120 sec BCAT1(WT) and BCAT1(C338S) had 4.29 ± 0.1 and 3.96 ± 0.2 labelled thiols whilst BCAT1(C335S) and BCAT1(C335/8S) had just 3.18 ± 0.1 and 2.84 ± 0.14 respectively demonstrating the cysteine thiol at C335 is more reactive than C338. After 15 min incubation with DTNB a total of 6.25 ± 0.2 free cysteine thiols were labelled for BCAT1(WT), 5.03 ± 0.1 for BCAT1(C335S), 5.22 ± 0.2 for BCAT1(C338S) and 3.95 ± 0.2 for BCAT1(C335/8S). This result confirms the mutation of C→S by site directed mutagenesis has been translated to the protein level (Figure 3.11).

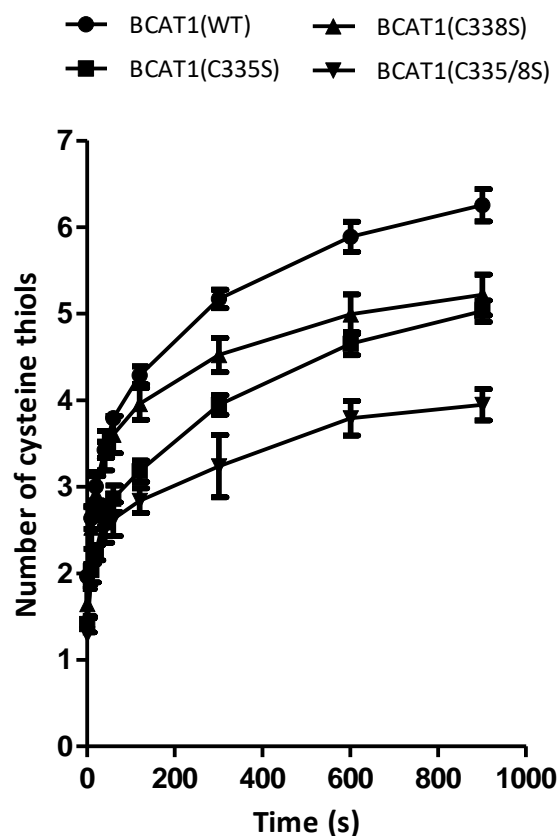


Figure 3.11 DTNB cysteine thiol titration of BCAT1(WT) and BCAT1 CXXC mutant protein. To verify the site directed mutagenesis of the CXXC motif translates to the protein level, purified BCAT1(WT) and BCAT1 CXXC motif mutants were titrated against DTNB. The graph illustrates the number of titratable cysteine thiols for BCAT1(WT) (circles), BCAT1(C335S) (squares), BCAT1(C338S) (triangles) and BCAT1(C335/8S) (inverted triangle). Data presented are mean \pm SEM(n=3).

3.5 Discussion

The aim of this chapter was to abrogate the antioxidant capacity of the BCAT1 CXXC motif by site directed mutagenesis substitution of amino acid Cysteine (C) to Serine (S) exchanging a thiol (-SH) group for a hydroxyl group (-OH) eliminating the ability of the Hydrogen to act as an electron donor and therefore abolishing the antioxidant activity of the CXXC motif.

The data presented show that the BCAT1 CXXC motif was successfully mutated in pCMV6-Entry vector as confirmed by DNA sequence analysis (Figure 3.4). In order to assess whether mutagenic substitution transferred to the protein level, BCAT1(WT), BCAT1(C335S), BCAT1(C338S) and BCAT1(C335/8S) mutant genes were transferred to a pET28a protein expression vector, where successful insertion was confirmed by NheI/SalI restriction enzyme digestion and DNA fragment analysis by agarose gel electrophoresis (Figure 3.5). To ensure that BCAT1 proteins will be correctly translated from pET28a-*BCAT1*, reading frame and sequence fidelity was verified by DNA sequence analysis (Figure 3.6). Induced overexpression of BCAT1(WT) and CXXC mutant proteins in *E.coli* BL21(DE3) cells was demonstrated by comparison to un-induced cells (Figure 3.7). Subsequently BCAT1(WT) and BCAT1 CXXC motif mutant(s) were purified by Ni-NTA and Ion exchange chromatography using the AKTA platform. Purification at various stages was monitored by SDS-PAGE (Figure 3.8), ultimately pure BCAT1 was confirmed by and western blot analysis (Figure 3.10).

To confirm that the CXXC cysteine mutations at the genomic level translated to the protein level, cysteine thiol analysis of the BCAT1(WT) and BCAT1 CXXC motif mutant proteins was quantitated by DTNB titration as illustrated in Figure 3.3. By using this

method, previous studies revealed that BCAT1(WT) contains 6 reactive cysteine thiols, including the 2 cysteine thiols of the CXXC motif (Davoodi et al. 1998). The results presented here agree with *Davoodi et al.* The DTNB titration data presented confirms the presence of 6 cysteine thiols for BCAT1(WT) as well as the successful elimination of C335, C338 and C335/8 from the CXXC motif mutated BCAT1 vector constructs (Figure 3.11). Interestingly, after just 120 sec the BCAT1(C338S) protein titrated an average of 3.96 ± 0.2 cysteine thiols compared with 3.18 ± 0.1 for the BCAT1(C335S) CXXC motif mutant protein (Figure 3.11). This relates to approximately 1 less labelled thiol group per molecule demonstrating the N-terminal C335 is more reactive than the C-terminal C338, supporting previous biochemical characterisation of the motif which identified C335 is more sensitive to oxidation than C338 (Coles, Hancock and Conway, 2012).

As well as differentially affecting the redox activity of the BCAT1 CXXC motif, previous studies demonstrated that mutagenesis of the motif differentially affects the aminotransferase metabolic activity of BCAT1 (Conway *et al.*, 2008), this is perhaps unsurprising given that the CXXC motif is located just 10 angstroms from the aminotransferase active site (Goto *et al.*, 2005). Conway *et al.*, 2008, showed that substitution of the BCAT1 C335 cysteine to serine resulted in a large decrease in the catalytic activity of the enzyme, reducing the K_{cat}/K_m from $108 \times 10^3 \text{ M}^{-1} \text{ s}^{-1}$ for BCAT1(WT) to $43 \times 10^3 \text{ M}^{-1} \text{ s}^{-1}$ for BCAT1(C335S), a reduction of 60% catalytic activity when measuring glutamate and using α -ketoisovalerate as the fixed substrate. This finding highlights the importance of the N-terminal CXXC motif cysteine (C335) with respect to the metabolic activity of BCAT1. By contrast the mutation of C338 residue resulted in an activity of $62 \times 10^3 \text{ M}^{-1} \text{ s}^{-1}$, a reduction of 30%, whilst mutation of both

the C335 and C338 results in a K_{cat}/K_m of $31 \times 10^3 \text{ M}^{-1} \text{ s}^{-1}$, a reduction of 71% (Conway *et al.*, 2008).

Whilst CXXC motif mutation results in a significant reduction in enzymatic turnover *in vitro*, under physiological GSH/GSSG ratios, the majority of the N-terminal C335 is largely S-glutathionylated, which protects BCAT1 enzymatic turnover (Conway *et al.*, 2008). The data presented by Conway *et al.*, 2008 indicate that the enzymatic activity of S-glutathionylated BCAT1(WT) and BCAT1(C338S) protein relates to 90 IU and 85 IU respectively (IU= μmol of valine formed per min), a reduction of just 5%. This highlights an important role for cellular GSH in maintaining the enzymatic activity of BCAT1 physiological settings.

These studies demonstrate mutation of the CXXC motif from C→S results in the change of only one atom in the BCAT1 protein, substituting Sulphur to Oxygen, however the effect on the enzymatic and antioxidant capacity of the protein can vary depending on whether the N or C-terminal residue is altered. In the presence of physiological levels of GSH mutation of the BCAT1(C338) retains enzymatic capacity comparable to BCAT(WT) whilst eliminating the antioxidant capacity, whilst BCAT1(C335/8) shows decreased enzymatic and antioxidant capacity. To elucidate the antioxidant role of the CXXC motif a comparison will be made between BCAT1(WT), BCAT1(C338S) and BCAT(C335/S) following overexpression in the AML cell line U937 (ATTC CRL-1593.2) which is the subject of the following chapter.

Chapter 4: Lentiviral transduction and overexpression of BCAT1(WT) and BCAT1 CXXC motif mutants in the myeloid cell line U937

4.1 Introduction

The ability to overexpress proteins in immortalised human cell lines has formed the backbone of leukaemia research over the last 30 years (Nuñez *et al.*, 1990; Thorsteinsdottir *et al.*, 2002). Retroviral vectors that integrate into the host genome are used to introduce transgenes to a wide range of cellular models (Spector *et al.*, 1990). Lentiviral vectors have become a popular choice because they infect both dividing and non-dividing cells due to their ability to cross the nuclear membrane (Naldini *et al.*, 1996; Kobilier *et al.*, 2012). Modern lentiviral vectors are the 3rd generation of modified HIV-1 virus, that have been iteratively engineered to reduce pathogenicity. The parental HIV genome containing nine genes has been reduced to three spread across four separate plasmids, that is aimed at eliminating the possibility of a replicative virus which could be reconstituted *in vivo* through a recombination event (Zufferey *et al.*, 1998).

The first generation of lentiviral vectors consisted of a two-plasmid system that separated the viral gene *env*, encoding envelope glycoproteins that facilitate attachment and entry into a host cell, and the remainder of the viral genome plus the transgene. Additionally, HIV-1 *env* genes were replaced or pseudo-typed with glycoprotein G of the Vesicular stomatitis virus (VSV-G), which recognizes the ubiquitously expressed low-density lipoprotein (LDL) receptor allowing the lentiviral

vector to transduce a wide range of cells (Cronin, Zhang and Reiser, 2005; Finkelshtein *et al.*, 2013).

Further safety improvements with the second generation eliminated virulence factors *Vpr*, *Vif*, *Vpu*, and *Nef* as well as separating essential replication and structural genes *Gag*, *Pol* and *Rev* from the transgene vector (Dull *et al.*, 1998). Finally, in the 3rd generation the 5' Long Terminal Repeat (LTR) was truncated, removing the viral promoter and Trans-activation response elements, which bind *tat* and stimulates promoter activity. This sequence was replaced with a recombinant 5'LTR driven by a Cytomegalovirus (CMV) promoter, that produces strong constitutive overexpression of the transgene (Miyoshi *et al.*, 1998). Production of infectious viral particles is achieved by co-transfection of transgene vector and packaging plasmids into a viral packaging cell line e.g. HEK293T (ATCC CRL-3216), which provide the components necessary for the cell line to manufacture infectious, replication incompetent virions (Merten, Hebben and Bovolenta, 2016). Over several days HEK293T cells produce the lentiviral particles, which are harvested from the culture medium. Upon viral transduction of the host cell, viral RNA is reverse transcribed and integrated into the host genome where co-expression of antibiotic resistance genes allows selection of stable transformants, see figure 4.1 (Merten, Hebben and Bovolenta, 2016).

During a transduction reaction the ratio of effective infectious viral particles and target cell number is known as the Multiplicity of Infection (MOI), where a 1:1 ratio represents a MOI equal to one (MOI = 1). The transduction efficiency for a given MOI varies depending on cell type, which itself may be dependent on the number LDL receptors available for interaction with VSV-G (Zhang *et al.*, 2004). It is recognised that

the transduction of leukaemia cell lines present a particular challenge, and generally require a higher viral titre compared to non-immune cells or undifferentiated hematopoietic cells (Swainson *et al.*, 2008). Although macrophages are a target for wild type HIV-1, myeloid cells in general are relatively refractory to infection by HIV-1 derived Lentivirus (Aquaro *et al.*, 2002). The reason for this is the myeloid-specific hydrolase (SAMHD1) that functions by dephosphorylating cellular dNTPs, reducing the cellular pool to a level that blocks reverse transcription of viral RNA (Hrecka *et al.*, 2011). Wild-type HIV-2 encodes a Vpx accessory protein, which binds SAMHD1 causing its degradation. However, the related Vpr protein as introduced in Lentivirus expression systems does not have the ability to degrade SAMHD1 in the same way as Vpx. Moreover, Vpx cannot be engineered to into a lentiviral system as the lentiviral virion cannot package Vpx (Bobadilla, Sunseri and Landau, 2013). Taken together, infection of monocytic cell lines such as THP1 (ATCC TIB-202) and U937 (ATCC CRL 1293.2) with Lentivirus requires MOIs an order of magnitude higher than many cell lines (Zhang *et al.*, 2004).

Integration of the lentivirus cDNA into the host genome is a semi-random event governed by the accessibility of nuclear chromatin, which varies depending on the cell type, cell cycle and proximity to the nuclear pore (Ciuffi, 2008). Additionally, the viral pre-integration complex (PIC) has been found to interact with a number of host proteins that facilitate integration (Ciuffi, 2008). For example, Lentiviral integrase associates with lens epithelium-derived growth factor (LEDGF), a transcriptional co-activator which contains a DNA binding AT hook motif that directs the PIC to relatively AT-rich regions (Cherepanov *et al.*, 2003). Lentiviral integration has been found to favour genes

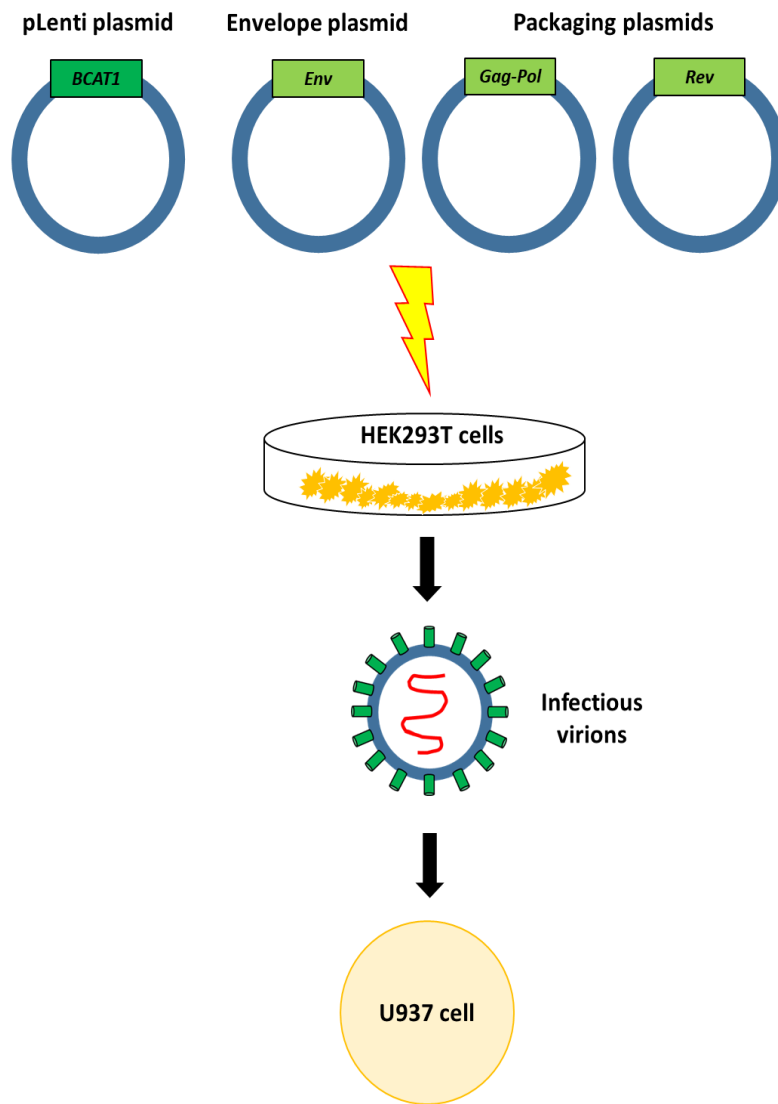


Figure 4.1 Production of Lentivirus using the third-generation system. Adherent HEK293T(ATCC CRL-3216) packaging cells are co-transfected with the pLenti envelope and packaging plasmids of the third-generation system. Viral particles containing the transgene are produced by HEK293T cells and secreted into the culture supernatant, which is collected, and filter purified. VSV-G pseudo-typed virions enter the cells via endocytosis mediated by the ubiquitously expressed low-density lipoprotein (LDL) receptor allowing transduction of a wide range of cells.

modulated by LEDGF which is proposed to act as a tether guiding PIC integration (Ciuffi and Bushman, 2006).

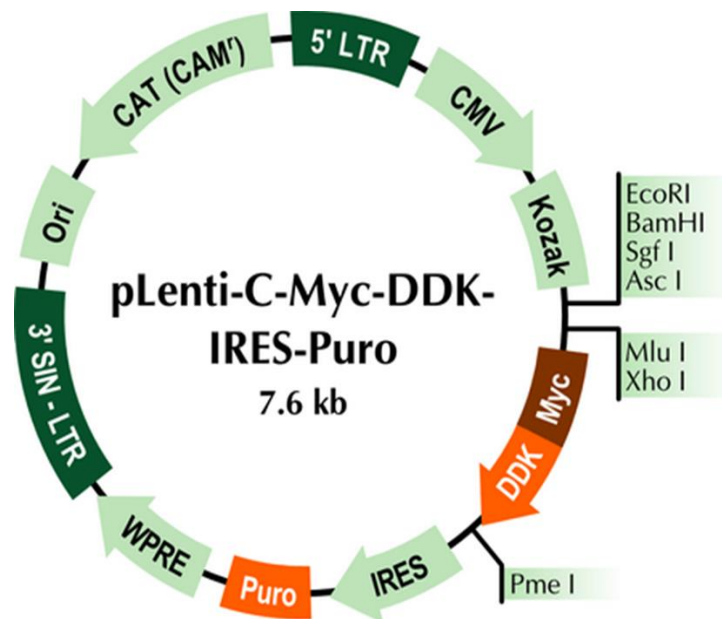
Quantification of lentiviral induced gene expression in transgenic cells at the transcript level is commonly performed by qPCR, which uses fluorescently labelled nucleotides to track the PCR amplification cDNA derived from target gene mRNA (Arya *et al.*, 2005). The quantitative end point of the reaction is the 'Crossing point' (Cp), the value at which fluorescence of the sample rises above the background noise. The Cp value is directly related to gene expression, since the Cp depends on the initial concentration of cDNA i.e. a sample with a higher initial concentration cDNA will take fewer cycles to cross the Cp threshold (Schmittgen and Livak, 2008). Although qPCR can be used to measure absolute transcript levels or copy numbers, this is not particularly relevant when examining gene overexpression, where relative change from the wild-type (WT) gene expression level is more pertinent

To this end, relative basic quantification, where fold change in gene expression is calculated using $-2^{\Delta\Delta C_p}$ method is widely used (Schmittgen and Livak, 2008). The equation $-2^{\Delta\Delta C_p} = (C_p \text{ Gene of interest} - C_p \text{ Internal control}) \text{ Sample A} - (C_p \text{ Gene of interest} - C_p \text{ Internal control}) \text{ Sample B}$, compares differences in Cp values between the overexpression sample (Sample A) and the WT control (Sample B). Given each cycle equates to a double the RNA content the fold change in target (gene of interest) mRNA is calculated by $2^{(x)}$ where $x = \Delta\Delta C_p$. To account for variation between sample concentrations both Sample A and B are normalised to a stably expressed internal or reference control.

Post transcriptional interference of mRNA can result in drastically reduced expression at the protein level (Schoenberg and Maquat, 2012). Therefore, it is advised that transgene expression change (qPCR) is supported by translation to protein. Protein expression is frequently validated through detection of a recombinant epitope tag that is affixed to the N or C-terminal of the transgene (Munro and Pelham, 1984). The pLenti Origene system used in this study employs a Myc/DDK FLAG system that allows detection post translation through western blotting, with an Anti-Myc/DDK (FLAG)-HRP mAb raised to DYKDDDDK epitope (Figure 4.2) (Einhauer and Jungbauer, 2001).

Using the techniques introduced above this part of the study aimed to stably transduce and overexpress BCAT1(WT) protein and the BCAT1 CXXC motif mutants BCAT1(C338S) and BCAT1(C335/8S), in U937 cells (a monocytic cell line of the myeloid lineage) using Origene's Lentiviral system (Figure 4.2) (Sundström and Nilsson, 1976). In this way, the hypothesised novel antioxidant capacity of the BCAT1 CXXC motif may be characterised in a robust AML cell system.

A)



B)

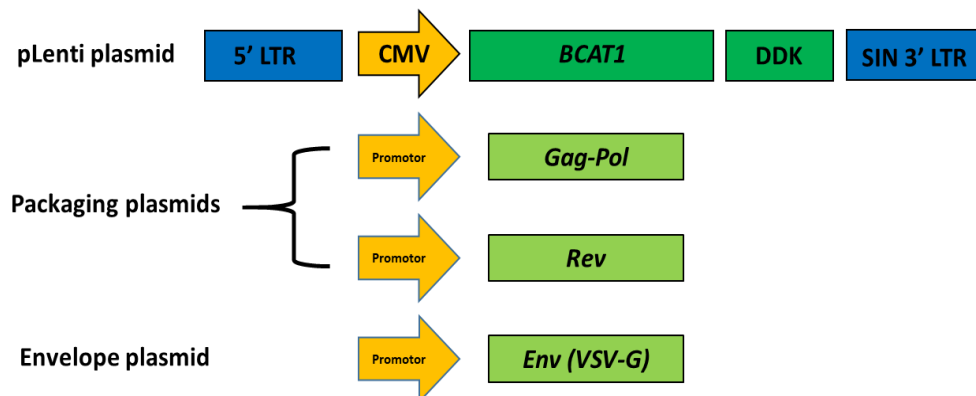


Figure 4.2 pLenti plasmid system for cellular transduction. A) Orgine’s pLenti plasmid features puromycin resistance gene(Puro) for selection of transgenic cells post transduction and a DDK epitope tag for transgenic protein detection transcription of which is driven by a CMV promoter. B) pLenti forms part of a third generation 4 plasmid system that separates viral packing genes *Gag/Pol*, *Rev* and *Env* onto separate elements. Only the pLenti element between 5’ and 3’ LTR is integrated into the genome of the host cell mitigating the formation of a replication competent virus *in vivo*.

4.2 Aims and Objectives

The aim of this chapter is the stable overexpression Empty Vector(EV), BCAT1(WT) and CXXC disrupted BCAT1(C338S) and (C335/8S) protein in immortalised monocyte cell line U937 (ATCC CRL 1293.2). In this way, 4 cell lines can be generated that will allow the antioxidant aspect of the BCAT1 CXXC motif to be studied at the cellular level:

1. U937-Control(EV)
2. U937-BCAT1(WT)
3. U937-BCAT1(C338S)
4. U937-BCAT1(C335/8S)

The BCAT1(C338S) mutant was selected on the basis that BCAT1 aminotransferase activity is preserved under physiological conditions, whereas the putative antioxidant activity is predicted to be diminished compared with BCAT1(WT). The BCAT1(C335/8S) mutant was selected since both BCAT1 aminotransferase and antioxidant activity is diminished, therefore, by comparing these cells lines the relative contributions of BCAT1 enzymatic and CXXC motif mediated effects can be distinguished. Finally, EV control cells, will evaluate the effect of the puromycin resistance gene which is under CMV bicistronic regulation. Overexpression of puromycin may affect cell growth parameters and must be controlled with respect to the various BCAT1 transgenic cells.

4.2.1 Objectives

- Subclone *BCAT1*(WT) and respective *BCAT1* CXXC motif mutant genes from the pCMV6-Entry construct to the Origene Lentiviral pLenti vector (Figure 4.2) and confirm successful ligation by DNA sequence analysis.
- Generate infectious Lentiviral particles containing the various pLenti-*BCAT1* constructs – *BCAT1*(WT), *BCAT1*(C338S), *BCAT1*(C335/8S) and Control(EV), using the viral packaging cell line, HEK293T (ATCC CRL-3216). Successful production of viral particles in culture supernatant will be determined by ELISA, targeting the p24 viral coat protein.
- Transfect U937 cells (ATCC CRL 1293.2) with respective Lentiviral particles creating four transgenic cell lines 1) U937-Control(EV), 2) U937-*BCAT1*(WT), 3) U937-*BCAT1*(C338S) and 4) U937-*BCAT1*(C335/8S). Puromycin will be used to select transgenic cells and ensure stable transfection.
- Validate stable transfection by evaluating *BCAT1* expression at the transcript level via qPCR. Confirm expression of *BCAT1* protein in WT, CXXC motif mutant and EV cell lines by Western Blot analysis targeting the Myc/DDK tag.

4.3 Methods

4.3.1 Subcloning pLenti-BCAT1 vector

BCAT1(WT) and CXXC motif mutants – *BCAT1*(C338S) and *BCAT1*(C335/8S) were subcloned from the respective pCMV6-*BCAT1* constructs (generated by site directed mutagenesis Section 2.6) into a pLenti destination vector (Figure 4.2, A) using Origene's precision shuttle system. Briefly 5 µg respective pCMV6-*BCAT1* construct and pLenti plasmids were digested with 2µL *Asi*I and *Mlu*I restriction endonucleases for 4-6 h. Following digestion, excised *BCAT1*(WT) and respective *BCAT1* CXXC motif mutant cDNA and linearized pLenti were separated by gel electrophoresis prior to gel purification and ligation. Competent *E.coli* α-Select Gold Efficiency cells (Bioline BIO-85027) were transformed with the ligation mixture and inoculated onto LB agar supplemented with 35µg/mL chloramphenicol to select for pLenti positive colonies. pLenti-*BCAT1* construct positive colonies were discriminated from colonies containing uncut or re-circularised pLenti by Colony PCR using the V2 and FTAG primers (Section 2.4) . pLenti-*BCAT1* positive colonies were expanded and pLenti-*BCAT1* plasmids purified prior to DNA sequence analysis using the V2 and FTAG sequencing primers. See section 2.5 to 2.8.

4.3.2 Transcription analysis of *BCAT1* expression

In order to select a model cell line appropriate for overexpression, *BCAT1* transcript levels were analysed in HL-60 (ATCC CCL-240), K562(ATCC CCL-243), U937(ATCC CRL1593.2) and THP1(ATCC TIB-202). Data was provided by <https://www.proteinatlas.org/cell>. U937 cells were selected based on their relatively

low background of BCAT1 expression in combination with favourable growth characteristics compared to THP1.

4.3.3 Stable Transduction of BCAT1(WT) and CXXC Motif Mutant U937 Cells

Lentiviral p'articles containing the pLenti empty vector (EV) control, *BCAT1*(WT), *BCAT1*(C338S) and *BCAT1*(C335/8S) vector constructs were generated using Origene's Lenti-vpak packaging system as described in Section 2.16. Viral titres were performed prior to U937 cell transduction as described in Section 2.17. To ensure maximum lentiviral transduction, U937 cells were subject to 'spinoculation as described in Section 2.20. Successful transfection of U937 cells was confirmed following puromycin selection by qPCR as described in Section 2.21. To confirm stable transfection and overexpression of *BCAT1*(WT), *BCAT1*(C338S) and *BCAT1*(C335/8S), transgenic U937 cells were verified by Western Blot analysis using the Anti-Myc/DDK (FLAG)-HRP mAb (OriGene) as described in Section 2.22. The *BCAT1*(WT), *BCAT1*(C338S), *BCAT1*(C335/8S) and *EV control* transgenic U937 cells were maintained in culture under 0.5 µg/ml puromycin selection pressure for up to 30 subcultures.

4.4 Results

4.4.1 Subcloning *BCAT1*(WT) and respective CXXC motif mutant clones to pLenti vector

To produce pLenti- *BCAT1* vectors, *BCAT1* and respective CXXC mutant cDNA was excised from the previously synthesised pCMV6 Entry vector constructs (see chapter 3), by restriction endonuclease digestion and isolated by gel electrophoresis. Successful excision of each *BCAT1* clone from respective pCMV6 Entry vectors was confirmed by the presence of 1.16 kb and 4.9 kb bands representing *BCAT1* and linearized pCMV6 respectively (Fig 4.4 Panel A). Successful insertion of *BCAT1* into destination vectors was confirmed by the presence of 1.16 kb and 6.9 kb fragment representing *BCAT1* and linearised pLenti respectively. (Fig.4.4 Panel B). pLenti-*BCAT1*(WT) and respective CXXC motif mutant cDNA sequence and reading frame fidelity was confirmed by DNA sequence analysis and NCBI-Blast alignment with pLenti sequence generated *in silico* using the Serial Cloner program (Appendix A). Mutant CXXC sequence variations were highlighted using the M-Coffee multiple sequence alignment tool (CRG, France) (Fig 4.5).

4.4.2 Transcription analysis of *BCAT1* expression

To determine the best cellular model for overexpression of *BCAT1*(WT) and CXXC motif mutants, native transcript levels on *BCAT1* in the myeloid cell lines - HL-60, K562, U937 and THP1 were examined using data from <https://www.proteinatlas.org/cell>. The analysis show that HL-60 and K562 both displays relatively high expression of *BCAT1* at 81.9 and 78.9 transcripts per million (TPM) (Figure 4.5). U937 displays lower expression at 48 TPM, a 41% reduction compared to HL-60. THP1 displays an even lower basal

expression of 29.5 TPM a 64% reduction compared to HL-60. On the basis of the data presented, U937 cells were selected for transduction.

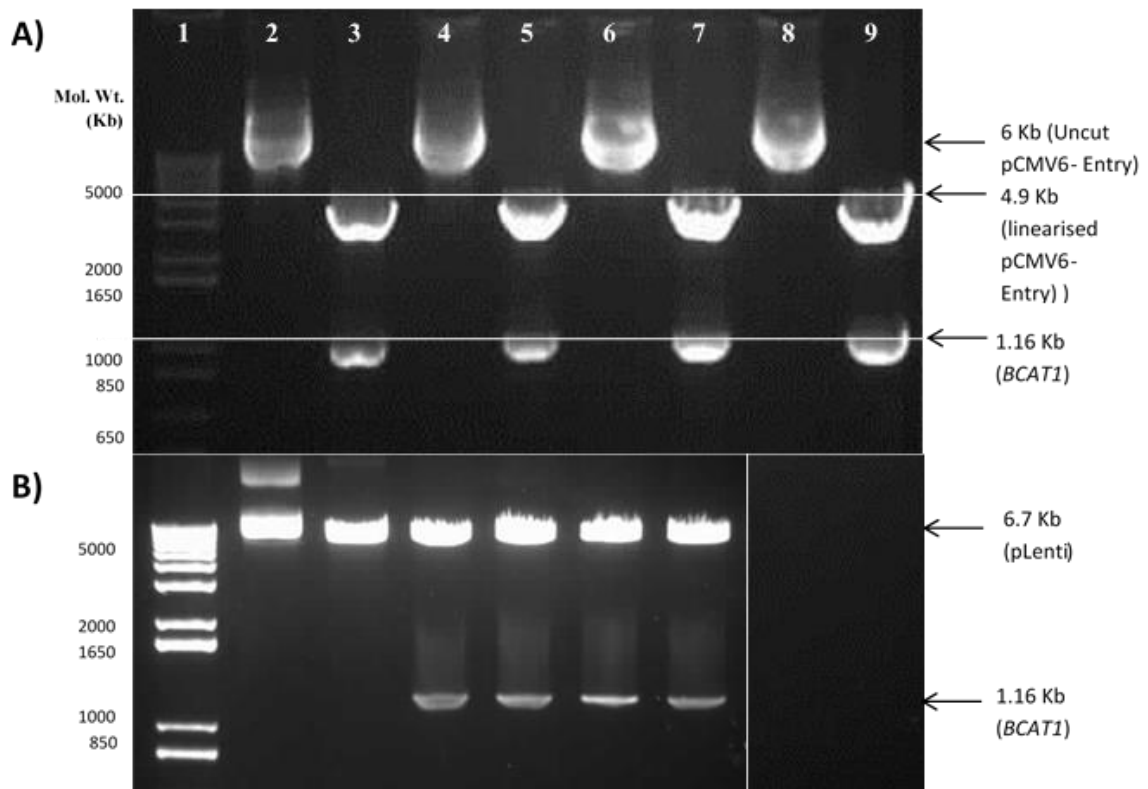


Figure 4.3 Subcloning *BCAT1* WT and CXXC motif mutants from pCMV6-Entry vector to pLenti destination vector. **A)** pCMV6-*BCAT1*(WT) and respective CXXC motif mutants (*C335S*, *C338S*, *C335/8S*) were AsiI and MluI digested and separated by agarose gel electrophoresis prior to ligation into pLenti destination vector. **B)** Recombinant pLenti-*BCAT1* constructs were digested and analysed by agarose gel electrophoresis to confirm *BCAT1* insertion. Gel loading was as follows:

- A)** Lane 2-9 100ng DNA per well. Lane 1: 5 μl 1 kb Plus DNA ladder. Lane 2: pCMV6-*BCAT1*(WT) (6 kb). Lane 3: digested pCMV6-*BCAT1*(WT) Lane 4: pCMV6-*BCAT1*(*C335S*) Lane 5: digested pCMV6-*BCAT1*(*C335S*) Lane 6: pCMV6-*BCAT1*(*C338S*) Lane 7: digested pCMV6-*BCAT1*(*C338S*) Lane 8: pCMV6-*BCAT1*(*C335/8S*) Lane 9: pCMV6-*BCAT1*(*C335/8S*)
- B)** Lane 2-7 100ng DNA per well. Lane 1: 5 μl 1 kb Plus DNA ladder. Lane 2: pLenti Lane 3: digested pLenti Lane 4: digested pLenti- *BCAT1*(WT) Lane 5: digested pLenti- *BCAT1*(*C335S*) Lane 6: digested pLenti- *BCAT1*(*C338S*) Lane 7: digested pLenti- *BCAT1*(*C338S*)

A)

pCMV6-BCAT	177	CTTTGTACAGTATATCAGAACTGGGCA	AACAACAC	CAGGCTGTACCAGAGCCAAACATCT
C335S	177	CTTTGTACAGTATATCAGAACTGGGCA	AACAACAG	CAGGCTGTACCAGAGCCAAACATCT
C338S	181	CTTTGTACAGTATATCAGAACTGGGCT	AACAACAC	CAGGCTGTACCAGAGCCAAACATCT
C335/8S	176	CTTTGTACAGTATATCAGAACTGGGCT	AACAACAG	CAGGCTGTACCAGAGCCAAACATCT

B)

pLenti-BCAT	174	CGCCTTTGTACAGTATATCAGAACTGGGCA	AACAACAC	CAGGCTGTACCAGAGCCAAACA
C335S	178	CGCCTTTGTACAGTATATCAGAACTGGGCA	AACAACAG	CAGGCTGTACCAGAGCCAAACA
C338S	179	CGCCTTTGTACAGTATATCAGAACTGGGCT	AACAACAC	CAGGCTGTACCAGAGCCAAACA
C335/8S	176	CGCCTTTGTACAGTATATCAGAACTGGGCT	AACAACAG	CAGGCTGTACCAGAGCCAAACA

Figure 4.4 Sequence alignment of pCMV6-Entry and pLenti constructs containing *BCAT1*(WT) and CXXC motif mutants. *BCAT1*(WT) and respective CXXC motif mutants were sub cloned from **A)** pCMV6-Entry constructs into **B)** pLenti destination vectors (Origene). Sequences were analysed using M-Coffee (OmicX, France) multiple sequence alignment tool. Base substitutions highlighted in white shows CXXC mutations carried over successfully following subcloning process. Full reading frame analysis of each construct shows no additional mutations, orientation and fidelity of the insert was verified against *in silico* pLenti-*BCAT1* using NCBI's BLAST tool (Data not shown).

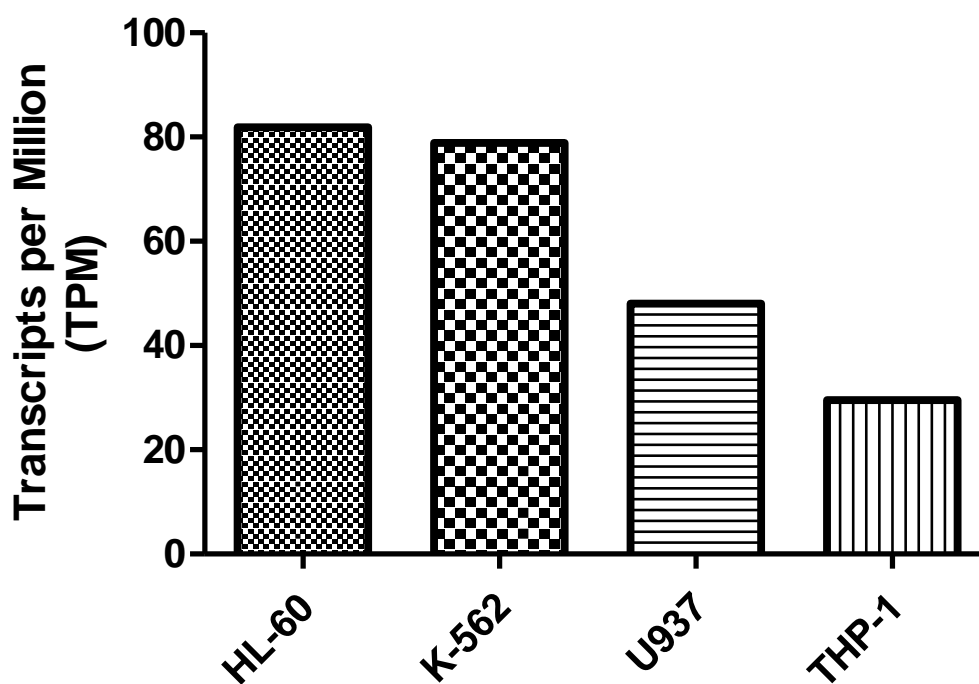


Figure 4.5 *BCAT1* transcript expression in immortalised leukaemia cell lines.

Comparison of *BCAT1* transcript levels in HL-60, K562, U937 and THP1. To select the appropriate model for transfection available cell lines were examined for basal *BCAT1* expression. Data provided by <https://www.proteinatlas.org/cell>

4.3.2 Lentiviral titre quantification

Following generation of infectious lentiviral particles containing the respective pLenti-*BCAT1* constructs generated by the HEK293T viral packaging cell, viral titre was assessed by measuring lentiviral coat protein p24 by ELISA using QuickTiter™ Lentivirus Titer Kit (Cell-Bio Labs no. VPK-107-T3) and sample titres were determined by comparison to p24 standard curve (Figure 4.6). The number of Lentiparticles is based on the assumption each viral particle contained an average of 2000 p24 coat protein molecules. The 4 viral constructs pLenti-*BCAT1(WT)*, pLenti-*BCAT1(C338S)*, pLenti-*BCAT1 (C335/8S)* and pLenti(EV) were measured at a density of 1.71×10^8 , 1.25×10^8 , 1.49×10^8 and 1.69×10^8 lentiparticles/mL respectively (Table 4.1).

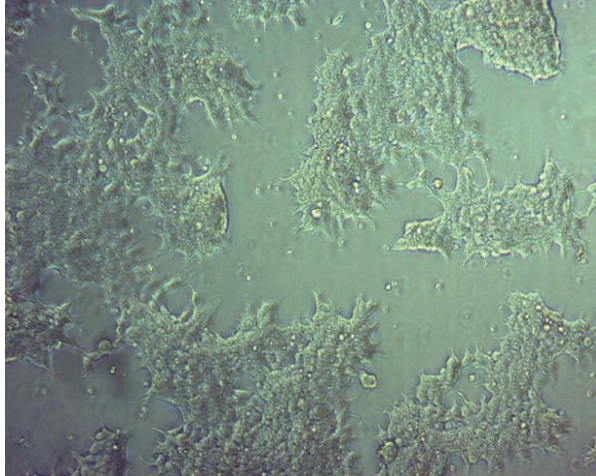
Table 4.1 Transducing units (TU) lentiviral titre calculated from p24 ELISA

<u>Lentiviral construct</u>	<u>p24(ng/mL)</u>	<u>Lentiparticles/mL</u>	<u>TU/mL</u>
pLenti- <i>BCAT1(WT)</i> -Myc-DDK	13.68	1.71E+08	1.71E+05
pLenti- <i>BCAT1(C338S)</i> -Myc-DDK	10.02	1.25E+08	1.25E+05
pLenti- <i>BCAT1(C335/8S)</i> -Myc-DDK	11.92	1.49E+08	1.49E+05
pLenti-Myc-DDK	13.51	1.69E+08	1.69E+05

4.4.3 Generation of *BCAT1* transgenic U937 cells

U937 cells were transduced with pLenti-*BCAT1* containing Lentivirus that integrates into the genome and induces constitutive expression of the *BCAT1* gene. Stable integration was selected for by puromycin resistance provided by the pLenti plasmid (Figure 4.2). A puromycin dose-response curve showed the lowest lethal dose of puromycin for U937 cells grown in a 96 well plate at a density of 0.5×10^6 cells/mL is $0.5 \mu\text{g/mL}$ (Fig 4.8, Panel A), therefore post transduction U937 cells were grown in complete RPMI supplemented with $0.5 \mu\text{g/mL}$ puromycin for several weeks until confluence demonstrating stable transduction. To confirm selection *wild-type* and transgenic U937 cells were grown in a 96 well plate at a density of 0.5×10^6 cells/mL supplemented with $0.5 \mu\text{g/mL}$ puromycin and viability was measured after 72 hours. Control U937 cells (non-transduced) display significantly reduced viability (12.1%) compared to EV, *BCAT1*(WT), *BCAT1*(C338S) and *BCAT1* (C335/8S) cells which retained 92.2, 98.3, 97.5 and 96.4% viability respectively (Fig 4.8 Panel B, n=3, One-way ANOVA $p < 0.0001$).

A)



B)

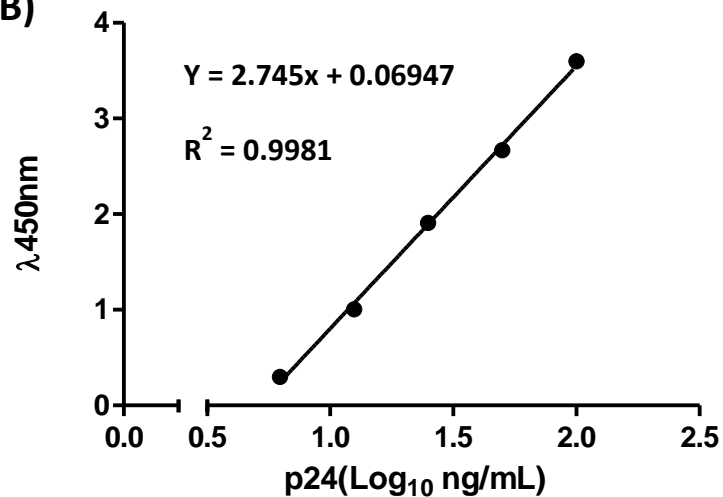


Figure 4.6 Generation and quantification of Lentivirus. Generation of infectious pLenti-*BCAT1* viral particles produced in HEK293T cells. **A)** Transduction of pLenti-*BCAT1* and packaging plasmids was carried out at approximately 70% confluence (100x magnification). Lentiviral particles were harvested from culture medium 2-3 days after transfection. **B)** Standard curve of p24 viral coat protein. Lentiviral concentration was determined by ELISA assay targeting Lentiviral associated p24 viral coat protein. ½ serial dilution was used to generate p24 standard curve plotted against absorbance at λ450nm. Standard was used to calculate the number of Lentiparticles (Table 4.1).

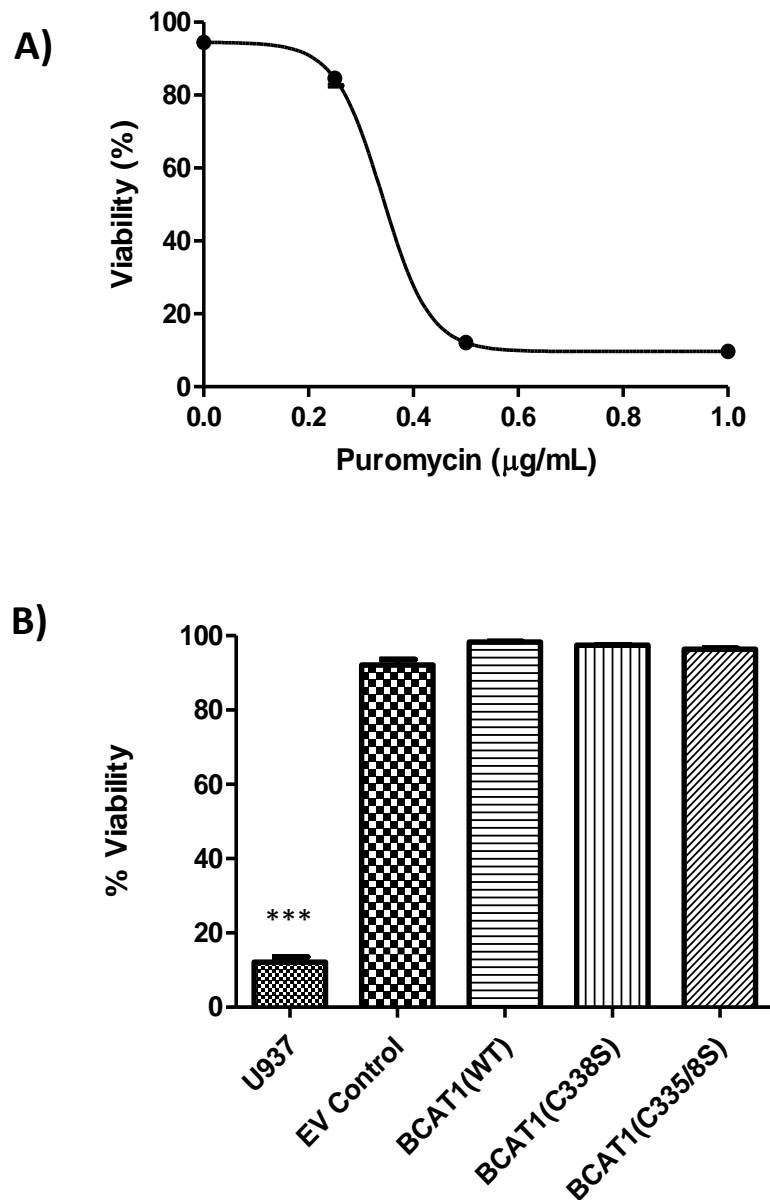


Figure 4.7 Antibiotic selection of transgenic cell lines. U937 puromycin cytotoxicity assay. **A)** Dose response curve for control U937 cells treated with 0-1 µg/mL puromycin for 72h (n=3, $R^2 = 0.9981$ as determined by non-linear regression). Minimum inhibitory concentration for selection of transgenic cell lines was determined as 0.5 µg/mL. **B)** Stable transduction of each transgenic cell line was confirmed through incubation with 0.5 µg/mL puromycin for 72h. Cell viability was determined by flow cytometric analysis (Viacount reagent, Merck-Millipore). (n=3, One-way ANOVA with Bonferroni post-hoc test, ***p<0.001)

4.3.5 Relative quantification of *BCAT1* expression

BCAT1(WT) and respective CXXC mutant motif transcript overexpression in Lentiviral transduced U937 (ATCC CRL1593.2) cells was measured by qPCR. Prior to the assay, total RNA was extracted from respective transgenic U937 cells using Bioline's isolate II RNA mini kit (BIO-52072) and checked for degradation by gel electrophoresis. The presence of distinct bands representing the 28S:18S ribosomal RNA subunits in a ratio ≥ 2 indicates intact RNA suitable for downstream analysis (Schroeder *et al.*, 2006) (Figure 4.8). The qPCR primers - *BCAT1*-F/*BCAT1*-R targeting *BCAT1*, and reference gene primers $\beta 2M$ -F/ $\beta 2M$ -R (Section 2.4), targeting reference gene Beta-2-microglobulin ($\beta 2M$), were assessed *in silico* by the NCBI primer blast tool, which predicted specific PCR products of 90 and 101 bp respectively (Figure 4.9, panel A), as well as potential non-specific primer dimer (Figure 4.9 panel B). Therefore, a gradient PCR to optimise assay annealing temperatures and eliminate non-specific products was performed. Non-specific products were detected by the presence of a low weight band in the amplification of *BCAT1* at 57, 59 and 61°C. No PCR product was seen at 63 and 64°C (Figure 4.9 panel A). Similarly, $\beta 2M$ amplification displayed non-specific bands at 57, 59 and 61°C and no PCR product was seen at 63 and 64°C (Figure 10 panel B). Another important parameter governing qPCR reliability is the relative cycling efficiency of the target and reference primers, therefore a calibration curve was generated for each primer pair. The amplification efficiency was calculated using the equation $e = 10^{-1/\text{slope}}$, where $1.8 \leq e \leq 2.2$ represents acceptable limits (Schmittgen and Livak, 2008). The data illustrate that *BCAT1* displays a cycling efficiency of 110% (Figure 4.11 panel A. $e = 2.21$, $r^2 = 0.99$) compared to 100% for $\beta 2M$ (Figure 4.11 panel B, $e = 2.0$, $r^2 = 0.99$). Expression

fold change was calculated using the $2^{-\Delta\Delta C_p}$ method (Section 2.21), where *BCAT1* expression is normalised to β 2M and compared between U937 non-transduced controls and respective transgenic U937 cells. The data show that mean expression increased 5.57 ± 0.76 fold for *BCAT1(WT)* and 5.93 ± 1.52 fold for *BCAT1(C338S)* which was significantly higher than the Empty Vector control, which increased modestly by 0.79 ± 0.48 fold (Figure 4.13 n=3, One-way ANOVA $p < 0.05$). *BCAT1(C335/8S)* displayed a fold change of 8.75 ± 4.19 , the highest average increase, although this increase was not significantly different from *BCAT1(WT)* or *BCAT1(C338S)* (Data summarised in Table 4.2).

Table 4.2 Fold change in *BCAT1* mRNA following transgenic overexpression

Cell line	Fold Expression change (Mean \pm SEM)
Control (EV)	0.79 ± 0.48
BCAT (WT)	5.57 ± 0.76
BCAT1 (C338S)	5.93 ± 1.52
BCAT1 (C335/8S)	8.75 ± 4.19

Representative qPCR amplification curves for fold expression change show where C_p threshold (horizontal red line) is breached at $C_p=21$ for U937-*BCAT1(WT)* (Dark Blue) vs $C_p= 24$ for U937 non-transduced controls (Blue) (Figure 4.12, panel A). Given β 2M reference genes (Orange/Yellow) are relatively stable for both U937 non-transduced controls and U937-*BCAT1(WT)*, this represents approximately an 8x fold increase in relative *BCAT1* expression. The data also show template controls (Purple), which display

non-specific amplification of BCAT1 primers after 27 cycles, denoting the detection limits of the assay at 63°C annealing temperature. Melt curve analysis reveals two distinct PCR products representing *BCAT1* (Blue) and β 2M (Orange) and non-specific PCR product (purple) in no template control wells. (Figure 4.12 panel B, n=3).

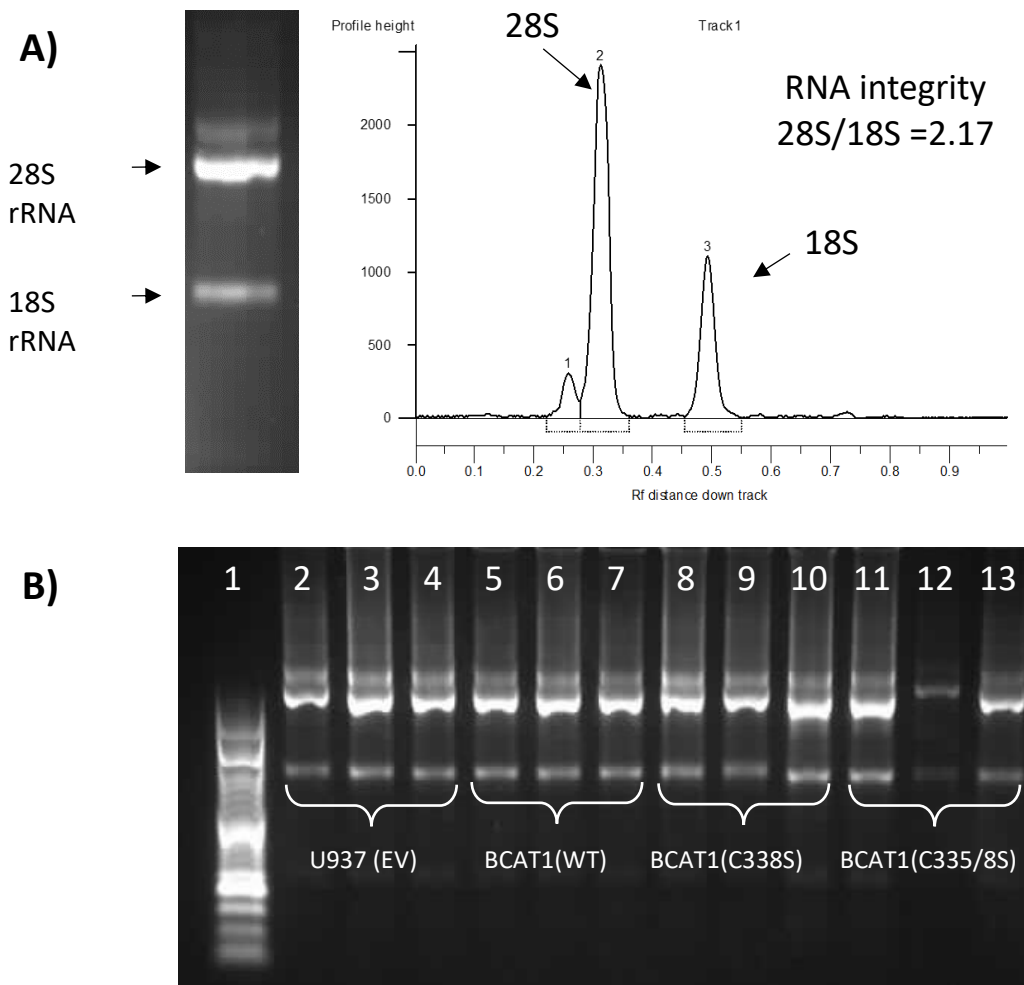


Figure 4.8 Analysis of RNA integrity extracted from U937 cell. A) Densitometric analysis of RNA agarose gels. Total RNA was extracted from transgenic and non-transgenic U937 cells using the isolate II RNA extraction kit (Bioline). Bands represent ribosomal subunits 28S and 18S. A 28S:18S rRNA ratio ≥ 2 indicates intact RNA suitable for downstream analysis(Full RNA analysis see Appendix B). Representative graphical presentation of band intensity displays desired 2:1 ratio. **B)** Representative agarose gel from RNA extracted from each transgenic U937 cell line. Gel loading is as follows:

Lane 1. 1ul 1kb plus DNA ladder **Lane 2-4.** 100ng U937-EV RNA **Lane 5-7.** U937-BCAT1(WT) RNA **Lane 8-10** 100ng U937-BCAT1(C338S) RNA **Lane 11-13.** 100ng U937-BCAT1(C335/8S) RNA

A) >[NM_001178094.1](#) Homo sapiens branched chain amino acid transaminase 1 (BCAT1);

```
product length = 90
Forward primer 1   TGGAGAATGGTCCTAAGCTG 20
Template       1484 ..... 1503

Reverse primer 1   GCACAATTGTCCAGTCGCTC 20
Template       1573 ..... 1554
```

>[NM_004048.4](#) Homo sapiens beta-2-microglobulin (B2M), mRNA

```
product length = 101
Forward primer 1   ATGAGTATGCCTGCCGTGTG 20
Template       317 ..... 336

Reverse primer 1   GGCATCTTCAAACCTCCATG 20
Template       417 ..... 398
```

B) 1 dimer for: BCAT1R
5-gcacaattgtccagtcgctc->
| ||||| |
<-ctcgctgacctgttaacacg-5

```
BCAT1F with BCAT1R
BCAT1F
5-tggagaatggtcctaagctg->
||| | | | |
<-ctcgctgacctgttaacacg-5
```

Figure 4.9 qPCR primer pair optimisation. **A)** Sequence alignment of qPCR primers vs BCAT1 transcript variant 5 (NM_01178094) and β 2M templates. qPCR Primers pairs BCAT1-F/R and β 2M -F/R PCR product was verified *in silico* using the NCBI primer-BLAST tool (<https://www.ncbi.nlm.nih.gov/tools/primer-blast>). Predicted product lengths of 90 and 101 base pairs respectively confirmed suitable target sequences. Predicted dimerisation of BCAT1 primers. **B)** BLAST alignment predicted two possible dimer formations therefore a gradient PCR to optimise annealing temperatures and eliminate non-specific amplification was performed. BCAT1 and β 2M primer sequences were provided by Hattori et al 2017.

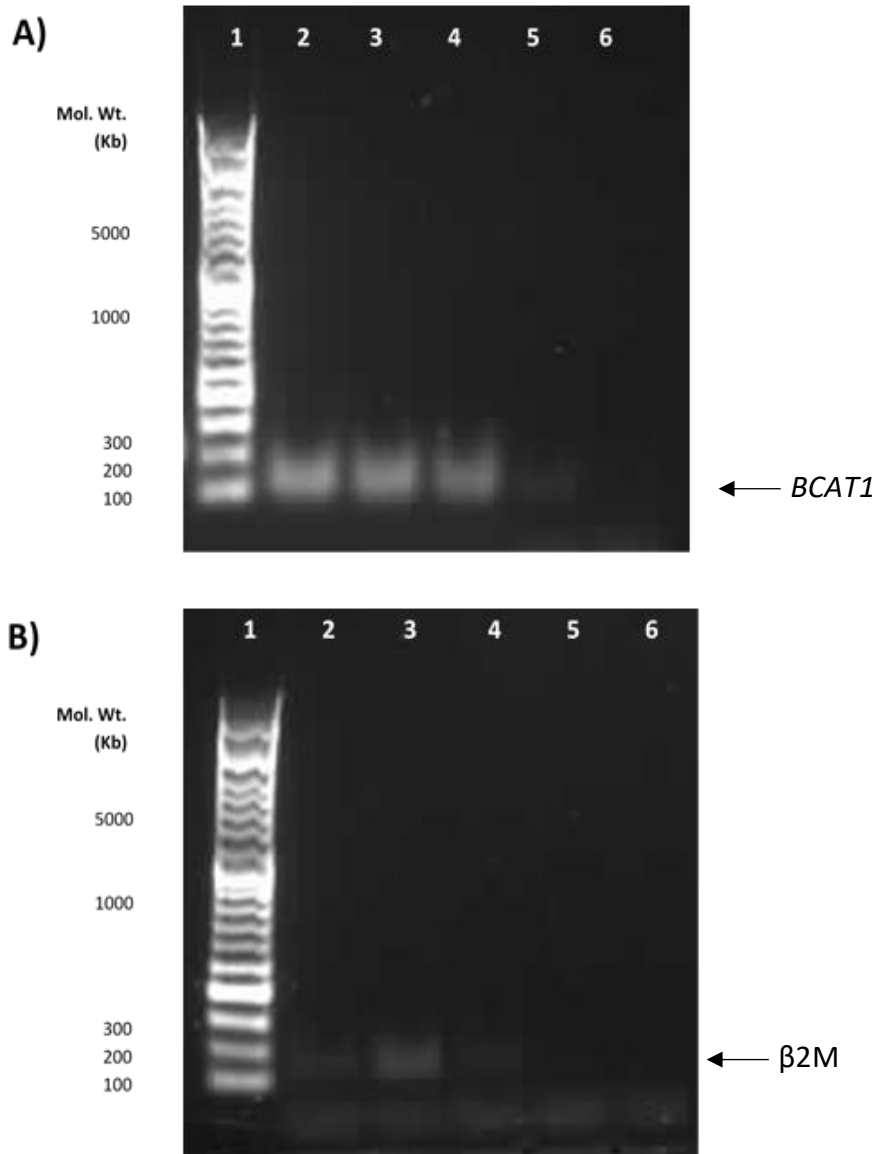


Figure 4.10 Optimisation of qPCR cycling parameters. Representative DNA agarose gel of gradient PCR products. Optimal annealing temperatures of qPCR primer pairs were determined by gradient PCR with no template to examine non-specific interactions e.g. primer dimers. PCR products were electrophoresed on a 1% agarose gel for 1 h. The minimum annealing temperature that produced ‘no’ non-specific product was selected for later qPCR runs. **A)** BCAT1-F and BCAT1-R primers. **B)** β 2M -F and β 2M -R. Loading for both gels is as follows: **Lane 1:** 1kb Ladder. **Lane 2:** 57°C **Lane 3:** 59°C **Lane 4:** 61°C **Lane 5:** 63°C and **Lane 6:** 64°C.

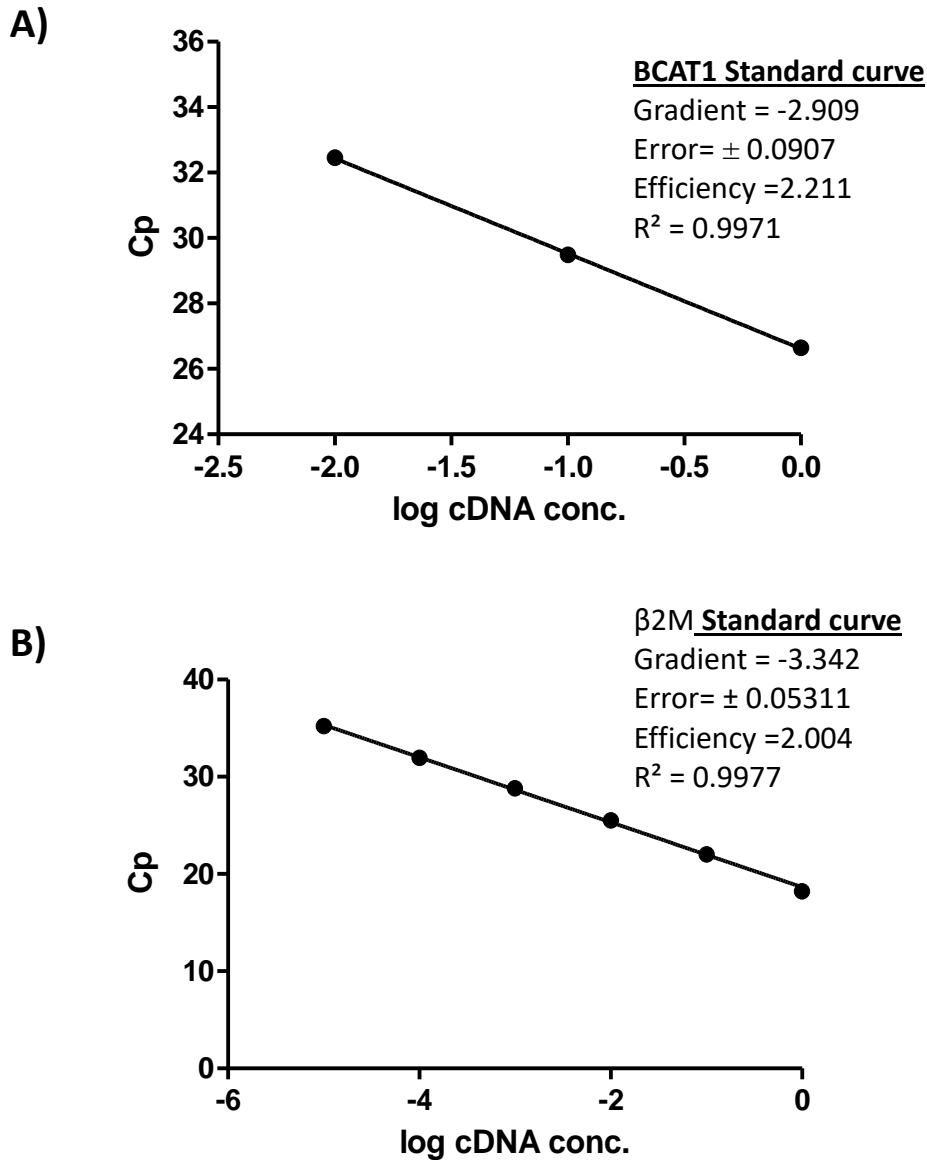


Figure 4.11 Calibration curves of BCAT1 and β2M primers. PCR amplification efficiency of the **A)** BCAT1 target gene and **B)** β2M reference gene was determined by generation of calibration curves. Following cDNA synthesis, a 10-fold serial dilution was performed and used as template for each data-point. Log cDNA concentration was plotted against the Crossing Point (Cp) value. Melt curve analysis confirmed target specific amplification (See appendices). Cycling efficiency was determined using the equation $E = 10^{(-1/m)}$ where E = efficiency, m = the slope of the standard curve. Data represents mean (n=2). Linear regression analysis was used to determine R^2 and gradient.

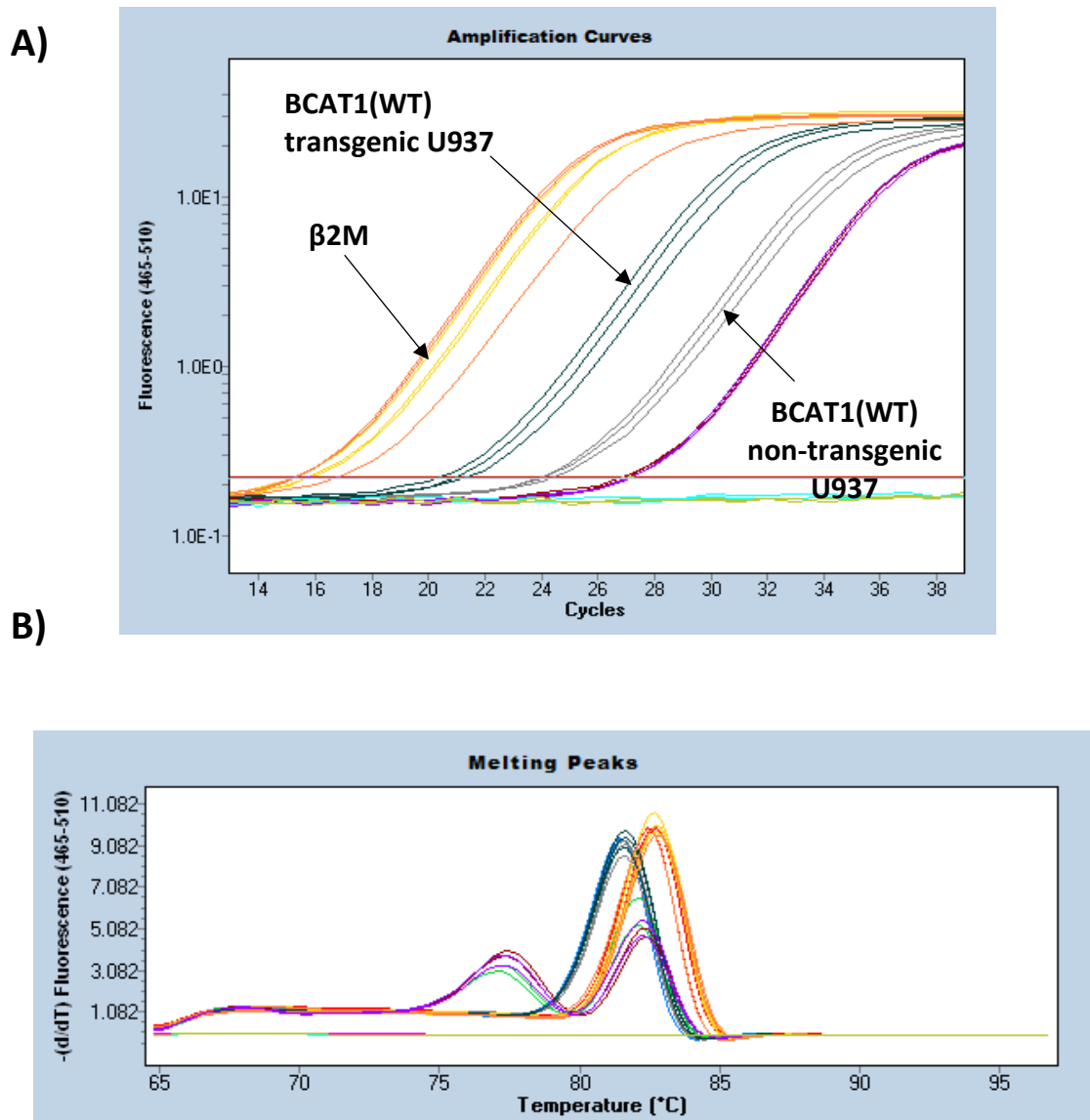


Figure 4.12 qPCR amplification curves and melt-curve analysis. **A)** Representative qPCR assay plot displaying comparative amplification of *BCAT1* target genes in U937 non-transduced control cells and U937-*BCAT1(WT)* overexpressing cells. Lines represent increasing fluorescence intensity U937 non-transduced (Blue), U937-*BCAT1(WT)* (Dark Blue), β 2M reference genes (Orange/Yellow), Crossing-point fluorescence threshold (horizontal red line). No template controls (Purple) display non-specific amplification of *BCAT1* primers after 27 cycles denoting the detection limit of the assay. **B)** Melt-curve analysis reveals two distinct PCR products representing *BCAT1* and β 2M and non-specific PCR products. (qPCR performed x12, n=3).

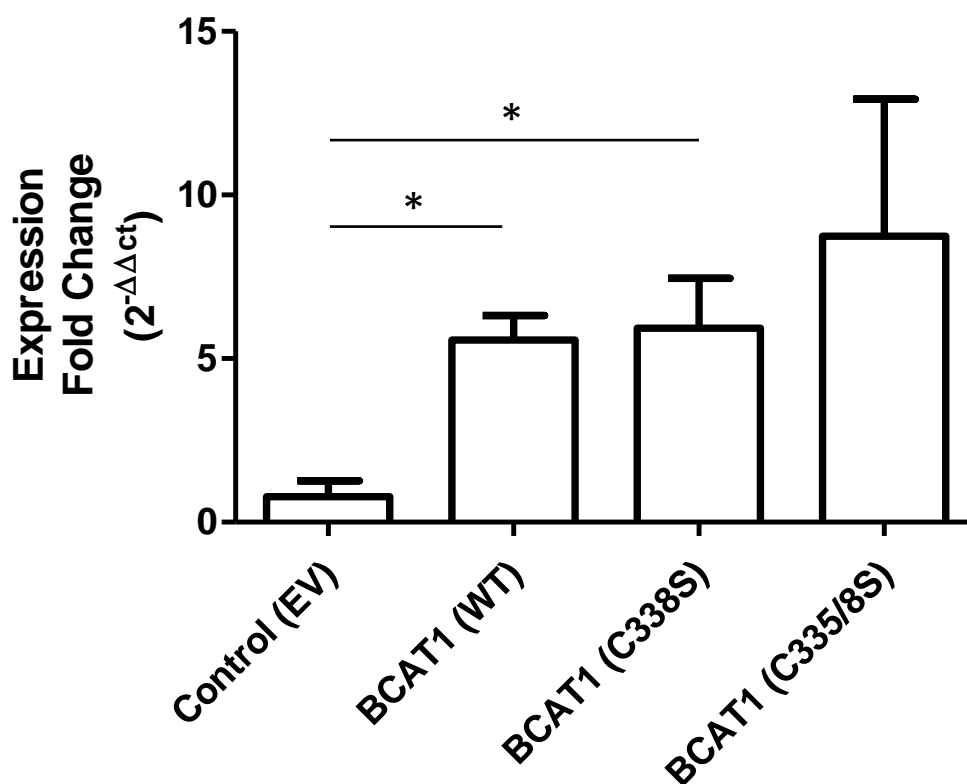


Figure 4.13 Fold expression change of BCAT1(WT) and CXXC motif mutants in transgenic U937 cells Fold expression change of transgenic cells compared to U937 transgenic EV control was quantified using relative quantification qPCR. Expression of *BCAT1* was calibrated against the reference gene Beta-2 Microglobulin (β 2M). Melt curve analysis confirmed amplification of two distinct products (Figure 4.12). Fold change was calculated using the $2^{-\Delta\Delta C_p}$ method (Data are mean \pm SD and analysed by one-way ANOVA with Bonferroni post-hoc test. * $p < 0.05$, $n = 3$).

4.3.6 Western blot detection of BCAT1 in U937

To ensure transcript overexpression translates to protein level, evaluation of BCAT1 transgenic protein from whole cell lysate was assessed by western blot analysis utilising the Anti-DDK (FLAG)-HRP mAb (OriGene). In order to define optimal detection parameters increasing loads of whole cell lysate from U937-BCAT1(WT) cells was incubated with different concentrations of Anti-DDK (FLAG) mAB (Origene clone OTI4C5) BCAT1 transgenic protein was detected in the range 1:1000 – 1:4000 therefore concentration of 1:2000 was selected for future experiments which concurred with the manufacturer's instructions (Figure 4.14). Following protein quantification by BCA assay, 30µg of whole cell lysate was loaded for each sample and separated by SDS-PAGE (Figure 4.15 Panel A). Presence of a 43kDa band signifies expression of transgenic Myc-DDK tagged BCAT1 protein in U937. BCAT1(WT) and BCAT1(C338S) was detected whilst no signal was detected for BCAT1(C335/8S) or Empty Vector (EV) control (Figure 4.15 B, n=3).

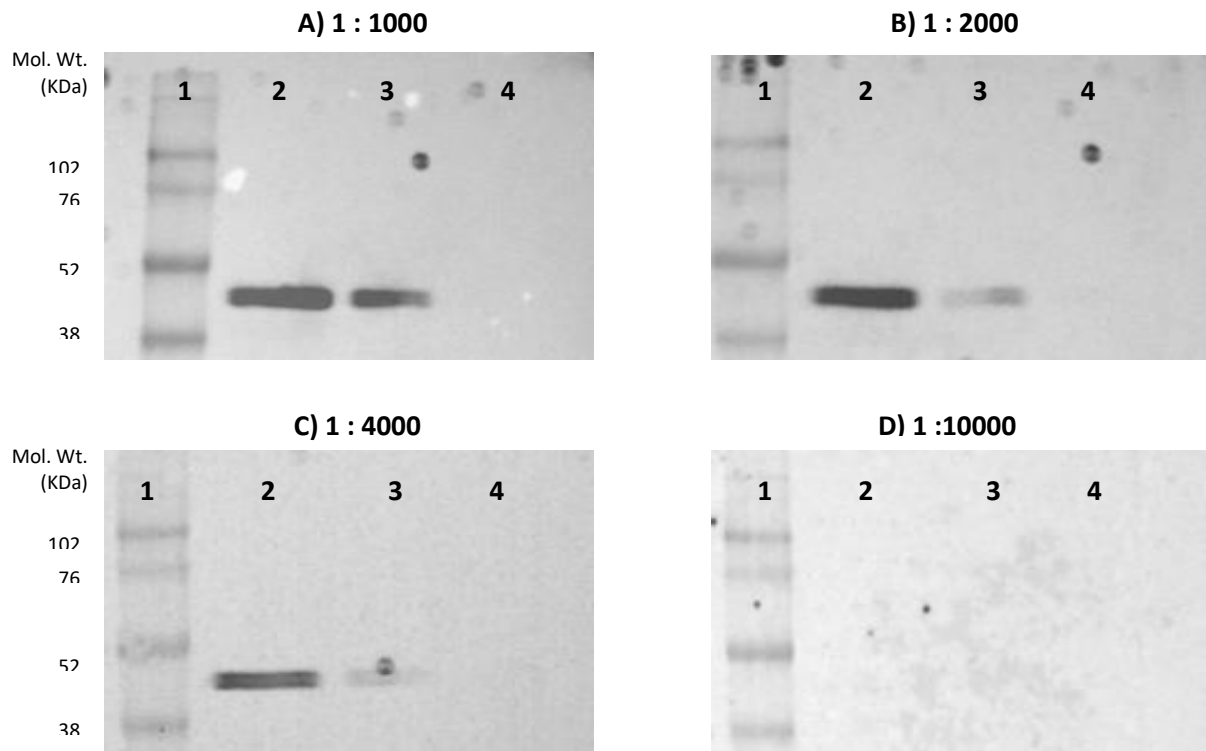


Figure 4. 14 Anti-Myc/DDK (FLAG) mAb titration by Western Blot analysis. In order to define optimal detection parameters, increasing loads of whole cell lysate from U937-*BCAT1(WT)* cells was incubated with different concentrations (**A** = 1:1000, **B** = 1:2000, **C** = 1:4000 and **D** = 1:10 000) of Anti-Myc/DDK (FLAG) mAb. Blots were loaded as follows: **Lane 1:** 5µl Full Range Rainbow Marker (Amersham) **Lane 2:** 30µg whole cell lysate, **Lane 3:** 15µg whole cell lysate and **Lane 4:** 5µg whole cell lysate.

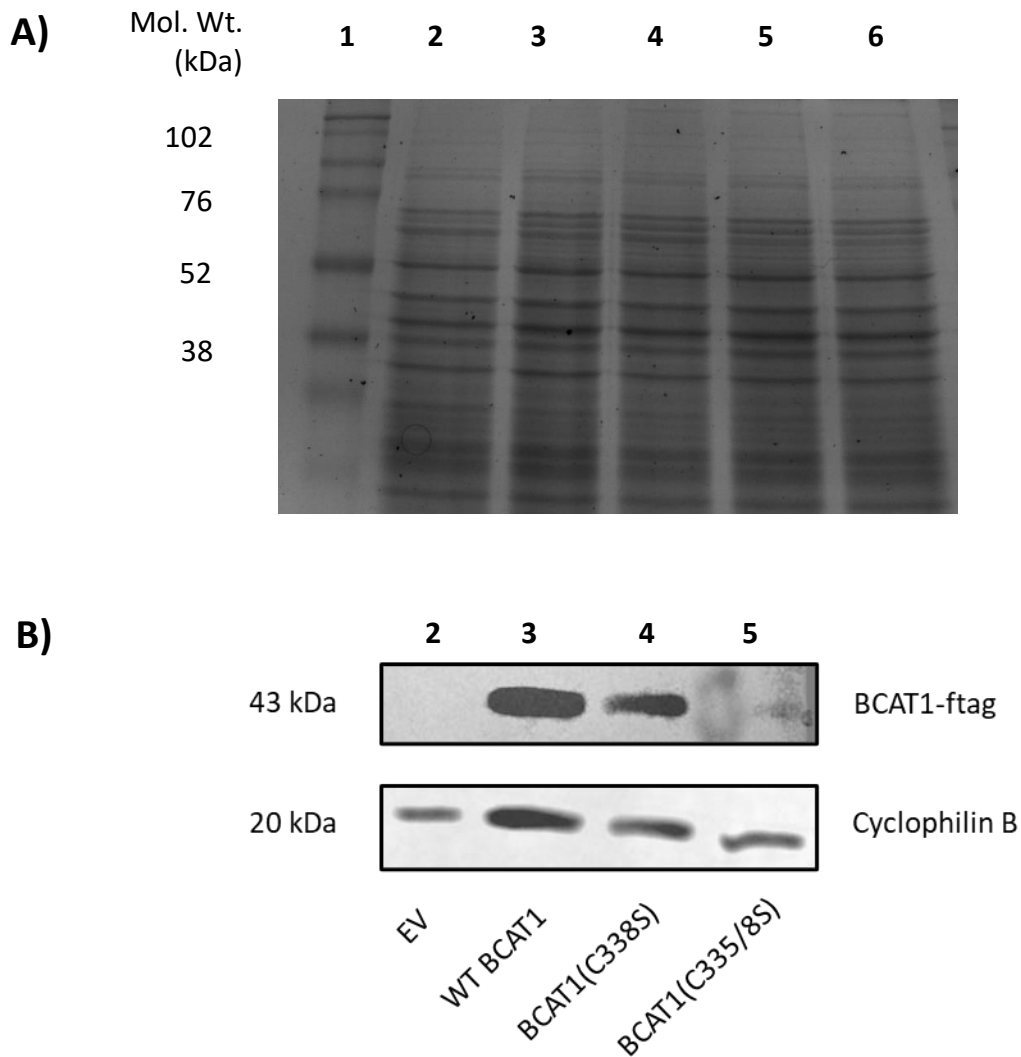


Figure 4.15 Protein expression validation of BCAT1(WT) and respective CXXC motif mutants in transgenic U937 cells SDS-PAGE and western blot analysis of U937 wild-type and transgenic cells. **A)** SDS-PAGE gel displays uniform equal sample loading prior to blotting. **B)** Detection of transgenic Myc/DDK tagged BCAT1 from whole cell lysate was by the BCAT1 Anti-Myc/DDK (FLAG) mAb. SDS-PAGE gels and Western blots were loaded as follows: **Lane 1.** 5ul Rainbow Ladder **Lane 2.** 30 μ g U937 non-transgenic whole cell lysate **Lane 3.** 30 μ g U937(EV) whole cell lysate **Lane 4.** 30 μ g U937-BCAT1(WT) whole cell lysate **Lane 5.** 30 μ g U937- BCAT1(C338S) whole cell lysate **Lane 6.** 30 μ g U937-BCAT1(C335/8S) whole cell lysate.

4.5 Discussion

The aim of this section was to generate a panel of transgenic AML cells that stably overexpress Control(EV), BCAT1(WT), BCAT1(C338S) and BCAT1(C338S) for subsequent *in vitro* characterisation (Chapter 5). Immortalised human cell line gene expression profiles reflect their underlying genetic abnormalities and correlate with cytogenetically analogous primary cell signatures, demonstrating them to be robust models for studying leukaemia (Andersson *et al.*, 2005; Rücker *et al.*, 2006). Since AML is characterised as a block in myeloid cell differentiation, the immortalised myeloid leukaemia cell lines, U937, HL-60, K562 and THP1, have all been successfully used to study differentiation of immature myeloid cells *in vitro* (Birnie, 1988; Park *et al.*, 2007; Yamamoto *et al.*, 2009; Huang *et al.*, 2014). Therefore, these cell lines are the ideal model to study the effect of *BCAT1(WT)* and *BCAT1* CXXC motif mutant overexpression in AML. Despite all these cell lines being myeloid in origin, significant variation in morphology, growth and expression profiles exist between cell lines, which must be considered when planning *in vitro* studies.

Expression of *BCAT1* mRNA transcript levels in the afore mentioned cell lines was examined using expression data provided by 'The Human Protein Atlas' (<http://www.proteinatlas.org>). Here it was theorised that the best cell model to examine the effect of *BCAT1(WT)* and respective CXXC motif mutant overexpression would be a cell line with a relatively low native BCAT1 expression, and therefore the highest expression delta post over-expression. Therefore, U937 was selected as the model cell line to explore the effect of *BCAT1 in vitro* based on relatively low basal *BCAT1* expression.

Infectious Lentiviral particles containing the pLenti-EV control, pLenti-*BCAT1(WT)*, pLenti-*BCAT1(C338S)* and *BCAT1(C335/8S)*, were subsequently generated in the HEK293T viral packaging cells using Origene's third generation Lenti-vpak packaging system (Origene ref: TR30022). Successful production of the virus in HEK293T cells was confirmed by physical titration utilising an ELISA which targeted viral coat protein p24 and quantified viral concentration by comparison against a known standard (Figure 4.6). However, physical viral titre i.e. the number of viral particles/mL, is notably different from functional viral titre which is quantified in Transducing Units (TU) and is the number of viral particles required to successfully transduce 1 cell (Klasse, 2015). Functional titre across various cell lines has been calculated using vector encoded reporter genes, for example green fluorescent protein (GFP) reporters are used to titrate viral concentration against the number of successfully transduced cells by flow cytometry. Using these methods the transduction efficiency of Lentiviral systems has been estimated to be 100-1000 fold lower than the physical titre (Kutner, Zhang and Reiser, 2009; Merten, Hebben and Bovolenta, 2016). Myeloid cells are relatively refractory to HIV-1 based Lentiviral infection due to myeloid-specific hydrolase SAMHD1 that that blocks reverse transcription of viral RNA (Hrecka *et al.*, 2011). Consequently Multiplicity of Infection (MOI) ratios required for the successful transduction of U937 cells are in the range of 80-100 (*Recommended lentivirus MOI for common cell lines*, Origene).

Given the refractory nature of myeloid U937 cells, a functional titre yield was calculated here by dividing physical yield by 1000, thus producing an estimated functional yield which ranged from 1.25 - 1.71×10^5 TU/mL across all pLenti vectors

(Table 4.1). This figure was comparable to the initial yield reported of HIV-1 based systems which ranged from $1 \times 10^{5-7}$ TU/mL (Dull *et al.*, 1998). In order to reach the recommended MOI of 80-100 for infection of refractory myeloid cells, a common step is to concentrate the viral suspension by ultracentrifugation at $80\,000 \times g$ increasing viral concentration 80-300 fold (Kutner, Zhang and Reiser, 2009). In place of this, centrifugal infection or 'spinoculation' where the initial transduction reaction is performed at up to $1200 \times g$ was performed here. This technique has been reported to increase viral transduction efficiency up to 40 fold, however other studies have reported more modest increases in efficiency (Tenser and Dunstan, 1980; O'Doherty, Swiggard and Malim, 2000).

Thus, using the 'spinoculation' method U937 cells were successfully transduced with Lentivirus containing pLenti-*BCAT1* and CXXC motif constructs. Successful transduction, where integration into the host genome and constitutive expression of CMV regulated genes, was confirmed by puromycin resistance for each transgenic U937 cell line (Figure 4.7). However, the number of Lentiviral integration events can vary in a dose dependant manner, resulting in different degrees of expression (Charrier *et al.*, 2011), therefore the level of *BCAT1* mRNA by qPCR was assessed. Fold changes in *BCAT1* transcript were significantly higher when compared with U937 non-transduced controls for *BCAT1(WT)* (5.57 ± 0.76 fold) and *BCAT1(C338S)* (5.93 ± 1.52 fold) whilst *BCAT1(C335/8S)* showed higher (8.75 ± 4.19 fold), with slight increase for pLenti-Control(EV) (0.79 ± 0.48 fold), which did not reach significance (Figure 4.13 and Table 4.2).

Gene expression under control of the Cytomegalovirus (CMV) promotor is widely used for ectopic gene overexpression, due to the relatively strong expression compared to other commonly used promotors (Xia *et al.*, 2006; Qin *et al.*, 2010). For example, CMV promotors were found to enhance expression 2-4 fold higher over Murine Leukaemia Virus (MLV) and 3-4 fold higher over Rous Sarcoma Virus long terminal repeat (RSV-LTR) (Pasleau *et al.*, 1985; Martin-Gallardo *et al.*, 1988). However, analysis of GFP reporter under CMV promotor control has shown that whilst CMV driven expression compares favourably to contemporary alternatives, such as the simian vacuolating virus 40 (SV-40) promotor, expression varies significantly depending on the gene and cell type (Qin *et al.*, 2010). A comparable study that used the CMV promotor driven vector and a lentiviral delivery system to overexpress the target genes in U937 reported a 5-10 fold increase in expression measured by qPCR (Kang *et al.*, 2014). These data reflect the fold-change gene expression of *BCAT1* as presented here (Table 4.2).

To confirm translation of *BCAT1* mRNA into protein, Western blot analysis was performed. These data revealed comparable levels of BCAT1(WT) and BCAT1(C338S) protein, reflecting the qPCR transcript expression data (Figure 4.16). However, BCAT1(C335/8S) expression was barely detectable and does not correlate with the qPCR data, which indicated relatively high yet variable expression of *BCAT1(C335/8S)* mRNA. Taken together, this may indicate that mutating both C335 and C338 residues results in post-transcriptional degradation by ribonucleases or post-translation degradation. The former explanation is previously demonstrated, where elimination of mRNA molecules by ribonucleases that are deemed 'non-functional' because they lack specific sequences, is demonstrated to play a role of transcriptional quality control (Sokhi *et al.*, 2013;

Chanfreau, 2017). In relation to *the BCAT1(335/8S)* transcript, is it possible that RNA interference by microRNAs or small interfering RNAs directed to the CXXC motif may, result in post-transcriptional silencing, which accounts for the more variable transcript expression of *BCAT1(C335/8S)* observed here (Dana *et al.*, 2017; O'Brien *et al.*, 2018). Alternatively, substitution of the N-terminal C335 residue of the CXXC motif which is S-glutathionylated at $\geq -280\text{mV}$ protecting the cysteine thiol from over oxidation and subsequent degradation, may have increased post-translation proteolysis (Grek *et al.*, 2013; Zhang *et al.*, 2018). Taken together, these combined theories potentially explain the variation in *BCAT1(C335/8S)* mRNA and lack of protein expression in the transgenic U937 cell model.

In summary, this chapter has demonstrated successful transduction and stable overexpression BCAT1(WT) and CXXC motif mutant BCAT1(C338S) at the transcript and protein level in the immortalised monocytic cell line U937. Degradation of BCAT1(C335/8S) either the transcript or protein level in U937 makes it unsuitable for examining the effect of abolishing the antioxidant capacity of the CXXC motif. Conversely the comparable expression levels BCAT1(WT) and BCAT1(C338S) detailed here and the comparable enzyme kinetics detailed in chapter 3 makes the transgenic U937- BCAT1(WT) and U937- BCAT1(C338S) a suitable model to evaluate the CXXC motif antioxidant hypothesis.

Chapter 5: The antioxidant role of the BCAT1-CXXC motif in oxidative stress induced differentiation and apoptosis in U937

5.1 Introduction

The metabolic role of BCAT1 in the cellular pathophysiology of cancer has been the subject of increasing interest in recent years and has been studied in various cancer models including AML (Zheng *et al.*, 2016; Raffel *et al.*, 2017; Thewes *et al.*, 2017; Xu *et al.*, 2018). BCAT1 catalyses the reversible deamination of Branched Chain Amino Acids (BCAA) Leucine, Isoleucine and Valine by transfer of an α -amino group to α -Ketoglutarate (α -KG) resulting in the production of Glutamate and Branched Chain Keto acids (BCKA). (Jamshid Davoodi *et al.*, 1998) BCKA are decarboxylated through the branched chain keto acid dehydrogenase complex (BCKADH) to Acetyl-CoA, which replenishes the Citric Acid Cycle (TCA) to produce ATP, however, where there is a build-up of BCKA, BCAT1 will favour the reverse reaction, generating BCAA and α -KG.

Through modulation of these key metabolites, BCAT1 has been demonstrated to exert diverse effects on key processes including proliferation, differentiation and epigenetic remodelling. For example in blast crisis CML (BC-CML), blocking BCAT1 expression or enzymatic activity induced cellular differentiation and impaired propagation *in vitro* and *in vivo* (Hattori *et al.*, 2017). In this model, BCAT1 drives leukaemia development through expression by increasing the intracellular pool of leucine, activating the mammalian target of rapamycin complex 1 (mTORC1), a key signalling complex that integrates upstream nutrient availability to downstream changes

in cell growth and survival (Laplante and Sabatini, 2009). Conversely in a published AML model, BCAT1 expression has been demonstrated to increase BCAA catabolism by restricting α -KG, leading to a DNA hypermethylation signature which is similar to IDH mutant cells, that produce the D-2-hydroxyglutarate (D-2-HG) oncometabolite, which is a competitive inhibitor of α -KG (Raffel, *et al.*, 2017). In another study this phenotype was associated with increased resistance to Reactive Oxygen Species (ROS) inducing Tyrosine Kinase Inhibitor therapy by BCAT1 mediated glutamate production, a precursor for the production major small molecule antioxidant GSH (Wang *et al.*, 2019). Whilst the metabolic effects of BCAT1 have received significant attention the antioxidant potential of BCAT1 CXXC motif has not been explored.

BCAT1 and the mitochondrial isoform BCAT2 both feature a conserved CXXC motif, which is characterised by two cysteine amino acids (C) separated by two other amino acids (X) located 10 angstroms from the active site. The metabolic activity of BCAT2 can be modulated by oxidation of CXXC motif cysteine thiol (-SH) groups, which form an intramolecular disulphide bond resulting in a conformational change that inactivates the enzyme (Myra E Conway, Poole and Hutson, 2004). Using the Nernst equation, Coles *et al* calculated the redox midpoint potential (E_m), that is the intracellular redox potential (E_h) at which the ratio of reduced/oxidised CXXC motif cysteines is equal to 1, was 80mV lower for BCAT1 CXXC motif compared to BCAT2 (Coles, Hancock and Conway, 2012). This demonstrated that the BCAT1 CXXC motif is more sensitive to oxidation or put another way it is more antioxidant (reductive) in nature than BCAT2.

Whilst oxidation of the BCAT2 CXXC motif results in enzymatic inactivation, oxidation of BCAT1 results in S-glutathionylation of the CXXC cysteine thiol groups, preventing disulphide bond formation and protecting the enzyme from inactivation (Conway *et al.*, 2008). Moreover, S-glutathionylation of BCAT1 links it to a wider antioxidant network, and importantly, deglutathionylation of BCAT1 using the GSH/glutaredoxin system suggests it may play an important role in cellular redox regulation. Interestingly, both BCAT1 and BCAT2 are reported to have equivalent sensitivities to reactive nitrogen species (RNS), suggesting that the decreased sensitivity of BCAT1 to ROS may be due to a putative oxidoreductase-like activity, similar to the human Glutaredoxin (Grx) and Thioredoxin enzymes (Rex) (Coles *et al.*, 2009, Coles *et al.*, 2012).

Redox systems such as the Grx and Trx systems are often dysregulated in malignant disease, which leads to defective control of redox homeostasis and consequent oxidative stress (Hanschmann *et al.*, 2013). Elevated ROS production promotes cellular growth through ROS regulated signalling pathways, however an excess of ROS can induce cellular differentiation and ultimately cell death as levels increase (Hole *et al.*, 2013; Lam *et al.*, 2018). In response to ROS, AML cells upregulate antioxidant enzymes such as Trx, which facilitate the reduction of other proteins by cysteine thiol-disulphide exchange, where interestingly the Trx oxidoreductase capacity is derived from its CXXC motif (Arnér and Holmgren, 2000; Collet and Messens, 2010; Kamal *et al.*, 2016). Trx expression is thus correlated with higher ROS production, which relates to poorer patient prognosis in AML (Chen *et al.* 2010). Moreover, inhibition of Trx increases AML cell sensitivity to the pro-oxidant Arsenic Trioxide (ATO), suggesting Trx

is protecting AML cells from ROS induced cell death (Jiang et al 2014). Whilst canonical antioxidants such as the Grx and Trx have been extensively studied, how the CXXC motif of BCAT1 affects the redox state of the cancer cell and how this impacts redox regulated processes such as proliferation, differentiation and survival remain unexplored.

5.2 Aims & Objectives

The aim of this chapter was to investigate the putative antioxidant effect of the BCAT1 CXXC motif on redox environment of the cell and how this affects redox mediated processes critical to the development of AML including, proliferation, apoptosis and differentiation, using the various U937 transgenic cells developed in Chapter 4.

5.2.1 Objectives

- *In vitro* growth characterisation of U937-(EV), U937-BCAT1(WT) and U937-BCAT1(C338S) cell lines. At each phase of growth (exponential/stationary/death) cell density and viability will be assessed by flow cytometric analysis. Concurrently the effect of the CXXC motif on redox environment of the cell will be analysed by comparison of intracellular ROS, redox potential (Eh), mitochondrial membrane potential (ψ_m) and GSH content in each cell line.
- Evaluate the capacity BCAT1 CXXC motif to ameliorate ROS induced apoptosis. U937-Control(EV), U937-BCAT1(WT) and U937-BCAT1(C338S) cell lines will be placed under serum starvation conditions inducing mitochondrially derived oxidative stress. Cellular survival will be monitored by flow cytometric analysis following 7AAD/Annexin V. Cellular ROS will be measured by 2',7' –dichlorofluorescein diacetate (DCFDA) staining.
- Evaluate the capacity BCAT1 CXXC motif to resist ROS induced differentiation. U937-Control(EV), U937-BCAT1(WT) and U937-BCAT1(C338S) cell lines will be induced to differentiate from monocyte to macrophage's using PMA. Following addition of PMA intracellular ROS will be measured by DCFDA staining. The level of cellular differentiation in each cell line will be compared by flow cytometric assessment of morphology and macrophagic cell surface markers CD36/CD11b.

5.3 Methods

5.3.1 Characterisation of BCAT1(WT) and CXXC Motif Mutant Transgenic Cells.

U937-Control(EV), U937-BCAT1(WT) and U937-BCAT1(C338S) transduced cells were cultured in T75 flasks seeded at 2×10^5 cells/mL in a total volume 10 mL and maintained at 37 °C and 5% CO₂ in complete RPMI-1640 for a total of 192 h. 100µL samples were taken at t=0 and at 24 h intervals from 0-96h and from 168-192 h. The number of viable/non-viable cells was determined by flow cytometry using Viacount staining as described in section 2.19. For each sample a minimum of 3×10^3 events were captured and cell viability and density were determined using the Easyfit algorithm (EasyCyte Software, Merck-Millipore).

Cellular proliferation during exponential phase was calculated using the equation: doubling time = $(t_1 - t_2) * \log(2) / (\log(n_1) - \log(n_2))$. Doubling time describes the time taken for cell number(n) to increase by a factor of two (2n) where t₁= initial time point, t₂=final time point and n₁ = initial cell concentration and n₂=final cell concentration (Roth, 2006 <http://www.doubling-time.com/compute.php>). Cell cycle analysis was performed for each transgenic cell line by Propidium Iodide (PI) staining as outlined in section 2.26. To evaluate intracellular ROS for each transgenic U937 cell line, DCFDA analysis was performed as described in section 2.27, following various treatments, including, serum starvation (section 2.30), Rotenone (section 2.31) and PMA induced differentiation (section 2.32). To monitor mitochondrial ROS levels following treatment, DiOC₂(3) assays were performed as outlined in section 2.31. Measurements of cellular 'reduced' to 'oxidised' glutathione levels (GSH/GSSG) were performed for each cell line following treatment as described in section 2.29.

5.3.2. Evaluation of the BCAT1 CXXC Motif in Myeloid Differentiation

To evaluate the effect of the BCAT1 CXXC motif on ROS mediated cellular processes, such as cellular differentiation, 1×10^6 cells/mL of each transgenic cell line was suspended in 0.5 mL complete RPMI \pm 1 to 10 ng/mL PMA and incubated for 72 h as described in section 2.32. To control for the contribution of cellular ROS in differentiation, 10 mM *N*-acetyl-L-cysteine (NAC) was added prior to incubation. Cellular differentiation was monitored for each transgenic U937 cell line over the 72 h period through expression of the myeloid markers CD11b and CD36 by flow cytometry (section 2.32 for flow cytometry gating strategy). CD11b⁺ and CD36⁺ positive cells were evaluated as an indication of cell surface expression level.

5.4 Results

5.4.1 Growth characterisation: Cell growth and density

To investigate the effect of the BCAT1 CXXC motif on the redox environment of the cell and how this impacts redox mediated processes critical to AML development including proliferation, apoptosis, and differentiation cell lines were initially characterised by *in vitro* flask cultures. U937-Control(EV), U937-BCAT1(WT) and U937-BCAT1(C338S) transgenic cells were cultured in T75 flasks seeded at 2×10^5 cells/mL in a total volume 10 mL and incubated in a cell culture incubator (37c 5% CO₂) for a total of 192 h. The data presented show that U937-BCAT(WT) and U937-BCAT1(C338S) reached significantly higher peak viable cell density at the end of the exponential growth phase (t=96h) compared to U937-(EV) control cells (Figure 5.1, $p < 0.001$). U937-BCAT(WT) cells plateaued at $1.57 \times 10^6 \pm 8.53 \times 10^4$ cells/mL compared to $1.51 \times 10^6 \pm 8.16 \times 10^4$ cells/mL for U937-BCAT1(C338S), and $1.01 \times 10^6 \pm 7.71 \times 10^4$ cells/mL for U937-Control(EV), equating to a relative increase in cell density of 155 % for BCAT1(WT) and 150 % for BCAT1(C338S) compared to the control (Figure 5.1, panel A). Analysis of cell proliferation over the exponential phase (t=24-72), revealed that both BCAT1 overexpressing U937 transgenic cell lines had significantly reduced doubling times compared to the control ($p < 0.001$, Figure 5.1, panel B). The data presented show that the doubling time for U937-BCAT1(WT) was 25.6 ± 0.7 h compared to 27.4 ± 0.6 h for U937-BCAT1(C338S) and 32.3 ± 1.6 h for the U937-Control(EV).

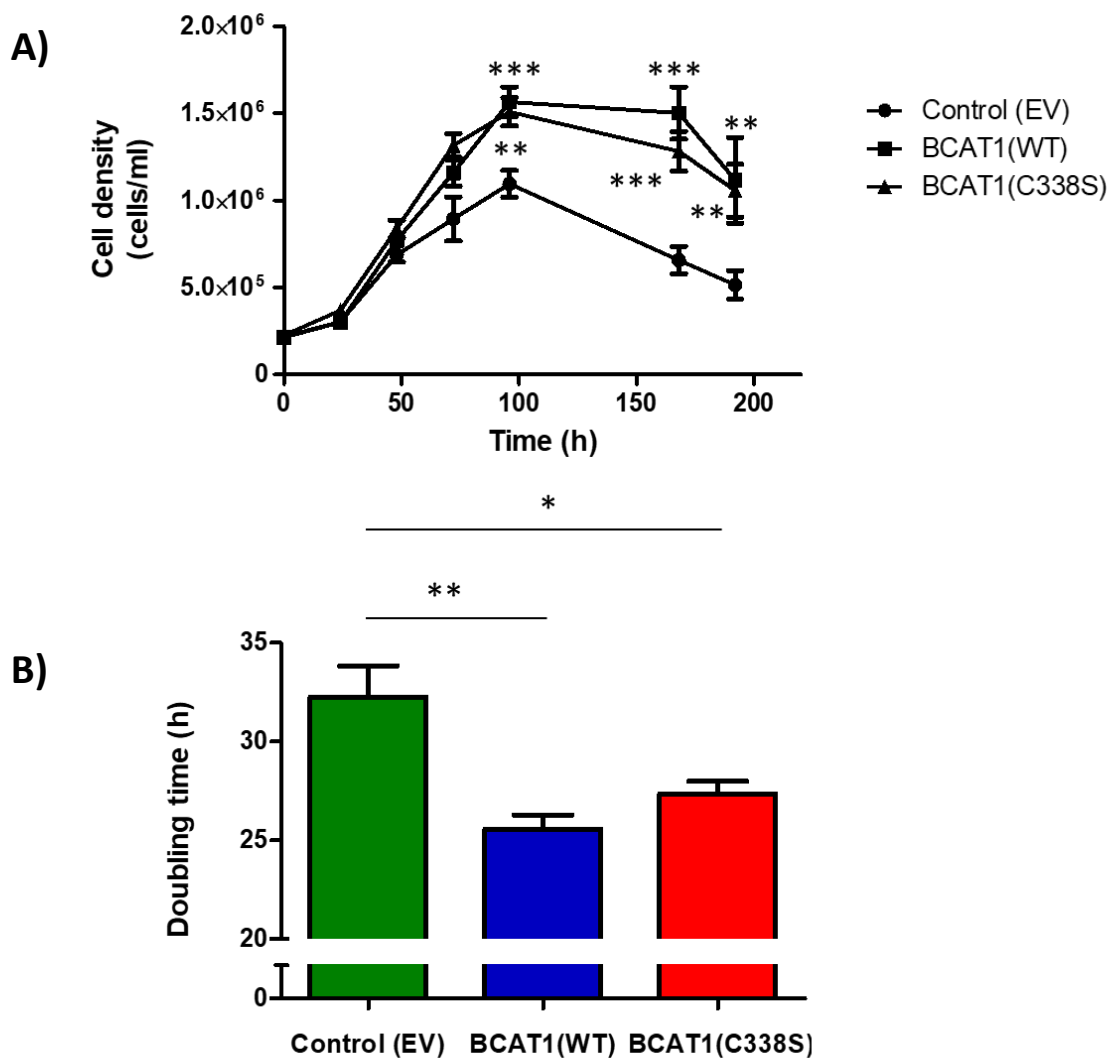


Figure 5.1 Growth profile of BCAT1 overexpressing and control U937 cells in culture.

A) T75 flasks were seeded with 2×10^6 BCAT1(WT), BCAT1(C338S) and Control(EV) U937 cells and cultured in 10mL of complete RPMI-1640. Viable cell counts were measured at 0h and after 24h, 48h, 72h, 96h, 168h and 192h. **B)** Doubling time was calculated between 24-72h. Data presented are mean \pm SEM (n=5). Data analysed by one/two-way ANOVA with Bonferroni post-hoc test (*p < 0.05, **p < 0.01, ***p < 0.001).

5.4.2 *Growth characterisation: Cell cycle analysis*

Analysis of DNA content at mid exponential phase (t=48), using PI staining shows that, both U937-BCAT1(WT) and U937-BCAT1(C338S) display a significantly higher proportion of cells in G2M phase $23.19\pm 1.4\%$ and $23.72\pm 1.2\%$ respectively, compared to the U937-Control(EV) $16.42\pm 1.4\%$ ($p < 0.01$, Figure 5.2)

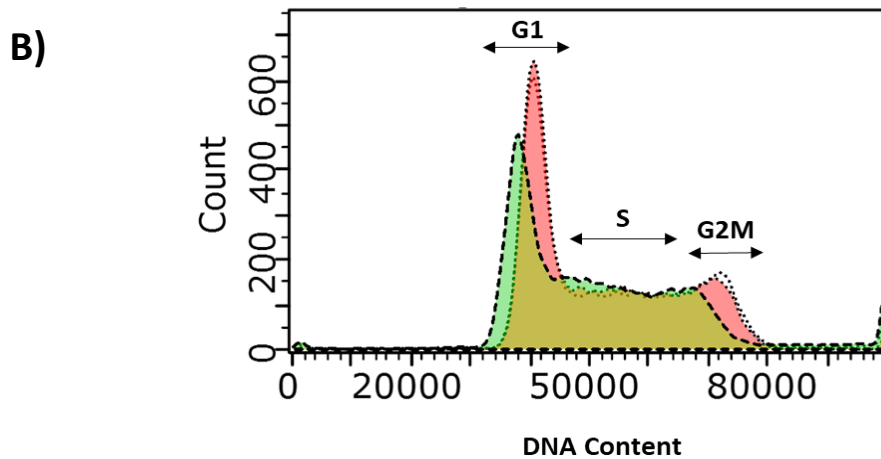
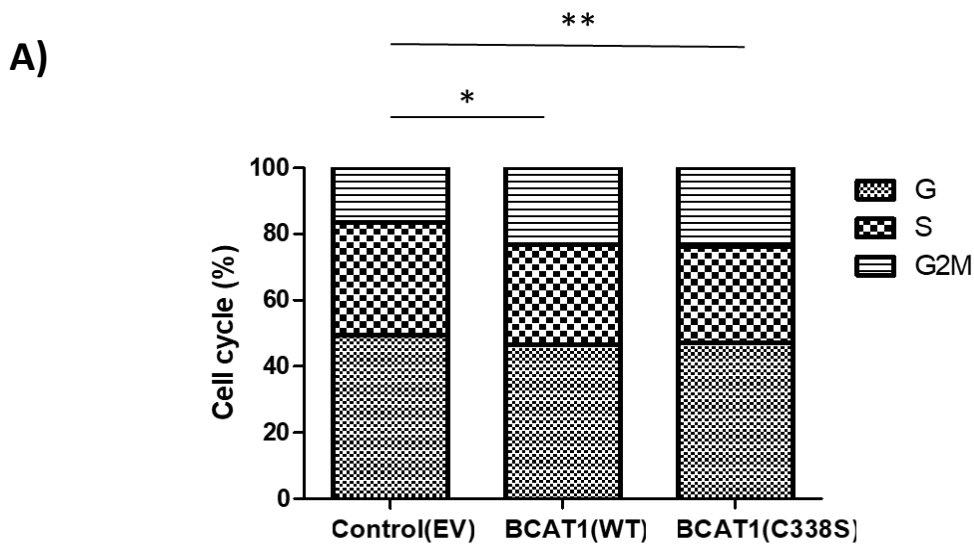


Figure 5.2 Effect of BCAT1(WT) and BCAT1(C338S) overexpression on cell cycle in U937 cells. **A)** Stacked bar chart displaying percentage of cells in G, S and G2M for U937 cell lines, proportion of G2M phase cells is significantly different between BCAT1(WT) and U937-BCAT1(C338S) compared to U937-Control(EV). **B)** Flow cytometry histograms displaying representative cell cycle data. U937-BCAT1(WT) (Dotted lines, no fill) and U937-BCAT1(C338S) (Dotted lines, red fill) cells display visibly higher proportion of dividing G2M cells represented by the 4n peak compared to the U937-Control(EV) (Dashed lines, green fill). Data presented are mean values (n=4) and analysed by One-way ANOVA, with Bonferroni post-hoc test (*p=0.05, **p=0.01)

5.4.3 Growth characterisation: Cell viability

To examine the effect of the BCAT1 CXXC motif on apoptosis in culture, the percentage of viable cells was measured by Viacount staining. Cell viability varied significantly between respective U937 transgenic cell lines from the late exponential phase (t=72) through to death phase (t=168/192). The data reveal that U937-BCAT1(WT) cells display consistently higher viability compared to U937-Control(EV) from t=72 onwards (Figure 5.3). U937-BCAT1(WT) cells were also significantly more viable (69.1±5.5%) compared to U937-BCAT1(C338S) (57.44±4.8%, $p<0.001$) and U937-Control(EV) (32.6±3.17%, $p<0.001$) at t=192 (Figure 5.3).

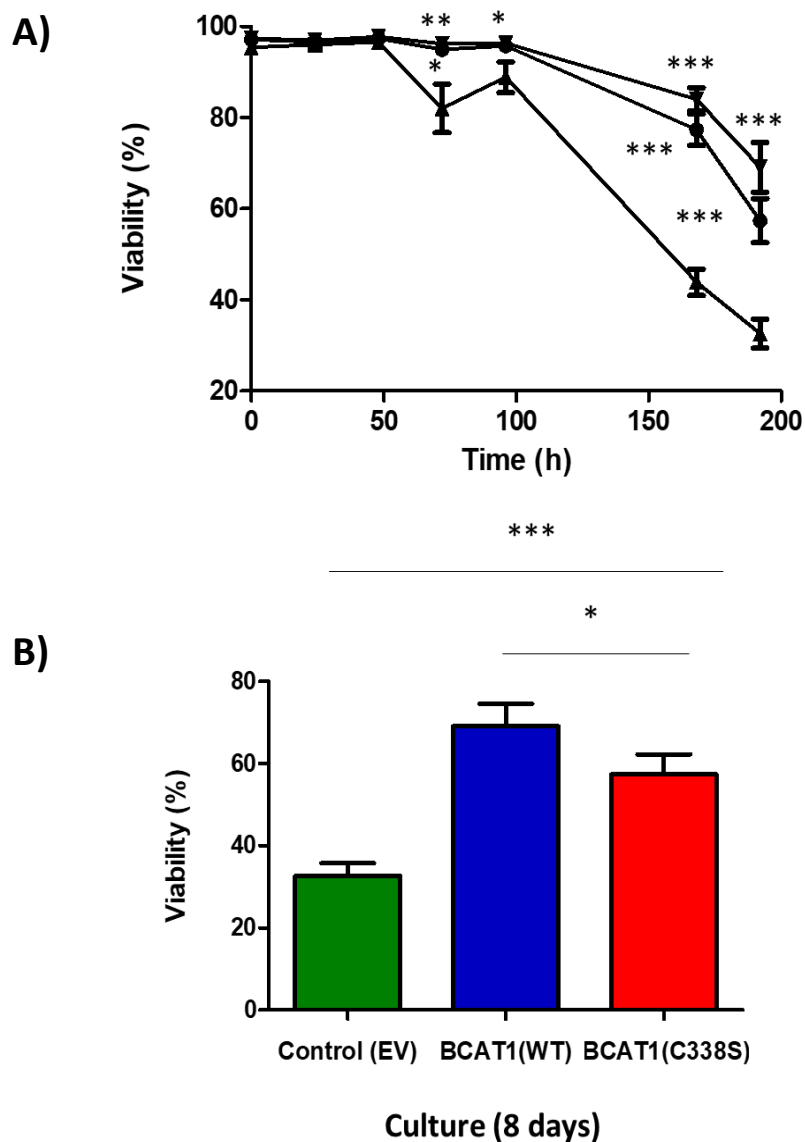


Figure 5.3 Viability profile of BCAT1 overexpressing and control U937 cells. **A)** T75 flasks were seeded with 2×10^6 cells and cultured in 10mL of complete RPMI. The percentage of viable cells was measured at 0h and after 24h, 48h, 72h, 96h, 168h and 192h. **B)** Bar chart displaying cellular viability in culture after 192h. U9937-BCAT1(WT) displays a significantly higher proportion of viable cells compared to U937-BCAT1(C338S) and U937-Control(EV) cells. Data presented are mean \pm SEM (n=4) Data analysed by One/ two-way ANOVA Bonferroni post-hoc test (*p<0.05, **p<0.01 and ***p<0.001)

5.4.4 Growth characterisation: Intracellular redox environment

The effect of the BCAT1 CXXC motif on the intracellular redox environment of the cell was evaluated at mid-exponential (t=48), stationary (t=96) and death phase (t=168). Mitochondrial membrane potential (ψ_m) was measured by staining with DiOC2(3) as previously described. A higher ψ_m is associated with increased mitochondrial ROS leakage, and therefore may impact the cellular redox environment (Suski *et al.*, 2012). Interestingly, the data show that ψ_m was consistently higher in U937-BCAT1(WT) and U937-BCAT1(C338S) cell lines compared to the U937-Control(EV) across all time points (Figure 5.4), although these data did not reach statistical significance. Next, intracellular ROS was measured using the DCFDA probe, where both U937-BCAT1(WT) and U937-BCAT1(C338S) displayed significantly decreased intracellular ROS compared to the U937-Control(EV) cells at t=96 and t=168 (Figure 5.5, $p < 0.001$ & $p < 0.01$ respectively). Moreover, these data correspond with intracellular redox potential (E_h), as measured calculating GSH/GSSG, which was significantly lower in U937-BCAT1(WT) and U937-BCAT1(C338S) cells compared to U937-Control(EV) at t=96 and t=168 (Figure 5.6, Panel B). The data show that total glutathione (GSH) content was also significantly increased in both BCAT1 overexpressing U937 transgenic cell lines compared to EV control at t=96. (Figure 5.6, Panel A)

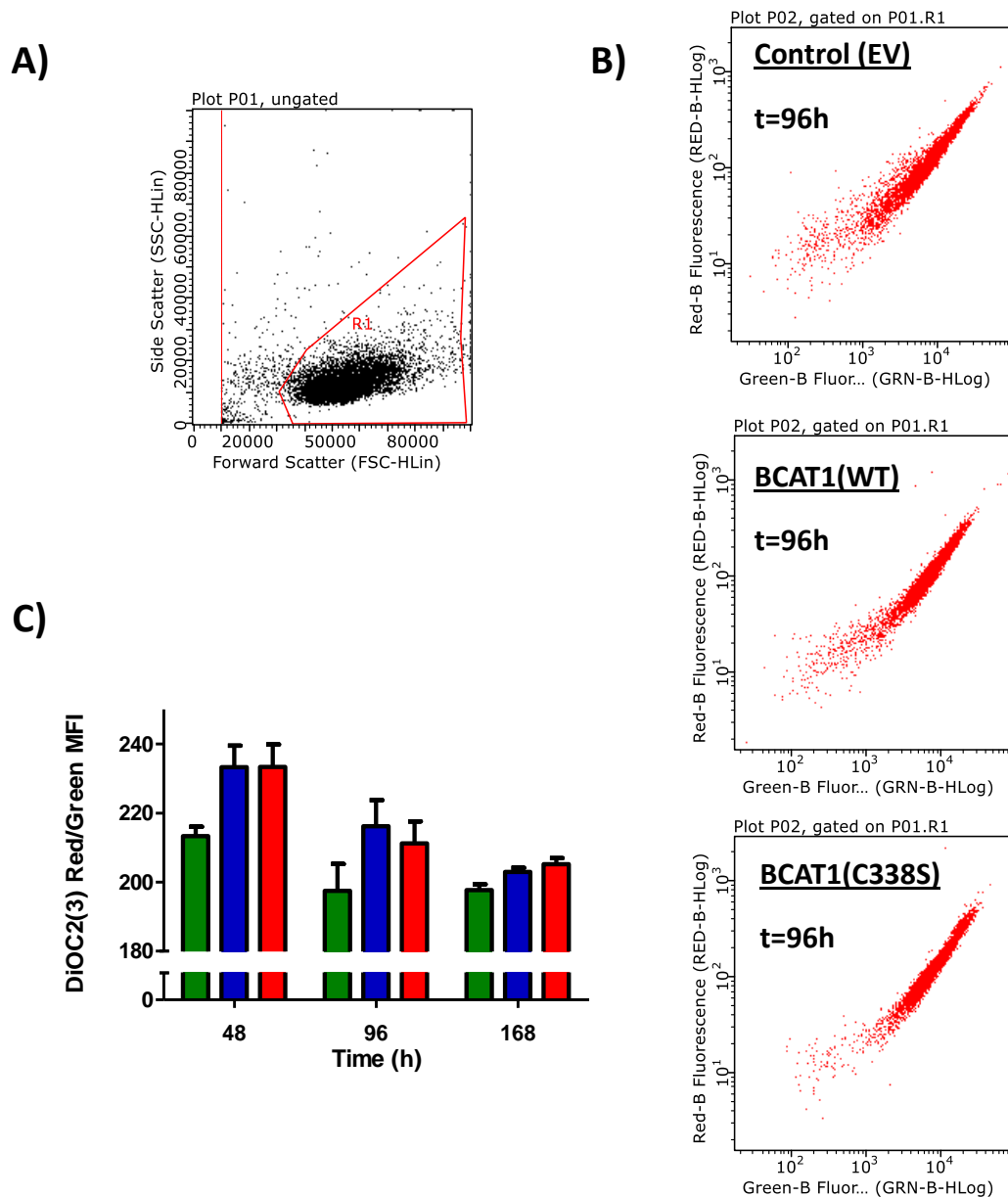


Figure 5.4 Effect of BCAT1(WT) and BCAT1(C338S) overexpression on mitochondrial membrane potential ($\Delta\Psi_m$). T75 flask culture samples were removed at exponential (48h), stationary (96h) and death phase (168h) and stained with DiOC2(3). **A)** Representative FSC vs SSC flow cytometric profile of DiOC2(3) treated U937 cells. **B)** Representative Green/Blue(FL1) vs Red/Blue(FL3) bivariate analysis gated on R1 after 96h. **C)** Bar chart displaying $\Delta\Psi_m$ (red/green MFI) of U937 cells. U937-BCAT1(WT) [blue] and U937-BCAT1(C338S) [red] display consistently increased $\Delta\Psi_m$ across all time points compared to U937-Control(EV) cells [green]. Data presented as mean \pm SEM (n=3). Data analysed by two-way ANOVA with Bonferroni post-test. Data not significant.

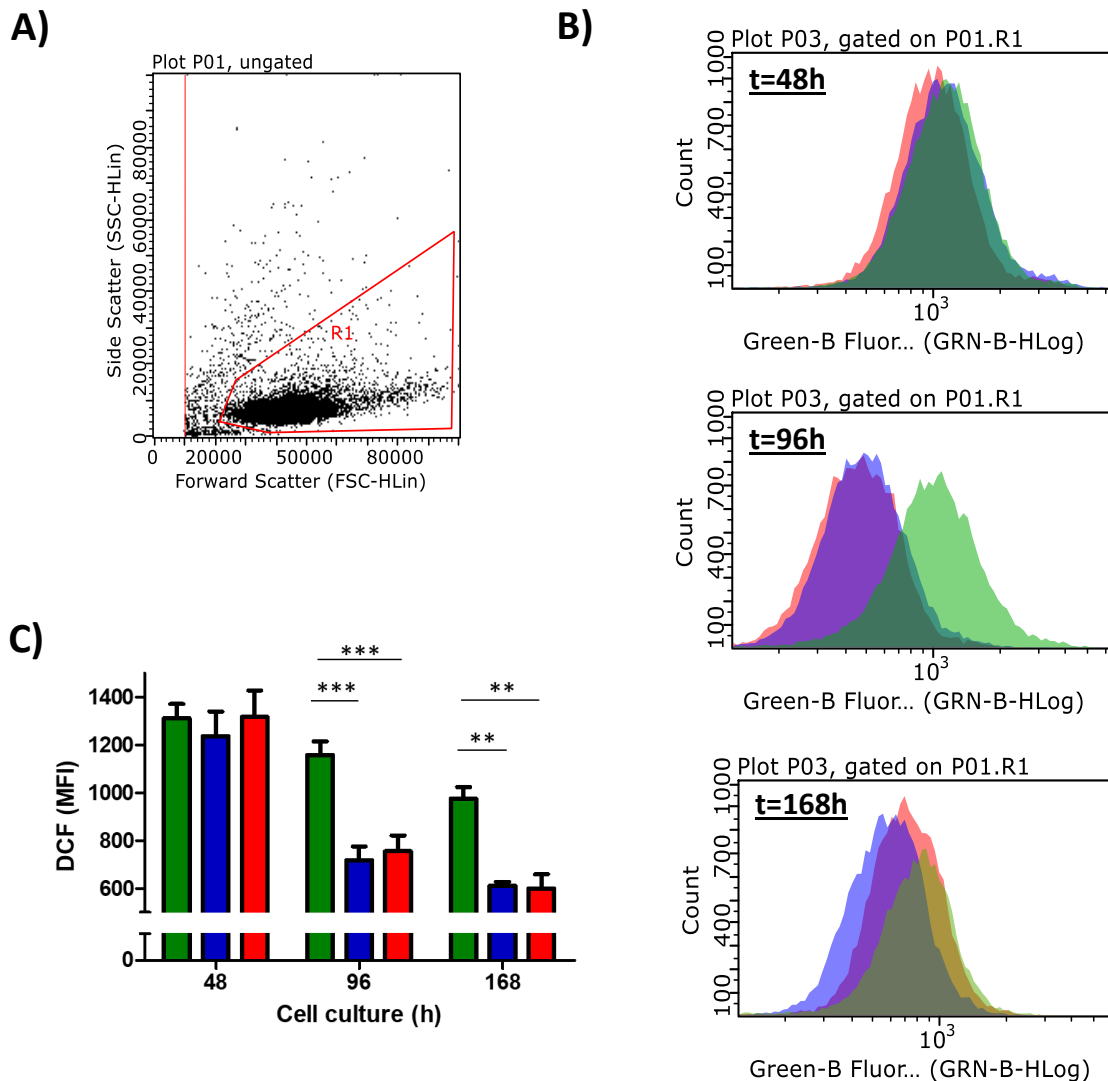


Figure 5.5 Effect of BCAT1(WT) and BCAT1(C338S) overexpression on Reactive Oxygen Species (ROS). **A)** Representative FSC vs SSC flow cytometric profile of DCFDA treated U937 cells. **B)** Representative green/blue(FL1) histograms gated on R1 after at exponential (48h), stationary (96h) and exponential (168h) showing U937-Control(EV) BCAT1(WT) [blue] and U937-BCAT1(C338S) cells. **C)** Bar chart displaying mean DCF signal (green/blue MFI) that equates to intracellular ROS levels. U937-BCAT1(WT) [blue] and U937-BCAT1(C338S) [red] display significantly decreased intracellular ROS at 96h and 168h compared to U937-Control(EV) cells [green]. Data presented as mean \pm SEM (n=4) analysed by two-way ANOVA with Bonferroni post-hoc test (**p<0.01 and ***p<0.001).

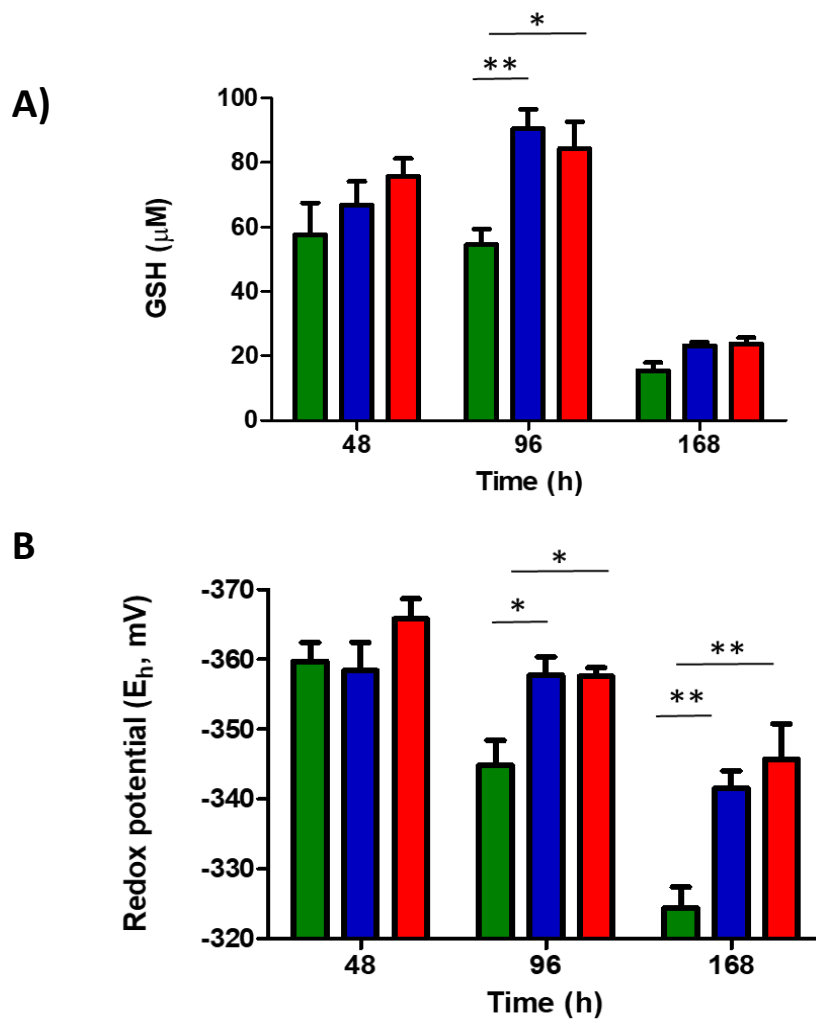


Figure 5.6 Effect of BCAT1(WT) and BCAT1(C338S) overexpression on intracellular glutathione and redox potential. **A)** Bar chart displaying total intracellular glutathione (GSH) content of viable cells. U937-BCAT1(WT) [blue], U937-BCAT1(C338S) [red] and U937-Control(EV) cells [green] measured at 48h, 96h and 168h. **B)** Bar chart displaying redox potential (E_h) of viable cells. E_h calculated from the Nernst equation using the ratio reduced/oxidised glutathione (GSH/GSSG). U937-BCAT1(WT) [blue], BCAT1(C338S) [red], and U937-Control(EV) [green]. were measured at 48h, 96h and 168h. Data presented as mean \pm SEM (n=3) and analysed by two-way ANOVA with Bonferroni post-hoc test (*p < 0.05 and **p < 0.01).

5.4.5 *The Antioxidant Effect of the CXXC Motif on Serum Starved Transgenic U937 cells*

In order to observe the potential antioxidant effect of the CXXC motif, each respective transgenic cell line was placed under an endogenous oxidative stress elicited by serum starvation (Scherz-Shouval *et al.*, 2007; Lee *et al.*, 2010). Cells were placed in complete RPMI $\pm 10\%$ FCS and $\pm 10\text{mM}$ NAC for 72h, and intracellular ROS levels were measured by DCFDA staining and flow cytometry. The data show that serum starvation resulted in increased the DCFDA signal across all cells lines, however U937-BCAT(WT) cells displayed a significantly lower overall DCFDA signal (1532 ± 50 MFI) overall, compared to either U937-BCAT1(C338S)(2553 ± 93 MFI) or U937-Control(EV) cells (3589 ± 154) (Figure 5.7, $p < 0.001$). Importantly, this effect was abrogated by the addition of 10mM of the antioxidant NAC, which significantly reduced DCFDA to 'normal' level signals and eliminated the observed differences between cell lines (Figure 5.7).

Next the effect of serum starvation on cell viability and apoptosis was measured by 7AAD/Annexin-V analysis. The data in Figure 5.8 and Table 5.1 illustrate that serum starvation significantly increases the percentage of non-viable cells (7AAD+ve) across all transgenic U937 cell lines, however U937-BCAT1(WT) cells display a substantially lower proportion of 7AAD+ve cells ($22.9\pm 2.5\%$) compared to either U937-BCAT1(C338S) ($38.3\pm 2.7\%$, $p < 0.01$) or U937-Control(EV) cells ($74.6\pm 1.2\%$, $p < 0.001$). Representative flow cytometric plots of this data show U937-BCAT1(WT) display a higher proportion of viable cells (lower left quadrant), with correspondingly lower levels of apoptotic (upper left quadrant) and dead cells (upper right quadrant) compared to U937-BCAT1(C338S) and U937-Control(EV) (Figure 5.8, Panel C). As with the intracellular ROS signal this effect was abrogated by the addition of NAC which significantly reduced the 7AAD+ve

population across all cells lines and abrogated the difference between BCAT1(WT) and BCAT1(C338) (Figure 5.8 Panel A).

Finally, the effect of serum starvation on cellular proliferation was examined. Cells were seeded at 5×10^5 cells/mL and proliferation was determined by total cell number after 72h in culture. The data show that U937-BCAT1(WT) and U937-BCAT1(C338S) cells display a final cell density of $1.04 \times 10^6 \pm 5.5 \times 10^4$ cells/mL and $1.04 \times 10^6 \pm 5.5 \times 10^4$, respectively, which represent a 108.4% ($p < 0.001$) and 102.2% ($p < 0.01$) increase in cell number (Figure 5.9). This finding is in contrast to U937-Control(EV) cells, which display a relative decrease in number by 17.42% to $4.13 \times 10^5 \pm 6.7 \times 10^4$ cells/mL after the same amount of time in culture (Figure 5.9). This demonstrates BCAT1 overexpressing cells underwent approximately one doubling whilst control cells were unable to proliferate in serum starved conditions.

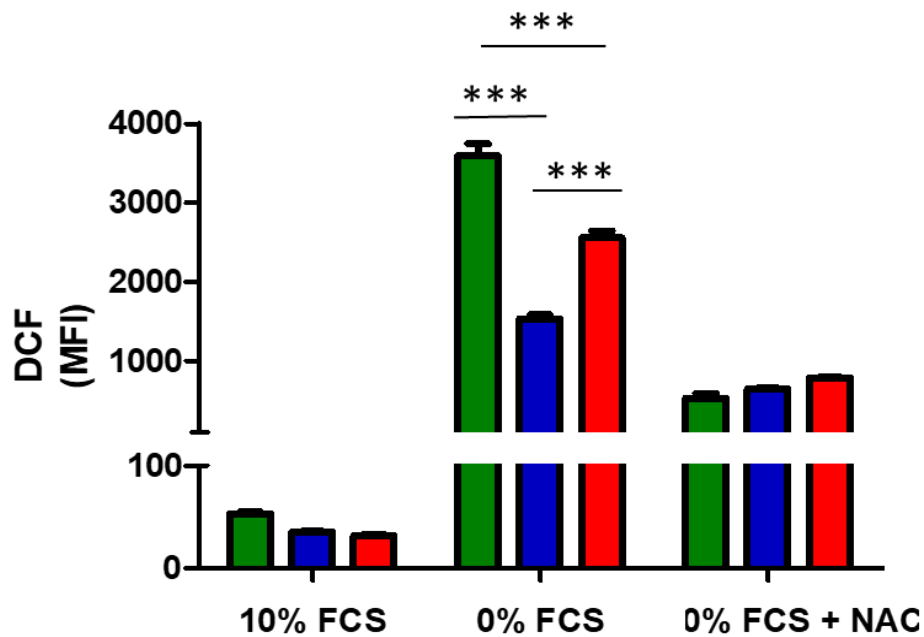


Figure 5.7 Effect of BCAT1(WT) and BCAT1(C338S) overexpression on intracellular ROS following serum starvation. Bar chart displaying Reactive Oxygen Species (ROS) generation following serum starvation. 5×10^4 cells per well were suspended in a 96 well plate with complete RPMI +/- 10% foetal calf serum (FCS) and +/- 10mM N-acetyl cysteine (NAC) and incubated for 72h prior to staining with intracellular ROS probe DCFDA. Serum starvation increases ROS signal across all cell lines, U937-Control(EV) [green], U937-BCAT1(WT) [blue] and U937-BCAT1(C338S) [red]. Addition of the antioxidant NAC abolishes differences in ROS signal across all cell lines. Data presented as mean \pm SEM (n=4), analysed by two-way ANOVA with Bonferroni post-hoc test (***) $p < 0.001$.

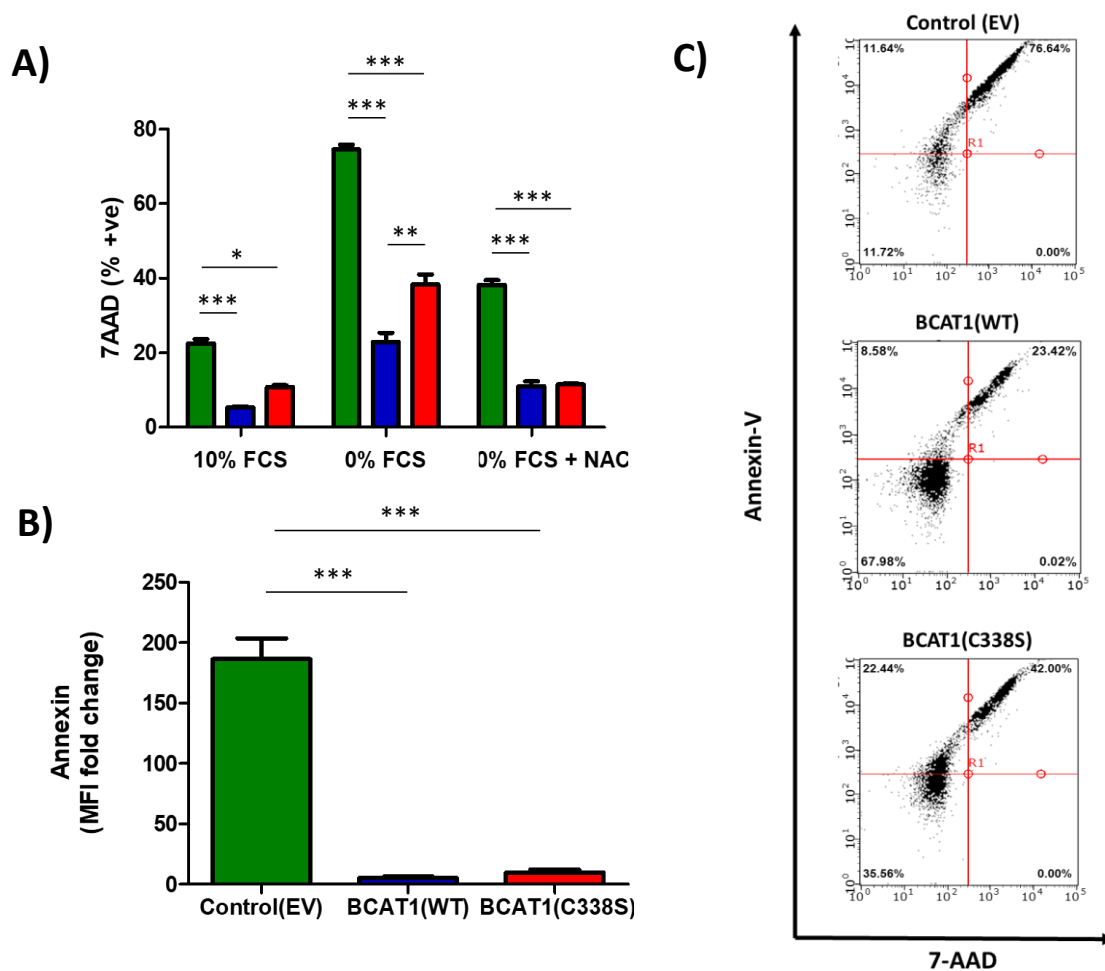


Figure 5.8 Effect of BCAT1(WT) and BCAT1(C338S) overexpression on 7AAD/Annexin in U937 cells following serum starvation. **A)** Bar chart summarising U937-Control(EV) [green], U937-BCAT1(WT) [blue] and U937-BCAT1(C338S) [red] cells cultured under serum starved conditions for 72h \pm 10mM NAC prior to viability analysis using 7AAD/Annexin-V. **B)** Data displaying fold change in Annexin-V following serum starvation, where U937-BCAT1(WT) and U937-BCAT1(C338S) display a significantly decreased fold change in Annexin-V signal compared to U937-Control(EV) cells. **C)** Representative bivariate flow cytometric plots for each cell line following serum starvation displaying percentage viable (lower left quadrant), apoptotic (upper left quadrant) and dead (upper right quadrant) cells (each plot represents 5000 events). Data presented as mean \pm SEM n=3, One/two-way ANOVA Bonferroni post-test (*p<0.05, **p<0.01 and ***p<0.001).

Table 5.1 Cell viability determined by 7AAD/ Annexin V staining following serum starvation summarised

	Viable (LL %)	Apoptotic (UL %)	Dead (UR %)
Control(EV)	14.0 ± 2.9	11.4 ± 1.0	74.6 ± 2.1
BCAT1(WT)	56.0 ± 12.2	21.1 ± 15.2	22.9 ± 4.4
BCAT1(C338)	42.8 ± 11.5	18.8 ± 6.9	38.3 ± 4.7

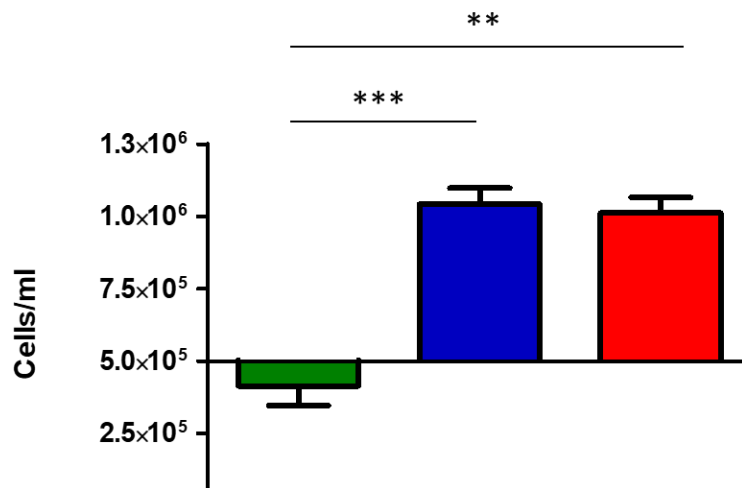


Figure 5.9 The effect of BCAT1(WT) and BCAT1(C338S) overexpression on cellular proliferation following serum starvation. 5×10^4 cells per well were suspended in a 96 well plate with complete RPMI - 10% fetal calf serum (FCS) and incubated for 72h prior to staining with Viacount reagent. U937-BCAT1(WT) [blue] and U937-BCAT1(C338S) [red] display increased proliferation compared to U937-Control(EV) cells [green]. Data presented as mean \pm SEM n=4, One-way ANOVA Bonferroni post-test (**p<0.01,***=p<0.001).

5.4.6 *The effect of the BCAT1 CXXC motif on PMA mediated cellular differentiation*

To examine the effect of BCAT1(WT) and BCAT1(C338S) overexpression on monocyte to macrophage differentiation, cellular morphology was examined by flow cytometry. Differentiated macrophages display increased granularity as a result of an increase in membrane bound organelles, which can be detected as an increase in side scatter (SSC) (Daigneault *et al.*, 2010). The data shows that U937-BCAT1(WT) and U937-BCAT1(C338S) cells display decreased SSC intensity compared to U937-Control(EV) cells in resting culture, indicating BCAT1 expression mediates a less differentiated U937 ground state (Figure 5.10).

To evaluate the effect of the BCAT1 CXXC motif on induced cellular differentiation, the transgenic U937 cells were incubated with PMA. PMA has been demonstrated to mediate differentiation in U937 cells in a ROS dependant manner (Yamamoto *et al.*, 2009), therefore PMA induced differentiation was explored across all cell lines. Intracellular ROS \pm PMA was measured by DCFDA staining, where the data shows that PMA increases DCFDA signal across all cell lines, however U937-BCAT1(WT) cells display significantly lower PMA induced DCFDA signal compared with U937-BCAT1(C338S) or U937-Control(EV) cells (Figure 5.11, $p < 0.05$ and $p < 0.001$ respectively).

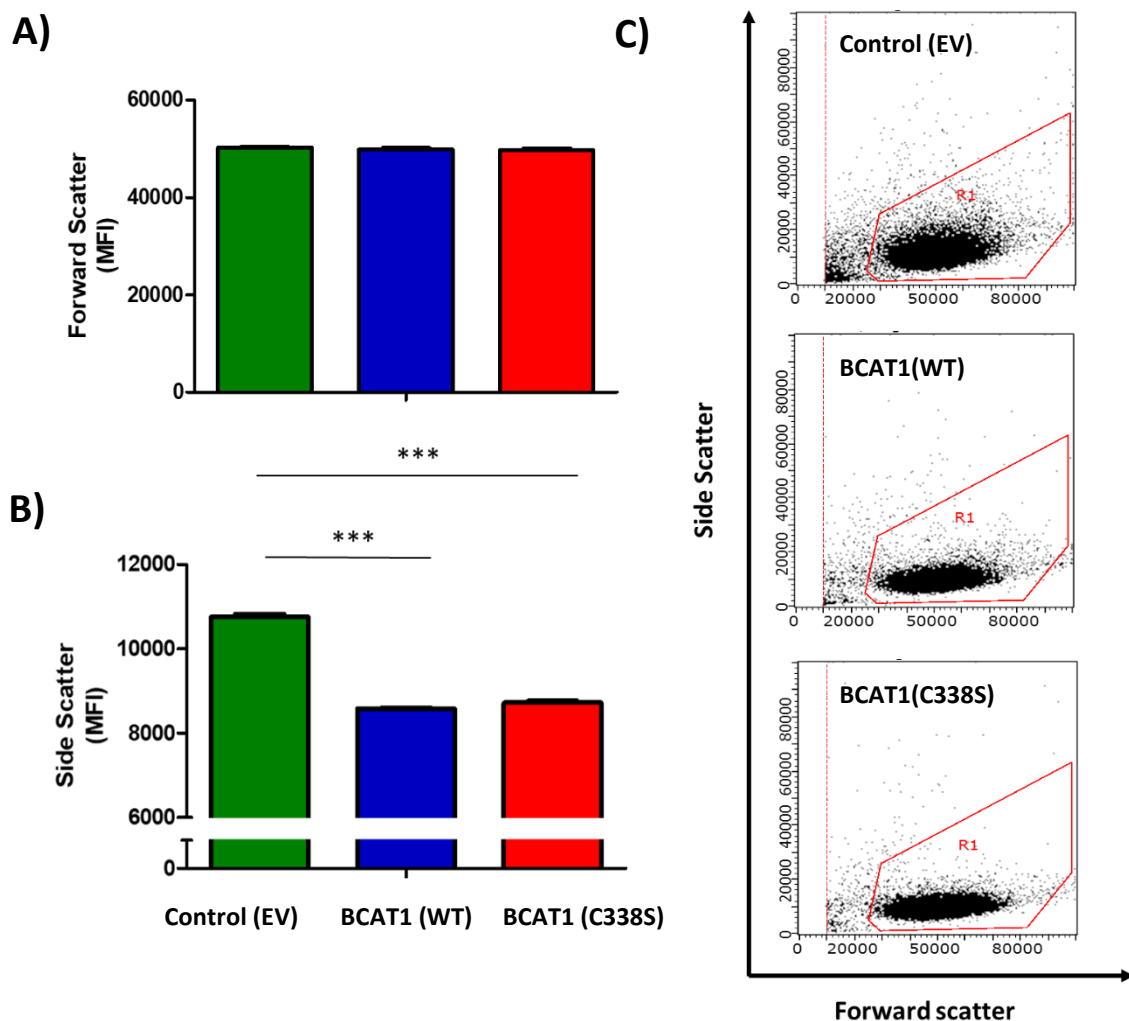


Figure 5.10 The effect of BCAT1(WT) and BCAT1(C338S) overexpression on cellular morphology. Bar charts displaying effect of BCAT1 overexpression on **A)** forward (FSC) and **B)** side scatter (SSC) measured by flow cytometry. BCAT1 overexpression has no effect on cell size as measured by forward FSC however U937-BCAT1(WT) and U937-BCAT1(C338S) display significantly reduced granularity as measured by SSC. **C)** Representative bivariate FSC vs SSC flow plots. U937-BCAT1(WT) [middle] and U937-BCAT1(C338S) [bottom] display visibly reduced side scatter compared to U937-Control(EV) [top] cells (each plot represents 5000 events). Data presented as mean \pm SEM, n=3. Analysed by One-way ANOVA Bonferroni post-test (***) $p < 0.001$.

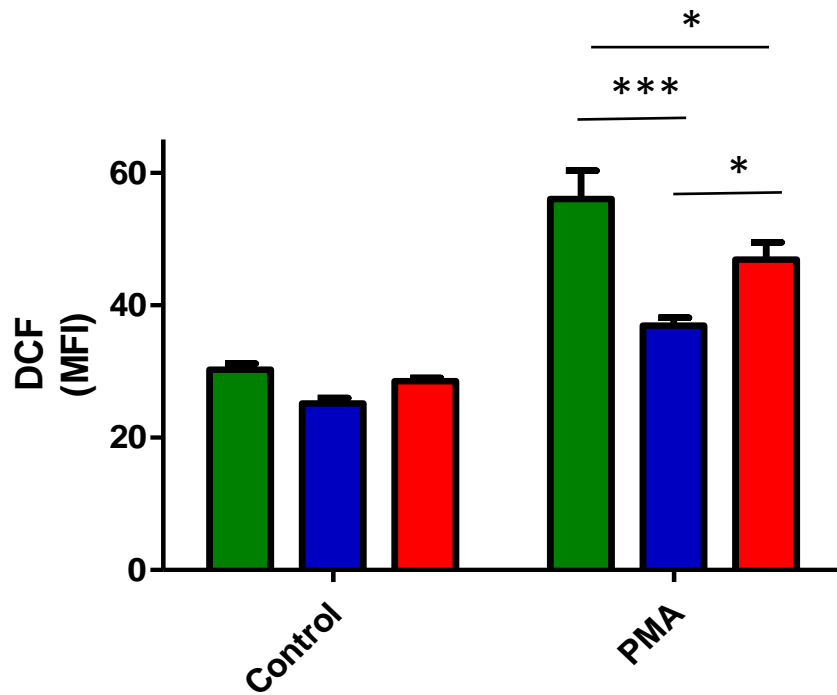


Figure 5.11 The effect of BCAT1(WT) and BCAT1(C338S) overexpression on Phorbol 12-myristate 13-acetate (PMA) induced Reactive Oxygen Species (ROS). Transgenic U937 cells were differentiated using PMA and intracellular ROS measured by DCFDA. Data show DCFDA signal before and after PMA treatment for U937-Control(EV) [green], U937-BCAT1(WT) [blue] and U937-BCAT1(C338S) [red]. Data presented as mean± SEM n=3 and analysed by two-way ANOVA Bonferroni post-test (*p<0.05 and***p<0.001).

The effect of the BCAT1 CXXC motif on cellular differentiation was analysed by expression of cell surface markers CD36 and CD11b, which distinguish a macrophage-type immunophenotype (Huh *et al.*, 1996; Misharin *et al.*, 2013). Here U937-BCAT1(WT) and U937-BCAT1(C338S) display significantly decreased baseline levels of CD36⁺ cells compared to U937-Control(EV) cells ($P < 0.001$), with CD36⁺ significantly lower in U937-BCAT1(WT) cells compared to U937-BCAT1(C338S) ($p < 0.01$, Figure 5.12, Panel C). PMA induced differentiation increases CD36 expression across all transgenic U937 cell lines, however U937-BCAT1(WT) displays a reduced percentage of CD36⁺ cells compared to U937-BCAT1(C338S) and U937-Control(EV). Moreover, PMA induced CD11b⁺ expression is also significantly reduced for U937-BCAT(WT) and U937-BCAT1(C338S) expressing cells compared to U937-Control(EV) cells. ($p < 0.05$, Figure 5.12, Panel D).

Given CD36 is known to play a role in monocyte and macrophagic cell to cell adhesion through receptor Thrombospondin-1 (TSP-1), cellular morphology was examined by phase contrast microscopy (Savill *et al.*, 1992; Ho Young Huh *et al.*, 1995). Following addition of PMA, visual examination revealed that U937-BCAT1(WT) cells displayed less cellular aggregation compared with U937-Control(EV) cells, a finding consistent with lower CD36 cell surface expression (Appendix D).

Finally, to confirm that the observation in myeloid differentiation markers CD36/CD11b was due to the CXXC motif, and not BCAT1 aminotransferase activity, cells were pre-treated with the BCAT1 competitive inhibitor, Gabapentin (Goto *et al.*). The maximal non-lethal inhibitory concentration of Gabapentin of 20 mM was determined by dose-response analysis (See Chapter 6). The data demonstrated that the addition of 20 mM Gabapentin was unable to restore the either CD36 or CD11b immunophenotype

to baseline, however the phenotype is effectively rescued by addition of 10mM of the antioxidant NAC demonstrating PMA mediated differentiation is primarily a redox driven process rather a metabolic one (Figure 5.12 Panel C +D).

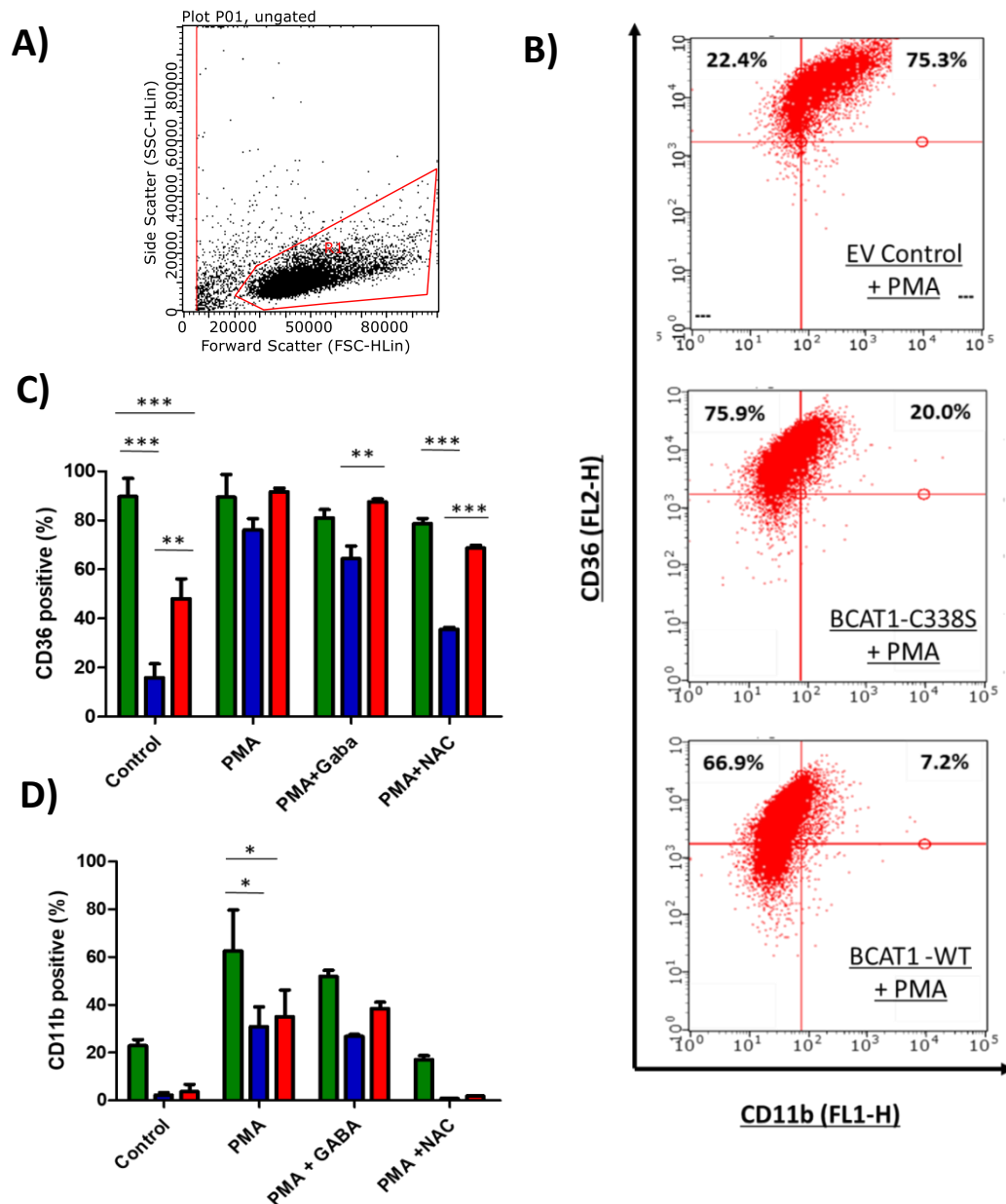


Figure 5.12 The effect of PMA treatment on the markers of myeloid differentiation CD36 and CD11b. **A)** Representative FSC vs SSC plot displaying gating of viable cells following PMA treatment. **B)** Representative green/blue (FL1) bivariate analysis gated on R1. CD36/CD11b⁻ (lower left quadrant), CD36⁺(upper left quadrant) and CD11b⁺ (upper right quadrant). Bar charts displaying percentage of **C)** CD36⁺ and **D)** CD11b⁺ cells under different treatment conditions where Control(EV) [green], U937-BCAT1(WT) [blue] and U937-BCAT1(C338S) [red]. Data presented as mean± SEM n=3 and analysed by two-way ANOVA Bonferroni post-hoc test (*p<0.05, **p<0.01 and ***p<0.001).

5.4 Discussion

The aim of this chapter was to determine the effect of the BCAT1 CXXC motif on the development of AML. To achieve this, it was necessary to attempt to separate the canonical metabolic activity and CXXC motif derived effects of BCAT1, in the model used here the differences between BCAT1(WT) and BCAT1(C338S) overexpressing U937 transgenic cell lines is taken to be indicative of this contribution. The rationale for this comes from the observation that cysteine to serine site directed mutagenesis of the C338 residue of the CXXC motif (i.e. CXXS) preserves the metabolic activity of the enzyme under physiological conditions (Conway *et al.*, 2008), whilst potentially abolishing the putative antioxidant activity compared to BCAT1(WT). Given development of AML results from a dysregulation of oncogenic processes such as cellular differentiation, proliferation and apoptosis (Testa and Riccioni, 2007; Olsson *et al.*, 2009; Akinduro *et al.*, 2018), these were the characteristics that were compared between the cell lines to explore the hypothesis that the BCAT1 CXXC motif contributes to the pathogenesis of AML, through modulation of ROS, a central component in AML development (Zhou, Shen and Claret, 2013; Sillar *et al.*, 2019).

The data presented here show that *in vitro* growth profiles for the transgenic cell lines, show an increased cell density for U937-BCAT1(WT) and U937-BCAT1(C338S) overexpressing cells compared to U937-Control(EV) (Figure 5.1). Additionally, cell cycle analysis during exponential growth phase revealed this was accompanied by a significant decrease in doubling time and G2M phase cells for both U937-BCAT1(WT) and U937BCAT(C338S) cells (Figure 5.2). However no significant difference in cell density

or cell cycle was observed between U937-BCAT1(WT) and U937-BCAT(C338S), demonstrating that this difference is due to the metabolic contribution of the enzyme.

Previous biochemical studies using *in vitro* enzyme kinetic data, demonstrate that BCAT1 metabolism favours the production α -KG and leucine (Davoodi *et al.*, 1998), however the current literature indicates that the direction of the reaction *in vivo* is context dependant. For example, in myeloid leukaemia, rapidly dividing blast crisis cells favour the forward reaction, whilst more quiescent leukemic stem cell populations in AML have been found to favour reverse reaction i.e. the production of glutamate and BCKA (Hattori *et al.*, 2017 and Raffel *et al.*, 2017). In transformed proliferating cells α -KG, anaplerotically replenishes the TCA cycle, whilst leucine activates mTOR stimulating growth and survival (Owen, Kalhan and Hanson, 2002; Laplante and Sabatini, 2009; Altman, Stine and Dang, 2016). Although direct measurements of these processes were beyond the scope for this study, it has been previously demonstrated BCAT1 overexpression promotes growth via mTOR by increasing the BCAA pool in a myeloid and breast cancer cell model (Hattori *et al.*, 2017; Zhang and Han, 2017). Therefore it is reasonable to speculate that increased cellular proliferation (Figure 5.1) and concurrent increase in G2M phase cells (Figure 5.2) observed from U937-BCAT1(WT) and U937-BCAT1(C338S) compared to U937-Control(EV) is due to increased levels of α -KG which feeds into the TCA cycle increasing ATP production. Supporting this idea, cell cycle has been demonstrated to be dependent on ATP production, where increasing ATP concentration induces depolymerization of the interphase microtubular network initiating cellular mitosis(Marcussen and Larsen, 1996).

Another factor to consider when examining the data presented in Figures 5.1 and 5.2 is the production of toxic ammonia. Cells in closed cultures experience a decrease in nutrient availability and an increase in toxic waste products, which ultimately limit growth and survival. An important waste product is ammonia, which has been reported to inhibit growth in cell cultures (Schneider, Marison and Von Stockar, 1996). The ammonium ion (NH_4^+) is produced as a by-product of glutamate metabolism through glutamate dehydrogenase, which also produces α -KG, however this reaction can also be performed by aminotransferases including BCAT1 without the producing toxic ammonium (Altman, Stine and Dang, 2016). Thus the significantly higher cell density observed from U937-BCAT1(WT) and U937-BCAT1(C338S) cells compared with the U937-Control(EV) after 96 h in culture (Figure 5.1) may be due to an increase in α -KG and leucine and a decrease in NH_4^+ metabolites.

Closer examination of cell viability at stationary (t_0 - 96h) and death phase (t_{96} - 192) shows that U937-BCAT1(WT) and U937-BCAT1(C338S) cells display an increased proportion of viable cells compared to U937-Control(EV) cells (Figure 5.3). Furthermore increased viability at these time points is related to a decrease in intracellular ROS (Figure 5.5) and increased GSH content (Figure 5.6), suggesting that during the stationary and death phase, the BCAT1 overexpressing cells may favour the reverse metabolic reaction, producing glutamate and BCKA (Hattori *et al.*, 2017 and Raffel *et al.*, 2017). This notion may be supported by previous studies which demonstrate that during stationary phase exhaustion of glutamine, which is supplemented in the culture medium and converted to glutamate via Glutaminase, would lead to a rapid decrease in the

availability of glutamate, shifting the reaction equilibrium of BCAT1 in favour of glutamate synthesis (Cluntun *et al.*, 2017).

The data presented in Figure 5.6 show an increase in total GSH for BCAT1 transgenic cells. GDH the most abundant low molecular weight thiol and integral part of cellular antioxidant defences (Lu, 2013). Cellular antioxidant enzymes including Glutathione peroxidase (GPx) and Peroxiredoxins (Prx) require GSH to act as an electron donor during the reductive elimination of H₂O₂, as well as to regenerate antioxidant enzymes to their reduced active forms (Forman, Zhang and Rinna, 2009). Glutamate is a precursor to the synthesis of the GSH, therefore, the increase in GSH observed for U937-BCAT1(WT) and U937-BCAT1(C338S) could be explained by the increased glutamate production via BCAT1 metabolic activity in these cells, as discussed previously.

GSH is known to modulate intracellular ROS and apoptosis, whereby inhibition of GSH synthesis in a human B lymphoma cell line leads to an increase in ROS and activation of apoptotic signalling cascades (Armstrong *et al.*, 2002; Circu and Aw, 2012). Interestingly, Hongbin *et al* demonstrate that BCAT1 overexpression increases cellular GSH content and that BCAT1 knockdown results in decreased GSH and increased ROS in human lung cancer cell lines PC-9 (Wang *et al.*, 2019). Thus, taken together, the *in vitro* characterisation of BCAT1 overexpressing U937 cell lines as presented here, seems to support hypothesis that the direction of the BCAT1 enzymatic reaction is dynamic and context dependant. During exponential phase, BCAT1 overexpression probably favours the forward reaction producing metabolites that support growth whilst during stationary phase the reverse reaction appears to be favoured producing glutamate and supporting GSH synthesis.

Whilst the metabolic contribution of BCAT1 accounts for the variation seen between BCAT1 overexpressing and EV control, U937-BCAT1(WT) also display significantly increased proportion of viable cells compared to BCAT1(C338S) at various time points (Figure 5.3). This observation may indicate CXXC derived protection from ROS mediated cell death, which is reported to impact cells in culture (Halliwell, 2003). The data presented in Figure 5.3 shows the difference in cell viability between U937-BCAT1(WT) and U937-Control(EV) at t=192 h is 36.5 %, whilst BCAT1(WT) and U937-Control(C338S) at t=192 h is 11.7 %. Therefore, the protective effect of BCAT1 on apoptosis may be quantified as 24.8% metabolic and 11.7% CXXC motif, roughly equating to 1/3rd of the effect measured. I hypothesised this effect would be due to exhaustion of media serum which is known to induce oxidative stress and apoptosis through mitochondrial ROS production. (Lee *et al.*, 2010; Braun *et al.*, 2011; Li, Chen and Gibson, 2013) Therefore in order to further interrogate the ability of the CXXC motif to protect against ROS mediated cell death I induced oxidative stress by serum starvation.

The ROS reactive probe, DCFDA was introduced to the culture to quantitate ROS production (Eruslanov and Kusmartsev, 2010). The data presented in Figure 5.7 show that following serum starvation, U937-BCAT1(WT) DCF signal was than less the U937-Control(EV) cells ($p < 0.001$) and also significantly less than the U937-BCAT1(C338S) cells ($p < 0.001$). Both BCAT1 overexpressing cells showed less ROS compared to the EV controls, however the data indicate that the CXXC motif may be responsible for approximately half the reduction in ROS (Figure 5.7). The metabolic activity of BCAT1 may also contribute to this effect by increasing the cellular pool of GSH, as previously discussed (Wang *et al.*, 2019).

The decrease in ROS observed in Figure 5.7 related to a decrease in cell death (Figure 5.8 and Table 5.1), where U937-BCAT1(WT) cells display a substantially lower proportion of 7AAD +ve cells compared to either U937-BCAT1(C338S) or U937-Control(EV) cells. Interestingly, addition of the cellular antioxidant 'NAC' equalised the DCF signal across all cell lines and nullified the percentage change in cell death seen between U937-BCAT1(WT) and U937-BCAT1(C338S) (Figure 5.7 and 5.8) demonstrating that these effects are redox mediated.

Serum starvation was used in this study to mediate an increase in endogenous cellular ROS. This technique has been widely used to study apoptosis in response to oxidative stress. HeLa cells deficient in mitochondrial electron transport chain display significantly reduced levels of superoxide in response to serum starvation, demonstrating that serum depleted induced ROS is mitochondrially derived (Li, Chen and Gibson, 2013). Another study demonstrated serum starvation increased DCF signal, which was rescued by the addition of NAC and catalase, supporting the notion serum starvation induces ROS and that the effects can be rescued by antioxidants (Scherz-Shouval *et al.*, 2007). The data here supports these observations where the DCF signal increases following serum starvation, moreover this increase in ROS is CXXC motif dependant where BCAT1(C338S) displays approximately a 50% reduction in ROS compared to BCAT1(WT) indicating the CXXC motif is functioning as an antioxidant against ROS mediated cell death .

The effect of CXXC motif's in ROS mediated cell death has been examined in the widely studied antioxidant protein Thioredoxin (Trx). Trx CXXC motif's form a catalytic reaction centre which acts as a protein disulphide oxidoreductase, reducing

intermolecular and intramolecular disulphide bonds of oxidised proteins (Collet and Messens, 2010). Thioredoxin can restore Peroxiredoxin to the reduced active form, and in the process the Trx CXXC motif becomes oxidised and forms an intramolecular disulphide bond, which is subsequently restored by Thioredoxin reductase (TR) using NADPH as reducing equivalent (Lee, Kim and Lee, 2013). Increased intracellular Trx is associated with reduced ROS and a decreased sensitivity to pro-oxidant treatment, whereby inhibiting Trx in a U937 AML model restores susceptibility to Arsenic Trioxide treatment (Wangpaichitr *et al.*, 2012; Tan *et al.*, 2014). Moreover Trx expression is increased by serum starvation induced oxidative stress in the monocytic AML cell line THP1, where it protects the cell from apoptosis by reducing the levels of ROS (Kim *et al.*, 2008).

Whilst the antioxidant effects of CXXC containing Trx system have been extensively studied, the potential antioxidant properties of the CXXC motif in proteins outside this canonical antioxidant system is less well understood. Recently cysteine to serine site directed mutagenesis of a CXXC motif in Mesencephalic astrocyte-derived neurotrophic factor (MANF) demonstrated that the motif provides protection from oxidative stress induced apoptosis and reduces intracellular ROS (Božok *et al.*, 2018). Whilst this study was performed in a neuronal cell model, it strongly supports the hypothesis that the CXXC motif can mediate ROS induced apoptosis.

The protective effect of the BCAT1 CXXC motif from oxidative stress induced apoptosis is clearly demonstrated here, however exactly how the CXXC motif functions as an antioxidant is yet to be fully understood. Previous work has demonstrated that the majority the BCAT1 CXXC motif is S-glutathionylated at cellular redox potentials that

relate to processes dysregulated in cancer i.e. proliferation (-260 to -210mV,) differentiation (-210 to 180mV) and apoptosis (-180 to -160 mV) (Schafer and Buettner, 2001 and Coles *et al.*, 2012), indicating the that BCAT1 CXXC motif may be buffering the cellular antioxidant network, by reducing intracellular GSSG to GSH. This notion is supported by an earlier biochemical study, which linked BCAT1 directly to the Trx and GSH redox networks (Conway *et al.*, 2008;). Furthermore, unpublished data from our group at the University of Worcester suggests that that BCAT1 CXXC motif can directly reduce H₂O₂ *in vitro* and can be regenerated by NADPH, suggesting a peroxidase like activity rather than a Trx like protein disulphide oxidoreductase role, although the precise activity *in vivo* remains to elucidated. Taken together, with the data presented for the transgenic U937 cells in this chapter, the evidence is mounting for BCAT1 as a cellular antioxidant.

Resisting differentiation is a feature of AML and occurs at a relatively oxidised intracellular redox potential (Schafer and Buettner, 2001). Therefore, it was hypothesised that the putative antioxidant properties of the BCAT1 CXXC motif would result in a more 'reduced' cellular environment and therefore less cellular differentiation would occur. To investigate this hypothesis, the ability of the BCAT1 CXXC motif to resist ROS mediated differentiation was examined by induction with PMA. Previous work in U937 cell line has shown that PMA induces expression of monocyte to macrophage markers CD36 and CD11b through generation of H₂O₂ increasing intracellular ROS as measured by DCF signalling. Moreover addition of catalase reduced intracellular H₂O₂ and blocked differentiation whilst ROS scavenger NAC decreased PMA induced expression of CD11b by 70%(Yamamoto *et al.*, 2009).

Initially, the effect of PMA in mediating cellular ROS was investigated. The DCFDA data shows that PMA treatment was linked with an increase in cellular ROS (Figure 5.11), where U937-BCAT1(WT) cells display significantly lower levels of ROS compared with both U937-BCAT1(C338S) and U937-Control(EV). This finding supports previous work linking ROS to PMA treatment (Yamamoto *et al.*, 2009) and further supports a role for the BCAT1 CXXC motif as an antioxidant. Interestingly, BCAT1 overexpressing transgenic cells display less granularity (Figure 5.10), suggesting that BCAT1 may be affecting the ability of U937 cells to differentiate. This finding is supported by the data presented in Figure 5.12, which illustrate that the percent of CD11b⁺ cells was significantly lower for BCAT1 overexpressing transgenic U937 cells compared with U937-Control(EV) following addition of PMA. However, there was no significant difference between U937-BCAT1(WT) and U937-BCAT1(C338S), suggesting that CD11b expression in part, may be due to the aminotransferase metabolic effect mediated by BCAT1 overexpression.

To investigate this further, the BCAT1 competitive inhibitor Gabapentin, which blocks the metabolic active site and not the CXXC motif (Goto *et al.*, 2005), was added to the system. When treated with PMA + Gabapentin U937-BCAT1(C338S) cells display increased proportion of CD11b⁺ cells compared with U937-BCAT1(WT), suggesting that this phenotype is in part driven by ROS. The addition of NAC restored the basal CD11b⁺ cell numbers, thus confirming PMA induced CD11b⁺ expression is mediated by ROS levels, which is supported by previous work (Yamamoto *et al.*, 2009).

The data presented here shows basal number of CD36⁺ cells (not PMA treated) is significantly higher for U937-BCAT1(C338S) compared with U937-BCAT1(WT) cells (Figure 5.12). This finding does not relate basal ROS levels observed by DCFDA analysis,

which was not significantly different across transgenic U937 cell lines (Figure 5.11), therefore, the percent CD36⁺ cell before PMA treatment does not appear to be a ROS mediated. However, CD36 has been found to be regulated in part by antioxidant transcription factor Nrf2, where under conditions of oxidative stress, Nrf2 translocates to the nucleus and initiates transcription of a number of antioxidant response genes, including CD36 (Ishii *et al.*, 2004). It is possible Nrf2 has been activated in U937-BCAT1(C338S) cells causing an increase in CD36⁺ cells and a concurrent decrease in ROS to levels comparable with U937-BCAT1(WT). Alternatively, it may be that substitution of the C338 cysteine to serine of the BCAT1 CXXC motif has initiated an oxidative stress signalling response. Work by Conway *et al.* demonstrated under reducing conditions, BCAT1 binds to several redox sensitive proteins that are associated with cytoskeletal remodelling, including, β -tubulin, Septin-4 and, Myosin-6 (Conway *et al.*, 2008). Importantly under oxidative stress, these proteins no longer bind to BCAT1, therefore it is possible that CD36 lies downstream of this response, which may account for the change in basal CD36⁺ seen here, however this needs further investigation.

Following addition of PMA, the DCF signal increases in a CXXC dependant manner (Figure 5.11), which is reflected by an increase in CD36⁺ cells (Figure 5.12). Moreover, the addition of Gabapentin had a negligible effect on the frequency of CD36⁺ cells, whilst the addition of NAC partially restored the baseline phenotype supporting the notion that this is a ROS mediated process. Examination of cell-cell adhesion by phase contrast microscopy revealed U937-BCAT1(WT) cells are visibly less aggregated compared to U937-Control(EV) following PMA treatment (Appendix D). These images support the flow cytometric data in Figure 5.12 which shows U937-BCAT1(WT) display a decrease

in CD36⁺ cells compared to U937- Control(EV) as CD36 is known to facilitate intracellular adhesion in monocytes(Pietsch, Erl and Lorenz, 1996). Given treatment with the CD36 ligand thrombospondin-1 has been demonstrated to induce apoptosis in primary leukaemia cells and cell lines (K. Li *et al.*, 2003), understanding the role of BCAT1 in redox mediated CD36 expression may be important for future treatment strategies targeting BCAT1, therefore the data presented in this chapter warrant further investigation.

In summary, here it has been demonstrated that BCAT1 overexpression may provide a metabolic proliferative advantage during exponential phase *in vitro*, whilst providing a survival advantage during stationary and death phase through a decrease in intracellular ROS and increase GSH content, which correlates with lowered cellular redox potentials. The data also demonstrate that the CXXC motif is able to modulate intracellular ROS in response serum starvation and PMA induced oxidative stress, where the CXXC motif provides protection from apoptosis and resists differentiation, both features of which are oncogenic processes dysregulated in the development of AML. Therefore, it may be possible to ameliorate these effects by targeting the metabolic activity and the CXXC motif antioxidant contribution of BCAT1 with competitive inhibitors and pro-oxidant therapies. This therapeutic possibility will be subject to investigation in chapter 6.

The work presented in this chapter was accepted for presentation at the 60th Annual American Society of Haematology Meeting, San Diego, USA (Nov, 2018) and the abstract was published in the Blood(Hillier J *et al.*, 2018).

Chapter 6: The effect of BCAT1 CXXC motif on treatment with Cytarabine and the pro-oxidant Rotenone in U937 cells.

6.1 Introduction

Acute Myeloid Leukaemia (AML) has a U.K. incidence of around 3,100 new cases/year approximately, which is ~30% of all leukaemia and survival remains below 15% for patients over the age of 60 (*Leukemia and Lymphoma Society, 2020*). Standard treatment for AML is a two-stage process that involves 1) an 'induction' stage, which aims to kill as many AML blast cells as possible to achieve minimum residual disease (MRD) and 2) a 'consolidation' stage, which aims to prevent relapse (Dombret and Gardin, 2016). During induction phase, high dose chemotherapeutic agents are administered, which interrupt cell division and therefore halt the proliferation of malignant cells. However these therapies are non-specific and target healthy and malignant dividing cells indiscriminately i.e. by disrupting DNA synthesis (Sigal *et al.*, 2010). For example, the widely used AML chemotherapeutic agent Cytarabine (1 β -arabinofuranosylcytosine, aka Ara-C), is a nucleoside analogue of the nucleic acid cytosine, where the ribose sugar of the sugar phosphate backbone for arabinose is substituted producing cytosine arabinose (Jimenez, Wilke and Costa-Lotufo, 2018). Ara-C is randomly incorporated into DNA during semiconservative replication in S-phase interrupting daughter strand synthesis, thus inhibiting all cell growth (Momparler, 2013). Older AML patients in particular respond poorly to this type of non-specific chemotherapy, and are therefore often put on low dose chemotherapy regimens that

are less effective at eradicating the disease, therefore there is a need to develop alternative targeted therapies for this cohort of patients in particular(Löwenberg *et al.*, 2011; Burnett, 2018).

Recently, pro-oxidant therapy, which kills cancer cells through generation of cytotoxic levels of ROS has emerged as an alternative effective treatment strategy to target cancer cells, for which AML cells with particular molecular mutations have responded to such therapies(Agathangelou *et al.*, 2015). Whilst pro-oxidant therapy does not target cancer cells specifically, malignant cells are considered more sensitive to oxidative stress (Zhang, Fang and Wang, 2014). Moreover, quiescent leukaemia stem cells (LSC's), which are not effectively targeted by agents that interrupt cell cycle, can be induced by ROS to exit the stem cell niche. Given these quiescent LSC's are the major cause of MRD (i.e. where a small proportion of leukemic cells remain post-induction therapy) and relapse in AML, targeting these cells with pro-oxidants is an attractive proposition (Jang and Sharkis, 2007). The pro-oxidant Arsenic Trioxide (ATO), is currently used to induce cell death and differentiation in Acute Promyelocytic Leukaemia (APL), and functions by inducing oxidative stress, DNA damage and the mitochondrial pathway of apoptosis i.e. Cytochrome-C release and activation of the caspase cascade(Zhang *et al.*, 2001; Kumar, Yedjou and Tchounwou, 2014).

Alternative ROS agents are currently under investigation for the treatment of AML, which induce ROS in a variety of ways including inhibition of antioxidant transcription factor NF- κ B, GSH depletion and inhibition of oxidative phosphorylation (Zhang, Fang and Wang, 2014). Inhibition of oxidative phosphorylation may represent a particularly attractive target, as AML cells are known to possess a reduced spare

respiratory chain reserve capacity, that is the amount of extra ATP that can be produced in response to increased energy demands (Sriskanthadevan *et al.*, 2015).

Rotenone is a naturally occurring compound found in the roots of several plant species that inhibits mitochondrial complex I, causing a reduction in ATP generation and incomplete transfer of electrons to oxygen resulting in ROS generation (Heinz *et al.*, 2017). Inhibition of oxidative phosphorylation by Rotenone has previously been demonstrated to induce cell death in a number of cancer models, including AML (N. Li *et al.*, 2003; Deng, Huang and Lin, 2010; Hu *et al.*, 2016). In these studies, Rotenone addition was found to initiate mitochondrial apoptosis following cell cycle arrest through activation of caspases, p53 and the pro-apoptotic downstream effector Bax, all of which are known to be redox regulated (Lee *et al.*, 2008). Moreover, in HL-60 cells, Rotenone induced apoptosis could be rescued by addition of antioxidant compounds, such as, NAC, GSH and Vitamin C, reinforcing the role of ROS in Rotenone mediated cell death (N. Li *et al.*, 2003). It has been demonstrated Ara-C initiates apoptosis through the same redox modulated signalling pathway as Rotenone following cell cycle arrest, for example siRNA mediated knockdown of the p53 targets 'Bax' and 'Puma' result in diminished apoptotic response to Ara-C (Vincelette and Yun, 2014).

In Chapter 5 it was demonstrated that BCAT1 expression reduces cellular ROS levels and decreases apoptosis in response to serum starvation induced oxidative stress. Because treatment with Ara-C and Rotenone can alter cellular ROS and induce mitochondrial apoptosis, I hypothesised that BCAT1 in AML may impact on these processes. Therefore, this Chapter investigated whether BCAT1 overexpression provides protection from apoptosis in Ara-C / Rotenone treated U937 transgenic cells. Since the

BCAT1 mediated protection from ROS appeared to involve both the antioxidant effect of the CXXC motif, as well as the metabolic contribution of BCAT1 enzyme, the BCAT1 metabolic inhibitor Gabapentin (Goto *et al.*, 2005) was also investigated. Rapamycin, an inhibitor of the downstream metabolic regulator of cell growth and survival 'mTOR' was also included, since BCAT1 was demonstrated to provide protection against apoptosis (Chapter 5)(Seto, 2012). In this way, knowledge of the pharmacological impact of these drug treatments with respect to BCAT1 overexpression may lead to the potential treatment stratification of AML patients.

6.2 Aims and Objectives

The aim of this study is to examine the effect of the BCAT1 CXXC motif in the treatment of AML. In the previous chapter it was demonstrated BCAT1 overexpression increases survival of U937 cells in response to oxidative stress by a combination of enzymatic and CXXC motif derived antioxidant mechanisms. Therefore, here the efficacy of inducing apoptosis with pro-oxidant therapy and the contribution of the CXXC motif to this process will be evaluated by treatment Rotenone, an inhibitor of mitochondrial complex I that generates endogenous ROS. Given targeted pro-oxidant treatment regimens will be delivered in combination with other therapeutic agents i.e. Cytarabine, Gabapentin and Rotenone, the effect of these agents, which target BCAT1 specifically, has also been examined.

6.2.1 Objectives

- Examine the anti-apoptotic effect of BCAT1 and the CXXC motif to treatment with standard chemotherapeutic Ara-C. Dose-response curves will be generated examining cell viability and cell density from which IC₅₀ calculations were made which will allow for direct comparisons of Ara-C sensitivity between U937-BCAT1(WT), U937-BCAT1(C338S) and U937-Control(EV) cell lines.
- Examine the anti-apoptotic and antioxidant effect of the BCAT1 CXXC motif to treatment with pro-oxidant therapy. Rotenone dose-response curves examining cell viability and cell density from which C₅₀ calculations will be generated for U937-BCAT1(WT), U937-BCAT1(C338S) and U937-Control(EV) cells. Rotenone induced ROS levels was monitored by flow cytometric analysis following DCFDA staining.
- Examine the anti-apoptotic effect of the BCAT1 CXXC motif on treatment with Gabapentin, a direct competitive inhibitor of BCAT1 and Rapamycin, inhibitor of downstream metabolic target mTOR. Gabapentin and Rapamycin dose-response curves and IC₅₀ calculations will be generated for U937-BCAT1(WT), (U937-BCAT1(C338S) and U937-Control(EV) allowing direct evaluation of the BCAT1 CXXC motif cells.

6.3 Methods

6.3.1. Dose Response Curves

Dose Response curves for Ara-C, Gabapentin, Rapamycin, H₂O₂ and Rotenone were generated by a ½ dilution series performed in a 96 well format at a cell density of 5x10⁴ cells/ well. Cells were incubated for 72 h in a cell culture incubator (5 % CO₂ and 37 °C). Following incubation absolute cellular density and viability was determined by flow cytometric analysis using the Viacount stain and Easy Fit cluster analysis algorithm, as described in Section 2.19. All data was normalised to the 'no treatment' control prior to calculation of IC₅₀ values using GraphPad Prism version 5.01 by non-linear regression.

6.3.2 Rotenone Generated ROS by DCFDA Assay

To confirm the involvement of ROS in Rotenone treated transgenic U937 cells, the DCFDA assay was performed as described in Section 2.27. A ½ dilution series of Rotenone was set up and seeded at a density of 5x10⁴ cells/well prior to incubation for 72 h in a cell culture incubator (5% CO₂ and 37 °C). Following incubation, 100µL of 2 µM DCFDA was added directly to the sample and incubated for a further 30 min at 37 °C, prior to flow cytometric analysis. For each sample 10-20 000 events were captured with Incyte software (Merck). Morphological changes were also examined by phase contrast light microscopy.

6.4 Results

6.4.1. Cytarabine Dose Response

To investigate the effect of BCAT1 and the CXXC motif on traditional chemotherapeutic treatment, U937-Control(EV), U937-BCAT1(WT) and U937-BCAT1(C338S) cells were incubated with Ara-C in a ½ dilution series in order to generate a dose response curve. IC₅₀ values were generated against cell density normalised to the 'no treatment control' i.e. the concentration required to reduce cell numbers by 50% (Sebaugh, 2011), show that U937-BCAT1(WT) (0.42±0.13 µM) and U937-BCAT1(C338S) (0.54±0.07 µM) were significantly more sensitive to Cytarabine treatment compared to U937-Control(EV) (2.4±0.07 µM) (Figure 6.1 and Table 6.1, p<0.001). Overall analysis of cell viability reveals that U937-BCAT1(C338S) cells are significantly more sensitive to treatment with Ara-C, compared with either U937-BCAT1(WT) and U937-Control(EV) at all concentrations, suggesting the CXXC motif is providing a protective effect against apoptosis when challenged with Ara-C (Figure 6.1, p<0.001). An increase in the percentage of viable cells at 25-50 µM across all cell lines indicates the presence of Ara-C resistant cell populations.

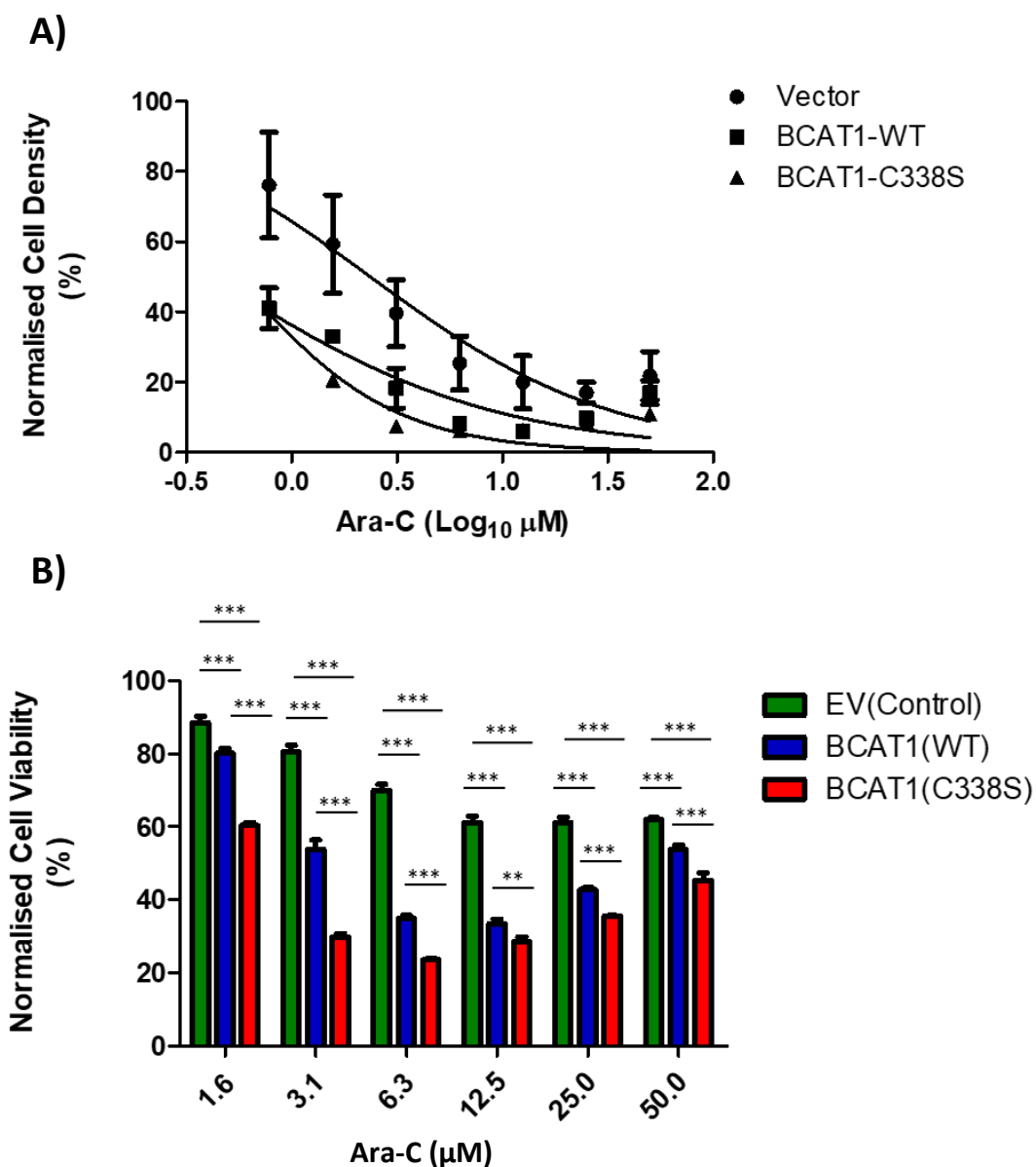


Figure 6.1. Cellular density and viability in response to Ara-C treatment. **A)** Dose response curve displaying cell density in response to Ara-C treatment normalised to no treatment control. Non-linear regression performed shows the IC₅₀ concentration for BCAT1(WT) is 0.42±0.13 μM, BCAT1(C338S) is 0.54±0.07 μM and BCAT1-Control(EV) is 2.4±0.07 μM, p<0.001. **B)** Bar chart representing cell viability following Ara-C treatment for U937-BCAT1(WT), U937-BCAT1(C338S) and U937-Control(EV). Data presented as mean ±SEM n=3 and analysed by 2-way ANOVA Bonferroni post-hoc test *p<0.05, **p<0.01 and***p<0.001.

6.4.2. Gabapentin Dose Response

To investigate the effect of blocking BCAT1 metabolism on cell density and viability, U937-Control(EV), U937-BCAT1(WT) and U937-BCAT1(C338S) cells were incubated with the BCAT1 metabolic activity inhibitor Gabapentin in a ½ dilution series to generate a dose response curve. Data presented in Figure 6.2 and summarised in Table 6.1 indicate that the IC₅₀ value for U937-BCAT1(WT) (28.7±1.1mM) is significantly lower for Gabapentin compared with either U937-BCAT1(C338S) (32.4±2.6mM) and U937-Control(EV) (33.8±1.2mM)(p<0.001). Analysis of cell viability supported this finding, where U937-BCAT1(WT) displays significantly reduced survival across multiple concentrations, compared with U937-Control(EV) cells. The U937-BCAT1(C338S) survival is highly comparable to control cells, showing no significant difference (Figure 6.2).

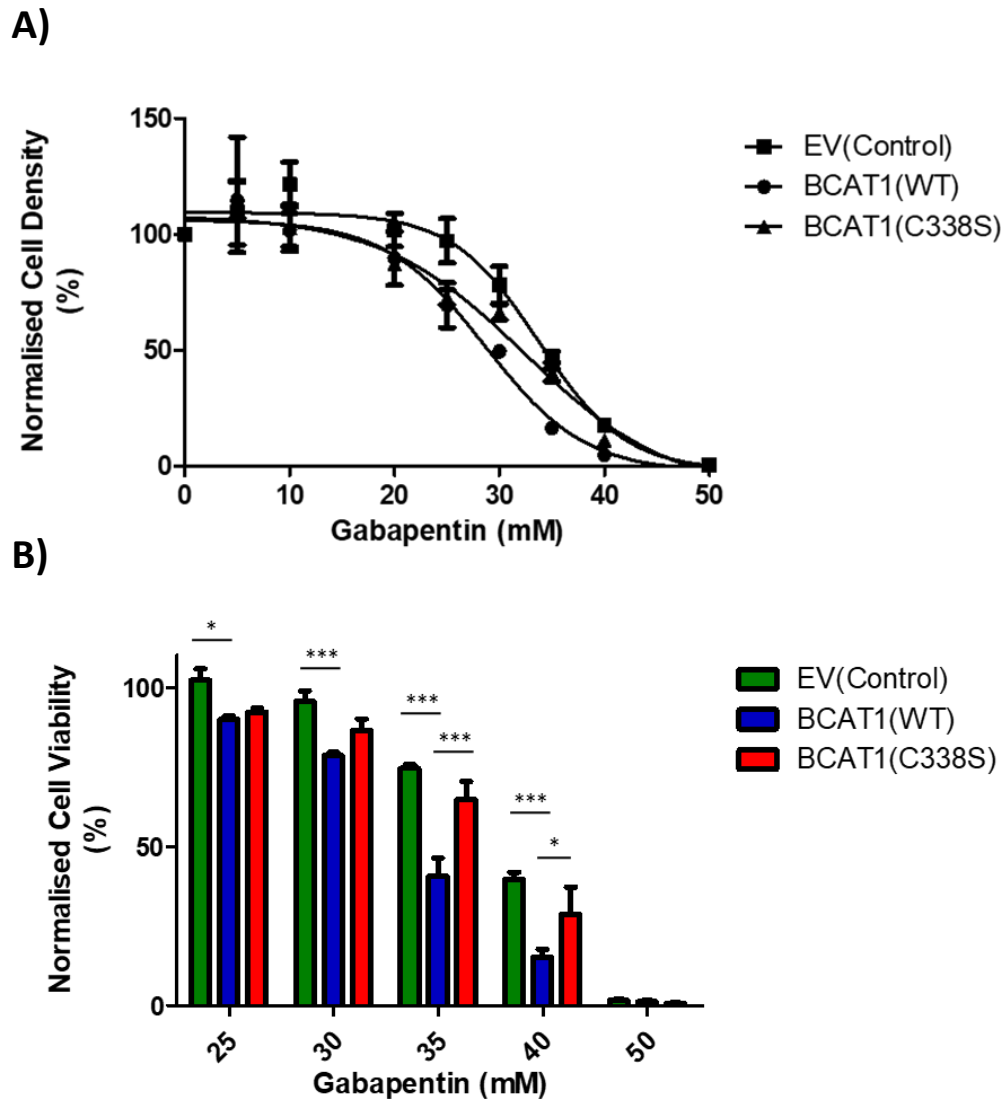


Figure 6.2 Cellular density and viability in response to Gabapentin treatment. A) Dose response curve displaying cell density in response to Gabapentin treatment normalised to no treatment control. Non-linear regression performed shows the IC_{50} concentration for U937-BCAT1(WT) is 28.7 ± 1.1 mM, U937-BCAT1(C338S) is 32.4 ± 2.6 mM and U937-Control(EV) is 33.8 ± 1.2 mM, $p < 0.001$. **B)** Bar chart representing cell viability following Gabapentin treatment for U937-BCAT1(WT), U937-BCAT1(C338S) and U937-Control(EV) cells. Data presented as mean \pm SEM $n=3$ and analysed by 2-way ANOVA with Bonferroni post-hoc test * $p < 0.05$, ** $p < 0.01$ and *** $p < 0.001$.

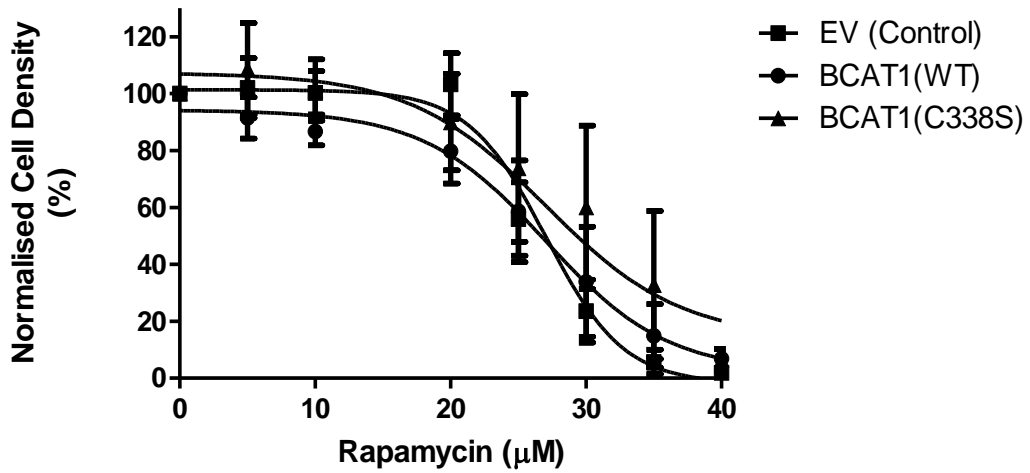
6.4.3. Rapamycin Dose Response

To investigate blocking the downstream metabolic effects of BCAT1 on cell density and viability, U937-Control(EV), U937-BCAT1(WT) and U937-BCAT1(C338S) cells were incubated with the mTOR inhibitor 'Rapamycin' in a ½ dilution series in order to generate a dose response curve. Data presented in Figure 6.3 and Table 6.1, show that IC₅₀ for U937-Control(EV) (36.9±25.9µM), U937-BCAT1(WT) (27.3±2.7µM), U937-BCAT1(C88S)(25.7±0.9µM) were not significantly different. Although Rapamycin had an overall effect of decreasing cell viability across all transgenic U937 cell lines the difference observed between cell lines for each treatment did not reach significance (Figure 6.3, panel B).

Table 6.1 Mean (±SEM) IC50 values for therapeutics across all cell lines

Cell line	Cytarabine (µM)	Gabapentin (mM)	Rapamycin (µM)	Rotenone (nM)
U937-Control(EV)	2.4 ± 0.07	33.8 ± 1.2	36.9 ± 25.9	20.7 ± 1.2
U937-BCAT1(WT)	0.42 ± 0.13	28.7 ± 1.1	27.3 ± 2.7	40.4 ± 1.1
U937-BCAT1(C338S)	0.54 ± 0.07	32.4 ± 2.6	25.7 ± 0.9	20.8 ± 1.1

A)



B)

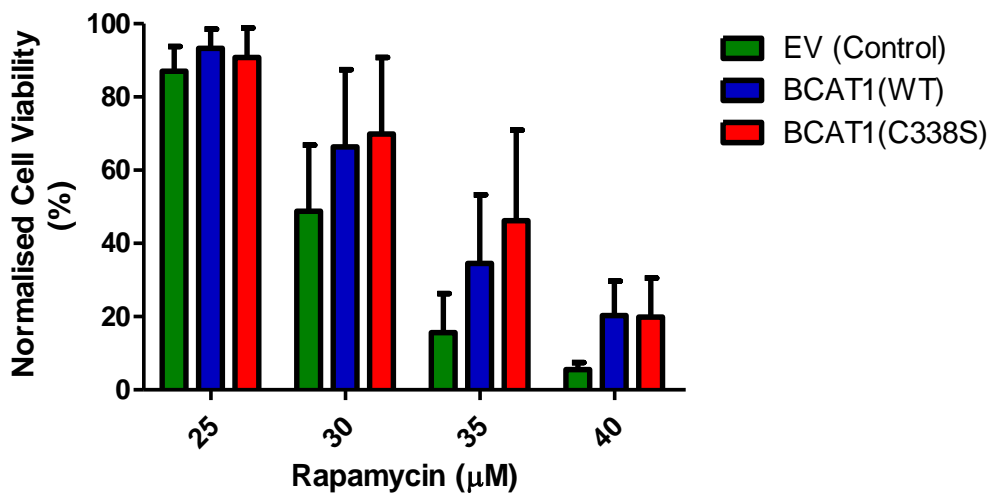


Figure 6.3 Cellular density and viability in response to Rapamycin treatment. A) Dose response curve displaying cell density in response to Rapamycin treatment for U937-BCAT1(WT), U937-BCAT1(C338S) and U937-Control(EV). IC_{50} values for each cell line as calculated by non-linear regression analysis were as follows: $27.3 \pm 2.7 \mu M$, $36.9 \pm 25.9 \mu M$ and $25.7 \pm 0.9 \mu M$ respectively, $p > 0.05$. B) Bar chart representing cell viability following Rapamycin treatment for U937-BCAT1(WT), U937-BCAT1(C338S) and U937-Control(EV). Data presented as mean \pm SEM $n=3$ and analysed by 2-way ANOVA with Bonferroni post-hoc test ($p > 0.05$).

6.4.4. Rotenone Dose Response

To investigate the effect of pro-oxidant treatment on cell density and cell viability, U937-Control(EV), U937-BCAT1(WT) and U937-BCAT1(C338S) cells were incubated with the complex I inhibitor, Rotenone, in a ½ dilution series in order to generate a dose response curve. The data presented in Table 6.1, show that the IC₅₀ value for U937-BCAT1(WT) at 40.4±1.1nM, was significantly higher than that of U937-BCAT1(C338S) at 20.8±1.1nM and U937-Control(EV) cells at 20.7±1.2nM (p<0.001). Additionally, the data shows that U937-BCAT1(C338S) cells show significantly less viability than U937-BCAT1(WT) cells across multiple Rotenone concentrations (Figure 6.4). Moreover U937-BCAT1(C338S) cells display significantly reduced levels of intracellular ROS at 60 nM Rotenone compared to U937-BCAT1(WT) (Figure 6.5, p<0.05), where ROS levels inversely correlate with viability, indicating that the CXXC motif provides an antioxidant protective effect against Rotenone induced ROS insult (Figure 6.5).

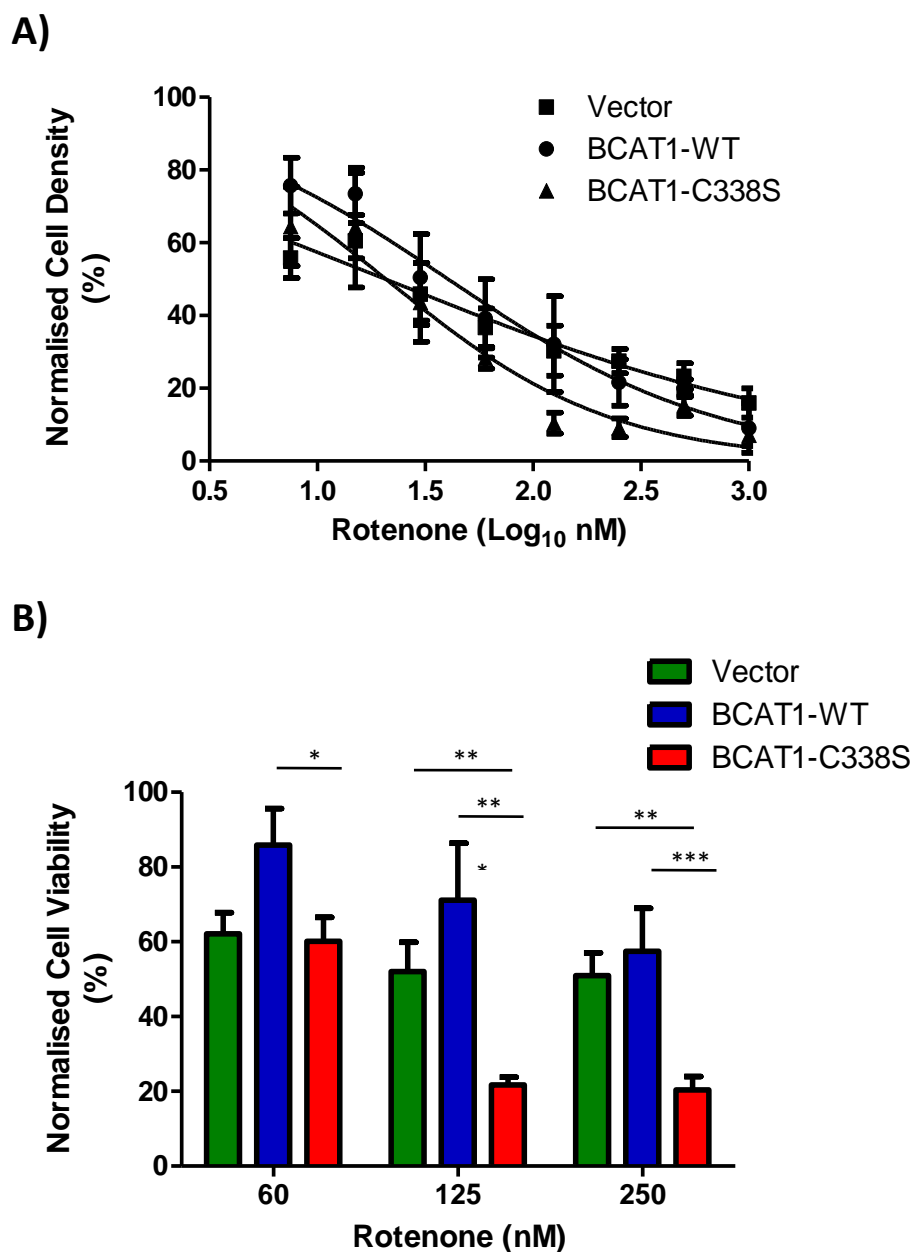


Figure 6.4 Cellular density and viability in response to Rotenone treatment. **A)** Dose response curve displaying cell density in response to Rotenone treatment for U9367-BCAT1(WT), U937-BCAT1(C338S) and U937-Control(EV). Non-linear regression analysis generated the IC₅₀ values for each as, 40.4±1.1nM, 20.8±1.1nM and 20.7±1.2nM, respectively (p<0.001). **B)** Bar chart representing cell viability following Rotenone treatment for U937-BCAT1(WT), U937-BCAT1(C338S) and U937-Control(EV). Data presented as mean ±SEM n=3 and analysed by 2-way ANOVA with Bonferroni post-hoc test (*p<0.05, **p<0.01 and ***p<0.001).

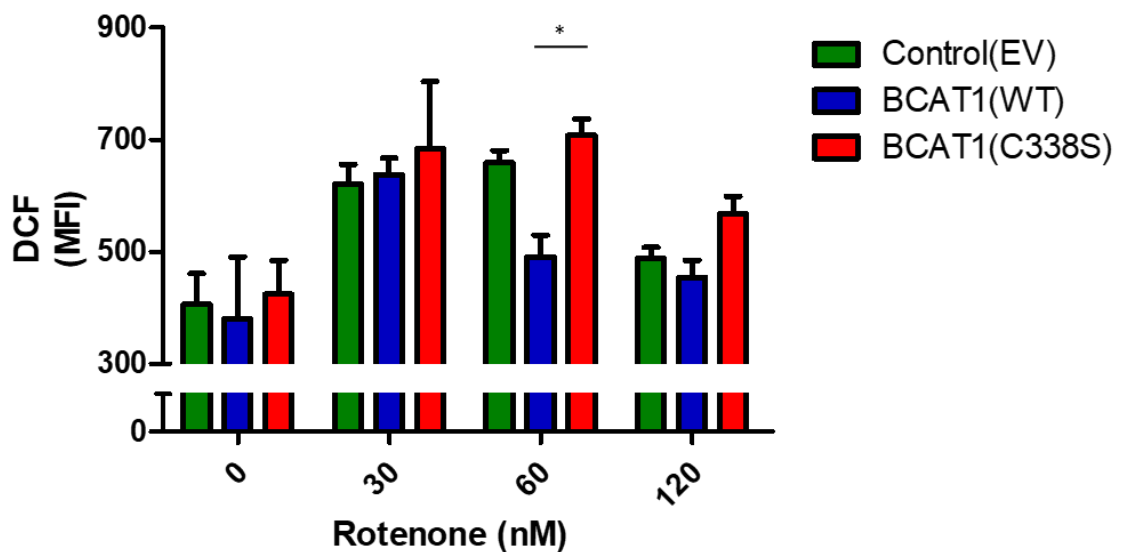


Figure 6.5 The effect of BCAT1 overexpression on intracellular ROS following Rotenone treatment. 5×10^4 cells per well were suspended in a 96 well plate with complete RPMI + Rotenone and incubated for 72 h prior to staining with DCFDA. Data presented show DCF signal for U937-BCAT(WT), U937-BCAT1(C338S) and U937-Control(EV). At 60 nM BCAT1(WT) displays significantly decreased intracellular ROS compared BCAT1(C338S) control. Data presented as mean \pm SEM n=4 and analysed by 2-way ANOVA Bonferroni post-hoc test (*p<0.05).

6.5 Discussion

The aim of this chapter was to examine the effect of the BCAT1 CXXC motif in the treatment of AML with a view to proposing a treatment strategy for AML patients stratified according to BCAT1 expression level i.e. BCAT1^{high} and BCAT1^{low}. Frontline treatment for AML involves intensive courses of non-specific drugs that are in many cases unsuitable for patients over 75 (Oran and Weisdorf, 2012), the age group for which AML diagnosis is most common, therefore there is need to identify more specific targeted therapies that can be administered in conjunction with lower dose traditional treatments (*Leukemia and Lymphoma Society*, 2020). For this reason, the growth and survival following treatment with pro-oxidant Rotenone, BCAT1 metabolic inhibitor Gabapentin and downstream inhibitor of mTOR Rapamycin, alongside common chemotherapeutic agent Ara-C was examined here.

The data presented in this chapter demonstrate that BCAT1 overexpressing U937 cells, were more sensitive to Ara-C treatment, displaying reduced IC₅₀ values compared to U937-Control(EV) cells (Table 6.1). As outlined in section 6.1, Ara-C is a nucleoside analogue that interrupts DNA synthesis preventing cell division stalling DNA replication during S-phase (Momparker, 2013). In Chapter 5, it was demonstrated that BCAT1 overexpressing cells display a significantly higher percentage of cells in G2M phase (Figure 5.2). This previous finding coupled with notion that Ara-C targets S-phase, would explain the increased sensitivity exhibited by BCAT1 overexpressing cells as demonstrated here in Figure 6.1. Additionally, the data here shows that U937-BCAT(WT) cells display significantly higher viability than U937-BCAT1(C338S) at all treatment concentrations when challenged with Ara-C (Figure 6.1), therefore the CXXC motif

appears to be providing a partial protective effect. To the best of knowledge, this is the first study of its kind to demonstrate this.

Previous studies show Ara-C induces cell death through the DNA damage response system via the ATR-Chk1-p53 pathway, resulting in cell cycle arrest and activation of mitochondrial apoptosis (Schenk *et al.*, 2012; Siddiqui *et al.*, 2013). To support this model, siRNA mediated knockdown of p53 targets BAX and Puma resulted in diminished apoptotic response to Ara-C (Vincelette and Yun, 2014). This pathway is ROS regulated through redox sensitive proteins upstream and downstream of the mitochondria, for example both p53 and the Cysteine-Aspartic proteases (Caspase) family of apoptotic effector proteins, are susceptible to oxidation of catalytic cysteine thiols in response to oxidative stress (Baker, Santos and Powis, 2000). Moreover, procaspase-9, procaspase-3 and caspase-3 are susceptible to S-glutathionylation, which decreases accessibility for proteolytic cleavage, resulting in resistance to apoptosis (Simon, Haj-Yehia and Levi-Schaffer, 2000; Redza-Dutordoir and Averill-Bates, 2016). Similarly it has been demonstrated that p53 is S-glutathionylated after oxidant treatment, decreasing DNA binding affinity, a process which was ameliorated by treatment with antioxidants (Sun *et al.*, 2003). These studies demonstrate a more reductive redox environment may protect against ROS induced mitochondrial apoptosis. Taken together with the data presented in Chapter 5, where it was demonstrated that metabolic and CXXC mediated BCAT1 effects lowers cellular ROS and increases the cellular GSH pool, it is plausible that BCAT1 may indirectly influence p53 and caspase activity, explaining why U937-BCAT1(WT) cells are more resistant to Ara-C mediated killing than either U937-BCAT1(C338S) and U937-Control(EV).

Given that BCAT1 expression reduces cellular ROS and increases the GSH pool, the possibility that BCAT1 low expressing AML cells may therefore be targeted by pro-oxidant treatment using Rotenone was explored. Strikingly, the data show that U937-BCAT1(WT) overexpressing cells display an IC₅₀ value that was double the concentration of U937-BCAT1(C338S) and U937-Control(EV) cells (Figure 6.5). Additionally, U937-BCAT1(WT) retained significantly more viability compared with U937-BCAT1(C338S) cells across multiple Rotenone concentrations, where increased survival related to decreased intracellular ROS (Figure 6.4 and 6.5). This data indicates that the BCAT1 CXXC motif survival advantage is conferred through a reduction in the cellular redox environment i.e. an antioxidant effect.

Rotenone is a 'pro-oxidant', that increases mitochondrial ROS generation through inhibition of complex I of the electron transport chain and has been shown to induce apoptosis in a wide range of cancer models including APL, neuroblastoma and liver cells (Deng, Huang and Lin, 2010; Sriskanthadevan *et al.*, 2015). In the breast cancer cell line, MCF-7, Rotenone induced apoptosis is mediated through an increase in the pro-apoptotic 'p53 target' Bax (Deng, Huang and Lin, 2010). Moreover, in the liver cell line, HepG2, Rotenone induced cytotoxicity resulted in the upregulation of - p53, Bax, and caspase-3, with down-regulation of Bcl-2 mRNA, indicating that Rotenone induced apoptosis is mediated through these previously described redox sensitive pathways (Deng, Huang and Lin, 2010; Siddiqui *et al.*, 2013). Given that the data presented here demonstrate that BCAT1 overexpression results in a CXXC dependant reduction in intracellular ROS following Rotenone treatment, it is possible that increased cell survival

as seen in U937-BCAT1(WT) is mediated by modulating these pathways, however, further research is required, which is beyond the scope of this thesis.

In Chapter 5, one of the most important observations was the demonstration that BCAT1 overexpression was linked to an increased survival in response to serum starvation induced oxidative stress (Figure 5.7). This observation was attributed to both the CXXC motif and metabolic aspect of BCAT1, therefore the efficacy of metabolic inhibitor Gabapentin was next investigated in the U937 transgenic cells. Gabapentin is a competitive inhibitor of BCAT1, and has been proposed to act as a leucine analogue (Goto *et al.*, 2005), however there are various hypotheses about the effects of Gabapentin treatment in leukaemia, which depend on the direction on the BCAT1 metabolic reaction (i.e. $\text{leucine} + \alpha\text{-KG} \rightarrow \alpha\text{-ketoisocaproate} + \text{Glutamate}$ or $\alpha\text{-ketoisocaproate} + \text{Glutamate} \rightarrow \text{Leucine} + \alpha\text{-KG}$, see Section 1.3). For example, in a CML model it has been demonstrated that Gabapentin decreases cell density, where it is proposed that treatment results in a decreased leucine production blocking mTOR activation (Hattori *et al.*, 2017). Conversely, Gabapentin treatment has been demonstrated to reduce BCAT1 metabolite Glutamate in neuronal cells (Tönjes *et al.*, 2013). Wang *et al* theorised that BCAT1 supplies Glutamate for GSH synthesis, thus protecting the BCAT1 overexpressing cell from ROS inducing Epidermal Growth Factor Receptor Tyrosine Kinase therapy (Wang *et al.*, 2019). Contrary to these studies, Grankvist *et al* demonstrated that Gabapentin can suppress cell density independent of BCAT1 mediated BCAA transamination, although they admit a convincing alternative mechanism remains unclear (Grankvist *et al.*, 2018). Here treatment with Gabapentin shows a decreased density and viability for U937-BCAT1(WT) significantly more than

U937-Control(EV) (Figure 6.2), supporting the notion that Gabapentin treatment is targeting the BCAT1 metabolic activity. However, this treatment effect is nullified for U937-BCAT1(C338S) cells, indicating that there is a redox component, perhaps in this context the increased ROS levels found in BCAT1(C338S) cells, that is providing a proliferative advantage compared to U937-BCAT1(WT). Moreover, these results may indicate that pro-oxidant treatment works antagonistically with Gabapentin in patients with high BCAT1 expression and warrants further investigation.

Finally, given that BCAT1 has been proposed to activate the growth and survival regulator mTOR, through leucine production (Hattori *et al.*, 2017), the efficacy of the mTOR inhibitor 'Rapamycin' was examined here. For U937-BCAT1(WT) and U937-BCAT1(EV) controls, no significant difference in density or viability was observed (Figure 6.3). This may suggest that for the U937 cell line, BCAT1 favours the leucine catabolism, and therefore mTOR activation remains unaffected by blocking BCAT1 activity, although this cannot be confirmed from the data presented here. Exploration of BCAT1 overexpression in multiple AML cell lines will be needed to elucidate this along with a metabolomics approach to evaluate BCAT1 metabolite changes, which is beyond the scope for this thesis.

In summary here we have demonstrated for the first time that BCAT1 CXXC motif protects against standard chemotherapeutic treatment with Ara-C and Rotenone mediated pro-oxidant treatment. Ultimately both treatment effects are likely to be redox mediated, possibly through cysteine thiol oxidation/ S-glutathionylation of the Caspase family and p53 resulting in differential expression of the BCL-2 pro and anti-apoptotic effectors, although further work is needed to confirm this. Given this, it may

be possible to further increase the efficacy of Ara-C treatment in BCAT1 overexpressing cells by combining treatment pro-oxidant therapies opening up a new therapeutic avenue for clinicians.

The work presented in this chapter was accepted for presentation at the Annual British Society of Haematology Meeting, Birmingham, UK (April, 2020) and the abstract was published in the British Journal for Haematology (Hillier J et al., 2020).

Chapter 7. Final Discussion and Future Work

7.1 Final Discussion

BCAT1 is an aminotransferase that catalyses the breakdown of Branched Chain Amino Acids (BCAA) leucine, isoleucine and valine by transfer of NH_3 from the BCAA to α -ketoglutarate (α -KG) forming the respective branched-chain alpha-keto acid (BCKA) and glutamate (J Davoodi *et al.*, 1998). These metabolites play important roles in a variety of cellular processes, including in cellular energetics, epigenetics and glutathione synthesis which are all dysregulated in AML. It is perhaps not surprising then that whilst expression of BCAT1 in healthy individuals is restricted to Haematopoietic Stem Cells (HSC) and the central nervous system (Hutson, 2001), it is highly dysregulated in numerous cancers, including AML, where it is generally associated with unfavourable outcomes (Xu *et al.*, 2016, 2018b). Recently, there has been increasing research interest in the metabolic effects of BCAT1, and several studies have examined the effect of BCAT1 silencing in myeloid leukaemia and various other cancer models (Tönjes *et al.*, 2013; Raffel *et al.*, 2017b; Zhang and Han, 2017; Wang *et al.*, 2019). However, currently there have been no studies examining the effect of the BCAT1 CXXC motif, a redox sensitive sequence conserved in the cytosolic and mitochondrial BCAT isoforms and a feature of many antioxidant enzymes (Fomenko and Gladyshev, 2003).

This project has examined the effect of overexpressing wild-type BCAT1 and CXXS motif mutant in U937 cells, in order to determine whether the CXXC motif is capable of modulating cellular oxidative stress and how this may affect processes important in the development of AML including proliferation and apoptosis. Mutating

the C338 cysteine residue to serine altered one atom from sulphur to oxygen (Figure 3.1), preserving the metabolic activity of the enzyme whilst abolishing the antioxidant capacity, therefore comparison of U937-BCAT1(WT) and U937-BCAT1(C338S) overexpressing cells against the U937-Control(EV) allowed the contribution of the CXXC motif to be elucidated.

In vitro characterisation of the transgenic U937 cells revealed that U937-BCAT(WT) and U937-BCAT1(C338S) overexpressing cells had a reduced doubling time as well as increased cell density and viability compared to U937-Control(EV), see Chapter 5. The reduction in doubling time during exponential growth was matched by an increased proportion of G2M phase cells, whilst increased cell density / viability related to lower levels of intracellular ROS / increased Glutathione (GSH) in BCAT1 overexpressing cells. Although U937-BCAT1(WT) displayed a consistently lower doubling time, intracellular ROS and higher GSH content than U937-BCAT1(C338S) failed to reach significance indicating that in this context these effects were predominantly due to BCAT1 metabolic activity.

Understanding the metabolic contribution of BCAT1 to the observations on cell growth and survival is not straightforward. Traditionally BCAT1 is seen as the first step in the catabolic breakdown of BCAAs leucine, isoleucine and valine (Figure 1.4), however *in vitro* enzyme kinetic data shows that BCAT1 favours BCAA anabolism i.e. the production of α -KG and Leucine (Conway *et al.*, 2008), however metabolomic studies indicate that the BCAT1 enzymatic reaction is context dependant, where proliferating cells favour the canonical reverse reaction (α -ketoisocaproate + Glutamate \rightarrow Leucine + α -KG) and quiescent cells favour the canonical forward reaction i.e. Leucine + α -KG \rightarrow

α -ketoisocaproate + Glutamate)(Raffel *et al.*, 2017; Wang *et al.*, 2019). The data presented in this thesis appears to agree with this interpretation, where an increased number of G2M phase cells during exponential growth indicates BCAT1 is stimulating growth through production of α -KG and leucine (Chapter 5). In this model of explanation, α -KG anaplerotically replenishes the TCA cycle, whilst leucine activates mTOR stimulating growth and survival (Pathways seen in Figure 1.7)(Zhang and Han, 2017).

Following exponential growth *in vitro* cell cultures enter a stationary phase, where peak cell densities are reached, here U937-BCAT1(WT) and U937-BCAT1(C338S) reached significantly higher cell density than U937-Control(EV)(Figure 5.1). An explanation for this result may lie in the much studied observation that cancer cells display an increased dependency on glutamine metabolism, which is converted to glutamate by Glutaminase and subsequently to α -KG by Glutamate dehydrogenase (GDH), thus producing the toxic ammonium ion (NH_4^+)(Altman, Stine and Dang, 2016). Aminotransferases, including BCAT1, allow conversion of Glutamate to α -KG without NH_4^+ production, which inhibits growth and survival in closed cultures(Schneider, Marison and Von Stockar, 1996).

Furthermore, it was shown that as *in vitro* cell cultures entered the stationary phase GSH content increased and intracellular ROS decreased in BCAT1 overexpressing cells suggesting that the transamination reaction mediated by BCAT1 has reversed during stationery and death phases i.e. leucine + α -KG \rightarrow α -ketoisocaproate + glutamate. Glutamate is a precursor for GSH synthesis which is the most abundant small molecule antioxidant, cellular antioxidant enzymes including Glutathione peroxidase

(GPx) and Peroxiredoxins (Prx) require GSH to act as an electron donor to in the reductive elimination of ROS and to regenerate antioxidant enzymes to their reduced active forms(Hanschmann *et al.*, 2013). Therefore, an increase in glutamate production should permit increased GSH synthesis and decreased ROS levels in BCAT1 overexpressing U937 transgenic cells, which the data presented in Chapter 5 support.

Following on from the stationary phase, *in vitro* cell cultures enter death phase, here after 192 h in culture U937-BCAT(WT) cells were significantly more viable than U937-BCAT1(C338S) (Figure 5.3), indicating that the BCAT1 CXXC motif may, in part, be ameliorating ROS driven apoptosis. To investigate this further U937 transgenic cells were placed under serum starvation to induce mitochondrial derived ROS (Li, Chen and Gibson, 2013). Serum starvation induced a cell line dependant increase in cellular ROS and where U937-Control(EV)> U937-BCAT1(C338S)> U937-BCAT1(WT), a finding which was associated with proportional increase in apoptosis (Figures 5.5, 5.7 and 5.8). Moreover, the serum starvation phenotype was rescued by across all cell lines by addition of antioxidant N-acetyl-cysteine (NAC), demonstrating this effect was, ROS driven and therefore redox mediated. However, given that U937-BCAT1(C338S) displayed lower ROS and concurrent apoptosis compared to U937-BCAT1(EV) it must be reiterated that there is evidence to suggest that a part of the effect of BCAT1 overexpression on U937 cell survival is likely due to the aminotransferase metabolic activity of BCAT1, presumably by production of glutamate as precursor to GSH, which is increased in both U937-BCAT1(WT) and U937-BCAT1(C338S) to equivalent levels (Figure 5.6).

AML is partially defined as a block in cellular differentiation, a cellular process which is taken to be redox mediated. Previous work has demonstrated that PMA induces differentiation in U937 cells through the ROS second messenger, H₂O₂(Yamamoto *et al.*, 2009). Moreover, recent work has demonstrated metabolic inhibition of BCAT1 suppresses production of Itaconate following lipopolysaccharide stimulation of macrophages(Papathanassiou *et al.*, 2017; Ko *et al.*, 2020). Given Itaconate is known to suppress Succinate Dehydrogenase(O'Neill and Artyomov, 2019), a known source of mitochondrial ROS, it was important to assess the impact of the CXXC motif on ROS following treatment with PMA.

In Chapter 5, treatment with PMA resulted in an increased ROS signal in a CXXC dependant manner i.e. ROS levels were greatest in U937-Control(EV) > U937-BCAT1(C338S) > U937BCAT1(WT). This observation related to a proportional change in PMA induced CD36 expression, a cell surface marker of monocyte differentiation(Huh *et al.*, 1996). Treatment with the BCAT1 inhibitor Gabapentin had a negligible effect on cellular ROS levels, however treatment with the antioxidant NAC effectively rescued the phenotype, reinforcing the notion PMA induced CD36 expression is ROS mediated, and that the BCAT1 CXXC modulates ROS levels in this process, thus causing a differentiation block.

Interestingly, BCAT1 overexpressing U937 cells displayed decreased basal percentage of CD36⁺ cells compared to control(EV) cells, despite displaying no significant difference in basal ROS levels. It is possible modifying the CXXC motif by cysteine to serine substitution may have disrupted a redox sensitive signalling cascade. Work by Conway *et al.*, 2008, demonstrated that under reducing conditions, BCAT1 binds to

several redox sensitive proteins that are associated with cytoskeletal remodelling. However, under oxidative stress, these proteins no longer bind to BCAT1. Moreover, through NEM alkylation studies, it was demonstrated that cysteine residues were essential to these redox interactions, where mutating the BCAT1 CXXC motif to SXXS, completely abolished these interactions (Conway *at al.*, 2008). The data in Figure 5.12 shows that U937-Control(EV) display the highest basal percentage of CD36⁺ cells followed by U937-BCAT1(C338S) and U937-BCAT1(WT) respectively. Given this, it may be that mutation of the C338 residue to serine has disrupted CXXC motif protein interactions that lie upstream of CD36, altering expression, however further proteomic studies are needed to elucidate this mechanism.

Having previously established a protective role for the BCAT1 CXXC motif in oxidative stress induced apoptosis (Figures 5.7 and 5.8), chapter 6 looked to evaluate if the BCAT1 CXXC motif could protect against treatment with the pro-oxidant Rotenone, or against the standard chemotherapeutic Ara-C, which is known to induce apoptosis through redox regulated pathways (Irwin, Rivera-Del Valle and Chandra, 2013). Indeed, the results show that the BCAT1 CXXC motif protects against Rotenone induced apoptosis, which related to lower levels of intracellular ROS levels (Figures 6.4 and 6.5). Conversely, both BCAT1(WT) and BCAT1(C338S) overexpressing U937 cells were demonstrated to be more sensitive than U937-Control(EV) cells to Ara-C treatment, perhaps reflecting the observation BCAT1 overexpressing cells display an increased proportion of G2M phase cells (Figure 5.2). Ara-C interrupts cell division during the preceding S-phase (Momparker, 2013) therefore increased Ara-C sensitivity in these cells would be expected.

Comparison between U937-BCAT1(WT) and U937-BCAT(C338S) cellular viability shows that the CXXC motif provide a small but significant protective effect following Ara-C treatment. This effect may be explained by the fact that Ara-C induced apoptosis has been demonstrated to be conducted through the ATR-Chk1-p53 pathway, resulting in activation mitochondrial mediated apoptosis, for which ROS is implicated(Liu, Chen and St. Clair, 2008). In summary, it appears that the mechanism of Ara-C mediated apoptosis in the context of BCAT1 overexpressing AML is complex. Whilst an increased S-phase may explain an increase in Ara-C sensitivity, reduced levels of ROS conferred by BCAT1 CXXC motif may in part negate the Ara-C sensitivity.

In conclusion, this thesis has demonstrated that the BCAT1 CXXC motif is able to modulate the intracellular redox environment in response to oxidative stress and that this impacts processes important to the development of AML, including cellular differentiation and apoptosis. Moreover, BCAT1 provides CXXC motif derived protection against pro-oxidant treatment whilst increasing sensitivity to treatment with standard chemotherapeutic Ara-C. This study therefore provides the first evidence to support the hypothesis set out in the introduction that the BCAT1 CXXC motif behaves as a novel antioxidant.

7.2 Future Work

Investigating BCAT1 CXXC motif derived CD36 expression

The data presented here show that CD36⁺ expression is reduced in U937-BCAT1(WT) cells compared to U937-BCAT1(C338S), however the mechanism for this difference remains unclear. CD36 has been identified to be under the control antioxidant transcription factor Nrf2 in macrophages (Ishii *et al.*, 2004). Nrf2 is redox

regulated, where under low ROS conditions, cytoplasmic Nrf2 interacts with KEAP1. However, under oxidative stress, KEAP1 undergoes cysteine thiol oxidation, which mediates the dissociation from Nrf2, which then translocates to the nucleus, inducing expression of numerous genes, including CD36 (Ishii *et al.*, 2004). It is possible that the BCAT1 CXXC motif is providing an antioxidant effect that is preventing disassociation of KEAP1 from Nrf2, explaining the decreased CD36 expression. Resolving the extent of Nrf2 expression in U937-BCAT1(WT) and U937-BCAT1(C388S) cells would be an important step to understanding the mechanism behind reduced CD36 expression seen in BCAT1 overexpressing cells. Moreover, the downregulation of CD36 in BCAT1 expressing cells may have implications for AML treatment, given that CD36 ligand 'Thrombospondin-1' has been shown to induce apoptosis and has been investigated as a possible therapeutic in CD36 positive cells (K. Li *et al.*, 2003). If the BCAT1 CXXC motif is indeed linked to a wider redox sensing network that involves Nrf2, it may be possible to induce CD36 expression with pro-oxidants, thus allowing combinational Thrombospondin-1 treatment for BCAT1^{high} AML patients.

CD36 stimulation has also been associated with actin polymerisation in macrophages, which links CD36 signalling to cellular migration, adhesion, and phagocytosis (Stuart *et al.*, 2007). Interestingly, as previously described in Chapter 5, work by Conway *et al.*, 2008 demonstrated that under reducing conditions BCAT1 binds to several redox sensitive proteins that are associated with cytoskeletal remodelling including β -tubulin, Septin-4 and Myosin-6, all of which disassociate under oxidative stress (Conway *et al.*, 2008). Mutation of the CXXC motif in this thesis may have altered a host of proteins that associate with BCAT1(WT) under 'reduced' and 'oxidised'

intracellular conditions. Therefore, a proteomic approach to compare proteins interactions with BCAT1(WT) and BCAT1(C338S) may uncover a previously unknown signalling components that links BCAT1 and cytoskeletal remodelling. The Conway et al., 2008 study demonstrated that these redox interactions occur in neural cells, however the nature of these interaction in healthy myeloid blood and myeloid leukaemia cells remains unknown. Indeed, superficially, U937-BCAT1(C338S) cells appear to exhibit more extraneous pseudopodia than U937-BCAT(WT) cells upon visual examination. Therefore, future work that incorporates migration assays may reveal a significant difference between the two cell lines.

Combinational Therapy investigations

The data presented in Chapter 6 illustrate that BCAT1 confers sensitivity to treatment to with Ara-C, whilst the CXXC motif provides protection against pro-oxidant Rotenone treatment. However, it is not known if Rotenone can be delivered in combination with Ara-C. Combinational therapies can be assessed by isobologram, which allows assessment of drug-drug interactions(Huang *et al.*, 2019). Drugs may work synergistically (where a lower dose is required in combination to achieve the same effect than if used alone), antagonistically (where a higher dose is required in combination to achieve the same effect than when used alone) or additive (dose required is the same as when used alone). Given pro-oxidant drugs may be delivered in conjunction with standard chemotherapy(Roboz *et al.*, 2008), examining the combinational effects in our U937 transgenic cells will allow the efficacy of pro-oxidant therapy in the targeted treatment of BCAT1 to be realistically assessed before primary cell investigations

Publications

- Hillier, J. et al. (2018) 'Identification and Characterisation of a Novel Antioxidant Activity for the BCAT1 CXXC Motif: Implications for Myeloid Leukaemia Development', *Blood. American Society of Haematology*, 132(Supplement 1), pp. 1473–1473. doi: 10.1182/blood-2018-99-118823.
- Hillier, J et al. (2020) ' BCAT1 increases sensitivity to Cytarabine and confers CXXC motif derived resistance to pro-oxidant treatment in Acute Myeloid Leukaemia cells', *British Journal of Haematology*, 189(Supplement 1), pp.4–294. <https://doi.org/10.1111/bjh.16638>

References

- Acute myeloid leukaemia - NHS* (no date). Available at: <https://www.nhs.uk/conditions/acute-myeloid-leukaemia/> (Accessed: 1 May 2020).
- Agathangelou, A. *et al.* (2015) 'Targeting the ataxia telangiectasia mutated-null phenotype in chronic lymphocytic leukemia with pro-oxidants', *Haematologica*, 100(8), pp. 1076–1085. doi: 10.3324/haematol.2014.115170.
- Akinduro, O. *et al.* (2018) 'Proliferation dynamics of acute myeloid leukaemia and haematopoietic progenitors competing for bone marrow space', *Nature Communications*, 9(1), pp. 1–12. doi: 10.1038/s41467-017-02376-5.
- Alfonso-Prieto, M. *et al.* (2009) 'The molecular mechanism of the catalase reaction', *Journal of the American Chemical Society*, 131(33), pp. 11751–11761. doi: 10.1021/ja9018572.
- Altman, B. J., Stine, Z. E. and Dang, C. V. (2016) 'From Krebs to clinic: Glutamine metabolism to cancer therapy', *Nature Reviews Cancer*. Nature Publishing Group, pp. 619–634. doi: 10.1038/nrc.2016.71.
- Andersson, A. *et al.* (2005) 'Gene expression profiling of leukemic cell lines reveals conserved molecular signatures among subtypes with specific genetic aberrations', *Leukemia*, 19(6), pp. 1042–1050. doi: 10.1038/sj.leu.2403749.
- Aquaro, S. *et al.* (2002) 'Macrophages and HIV infection: therapeutical approaches toward this strategic virus reservoir.', *Antiviral research*, 55(2), pp. 209–25. doi: 10.1016/s0166-3542(02)00052-9.
- Arai, F. *et al.* (2004) 'Tie2/angiopoietin-1 signaling regulates hematopoietic stem cell quiescence in the bone marrow niche', *Cell*, 118(2), pp. 149–161. doi: 10.1016/j.cell.2004.07.004.
- Arber, D. A. *et al.* (2016) 'The 2016 revision to the World Health Organization classification of myeloid neoplasms and acute leukemia', *Blood*. American Society of Hematology, pp. 2391–2405. doi: 10.1182/blood-2016-03-643544.

Arber, D. A. *et al.* (no date) 'The 2016 revision to the World Health Organization classification of myeloid neoplasms and acute leukemia'. doi: 10.1182/blood-2016-03-643544.

Armstrong, J. S. *et al.* (2002) 'Role of glutathione depletion and reactive oxygen species generation in apoptotic signaling in a human B lymphoma cell line', *Cell Death and Differentiation*, 9(3), pp. 252–263. doi: 10.1038/sj.cdd.4400959.

Arnér, E. S. and Holmgren, A. (2000) 'Physiological functions of thioredoxin and thioredoxin reductase.', *European journal of biochemistry*, 267(20), pp. 6102–9. Available at: <http://www.ncbi.nlm.nih.gov/pubmed/11012661> (Accessed: 1 August 2018).

Arnér, E. S. J. and Holmgren, A. (2000) 'Physiological functions of thioredoxin and thioredoxin reductase', *European Journal of Biochemistry*, 267(20), pp. 6102–6109. doi: 10.1046/j.1432-1327.2000.01701.x.

Arya, M. *et al.* (2005) 'Basic principles of real-time quantitative PCR', *Expert Review of Molecular Diagnostics*, pp. 209–219. doi: 10.1586/14737159.5.2.209.

Baker, A., Santos, B. Dos and Powis, G. (2000) 'Redox control of caspase-3 activity by thioredoxin and other reduced proteins', *Biochemical and Biophysical Research Communications*, 268(1), pp. 78–81. doi: 10.1006/bbrc.1999.1908.

Baran, C. *et al.* (2004) 'The Role of ROS and RNS in Regulating Life and Death of Blood Monocytes', *Current Pharmaceutical Design*, 10(8), pp. 855–866. doi: 10.2174/1381612043452866.

Battin, E. E. and Brumaghim, J. L. (2009) 'Antioxidant activity of sulfur and selenium: A review of reactive oxygen species scavenging, glutathione peroxidase, and metal-binding antioxidant mechanisms', *Cell Biochemistry and Biophysics*. Springer, pp. 1–23. doi: 10.1007/s12013-009-9054-7.

Bedard, K. and Krause, K. H. (2007) 'The NOX family of ROS-generating NADPH oxidases: Physiology and pathophysiology', *Physiological Reviews*, pp. 245–313. doi: 10.1152/physrev.00044.2005.

- Bennett, J. M. *et al.* (1976) 'Proposals for the Classification of the Acute Leukaemias French-American-British (FAB) Co-operative Group', *British Journal of Haematology*, 33(4), pp. 451–458. doi: 10.1111/j.1365-2141.1976.tb03563.x.
- Birnie, G. D. (1988) 'The HL60 cell line: A model system for studying human myeloid cell differentiation', *British Journal of Cancer*, 58(SUPPL. 9), pp. 41–45.
- Bobadilla, S., Sunseri, N. and Landau, N. R. (2013) 'Efficient transduction of myeloid cells by an HIV-1-derived lentiviral vector that packages the Vpx accessory protein', *Gene Therapy*, 20(5), pp. 514–520. doi: 10.1038/gt.2012.61.
- Boulais, P. E. and Frenette, P. S. (2015) 'Making sense of hematopoietic stem cell niches', *Blood*, 125(17), pp. 2621–2629. doi: 10.1182/blood-2014-09-570192.
- Božok, V. *et al.* (2018) 'Antioxidative CXXC Peptide Motif From Mesencephalic Astrocyte-Derived Neurotrophic Factor Antagonizes Programmed Cell Death', *Frontiers in Cell and Developmental Biology*, 6(SEP), p. 106. doi: 10.3389/fcell.2018.00106.
- Brandes, R. P., Weissmann, N. and Schröder, K. (2014) 'Nox family NADPH oxidases: Molecular mechanisms of activation', *Free Radical Biology and Medicine*. Elsevier Inc., pp. 208–226. doi: 10.1016/j.freeradbiomed.2014.07.046.
- Braun, F. *et al.* (2011) 'Serum-Nutrient Starvation Induces Cell Death Mediated by Bax and Puma That Is Counteracted by p21 and Unmasked by Bcl-xL Inhibition', *PLoS ONE*. Edited by A. L. Gartel, 6(8), p. e23577. doi: 10.1371/journal.pone.0023577.
- Bromberg, O. *et al.* (2012) 'Osteoblastic N-cadherin is not required for microenvironmental support and regulation of hematopoietic stem and progenitor cells', *Blood*, 120(2), pp. 303–313. doi: 10.1182/blood-2011-09-377853.
- Bunting, J. R. *et al.* (1989) 'Fluorescent cationic probes of mitochondria. Metrics and mechanism of interaction', *Biophysical Journal*, 56(5), pp. 979–993. doi: 10.1016/S0006-3495(89)82743-2.
- Burda, P., Laslo, P. and Stopka, T. (2010) 'The role of PU.1 and GATA-1 transcription factors during normal and leukemogenic hematopoiesis', *Leukemia*. Nature Publishing

Group, pp. 1249–1257. doi: 10.1038/leu.2010.104.

Burnett, A. K. (2013) 'The challenge of AML in older patients', *Mediterranean Journal of Hematology and Infectious Diseases*. Universita Cattolica del Sacro Cuore. doi: 10.4084/mjhid.2013.038.

Burnett, A. K. (2018) 'Treatment of Older Patients With Newly Diagnosed AML Unfit for Traditional Therapy', *Clinical Lymphoma, Myeloma and Leukemia*. Elsevier Inc., pp. 553–557. doi: 10.1016/j.clml.2018.06.027.

Cadet, J. and Richard Wagner, J. (2013) 'DNA base damage by reactive oxygen species, oxidizing agents, and UV radiation', *Cold Spring Harbor Perspectives in Biology*, 5(2). doi: 10.1101/cshperspect.a012559.

Cairolì, R. *et al.* (2006) 'Prognostic impact of c-KIT mutations in core binding factor leukemias: An Italian retrospective study', *Blood*, 107(9), pp. 3463–3468. doi: 10.1182/blood-2005-09-3640.

Cauchy, P. *et al.* (2015) 'Chronic FLT3-ITD Signaling in Acute Myeloid Leukemia Is Connected to a Specific Chromatin Signature.', *Cell reports*, 12(5), pp. 821–36. doi: 10.1016/j.celrep.2015.06.069.

Chan, E. Y. (2009) 'mTORC1 phosphorylates the ULK1-mAtg13-FIP200 autophagy regulatory complex', *Science Signaling*. American Association for the Advancement of Science, pp. pe51–pe51. doi: 10.1126/scisignal.284pe51.

Chanfreau, G. F. (2017) 'Impact of RNA Modifications and RNA-Modifying Enzymes on Eukaryotic Ribonucleases', in *Enzymes*. Academic Press, pp. 299–329. doi: 10.1016/bs.enz.2017.03.008.

Chang, I.-W. *et al.* (2016) 'BCAT1 overexpression is an indicator of poor prognosis in patients with urothelial carcinomas of the upper urinary tract and urinary bladder', *Histopathology*, 68(4), pp. 520–532. doi: 10.1111/his.12778.

Charrier, S. *et al.* (2011) 'Quantification of lentiviral vector copy numbers in individual hematopoietic colony-forming cells shows vector dose-dependent effects on the

frequency and level of transduction', *Gene Therapy*, 18(5), pp. 479–487. doi: 10.1038/gt.2010.163.

Cherepanov, P. *et al.* (2003) 'HIV-1 integrase forms stable tetramers and associates with LEDGF/p75 protein in human cells', *Journal of Biological Chemistry*, 278(1), pp. 372–381. doi: 10.1074/jbc.M209278200.

Circu, M. L. and Aw, T. Y. (2012) 'Glutathione and modulation of cell apoptosis', *Biochimica et Biophysica Acta - Molecular Cell Research*. NIH Public Access, pp. 1767–1777. doi: 10.1016/j.bbamcr.2012.06.019.

Ciuffi, A. (2008) 'Mechanisms Governing Lentivirus Integration Site Selection', *Current Gene Therapy*, 8(6), pp. 419–429. doi: 10.2174/156652308786848021.

Cluntun, A. A. *et al.* (2017) 'Glutamine Metabolism in Cancer: Understanding the Heterogeneity', *Trends in Cancer*. Cell Press, pp. 169–180. doi: 10.1016/j.trecan.2017.01.005.

Coles, S. J. *et al.* (2009) 'S-nitrosoglutathione inactivation of the mitochondrial and cytosolic BCAT proteins: S-nitrosation and s-thiolation', *Biochemistry*, 48(3), pp. 645–656. doi: 10.1021/bi801805h.

Coles, S. J., Hancock, J. T. and Conway, M. E. (2012) 'Differential redox potential between the human cytosolic and mitochondrial branched-chain aminotransferase', *Acta Biochimica et Biophysica Sinica*, 44(2), pp. 172–176. doi: 10.1093/abbs/gmr103.

Coles, S. J. and Wadley, A. J. (1995) *Can BCAT1 expression level help predict disease progression in chronic lymphocytic leukaemia*. Available at: <https://www.ncbi.nlm.nih.gov/geo/> (Accessed: 22 July 2020).

Collet, J. F. and Messens, J. (2010) 'Structure, function, and mechanism of thioredoxin proteins', *Antioxidants and Redox Signaling*. Mary Ann Liebert, Inc. 140 Huguenot Street, 3rd Floor New Rochelle, NY 10801 USA , pp. 1205–1216. doi: 10.1089/ars.2010.3114.

Conway, M. E. *et al.* (2008) 'Regulatory control of human cytosolic branched-chain

aminotransferase by oxidation and S-glutathionylation and its interactions with redox sensitive neuronal proteins', *Biochemistry*, 47(19), pp. 5465–5479. doi: 10.1021/bi800303h.

Conway, Myra E, Poole, L. B. and Hutson, S. M. (2004) 'Roles for cysteine residues in the regulatory CXXC motif of human mitochondrial branched chain aminotransferase enzyme.', *Biochemistry*, 43(23), pp. 7356–64. doi: 10.1021/bi0498050.

Conway, Myra E., Poole, L. B. and Hutson, S. M. (2004) 'Roles for cysteine residues in the regulatory CXXC motif of human mitochondrial branched chain aminotransferase enzyme', *Biochemistry*, 43(23), pp. 7356–7364. doi: 10.1021/bi0498050.

Coombs, C. C., Tavakkoli, M. and Tallman, M. S. (2015) 'Acute promyelocytic leukemia: where did we start, where are we now, and the future.', *Blood cancer journal*, 5(4), p. e304. doi: 10.1038/bcj.2015.25.

Cronin, J., Zhang, X.-Y. and Reiser, J. (2005) 'Altering the Tropism of Lentiviral Vectors through Pseudotyping', *Current Gene Therapy*, 5(4), pp. 387–398. doi: 10.2174/1566523054546224.

Daigneault, M. *et al.* (2010) 'The Identification of Markers of Macrophage Differentiation in PMA-Stimulated THP-1 Cells and Monocyte-Derived Macrophages'. doi: 10.1371/journal.pone.0008668.

Dana, H. *et al.* (2017) 'Molecular Mechanisms and Biological Functions of siRNA.', *International journal of biomedical science : IJBS*, 13(2), pp. 48–57. Available at: <http://www.ncbi.nlm.nih.gov/pubmed/28824341> (Accessed: 14 April 2020).

Davoodi, J *et al.* (1998) 'Overexpression and characterization of the human mitochondrial and cytosolic branched-chain aminotransferases.', *The Journal of biological chemistry*, 273(9), pp. 4982–9. doi: 10.1074/jbc.273.9.4982.

Davoodi, Jamshid *et al.* (1998) 'Overexpression and characterization of the human mitochondrial and cytosolic branched-chain aminotransferases', *Journal of Biological Chemistry*, 273(9), pp. 4982–4989. doi: 10.1074/jbc.273.9.4982.

Definitive hematopoietic stem cells first develop within the major arterial regions of the mouse embryo (no date). Available at:

<https://www.ncbi.nlm.nih.gov/pmc/articles/PMC212758/> (Accessed: 29 April 2020).

Degos, L. *et al.* (1995) 'All-trans-retinoic acid as a differentiating agent in the treatment of acute promyelocytic leukemia [see comments]', *Blood*, 85(10). Available at:

<http://www.bloodjournal.org/content/85/10/2643.short?sso-checked=true> (Accessed: 16 March 2018).

Deng, Y. T., Huang, H. C. and Lin, J. K. (2010) 'Rotenone induces apoptosis in MCF-7 human breast cancer cell-mediated ROS through JNK and p38 signaling', *Molecular Carcinogenesis*, 49(2), pp. 141–151. doi: 10.1002/mc.20583.

Deynoux, M. *et al.* (2016) 'Hypoxia and Hypoxia-Inducible Factors in Leukemias.', *Frontiers in oncology*, 6, p. 41. doi: 10.3389/fonc.2016.00041.

Dhakshinamoorthy, S. *et al.* (2005) 'Bach1 competes with Nrf2 leading to negative regulation of the antioxidant response element (ARE)-mediated NAD(P)H:quinone oxidoreductase 1 gene expression and induction in response to antioxidants', *Journal of Biological Chemistry*, 280(17), pp. 16891–16900. doi: 10.1074/jbc.M500166200.

Ding, L. and Morrison, S. J. (2013) 'Haematopoietic stem cells and early lymphoid progenitors occupy distinct bone marrow niches', *Nature*, 495(7440), pp. 231–235. doi: 10.1038/nature11885.

Döhner, H., Weisdorf, D. J. and Bloomfield, C. D. (2015) 'Acute myeloid leukemia', *New England Journal of Medicine*. Edited by D. L. Longo. Massachusetts Medical Society, pp. 1136–1152. doi: 10.1056/NEJMra1406184.

Dombret, H. and Gardin, C. (2016) 'An update of current treatments for adult acute myeloid leukemia', *Blood*. American Society of Hematology, pp. 53–61. doi: 10.1182/blood-2015-08-604520.

Downing, J. R. (2003) 'The core-binding factor leukemias: lessons learned from murine models', *Current Opinion in Genetics & Development*, 13(1), pp. 48–54. doi: 10.1016/S0959-437X(02)00018-7.

- Dröge, W. (2002) 'Free Radicals in the Physiological Control of Cell Function', *Physiological Reviews*, 82(1), pp. 47–95. doi: 10.1152/physrev.00018.2001.
- Drolle, H. *et al.* (2015) 'Hypoxia regulates proliferation of acute myeloid leukemia and sensitivity against chemotherapy', *Leukemia Research*, 39(7), pp. 779–785. doi: 10.1016/j.leukres.2015.04.019.
- Dull, T. *et al.* (1998) 'A third-generation lentivirus vector with a conditional packaging system.', *Journal of virology*, 72(11), pp. 8463–71. Available at: <http://www.ncbi.nlm.nih.gov/pubmed/9765382> (Accessed: 10 December 2019).
- Einhauer, A. and Jungbauer, A. (2001) 'The FLAGTM peptide, a versatile fusion tag for the purification of recombinant proteins', *Journal of Biochemical and Biophysical Methods*, pp. 455–465. doi: 10.1016/S0165-022X(01)00213-5.
- Emadi, A. (2015) 'Exploiting AML vulnerability: glutamine dependency.', *Blood*, 126(11), pp. 1269–70. doi: 10.1182/blood-2015-07-659508.
- Eruslanov, E. and Kusmartsev, S. (2010) 'Identification of ROS using oxidized DCFDA and flow-cytometry', *Methods in Molecular Biology*, 594, pp. 57–72. doi: 10.1007/978-1-60761-411-1_4.
- Escribano, L. *et al.* (1998) 'Expression of the c-kit (CD117) molecule in normal and malignant hematopoiesis', *Leukemia and Lymphoma*. Informa Healthcare, pp. 459–466. doi: 10.3109/10428199809057558.
- Facts and Statistics | Leukemia and Lymphoma Society* (no date). Available at: <https://www.lls.org/facts-and-statistics/facts-and-statistics-overview/facts-and-statistics> (Accessed: 29 April 2020).
- Fato, R. *et al.* (2009) 'Differential effects of mitochondrial Complex I inhibitors on production of reactive oxygen species', *Biochimica et Biophysica Acta - Bioenergetics*, 1787(5), pp. 384–392. doi: 10.1016/j.bbabi.2008.11.003.
- Feng, J.-H. *et al.* (2012) 'Prognostic significance of IDH1 mutations in acute myeloid leukemia: a meta-analysis.', *American journal of blood research*, 2(4), pp. 254–64. doi:

10.3892/mco.2013.222.

Finkelshtein, D. *et al.* (2013) 'LDL receptor and its family members serve as the cellular receptors for vesicular stomatitis virus', *Proceedings of the National Academy of Sciences of the United States of America*, 110(18), pp. 7306–7311. doi: 10.1073/pnas.1214441110.

Fomenko, D. E. and Gladyshev, V. N. (2003) 'Identity and Functions of CxxC-Derived Motifs ⁺', *Biochemistry*, 42(38), pp. 11214–11225. doi: 10.1021/bi034459s.

Forman, H. J., Zhang, H. and Rinna, A. (2009) 'Glutathione: Overview of its protective roles, measurement, and biosynthesis', *Molecular Aspects of Medicine*. NIH Public Access, pp. 1–12. doi: 10.1016/j.mam.2008.08.006.

Fridovich, I. (1983) 'Superoxide Radical: An Endogenous Toxicant', *Annual Review of Pharmacology and Toxicology*, 23(1), pp. 239–257. doi: 10.1146/annurev.pa.23.040183.001323.

Galloway, J. L. *et al.* (2005) 'Loss of Gata1 but not Gata2 converts erythropoiesis to myelopoiesis in zebrafish embryos', *Developmental Cell*, 8(1), pp. 109–116. doi: 10.1016/j.devcel.2004.12.001.

Gary Gilliland, D. and Griffin, J. D. (2002a) 'The roles of FLT3 in hematopoiesis and leukemia', *Blood*, pp. 1532–1542. doi: 10.1182/blood-2002-02-0492.

Gary Gilliland, D. and Griffin, J. D. (2002b) 'The roles of FLT3 in hematopoiesis and leukemia', *Blood*, 100(5), pp. 1532–1542. doi: 10.1182/blood-2002-02-0492.

Godfrey, R. *et al.* (2012) 'Cell transformation by FLT3 ITD in acute myeloid leukemia involves oxidative inactivation of the tumor suppressor protein-tyrosine phosphatase DEP-1/ PTPRJ', *Blood*, 119(19), pp. 4499–4511. doi: 10.1182/blood-2011-02-336446.

Gorrini, C., Harris, I. S. and Mak, T. W. (2013) 'Modulation of oxidative stress as an anticancer strategy', *Nature Reviews Drug Discovery*, pp. 931–947. doi: 10.1038/nrd4002.

Goto, M. *et al.* (2005) 'Structural determinants for branched-chain aminotransferase

- isozyme-specific inhibition by the anticonvulsant drug gabapentin', *Journal of Biological Chemistry*, 280(44), pp. 37246–37256. doi: 10.1074/jbc.M506486200.
- Grankvist, N. *et al.* (2018) 'Gabapentin Can Suppress Cell Proliferation Independent of the Cytosolic Branched-Chain Amino Acid Transferase 1 (BCAT1)', *Biochemistry*, 57(49), pp. 6762–6766. doi: 10.1021/acs.biochem.8b01031.
- Greenbaum, A. *et al.* (2013) 'CXCL12 in early mesenchymal progenitors is required for haematopoietic stem-cell maintenance', *Nature*, 495(7440), pp. 227–230. doi: 10.1038/nature11926.
- Grek, C. L. *et al.* (2013) 'Causes and consequences of cysteine s-glutathionylation', *Journal of Biological Chemistry*. American Society for Biochemistry and Molecular Biology, pp. 26497–26504. doi: 10.1074/jbc.R113.461368.
- Grimwade, D. *et al.* (2010) 'Refinement of cytogenetic classification in acute myeloid leukemia: determination of prognostic significance of rare recurring chromosomal abnormalities among 5876 younger adult patients treated in the United Kingdom Medical Research Council trials.', *Blood*, 116(3), pp. 354–65. doi: 10.1182/blood-2009-11-254441.
- Halliwell, B. (2003) 'Oxidative stress in cell culture: An under-appreciated problem?', *FEBS Letters*, 540(1–3), pp. 3–6. doi: 10.1016/S0014-5793(03)00235-7.
- Hanahan, D. and Weinberg, R. A. (2011) 'Hallmarks of cancer: The next generation', *Cell*, 144(5), pp. 646–674. doi: 10.1016/j.cell.2011.02.013.
- Hanschmann, E. M. *et al.* (2013) 'Thioredoxins, glutaredoxins, and peroxiredoxins-molecular mechanisms and health significance: From cofactors to antioxidants to redox signaling', *Antioxidants and Redox Signaling*. Mary Ann Liebert, Inc., pp. 1539–1605. doi: 10.1089/ars.2012.4599.
- Hattori, A. *et al.* (2017) 'Cancer progression by reprogrammed BCAA metabolism in myeloid leukaemia', *Nature*, 545(7655), pp. 500–504. doi: 10.1038/nature22314.
- Vander Heiden, M., Cantley, L. and Thompson, C. (2009) 'Understanding the Warburg

effect: The metabolic Requirements of cell proliferation', *Science*, 324(5930), pp. 1029–1033. doi: 10.1126/science.1160809.Understanding.

Heinz, S. *et al.* (2017) 'Mechanistic Investigations of the Mitochondrial Complex I Inhibitor Rotenone in the Context of Pharmacological and Safety Evaluation', *Scientific Reports*, 7(1), pp. 1–13. doi: 10.1038/srep45465.

Ho Young Huh *et al.* (1995) 'CD36 induction on human monocytes upon adhesion to tumor necrosis factor- activated endothelial cells', *Journal of Biological Chemistry*, 270(11), pp. 6267–6271. doi: 10.1074/jbc.270.11.6267.

Hole, Paul S *et al.* (2013) 'Overproduction of NOX-derived ROS in AML promotes proliferation and is associated with defective oxidative stress signaling.', *Blood*, 122(19), pp. 3322–30. doi: 10.1182/blood-2013-04-491944.

Hole, Paul S. *et al.* (2013) 'Overproduction of NOX-derived ROS in AML promotes proliferation and is associated with defective oxidative stress signaling', *Blood*, 122(9), pp. 3322–3330. doi: 10.1182/blood-2013-04-491944.

Hrecka, K. *et al.* (2011) 'Vpx relieves inhibition of HIV-1 infection of macrophages mediated by the SAMHD1 protein', *Nature*, 474(7353), pp. 658–661. doi: 10.1038/nature10195.

Hu, W. *et al.* (2016) 'Rotenone induces apoptosis in human lung cancer cells by regulating autophagic flux', *IUBMB Life*, 68(5), pp. 388–393. doi: 10.1002/iub.1493.

Huang, R. *et al.* (2014) 'Megakaryocytic differentiation of K562 cells induced by PMA reduced the activity of respiratory chain complex IV', *PLoS ONE*, 9(5). doi: 10.1371/journal.pone.0096246.

Huang, R. Y. *et al.* (2019) 'Isobologram analysis: A comprehensive review of methodology and current research', *Frontiers in Pharmacology*. Frontiers Media S.A. doi: 10.3389/fphar.2019.01222.

Huh, H. Y. *et al.* (1996) *Regulated Expression of CD36 During Monocyte-to-Macrophage Differentiation: Potential Role of CD36 in Foam Cell Formation.*

Hutson, S. (2001) 'Structure and function of branched chain aminotransferases', *Progress in Nucleic Acid Research and Molecular Biology*. Academic Press Inc., pp. 175–206. doi: 10.1016/s0079-6603(01)70017-7.

Inoki, K., Corradetti, M. N. and Guan, K. L. (2005) 'Dysregulation of the TSC-mTOR pathway in human disease', *Nature Genetics*, pp. 19–24. doi: 10.1038/ng1494.

International Union of Pure and Applied Chemistry. Commission on Equilibrium Data. *et al.* (1979) *Ionisation constants of organic acids in aqueous solution*. Oxford ;;New York: Pergamon Press.

Irwin, M. E., Rivera-Del Valle, N. and Chandra, J. (2013) 'Redox control of leukemia: From molecular mechanisms to therapeutic opportunities', *Antioxidants and Redox Signaling*. Mary Ann Liebert, Inc., pp. 1349–1383. doi: 10.1089/ars.2011.4258.

Ishii, T. *et al.* (2004) 'Role of Nrf2 in the Regulation of CD36 and Stress Protein Expression in Murine Macrophages', *Circulation Research*, 94(5), pp. 609–616. doi: 10.1161/01.RES.0000119171.44657.45.

Ivanovs, A. *et al.* (2017) 'Human haematopoietic stem cell development: From the embryo to the dish', *Development (Cambridge)*. Company of Biologists Ltd, pp. 2323–2337. doi: 10.1242/dev.134866.

Jacque, N. *et al.* (2015) 'Targeting glutaminolysis has antileukemic activity in acute myeloid leukemia and synergizes with BCL-2 inhibition', *Blood*, 126(11), pp. 1346–1356. doi: 10.1182/blood-2015-01-621870.

Jagannathan-Bogdan, M. and Zon, L. I. (2013) 'Hematopoiesis', *Development (Cambridge)*, 140(12), pp. 2463–2467. doi: 10.1242/dev.083147.

Jang, Y. Y. and Sharkis, S. J. (2007) 'A low level of reactive oxygen species selects for primitive hematopoietic stem cells that may reside in the low-oxygenic niche', *Blood*, 110(8), pp. 3056–3063. doi: 10.1182/blood-2007-05-087759.

Jayavelu, A. K. *et al.* (2016) 'NOX4-driven ROS formation mediates PTP inactivation and cell transformation in FLT3ITD-positive AML cells', *Leukemia*, 30(2), pp. 473–483. doi:

10.1038/leu.2015.234.

Jewell, J. L., Russell, R. C. and Guan, K.-L. (2013) 'Amino acid signalling upstream of mTOR.', *Nature reviews. Molecular cell biology*, 14(3). doi: 10.1038/nrm3522.

Jimenez, P. C., Wilke, D. V. and Costa-Lotufo, L. V. (2018) 'Marine drugs for cancer: Surfacing biotechnological innovations from the oceans', *Clinics*. Universidade de Sao Paulo. doi: 10.6061/clinics/2018/e482s.

Jin, L. and Zhou, Y. (2019) 'Crucial role of the pentose phosphate pathway in malignant tumors (review)', *Oncology Letters*, 17(5), pp. 4213–4221. doi: 10.3892/ol.2019.10112.

Kamal, A. M. *et al.* (2016) 'Expression of thioredoxin-1 (TXN) and its relation with oxidative DNA damage and treatment outcome in adult AML and ALL: A comparative study', *Hematology*, 21(10), pp. 567–575. doi: 10.1080/10245332.2016.1173341.

Kang, W. *et al.* (2014) 'Anti-tat Hutat2: Fc mediated protection against tat-induced neurotoxicity and HIV-1 replication in human monocyte-derived macrophages', *Journal of Neuroinflammation*, 11(1), p. 195. doi: 10.1186/s12974-014-0195-2.

Karathedath, S. *et al.* (2017) 'Role of NF-E2 related factor 2 (Nrf2) on chemotherapy resistance in acute myeloid leukemia (AML) and the effect of pharmacological inhibition of Nrf2', *PLoS ONE*, 12(5). doi: 10.1371/journal.pone.0177227.

Kiel, M. J. *et al.* (2005) 'SLAM family receptors distinguish hematopoietic stem and progenitor cells and reveal endothelial niches for stem cells', *Cell*, 121(7), pp. 1109–1121. doi: 10.1016/j.cell.2005.05.026.

Kim, S. H. *et al.* (2008) 'Identification of human thioredoxin as a novel IFN-gamma-induced factor: Mechanism of induction and its role in cytokine production', *BMC Immunology*, 9(1), pp. 1–15. doi: 10.1186/1471-2172-9-64.

Klasse, P. J. (2015) 'Molecular determinants of the ratio of inert to infectious virus particles', in *Progress in Molecular Biology and Translational Science*. Elsevier B.V., pp. 285–326. doi: 10.1016/bs.pmbts.2014.10.012.

Ko, J.-H. *et al.* (2020) 'BCAT1 affects mitochondrial metabolism independently of

- leucine transamination in activated human macrophages', *Journal of Cell Science*, 133(22), p. jcs.247957. doi: 10.1242/jcs.247957.
- Kobiler, O. *et al.* (2012) 'Virus strategies for passing the nuclear envelope barrier', *Nucleus (United States)*. doi: 10.4161/nucl.21979.
- Kumar, S., Yedjou, C. G. and Tchounwou, P. B. (2014) 'Arsenic trioxide induces oxidative stress, DNA damage, and mitochondrial pathway of apoptosis in human leukemia (HL-60) cells', *Journal of Experimental and Clinical Cancer Research*, 33(1). doi: 10.1186/1756-9966-33-42.
- Kutner, R. H., Zhang, X. Y. and Reiser, J. (2009) 'Production, concentration and titration of pseudotyped HIV-1-based lentiviral vectors', *Nature Protocols*, 4(4), pp. 495–505. doi: 10.1038/nprot.2009.22.
- Lacaud, G. *et al.* (2002) 'Runx1 is essential for hematopoietic commitment at the hemangioblast stage of development in vitro', *Blood*, 100(2), pp. 458–466. doi: 10.1182/blood-2001-12-0321.
- Lam, C. F. *et al.* (2018) 'Reactive oxygen species activate differentiation gene transcription of acute myeloid leukemia cells via the JNK/c-JUN signaling pathway', *Leukemia Research*, 68, pp. 112–119. doi: 10.1016/j.leukres.2018.03.012.
- Laplante, M. and Sabatini, D. M. (2009) 'mTOR signaling at a glance', *Journal of Cell Science*, 122(20), pp. 3589–3594. doi: 10.1242/jcs.051011.
- Lee, J. *et al.* (2008) 'Essential roles of caspases and their upstream regulators in rotenone-induced apoptosis', *Biochemical and Biophysical Research Communications*, 371(1), pp. 33–38. doi: 10.1016/j.bbrc.2008.03.149.
- Lee, S. B. *et al.* (2010) 'Serum deprivation-induced reactive oxygen species production is mediated by Romo1', *Apoptosis*, 15(2), pp. 204–218. doi: 10.1007/s10495-009-0411-1.
- Lee, S., Kim, S. M. and Lee, R. T. (2013) 'Thioredoxin and thioredoxin target proteins: From molecular mechanisms to functional significance', *Antioxidants and Redox*

Signaling. Mary Ann Liebert, Inc., pp. 1165–1207. doi: 10.1089/ars.2011.4322.

Leslie, N. R. *et al.* (2003) 'Redox regulation of PI 3-kinase signalling via inactivation of PTEN.', *The EMBO journal*, 22(20), pp. 5501–10. doi: 10.1093/emboj/cdg513.

Leukaemia (all subtypes combined) statistics | Cancer Research UK (no date). Available at: <https://www.cancerresearchuk.org/health-professional/cancer-statistics/statistics-by-cancer-type/leukaemia#heading-Zero> (Accessed: 1 May 2020).

Leukaemia | Cancer Research UK (no date). Available at: <https://www.cancerresearchuk.org/about-cancer/leukaemia> (Accessed: 1 May 2020).

Li, K. *et al.* (2003) 'Thrombospondin-1 induces apoptosis in primary leukemia and cell lines mediated by CD36 and Caspase-3', *International Journal of Molecular Medicine*. doi: 10.3892/ijmm.12.6.995.

Li, L., Chen, Y. and Gibson, S. B. (2013) 'Starvation-induced autophagy is regulated by mitochondrial reactive oxygen species leading to AMPK activation', *Cellular Signalling*, 25(1), pp. 50–65. doi: 10.1016/j.cellsig.2012.09.020.

Li, N. *et al.* (2003) 'Mitochondrial complex I inhibitor rotenone induces apoptosis through enhancing mitochondrial reactive oxygen species production', *Journal of Biological Chemistry*, 278(10), pp. 8516–8525. doi: 10.1074/jbc.M210432200.

Li, S. *et al.* (2000) 'The role of cellular glutathione peroxidase redox regulation in the suppression of tumor cell growth by manganese superoxide dismutase', *Cancer Research*, 60(14), pp. 3927–3939.

Liberti, M. V. and Locasale, J. W. (2016) 'The Warburg Effect: How Does it Benefit Cancer Cells?', *Trends in Biochemical Sciences*. Elsevier Ltd, pp. 211–218. doi: 10.1016/j.tibs.2015.12.001.

Liu, B., Chen, Y. and St. Clair, D. K. (2008) 'ROS and p53: A versatile partnership', *Free Radical Biology and Medicine*. NIH Public Access, pp. 1529–1535. doi: 10.1016/j.freeradbiomed.2008.01.011.

Loft, S. and Poulsen, H. E. (1996) 'Cancer risk and oxidative DNA damage in man',

Journal of Molecular Medicine. Springer Verlag, pp. 297–312. doi: 10.1007/BF00207507.

Loft, S. and Poulsen, H. E. (1998) 'Estimation of oxidative DNA damage in man from urinary excretion of repair products.', *Acta biochimica Polonica*, 45(1), pp. 133–44. Available at: <http://www.ncbi.nlm.nih.gov/pubmed/9701506> (Accessed: 29 April 2020).

Löwenberg, B. *et al.* (2011) 'Cytarabine Dose for Acute Myeloid Leukemia', *New England Journal of Medicine*, 364(11), pp. 1027–1036. doi: 10.1056/NEJMoa1010222.

Lu, S. C. (2013) 'Glutathione synthesis', *Biochimica et Biophysica Acta - General Subjects*. NIH Public Access, pp. 3143–3153. doi: 10.1016/j.bbagen.2012.09.008.

Lushchak, V. I. (2014) 'Free radicals, reactive oxygen species, oxidative stress and its classification', *Chemico-Biological Interactions*. Elsevier Ireland Ltd, pp. 164–175. doi: 10.1016/j.cbi.2014.10.016.

Marcussen, M. and Larsen, P. J. (1996) 'Cell Cycle-Dependent Regulation of Cellular ATP Concentration, and Depolymerization of the Interphase Microtubular Network Induced by Elevated Cellular ATP Concentration in Whole Fibroblasts', *Cell Motility and the Cytoskeleton*, 35(2), pp. 94–99. doi: 10.1002/(SICI)1097-0169(1996)35:2<94::AID-CM2>3.0.CO;2-I.

Marengo, B. *et al.* (2016) 'Redox homeostasis and cellular antioxidant systems: Crucial players in cancer growth and therapy', *Oxidative Medicine and Cellular Longevity*, 2016. doi: 10.1155/2016/6235641.

Martin-Gallardo, A. *et al.* (1988) 'A comparison of bovine growth-hormone gene expression in mouse L cells directed by the Moloney murine-leukemia virus long terminal repeat, simian virus-40 early promoter or cytomegalovirus immediate-early promoter', *Gene*, 70(1), pp. 51–56. doi: 10.1016/0378-1119(88)90103-5.

Martínez, M. C. and Andriantsitohaina, R. (2009) 'Reactive nitrogen species: Molecular mechanisms and potential significance in health and disease', *Antioxidants and Redox Signaling*. Mary Ann Liebert Inc., pp. 669–702. doi: 10.1089/ars.2007.1993.

Matsunaga, T. *et al.* (2012) 'Elevated HIF-1 α expression of acute myelogenous leukemia stem cells in the endosteal hypoxic zone may be a cause of minimal residual disease in bone marrow after chemotherapy', *Leukemia Research*, pp. e122-4. doi: 10.1016/j.leukres.2012.02.028.

Mclvor, Z. *et al.* (2003) 'Transient expression of PU.1 commits multipotent progenitors to a myeloid fate whereas continued expression favors macrophage over granulocyte differentiation', *Experimental Hematology*, 31(1), pp. 39–47. doi: 10.1016/S0301-472X(02)01017-2.

Medeiros, B. C. *et al.* (2017) 'Isocitrate dehydrogenase mutations in myeloid malignancies', *Leukemia*. The Author(s), pp. 272–281. Available at: <http://dx.doi.org/10.1038/leu.2016.275>.

Merten, O. W., Hebben, M. and Bovolenta, C. (2016) 'Production of lentiviral vectors', *Molecular Therapy - Methods and Clinical Development*. Elsevier Inc, p. 16017. doi: 10.1038/mtm.2016.17.

Miki, H. and Funato, Y. (2012) 'Regulation of intracellular signalling through cysteine oxidation by reactive oxygen species.', *Journal of biochemistry*, 151(3), pp. 255–61. doi: 10.1093/jb/mvs006.

Mikkola, H. K. A. and Orkin, S. H. (2006) 'The journey of developing hematopoietic stem cells', *Development*. The Company of Biologists Ltd, pp. 3733–3744. doi: 10.1242/dev.02568.

Misharin, A. V. *et al.* (2013) 'Flow cytometric analysis of macrophages and dendritic cell subsets in the mouse lung', *American Journal of Respiratory Cell and Molecular Biology*, 49(4), pp. 503–510. doi: 10.1165/rcmb.2013-0086MA.

Miyoshi, H. *et al.* (1998) 'Development of a self-inactivating lentivirus vector.', *Journal of virology*, 72(10), pp. 8150–7. Available at: <http://www.ncbi.nlm.nih.gov/pubmed/9733856> (Accessed: 10 December 2019).

Moloney, J. N. *et al.* (2017) 'Nuclear membrane-localised NOX4D generates pro-survival ROS in FLT3-ITD-expressing AML', *Oncotarget*, 8(62), pp. 105440–105457. doi:

10.18632/oncotarget.22241.

Momparler, R. L. (2013) 'Optimization of cytarabine (ARA-C) therapy for acute myeloid leukemia', *Experimental Hematology and Oncology*. BioMed Central Ltd., p. 20. doi: 10.1186/2162-3619-2-20.

Morotti, A. *et al.* (2015) 'The Role of PTEN in Myeloid Malignancies.', *Hematology reports*, 7(4), p. 5844. doi: 10.4081/hr.2015.6027.

Morrison, S. J. and Scadden, D. T. (2014) 'The bone marrow niche for haematopoietic stem cells', *Nature*. Nature Publishing Group, pp. 327–334. doi: 10.1038/nature12984.

Mrozek, K. and Bloomfield, C. D. (2008) 'Clinical Significance of the Most Common Chromosome Translocations in Adult Acute Myeloid Leukemia', *JNCI Monographs*, 2008(39), pp. 52–57. doi: 10.1093/jncimonographs/lgn003.

Mrózek, K., Heerema, N. A. and Bloomfield, C. D. (2004) 'Cytogenetics in acute leukemia.', *Blood reviews*, 18(2), pp. 115–36. doi: 10.1016/S0268-960X(03)00040-7.

Munro, S. and Pelham, H. R. (1984) 'Use of peptide tagging to detect proteins expressed from cloned genes: deletion mapping functional domains of *Drosophila* hsp 70.', *The EMBO journal*, 3(13), pp. 3087–93. Available at: <http://www.ncbi.nlm.nih.gov/pubmed/6526011> (Accessed: 10 December 2019).

Murphy, M. P. (2009) 'How mitochondria produce reactive oxygen species', *Biochemical Journal*. Portland Press Ltd, pp. 1–13. doi: 10.1042/BJ20081386.

Naldini, L. *et al.* (1996) 'In vivo gene delivery and stable transduction of nondividing cells by a lentiviral vector', *Science*, 272(5259), pp. 263–267. doi: 10.1126/science.272.5259.263.

Nerlov, C. *et al.* (2000) 'GATA-1 interacts with the myeloid PU.1 transcription factor and represses PU.1-dependent transcription', *Blood*, 95(8), pp. 2543–2551. doi: 10.1182/blood.v95.8.2543.008k19_2543_2551.

Nuñez, G. *et al.* (1990) 'Deregulated Bcl-2 gene expression selectively prolongs survival of growth factor-deprived hemopoietic cell lines.', *Journal of immunology (Baltimore)*,

Md. : 1950), 144(9), pp. 3602–10. Available at:

<http://www.ncbi.nlm.nih.gov/pubmed/2184193> (Accessed: 3 December 2019).

O'Brien, J. *et al.* (2018) 'Overview of microRNA biogenesis, mechanisms of actions, and circulation', *Frontiers in Endocrinology*. Frontiers Media S.A., p. 402. doi: 10.3389/fendo.2018.00402.

O'Doherty, U., Swiggard, W. J. and Malim, M. H. (2000) 'Human Immunodeficiency Virus Type 1 Spinoculation Enhances Infection through Virus Binding', *Journal of Virology*, 74(21), pp. 10074–10080. doi: 10.1128/jvi.74.21.10074-10080.2000.

O'Neill, L. A. J. and Artyomov, M. N. (2019) 'Itaconate: the poster child of metabolic reprogramming in macrophage function', *Nature Reviews Immunology*. Nature Publishing Group, pp. 273–281. doi: 10.1038/s41577-019-0128-5.

Olayanju, A. *et al.* (2015) 'Brusatol provokes a rapid and transient inhibition of Nrf2 signaling and sensitizes mammalian cells to chemical toxicity - Implications for therapeutic targeting of Nrf2', *Free Radical Biology and Medicine*, 78, pp. 202–212. doi: 10.1016/j.freeradbiomed.2014.11.003.

Olsson, I. *et al.* (2009) 'Cell differentiation in acute myeloid leukemia', *European Journal of Haematology*, 57(1), pp. 1–16. doi: 10.1111/j.1600-0609.1996.tb00483.x.

Oppliger, W. *et al.* (2012) 'Article Glutaminolysis Activates Rag-mTORC1 Signaling', pp. 349–358. doi: 10.1016/j.molcel.2012.05.043.

Oran, B. and Weisdorf, D. J. (2012) 'Survival for older patients with acute myeloid leukemia: a population-based study.', *Haematologica*, 97(12), pp. 1916–24. doi: 10.3324/haematol.2012.066100.

Orkin, S. H. and Zon, L. I. (no date) 'Leading Edge Hematopoiesis: An Evolving Paradigm for Stem Cell Biology'. doi: 10.1016/j.cell.2008.01.025.

Østgård, L. *et al.* (2015) 'Comorbidity and performance status in acute myeloid leukemia patients: a nation-wide population-based cohort study', *Leukemia*, 29, pp. 548–555. doi: 10.1038/leu.2014.234.

- Ouellette, R. J. and Rawn, J. D. (2018) *Organic Chemistry*. Academic Press. doi: 10.1016/B978-0-12-812838-1.50028-1.
- Owen, O. E., Kalhan, S. C. and Hanson, R. W. (2002) 'The key role of anaplerosis and cataplerosis for citric acid cycle function', *Journal of Biological Chemistry*. American Society for Biochemistry and Molecular Biology, pp. 30409–30412. doi: 10.1074/jbc.R200006200.
- Panday, A. *et al.* (2015) 'NADPH oxidases: An overview from structure to innate immunity-associated pathologies', *Cellular and Molecular Immunology*. Chinese Soc Immunology, pp. 5–23. doi: 10.1038/cmi.2014.89.
- Papathanassiou, A. E. *et al.* (2017) 'BCAT1 controls metabolic reprogramming in activated human macrophages and is associated with inflammatory diseases', *Nature Communications*, 8(1), pp. 1–13. doi: 10.1038/ncomms16040.
- Park, E. K. *et al.* (2007) 'Optimized THP-1 differentiation is required for the detection of responses to weak stimuli', *Inflammation Research*, 56(1), pp. 45–50. doi: 10.1007/s00011-007-6115-5.
- Pasleau, F. *et al.* (1985) 'Growth hormone gene expression in eukaryotic cells directed by the Rous sarcoma virus long terminal repeat or cytomegalovirus immediate-early promoter', *Gene*, 38(1–3), pp. 227–232. doi: 10.1016/0378-1119(85)90221-5.
- Pietsch, A., Erl, W. and Lorenz, R. L. (1996) 'Lovastatin reduces expression of the combined adhesion and scavenger receptor CD36 in human monocytic cells', *Biochemical Pharmacology*, 52(3), pp. 433–439. doi: 10.1016/0006-2952(96)00245-6.
- Pietsch, E. C. *et al.* (2003) 'Nrf2 mediates the induction of ferritin H in response to xenobiotics and cancer chemopreventive dithiolethiones', *Journal of Biological Chemistry*, 278(4), pp. 2361–2369. doi: 10.1074/jbc.M210664200.
- Potter, M., Newport, E. and Morten, K. J. (2016) 'The Warburg effect: 80 years on', *Biochemical Society Transactions*, 44(5), pp. 1499–1505. doi: 10.1042/BST20160094.
- Qin, J. Y. *et al.* (2010) 'Systematic Comparison of Constitutive Promoters and the

Doxycycline-Inducible Promoter', *PLoS ONE*. Edited by I. A. Hansen, 5(5), p. e10611. doi: 10.1371/journal.pone.0010611.

Rabbitts, T. H. (1998) 'LMO T-cell translocation oncogenes typify genes activated by chromosomal translocations that alter transcription and developmental processes', *Genes and Development*. Cold Spring Harbor Laboratory Press, pp. 2651–2657. doi: 10.1101/gad.12.17.2651.

Radak, Z. and Boldogh, I. (2010) '8-Oxo-7,8-dihydroguanine: Links to gene expression, aging, and defense against oxidative stress', *Free Radical Biology and Medicine*, 49(4), pp. 587–596. doi: 10.1016/j.freeradbiomed.2010.05.008.

Raffel, S., Falcone, M., Kneisel, N., Hansson, J., Wang, W., Lutz, C., Bullinger, L., Poschet, G., Nonnenmacher, Y., Barnert, A., Bahr, C., Zeisberger, P., Przybylla, A., Sohn, M., Tönjes, M., Erez, A., Adler, L., Jensen, P., Scholl, C., Fröhling, S., Cocciardi, S., Wuchter, P., Thiede, C., Flörcken, A., Westermann, J., Ehninger, G., Lichter, P., Hiller, K., Hell, Rüdiger, *et al.* (2017a) 'BCAT1 restricts α KG levels in AML stem cells leading to IDHmut-like DNA hypermethylation', *Nature*, 551(7680), pp. 384–388. doi: 10.1038/nature24294.

Raffel, S., Falcone, M., Kneisel, N., Hansson, J., Wang, W., Lutz, C., Bullinger, L., Poschet, G., Nonnenmacher, Y., Barnert, A., Bahr, C., Zeisberger, P., Przybylla, A., Sohn, M., Tönjes, M., Erez, A., Adler, L., Jensen, P., Scholl, C., Fröhling, S., Cocciardi, S., Wuchter, P., Thiede, C., Flörcken, A., Westermann, J., Ehninger, G., Lichter, P., Hiller, K., Hell, Rüdiger, *et al.* (2017b) 'BCAT1 restricts α KG levels in AML stem cells leading to IDHmut-like DNA hypermethylation', *Nature*, 551(7680), pp. 384–388. doi: 10.1038/nature24294.

Raffel, S., Falcone, M., Kneisel, N., Hansson, J., Wang, W., Lutz, C., Bullinger, L., Poschet, G., Nonnenmacher, Y., Barnert, A., Bahr, C., Zeisberger, P., Przybylla, A., Sohn, M., Tönjes, M., Erez, A., Adler, L., Jensen, P., Scholl, C., Fröhling, S., Cocciardi, S., Wuchter, P., Thiede, C., Flörcken, A., Westermann, J., Ehninger, G., Lichter, P., Hiller, K., Hell, Rüdiger, *et al.* (2017) 'BCAT1 restricts α KG levels in AML stem cells leading to IDHmut-like DNA hypermethylation', *Nature*, 551(7680), pp. 384–388. doi:

10.1038/nature24294.

Ray, P. D., Huang, B. W. and Tsuji, Y. (2012) 'Reactive oxygen species (ROS) homeostasis and redox regulation in cellular signaling', *Cellular Signalling*. NIH Public Access, pp. 981–990. doi: 10.1016/j.cellsig.2012.01.008.

Recommended lentivirus MOI for common cell lines (no date).

Redza-Dutordoir, M. and Averill-Bates, D. A. (2016) 'Activation of apoptosis signalling pathways by reactive oxygen species', *Biochimica et Biophysica Acta - Molecular Cell Research*. Elsevier B.V., pp. 2977–2992. doi: 10.1016/j.bbamcr.2016.09.012.

Reinhardt, H. C. and Schumacher, B. (2012) 'The p53 network: cellular and systemic DNA damage responses in aging and cancer', *Trends in Genetics*, 28(3), pp. 128–136. doi: 10.1016/j.tig.2011.12.002.

Rekhtman, N. *et al.* (2003) 'PU.1 and pRB Interact and Cooperate To Repress GATA-1 and Block Erythroid Differentiation', *Molecular and Cellular Biology*, 23(21), pp. 7460–7474. doi: 10.1128/mcb.23.21.7460-7474.2003.

Rhee, S. G. (2016) 'Overview on Peroxiredoxin.', *Molecules and cells*, 39(1), pp. 1–5. doi: 10.14348/molcells.2016.2368.

Rhodes, J. *et al.* (2005) 'Interplay of pu.1 and Gata1 determines myelo-erythroid progenitor cell fate in zebrafish', *Developmental Cell*, 8(1), pp. 97–108. doi: 10.1016/j.devcel.2004.11.014.

Roboz, G. J. *et al.* (2008) 'Arsenic trioxide and low-dose cytarabine in older patients with untreated acute myeloid leukemia, excluding acute promyelocytic leukemia', *Cancer*, 113(9), pp. 2504–2511. doi: 10.1002/cncr.23855.

Rosenbauer, F. *et al.* (2004) 'Acute myeloid leukemia induced by graded reduction of a lineage-specific transcription factor, PU.1', *Nature Genetics*, 36(6), pp. 624–630. doi: 10.1038/ng1361.

Roszkowski, K. *et al.* (2011) 'Oxidative damage DNA: 8-oxogua and 8-oxodG as molecular markers of cancer', *Medical Science Monitor*, 17(6), p. CR329. doi:

10.12659/MSM.881805.

Rücker, F. G. *et al.* (2006) 'Molecular profiling reveals myeloid leukemia cell lines to be faithful model systems characterized by distinct genomic aberrations', *Leukemia*, 20(6), pp. 994–1001. doi: 10.1038/sj.leu.2404235.

Sambrook, J. and Russell, D. W. (2006) 'SDS-Polyacrylamide Gel Electrophoresis of Proteins', *CSH Protocols*. doi: 10.1101/pdb.prot4540.

Savill, J. *et al.* (1992) 'Thrombospondin cooperates with CD36 and the vitronectin receptor in macrophage recognition of neutrophils undergoing apoptosis', *Journal of Clinical Investigation*, 90(4), pp. 1513–1522. doi: 10.1172/JCI116019.

Schafer, F Q and Buettner, G. R. (2001) 'Redox environment of the cell as viewed through the redox state of the glutathione disulfide/glutathione couple.', *Free radical biology & medicine*, 30(11), pp. 1191–1212.

Schafer, Freya Q. and Buettner, G. R. (2001) 'Redox environment of the cell as viewed through the redox state of the glutathione disulfide/glutathione couple', *Free Radical Biology and Medicine*, pp. 1191–1212. doi: 10.1016/S0891-5849(01)00480-4.

Schenk, E. L. *et al.* (2012) 'Effects of selective checkpoint kinase 1 inhibition on cytarabine cytotoxicity in acute myelogenous leukemia cells in vitro', *Clinical Cancer Research*, 18(19), pp. 5364–5373. doi: 10.1158/1078-0432.CCR-12-0961.

Scherz-Shouval, R. *et al.* (2007) 'Reactive oxygen species are essential for autophagy and specifically regulate the activity of Atg4', *EMBO Journal*, 26(7), pp. 1749–1760. doi: 10.1038/sj.emboj.7601623.

Schieber, M. and Chandel, N. S. (2014) 'ROS function in redox signaling and oxidative stress', *Current Biology*. Cell Press, p. R453. doi: 10.1016/j.cub.2014.03.034.

Schlenk, R. F. *et al.* (2008) 'Mutations and Treatment Outcome in Cytogenetically Normal Acute Myeloid Leukemia', *New England Journal of Medicine*, 358(18), pp. 1909–1918. doi: 10.1056/NEJMoa074306.

Schmittgen, T. D. and Livak, K. J. (2008) 'Analyzing real-time PCR data by the

comparative CT method', *Nature Protocols*, 3(6), pp. 1101–1108. doi: 10.1038/nprot.2008.73.

Schneider, M., Marison, I. W. and Von Stockar, U. (1996) 'The importance of ammonia in mammalian cell culture', *Journal of Biotechnology*. Elsevier B.V., pp. 161–185. doi: 10.1016/0168-1656(95)00196-4.

Schoenberg, D. R. and Maquat, L. E. (2012) 'Regulation of cytoplasmic mRNA decay', *Nature Reviews Genetics*, pp. 246–259. doi: 10.1038/nrg3160.

Schroeder, A. *et al.* (2006) 'The RIN: An RNA integrity number for assigning integrity values to RNA measurements', *BMC Molecular Biology*, 7(1), p. 3. doi: 10.1186/1471-2199-7-3.

Sebaugh, J. L. (2011) 'Guidelines for accurate EC50/IC50 estimation', *Pharmaceutical Statistics*, 10(2), pp. 128–134. doi: 10.1002/pst.426.

Seto, B. (2012) 'Rapamycin and mTOR: a serendipitous discovery and implications for breast cancer', *Clinical and Translational Medicine*, 1(1), p. 29. doi: 10.1186/2001-1326-1-29.

Sheen, J. H. *et al.* (2011) 'Defective Regulation of Autophagy upon Leucine Deprivation Reveals a Targetable Liability of Human Melanoma Cells In Vitro and In Vivo', *Cancer Cell*, 19(5), pp. 613–628. doi: 10.1016/j.ccr.2011.03.012.

Shivdasani, R. A., Mayer, E. L. and Orkin, S. H. (1995) 'Absence of blood formation in mice lacking the T-cell leukaemia oncogene tal-1/SCL', *Nature*, 373(6513), pp. 432–434. doi: 10.1038/373432a0.

Siddiqui, M. A. *et al.* (2013) 'Rotenone-induced oxidative stress and apoptosis in human liver HepG2 cells', *Molecular and Cellular Biochemistry*, 384(1–2), pp. 59–69. doi: 10.1007/s11010-013-1781-9.

Sigal, D. S. *et al.* (2010) 'Beyond hairy cell: The activity of cladribine in other hematologic malignancies', *Blood*. American Society of Hematology, pp. 2884–2896. doi: 10.1182/blood-2010-02-246140.

- Sillar, J. R. *et al.* (2019) 'The role of reactive oxygen species in acute myeloid leukaemia', *International Journal of Molecular Sciences*. MDPI AG. doi: 10.3390/ijms20236003.
- Simon, H. U., Haj-Yehia, A. and Levi-Schaffer, F. (2000) 'Role of reactive oxygen species (ROS) in apoptosis induction', *Apoptosis*, 5(5), pp. 415–418. doi: 10.1023/A:1009616228304.
- Singh, A. *et al.* (2006) 'Glutathione peroxidase 2, the major cigarette smoke-inducible isoform of GPX in lungs, is regulated by Nrf2', *American Journal of Respiratory Cell and Molecular Biology*, 35(6), pp. 639–650. doi: 10.1165/rcmb.2005-0325OC.
- Sokhi, U. K. *et al.* (2013) 'Human polynucleotide phosphorylase (hPNPaseold-35). Should I eat you or not-that is the question?', in *Advances in Cancer Research*. Academic Press Inc., pp. 161–190. doi: 10.1016/B978-0-12-407190-2.00005-8.
- Song, Y. *et al.* (2020) 'Prognostic significance of branched-chain amino acid transferase 1 and CD133 in triple-negative breast cancer', *BMC Cancer*, 20(1), p. 584. doi: 10.1186/s12885-020-07070-2.
- Spector, D. H. *et al.* (1990) 'Human immunodeficiency virus pseudotypes with expanded cellular and species tropism.', *Journal of virology*, 64(5), pp. 2298–308. Available at: <http://www.ncbi.nlm.nih.gov/pubmed/1691314> (Accessed: 10 December 2019).
- Spencer, J. A. *et al.* (2014) 'Direct measurement of local oxygen concentration in the bone marrow of live animals', *Nature*, 508(7495), pp. 269–273. doi: 10.1038/nature13034.
- Sporn, M. B. and Libby, K. T. (2012) 'NRF2 and cancer: The Good, the bad and the importance of context', *Nature Reviews Cancer*, pp. 564–571. doi: 10.1038/nrc3278.
- Sriskanthadevan, S. *et al.* (2015) 'AML cells have low spare reserve capacity in their respiratory chain that renders them susceptible to oxidative metabolic stress', *Blood*, 125(13), pp. 2120–2130. doi: 10.1182/blood-2014-08-594408.

- Stuart, L. M. *et al.* (2007) 'CD36 signals to the actin cytoskeleton and regulates microglial migration via a p130Cas complex', *Journal of Biological Chemistry*, 282(37), pp. 27392–27401. doi: 10.1074/jbc.M702887200.
- Suda, T., Takubo, K. and Semenza, G. L. (2011) 'Metabolic regulation of hematopoietic stem cells in the hypoxic niche', *Cell Stem Cell*, pp. 298–310. doi: 10.1016/j.stem.2011.09.010.
- Sugiyama, T. *et al.* (2006) 'Maintenance of the Hematopoietic Stem Cell Pool by CXCL12-CXCR4 Chemokine Signaling in Bone Marrow Stromal Cell Niches', *Immunity*, 25(6), pp. 977–988. doi: 10.1016/j.immuni.2006.10.016.
- Sun, X. Z. *et al.* (2003) 'Formation of Disulfide Bond in p53 Correlates with Inhibition of DNA Binding and Tetramerization', *Antioxidants and Redox Signaling*, 5(5), pp. 655–665. doi: 10.1089/152308603770310338.
- Sundström, C. and Nilsson, K. (1976) 'Establishment and characterization of a human histiocytic lymphoma cell line (U-937)', *International Journal of Cancer*, 17(5), pp. 565–577. doi: 10.1002/ijc.2910170504.
- Surh, Y. J. *et al.* (2009) 'Role of Nrf2-mediated heme oxygenase-1 upregulation in adaptive survival response to nitrosative stress', *Archives of Pharmacal Research*, pp. 1163–1176. doi: 10.1007/s12272-009-1807-8.
- Suski, J. M. *et al.* (2012) 'Relation between mitochondrial membrane potential and ROS formation', *Methods in Molecular Biology*, 810, pp. 183–205. doi: 10.1007/978-1-61779-382-0_12.
- Suzuki, R. (2014) 'Clinical characteristics and prognostic implications of NPM1 mutations in acute myeloid leukemia'. doi: 10.1182/blood-2005-04-1733.
- Swainson, L. *et al.* (2008) 'Lentiviral transduction of immune cells.', *Methods in molecular biology (Clifton, N.J.)*, 415, pp. 301–320. doi: 10.1007/978-1-59745-570-1_18.
- Takubo, K. *et al.* (2010) 'Regulation of the HIF-1 α level is essential for hematopoietic

- stem cells', *Cell Stem Cell*, 7(3), pp. 391–402. doi: 10.1016/j.stem.2010.06.020.
- Tan, Y. *et al.* (2014) 'Thioredoxin-1 inhibitor PX-12 induces human acute myeloid leukemia cell apoptosis and enhances the sensitivity of cells to arsenic trioxide.', *International journal of clinical and experimental pathology*, 7(8), pp. 4765–73. Available at: <http://www.ncbi.nlm.nih.gov/pubmed/25197347> (Accessed: 31 October 2019).
- Tenser, R. B. and Dunstan, M. E. (1980) 'Mechanisms of herpes simplex virus infectivity enhanced by ultracentrifugal inoculation.', *Infection and immunity*, 30(1), pp. 193–7. Available at: <http://www.ncbi.nlm.nih.gov/pubmed/6254878> (Accessed: 14 April 2020).
- Testa, U. *et al.* (2016) 'Oxidative stress and hypoxia in normal and leukemic stem cells', *Experimental Hematology*, 44(7), pp. 540–560. doi: 10.1016/j.exphem.2016.04.012.
- Testa, U. and Riccioni, R. (2007) 'Deregulation of apoptosis in acute myeloid leukemia', *Haematologica*, 92(1), pp. 81–94. doi: 10.3324/haematol.10279.
- Thewes, V. *et al.* (2017) 'The branched-chain amino acid transaminase 1 sustains growth of antiestrogen-resistant and ER α -negative breast cancer', *Oncogene*, 36(29), pp. 4124–4134. doi: 10.1038/onc.2017.32.
- Thorsteinsdottir, U. *et al.* (2002) 'Overexpression of the myeloid leukemia-associated Hoxa9 gene in bone marrow cells induces stem cell expansion', *Blood*, 99(1), pp. 121–129. doi: 10.1182/blood.V99.1.121.
- Tonelli, C., Chio, I. I. C. and Tuveson, D. A. (2018) 'Transcriptional Regulation by Nrf2', *Antioxidants and Redox Signaling*. Mary Ann Liebert Inc., pp. 1727–1745. doi: 10.1089/ars.2017.7342.
- Tönjes, M. *et al.* (2013) 'BCAT1 promotes cell proliferation through amino acid catabolism in gliomas carrying wild-type IDH1.', *Nature medicine*, 19(7), pp. 901–8. doi: 10.1038/nm.3217.
- Verhaak, R. G. W. *et al.* (2005) 'Mutations in nucleophosmin (NPM1) in acute myeloid

leukemia (AML): association with other gene abnormalities and previously established gene expression signatures and their favorable prognostic significance.', *Blood*, 106(12), pp. 3747–54. doi: 10.1182/blood-2005-05-2168.

Vincelette, N. D. and Yun, S. (2014) 'Assessing the Mechanism of Cytarabine-Induced Killing in Acute Leukemia', *Blood*, 124(21), pp. 5210–5210. doi: 10.1182/blood.v124.21.5210.5210.

Wang, Y. *et al.* (2019) 'Branched-Chain Amino Acid Metabolic Reprogramming Orchestrates Drug Resistance to EGFR Tyrosine Kinase Inhibitors', *Cell Reports*, 28(2), pp. 512-525.e6. doi: 10.1016/j.celrep.2019.06.026.

Wangpaichitr, M. *et al.* (2012) 'The relationship of thioredoxin-1 and cisplatin resistance: Its impact on ROS and oxidative metabolism in lung cancer cells', *Molecular Cancer Therapeutics*, 11(3), pp. 604–615. doi: 10.1158/1535-7163.MCT-11-0599.

Ward, P. S. and Thompson, C. B. (2012) 'Metabolic Reprogramming: A Cancer Hallmark Even Warburg Did Not Anticipate', *Cancer Cell*. NIH Public Access, pp. 297–308. doi: 10.1016/j.ccr.2012.02.014.

Weiskopf, K. *et al.* (2016) 'Myeloid Cell Origins, Differentiation, and Clinical Implications', *Microbiology Spectrum*, 4(5). doi: 10.1128/microbiolspec.mchd-0031-2016.

Winterbourn, C. C. (1995) 'Toxicity of iron and hydrogen peroxide: the Fenton reaction', *Toxicology Letters*, 82–83(C), pp. 969–974. doi: 10.1016/0378-4274(95)03532-X.

Winther, J. R. and Thorpe, C. (2014) 'Quantification of thiols and disulfides', *Biochimica et Biophysica Acta - General Subjects*. NIH Public Access, pp. 838–846. doi: 10.1016/j.bbagen.2013.03.031.

Woo, H. A. *et al.* (2010) 'Inactivation of Peroxiredoxin I by Phosphorylation Allows Localized H₂O₂ Accumulation for Cell Signaling', *Cell*, 140(4), pp. 517–528. doi: 10.1016/j.cell.2010.01.009.

- Wouters, B. J. and Delwel, R. (2016) 'Epigenetics and approaches to targeted epigenetic therapy in acute myeloid leukemia.', *Blood*, 127(1), pp. 42–52. doi: 10.1182/blood-2015-07-604512.
- Xia, W. *et al.* (2006) 'High levels of protein expression using different mammalian CMV promoters in several cell lines', *Protein Expression and Purification*, 45(1), pp. 115–124. doi: 10.1016/j.pep.2005.07.008.
- Xu, J., Ji, J. and Yan, X. H. (2012) 'Cross-Talk between AMPK and mTOR in Regulating Energy Balance', *Critical Reviews in Food Science and Nutrition*, pp. 373–381. doi: 10.1080/10408398.2010.500245.
- Xu, M. *et al.* (2016) 'BCAT1 promotes tumor cell migration and invasion in hepatocellular carcinoma', *Oncology Letters*, 12(4), pp. 2648–2656. doi: 10.3892/ol.2016.4969.
- Xu, W. *et al.* (2011) 'Oncometabolite 2-Hydroxyglutarate Is a Competitive Inhibitor of α -Ketoglutarate-Dependent Dioxygenases', *Cancer Cell*, 19(1), pp. 17–30. doi: 10.1016/J.CCR.2010.12.014.
- Xu, Y. *et al.* (2018a) 'Overexpression of BCAT1 is a prognostic marker in gastric cancer', *Human Pathology*, 75, pp. 41–46. doi: 10.1016/j.humpath.2018.02.003.
- Xu, Y. *et al.* (2018b) 'Overexpression of BCAT1 is a prognostic marker in gastric cancer', *Human Pathology*, 75, pp. 41–46. doi: 10.1016/j.humpath.2018.02.003.
- Yamamoto, T. *et al.* (2009) 'Role of catalase in monocytic differentiation of U937 cells by TPA: Hydrogen peroxide as a second messenger', *Leukemia*, 23(4), pp. 761–769. doi: 10.1038/leu.2008.353.
- Ye, Z. W. *et al.* (2015) 'Oxidative stress, redox regulation and diseases of cellular differentiation', *Biochimica et Biophysica Acta - General Subjects*. Elsevier, pp. 1607–1621. doi: 10.1016/j.bbagen.2014.11.010.
- Yoshihara, H. *et al.* (2007) 'Thrombopoietin/MPL Signaling Regulates Hematopoietic Stem Cell Quiescence and Interaction with the Osteoblastic Niche', *Cell Stem Cell*, 1(6),

pp. 685–697. doi: 10.1016/j.stem.2007.10.020.

Yu, X. *et al.* (2018) 'Itaconate: an emerging determinant of inflammation in activated macrophages', *Immunology & Cell Biology*, 97(2), p. imcb.12218. doi: 10.1111/imcb.12218.

Zhang, B. *et al.* (2004) 'The significance of controlled conditions in lentiviral vector titration and in the use of multiplicity of infection (MOI) for predicting gene transfer events', *Genetic Vaccines and Therapy*, 2. doi: 10.1186/1479-0556-2-6.

Zhang, H., Fang, H. and Wang, K. (2014) 'Reactive oxygen species in eradicating acute myeloid leukemic stem cells', *Stem Cell Investigation*, 1(1), pp. 1–10. doi: 10.3978/j.issn.2306-9759.2014.04.03.

Zhang, J. *et al.* (2003) 'Identification of the haematopoietic stem cell niche and control of the niche size', *Nature*, 425(6960), pp. 836–841. doi: 10.1038/nature02041.

Zhang, J. *et al.* (2018) 'An evolving understanding of the S-glutathionylation cycle in pathways of redox regulation', *Free Radical Biology and Medicine*. Elsevier Inc., pp. 204–216. doi: 10.1016/j.freeradbiomed.2018.03.038.

Zhang, L. and Han, J. (2017) 'Branched-chain amino acid transaminase 1 (BCAT1) promotes the growth of breast cancer cells through improving mTOR-mediated mitochondrial biogenesis and function', *Biochemical and Biophysical Research Communications*, 486(2), pp. 224–231. doi: 10.1016/j.bbrc.2017.02.101.

Zhang, P. *et al.* (1999) 'Negative cross-talk between hematopoietic regulators: GATA proteins repress PU.1', *Proceedings of the National Academy of Sciences of the United States of America*, 96(15), pp. 8705–8710. doi: 10.1073/pnas.96.15.8705.

Zhang, T. D. *et al.* (2001) 'Arsenic trioxide, a therapeutic agent for APL', *Oncogene*. *Oncogene*, pp. 7146–7153. doi: 10.1038/sj.onc.1204762.

Zheng, Y. H. *et al.* (2016) 'BCAT1, a key prognostic predictor of hepatocellular carcinoma, promotes cell proliferation and induces chemoresistance to cisplatin', *Liver International*, 36(12), pp. 1836–1847. doi: 10.1111/liv.13178.

Zhou, F., Shen, Q. and Claret, F. X. (2013) 'Novel roles of reactive oxygen species in the pathogenesis of acute myeloid leukemia', *Journal of Leukocyte Biology*, 94(3), pp. 423–429. doi: 10.1189/jlb.0113006.

Zhou, Yang *et al.* (2015) 'Sulfiredoxin-1 Attenuates Oxidative Stress via Nrf2/ARE Pathway and 2-Cys Prdxs After Oxygen-Glucose Deprivation in Astrocytes', *Journal of Molecular Neuroscience*, 55(4), pp. 941–950. doi: 10.1007/s12031-014-0449-6.

Zou, H. *et al.* (2019) 'Data mining of the expression and regulatory role of BCAT1 in hepatocellular carcinoma', *Oncology Letters*, 18(6), pp. 5879–5888. doi: 10.3892/ol.2019.10932.

Zufferey, R. *et al.* (1998) 'Self-inactivating lentivirus vector for safe and efficient in vivo gene delivery.', *Journal of virology*, 72(12), pp. 9873–80. Available at: <http://www.ncbi.nlm.nih.gov/pubmed/9811723> (Accessed: 10 December 2019).

Appendices

Appendix A. NCBI Blast vector sequence alignments

Legend: Start codon = **ATG**
Stop codon = **GAT**
C335S codon = **GCA**
C338S codon = **ACA**

n.b. mutagenized bases displayed in red font

Primer: VP1.5

Query: pCMV6-BCAT1(WT)

Subject: serial cloner *in silico* pCMV6-BCAT1(WT)

```
Query 137 ACCGAGGAGATCTGCCGCCGCGATCGCCATGGATTGCAGTAACGGATGCTCCGCAGAGTG 196
          |||
Sbjct 1001 ACCGAGGAGATCTGCCGCCGCGATCGCCATGGATTGCAGTAACGGATGCTCCGCAGAGTG 1060

Query 197 TACCGGAGAAGGAGGATCAAAAGAGGTGGTGGGGACTTTTAAGGCTAAAGACCTAATAGT 256
          |||
Sbjct 1061 TACCGGAGAAGGAGGATCAAAAGAGGTGGTGGGGACTTTTAAGGCTAAAGACCTAATAGT 1120

Query 257 CACACCAGCTACCATTTTAAAGGAAAAACCAGACCCCAATAATCTGGTTTTTGGAACTGT 316
          |||
Sbjct 1121 CACACCAGCTACCATTTTAAAGGAAAAACCAGACCCCAATAATCTGGTTTTTGGAACTGT 1180

Query 317 GTTCACGGATCATATGCTGACGGTGGAGTGGTCCTCAGAGTTTGGATGGGAGAAACCTCA 376
          |||
Sbjct 1181 GTTCACGGATCATATGCTGACGGTGGAGTGGTCCTCAGAGTTTGGATGGGAGAAACCTCA 1240

Query 377 TATCAAGCCTCTTCAGAACCTGTCAATGCACCCTGGCTCATCAGCTTTGCACTATGCAGT 436
          |||
Sbjct 1241 TATCAAGCCTCTTCAGAACCTGTCAATGCACCCTGGCTCATCAGCTTTGCACTATGCAGT 1300

Query 437 GGAATTATTTGAAGGATTGAAGGCATTTTCGAGGAGTAGATAATAAAATTCGACTGTTTCA 496
          |||
Sbjct 1301 GGAATTATTTGAAGGATTGAAGGCATTTTCGAGGAGTAGATAATAAAATTCGACTGTTTCA 1360

Query 497 GCCAAACCTCAACATGGATAGAATGTATCGCTCTGCTGTGAGGGCAACTCTGCCGGTATT 556
          |||
Sbjct 1361 GCCAAACCTCAACATGGATAGAATGTATCGCTCTGCTGTGAGGGCAACTCTGCCGGTATT 1420

Query 557 TGACAAAGAAGAGCTCTTAGAGTGTATTCAACAGCTTGTGAAATTGGATCAAGAATGGGT 616
          |||
Sbjct 1421 TGACAAAGAAGAGCTCTTAGAGTGTATTCAACAGCTTGTGAAATTGGATCAAGAATGGGT 1480

Query 617 CCCATATTCAACATCTGCTAGTCTGTATATTCGTCCACATTTCATTGGAAGTGGAGCTTC 676
          |||
Sbjct 1481 CCCATATTCAACATCTGCTAGTCTGTATATTCGTCCACATTTCATTGGAAGTGGAGCTTC 1540

Query 677 TCTTGGAGTCAAGAAGCCTACCAAAGCCCTGCTCTTTGTACTCTTGAGCCCAGTGGGACC 736
          |||
Sbjct 1541 TCTTGGAGTCAAGAAGCCTACCAAAGCCCTGCTCTTTGTACTCTTGAGCCCAGTGGGACC 1600

Query 737 TTATTTTCAAGTGGAAACCTTTAATCCAGTGTCCCTGTGGGCCAATCCCAAGTATGTAAG 796
          |||
Sbjct 1601 TTATTTTCAAGTGGAAACCTTTAATCCAGTGTCCCTGTGGGCCAATCCCAAGTATGTAAG 1660

Query 797 AGCCTGAAAAGGTGGAAGTGGGGACTGCAAGATGGGAGGGAATTACGGCTCATCTCTTTT 856
          |||
Sbjct 1661 AGCCTGAAAAGGTGGAAGTGGGGACTGCAAGATGGGAGGGAATTACGGCTCATCTCTTTT 1720
```

Primer XL39

Query: pCMV6-BCAT1(WT)

Subject: serial cloner *in silico* pCMV6-BCAT1(WT)

```
Query 141 TTGCTGCCAGATCCTCTTCTGAGATGAGTTTCTGCTCGAGCGGCCGCTACGCGTGATA 200
          |||
Sbjct 2238 TTGCTGCCAGATCCTCTTCTGAGATGAGTTTCTGCTCGAGCGGCCGCTACGCGTGATA 2179

Query 201 GCACAATTGTCCAGTCGCTCTCTTCTCTCCATACTGGATATCAGTTAATTTGCTCAAGA 260
          |||
Sbjct 2178 GCACAATTGTCCAGTCGCTCTCTTCTCTCCATACTGGATATCAGTTAATTTGCTCAAGA 2119

Query 261 TCGCGCTTGCCAGCTTAGGACCATTCTCCATAGTTGGAATGTGTATTGTCTCGCCTTTGT 320
          |||
Sbjct 2118 TCGCGCTTGCCAGCTTAGGACCATTCTCCATAGTTGGAATGTGTATTGTCTCGCCTTTGT 2059

Query 321 ACAGTATATCAGAAACTGGGCAAACAACACAGGCTGTACCAGAGCCAAACATCTCTCTCA 380
          |||
Sbjct 2058 ACAGTATATCAGAAACTGGGCAAACAACACAGGCTGTACCAGAGCCAAACATCTCTCTCA 1999

Query 381 CTCTGTTCCCTCCAGGGCTGTTGTCAAGTCATCCATGGTGAGGTATCTCTCTGACACCT 440
          |||
Sbjct 1998 CTCTGTTCCCTCCAGGGCTGTTGTCAAGTCATCCATGGTGAGGTATCTCTCTGACACCT 1939

Query 441 TAAATTCACCCCACTGATGTGCCAGGTCCAGAATGCACCGCCTTGCTACTCCTGGAAGAA 500
          |||
Sbjct 1938 TAAATTCACCCCACTGATGTGCCAGGTCCAGAATGCACCGCCTTGCTACTCCTGGAAGAA 1879

Query 501 TGATGCCATCTAGTGGAGGAGTTGCCAGTTCTTCTTCTCCATCTTCATTTATCCAGTAAA 560
          |||
Sbjct 1878 TGATGCCATCTAGTGGAGGAGTTGCCAGTTCTTCTTCTCCATCTTCATTTATCCAGTAAA 1819

Query 561 GAAAAAGATTCATAGTTCCTCACTTCAGTGATCTGATGGTCCTCTCCATAGAGCCACAGGA 620
          |||
Sbjct 1818 GAAAAAGATTCATAGTTCCTCACTTCAGTGATCTGATGGTCCTCTCCATAGAGCCACAGGA 1759

Query 621 CCTGCTGACACCCATTATCTACTGCTTCACATTGGGCAAAAAGAGATGAGCCGTAATTCC 680
          |||
Sbjct 1758 CCTGCTGACACCCATTATCTACTGCTTCACATTGGGCAAAAAGAGATGAGCCGTAATTCC 1699

Query 681 CTCCCATCTTGCAGTCCCAGTTCCACCTTTCCAGGCTTTACATACTTGGGATTGGCCC 740
          |||
Sbjct 1698 CTCCCATCTTGCAGTCCCAGTTCCACCTTTCCAGGCTTTACATACTTGGGATTGGCCC 1639

Query 741 ACAGGGACACTGGATTAAAGGTTCCACTTGAAAAATAA
          |||
Sbjct 1638 ACAGGGACACTGGATTAAAGGTTCCACTTGAAAAATAA
```

Primer VP1.5
Query: pCMV6-BCAT1(C335S)
Subject: serial cloner *in silico* pCMV6-BCAT1(WT)

```

Query 135   ACCGAGGAGATCTGCCGCCGCGATCGCCATGGATTGCAGTAACGGATGCTCCGCAGAGTG   194
          |||
Sbjct 1001  ACCGAGGAGATCTGCCGCCGCGATCGCCATGGATTGCAGTAACGGATGCTCCGCAGAGTG   1060

Query 195   TACCGGAGAAGGAGGATCAAAAAGAGGTGGTGGGGACTTTTAAGGCTAAAGACCTAATAGT   254
          |||
Sbjct 1061  TACCGGAGAAGGAGGATCAAAAAGAGGTGGTGGGGACTTTTAAGGCTAAAGACCTAATAGT   1120

Query 255   CACACCAGCTACCATTTTAAAGGAAAAACCAGACCCCAATAATCTGGTTTTTGGAACTGT   314
          |||
Sbjct 1121  CACACCAGCTACCATTTTAAAGGAAAAACCAGACCCCAATAATCTGGTTTTTGGAACTGT   1180

Query 315   GTTCACGGATCATATGCTGACGGTGGAGTGGTCCTCAGAGTTTGGATGGGAGAAACCTCA   374
          |||
Sbjct 1181  GTTCACGGATCATATGCTGACGGTGGAGTGGTCCTCAGAGTTTGGATGGGAGAAACCTCA   1240

Query 375   TATCAAGCCTCTTCAGAACCTGTCAATGCACCCTGGCTCATCAGCTTTGCACTATGCAGT   434
          |||
Sbjct 1241  TATCAAGCCTCTTCAGAACCTGTCAATGCACCCTGGCTCATCAGCTTTGCACTATGCAGT   1300

Query 435   GGAATTATTTGAAGGATTGAAGGCATTTCGAGGAGTAGATAATAAAATTCGACTGTTTCA   494
          |||
Sbjct 1301  GGAATTATTTGAAGGATTGAAGGCATTTCGAGGAGTAGATAATAAAATTCGACTGTTTCA   1360

Query 495   GCCAAACCTCAACATGGATAGAATGTATCGCTCTGCTGTGAGGGCAACTCTGCCGGTATT   554
          |||
Sbjct 1361  GCCAAACCTCAACATGGATAGAATGTATCGCTCTGCTGTGAGGGCAACTCTGCCGGTATT   1420

Query 555   TGACAAAGAAGAGCTCTTAGAGTGTATTCAACAGCTTGTGAAATTGGATCAAGAATGGGT   614
          |||
Sbjct 1421  TGACAAAGAAGAGCTCTTAGAGTGTATTCAACAGCTTGTGAAATTGGATCAAGAATGGGT   1480

Query 615   CCCATATTCAACATCTGCTAGTCTGTATATTCGTCTACATTCATTGGAAGTGGAGCCTTC   674
          |||
Sbjct 1481  CCCATATTCAACATCTGCTAGTCTGTATATTCGTCTACATTCATTGGAAGTGGAGCCTTC   1540

Query 675   TCTTGGAGTCAAGAAGCCTACCAAAGCCCTGCTCTTTGTACTCTTGAGCCCAGTGGGACC   734
          |||
Sbjct 1541  TCTTGGAGTCAAGAAGCCTACCAAAGCCCTGCTCTTTGTACTCTTGAGCCCAGTGGGACC   1600

Query 735   TTATTTTTCAAGTGGAACCTTTAATCCAGTGTCCCTGTGGGCCAATCCCAAGTATGTAAG   794
          |||
Sbjct 1601  TTATTTTTCAAGTGGAACCTTTAATCCAGTGTCCCTGTGGGCCAATCCCAAGTATGTAAG   1660

Query 795   AGCCTGGAAAGGTGGAAGTGGGGACTGCAAGATGGGAGGGAATTACGGCTCATCTCTTTT   854
          |||
Sbjct 1661  AGCCTGGAAAGGTGGAAGTGGGGACTGCAAGATGGGAGGGAATTACGGCTCATCTCTTTT   1720

Query 855   TGCCCAATGTGAAGCAGTAGATAAT 879
          |||
Sbjct 1721  TGCCCAATGTGAAGCAGTAGATAAT 1745

```

Primer FTAGR

Query: pCMV6-BCAT1(C335S)

Subject: serial cloner *in silico* pCMV6-BCAT1(WT)

```
Query 12 GATCCTCTTCTGAGATGAGTTTCTGCTCGAGCGGCCGCGTACGCGTGATAGCACAATTG 71
|
Sbjct 2229 GATCCTCTTCTGAGATGAGTTTCTGCTCGAGCGGCCGCGTACGCGTGATAGCACAATTG 2170
|
Query 72 TCCAGTCGCTCTCTTCTCTTCCATACTGGATATCAGTTAATTTGCTCAAGATGCGGCTTG 131
|
Sbjct 2169 TCCAGTCGCTCTCTTCTCTTCCATACTGGATATCAGTTAATTTGCTCAAGATGCGGCTTG 2110
|
Query 132 CCAGCTTAGGACCATTCTCCATAGTTGGAATGTGTATTGTCTCGCCTTTGTACAGTATAT 191
|
Sbjct 2109 CCAGCTTAGGACCATTCTCCATAGTTGGAATGTGTATTGTCTCGCCTTTGTACAGTATAT 2050
|
Query 192 CAGAACTGGGCAAACAACAGAGGCTGTACCAGAGCCAAACATCTCTCTCACTCTGTTCC 251
|
Sbjct 2049 CAGAACTGGGCAAACAACAGAGGCTGTACCAGAGCCAAACATCTCTCTCACTCTGTTCC 1990
|
Query 252 CCTCCAGGGCTGTTGTCAAGTCATCCATGGTGAGGTATCTCTCTGACACCTTAAATTCAC 311
|
Sbjct 1989 CCTCCAGGGCTGTTGTCAAGTCATCCATGGTGAGGTATCTCTCTGACACCTTAAATTCAC 1930
|
Query 312 CCCACTGATGTGCCAGGTCCAGAATGCACCGCCTTGCTCACTCCTGGAAGAATGATGCCAT 371
|
Sbjct 1929 CCCACTGATGTGCCAGGTCCAGAATGCACCGCCTTGCTCACTCCTGGAAGAATGATGCCAT 1870
|
Query 372 CTAGTGGAGGAGTTGCCAGTTCTTCTTCTCCATCTTCATTTATCCAGTAAAGAAAAGAT 431
|
Sbjct 1869 CTAGTGGAGGAGTTGCCAGTTCTTCTTCTCCATCTTCATTTATCCAGTAAAGAAAAGAT 1810
|
Query 432 TCATAGTTCCCACTTCAGTGATCTGATGGTCCTCTCCATAGAGCCACAGGACCTGCTGAC 491
|
Sbjct 1809 TCATAGTTCCCACTTCAGTGATCTGATGGTCCTCTCCATAGAGCCACAGGACCTGCTGAC 1750
|
Query 492 ACCCATTATCTACTGCTTCACATTGGGCAAAAAGAGATGAGCCGTAATTCCTCCCATCT 551
|
Sbjct 1749 ACCCATTATCTACTGCTTCACATTGGGCAAAAAGAGATGAGCCGTAATTCCTCCCATCT 1690
|
Query 552 TGCAGTCCCCAGTTCCACCTTTCCAGGCTCTTACATACTTGGGATTGGCCCACAGGGACA 611
|
Sbjct 1689 TGCAGTCCCCAGTTCCACCTTTCCAGGCTCTTACATACTTGGGATTGGCCCACAGGGACA 1630
|
Query 612 CTGGATTAAAGGTTCCACTTGAAAAATAAGGTCCCACTGGGCTCAAGAGTACAAAGAGCA 671
|
Sbjct 1629 CTGGATTAAAGGTTCCACTTGAAAAATAAGGTCCCACTGGGCTCAAGAGTACAAAGAGCA 1570
```

Primer VP1.5

Query: pCMV6-BCAT1(C338S)

Subject: serial cloner *in silico* pCMV6-BCAT1(WT)

```
Query 138 ACCGAGGAGATCTGCCGCCGCGATCGCCATGGATTGCAGTAACGGATGCTCCGCAGAGTG 197
          |||
Sbjct 1001 ACCGAGGAGATCTGCCGCCGCGATCGCCATGGATTGCAGTAACGGATGCTCCGCAGAGTG 1060

Query 198 TACCGGAGAAGGAGGATCAAAAAGAGGTGGTGGGGACTTTTAAGGCTAAAGACCTAATAGT 257
          |||
Sbjct 1061 TACCGGAGAAGGAGGATCAAAAAGAGGTGGTGGGGACTTTTAAGGCTAAAGACCTAATAGT 1120

Query 258 CACACCAGCTACCATTTTAAAGGAAAAACCAGACCCCAATAATCTGGTTTTTGGAACTGT 317
          |||
Sbjct 1121 CACACCAGCTACCATTTTAAAGGAAAAACCAGACCCCAATAATCTGGTTTTTGGAACTGT 1180

Query 318 GTTCACGGATCATATGCTGACGGTGGAGTGGTCCTCAGAGTTTGGATGGGAGAAACCTCA 377
          |||
Sbjct 1181 GTTCACGGATCATATGCTGACGGTGGAGTGGTCCTCAGAGTTTGGATGGGAGAAACCTCA 1240

Query 378 TATCAAGCCTCTTCAGAACCTGTCAATGCACCCTGGCTCATCAGCTTTGCACTATGCAGT 437
          |||
Sbjct 1241 TATCAAGCCTCTTCAGAACCTGTCAATGCACCCTGGCTCATCAGCTTTGCACTATGCAGT 1300

Query 438 GGAATTATTTGAAGGATTGAAGGCATTTTCGAGGAGTAGATAATAAAATTCGACTGTTTCA 497
          |||
Sbjct 1301 GGAATTATTTGAAGGATTGAAGGCATTTTCGAGGAGTAGATAATAAAATTCGACTGTTTCA 1360

Query 498 GCCAAACCTCAACATGGATAGAATGTATCGCTCTGCTGTGAGGGCAACTCTGCCGGTATT 557
          |||
Sbjct 1361 GCCAAACCTCAACATGGATAGAATGTATCGCTCTGCTGTGAGGGCAACTCTGCCGGTATT 1420

Query 558 TGACAAAGAAGAGCTCTTAGAGTGTATTCAACAGCTTGTGAAATTGGATCAAGAATGGGT 617
          |||
Sbjct 1421 TGACAAAGAAGAGCTCTTAGAGTGTATTCAACAGCTTGTGAAATTGGATCAAGAATGGGT 1480

Query 618 CCCATATTCAACATCTGCTAGTCTGTATATTCGTCTTACATTCATTGGAAGTGGAGCTTC 677
          |||
Sbjct 1481 CCCATATTCAACATCTGCTAGTCTGTATATTCGTCTTACATTCATTGGAAGTGGAGCTTC 1540

Query 678 TCTTGGAGTCAAGAAGCCTACCAAAGCCCTGCTCTTTGTACTCTTGAGCCCAGTGGGACC 737
          |||
Sbjct 1541 TCTTGGAGTCAAGAAGCCTACCAAAGCCCTGCTCTTTGTACTCTTGAGCCCAGTGGGACC 1600

Query 738 TTATTTTCAAGTGGAACTTTAATCCAGTGTCCCTGTGGGCCAATCCCAAGTATGTAAG 797
          |||
Sbjct 1601 TTATTTTCAAGTGGAACTTTAATCCAGTGTCCCTGTGGGCCAATCCCAAGTATGTAAG 1660

Query 798 AGCCTGGAAAGGTGGAAGTGGGGACTGCAAGATGGGAGGGAATTACGGCTCATCTCTTTT 857
          |||
Sbjct 1661 AGCCTGGAAAGGTGGAAGTGGGGACTGCAAGATGGGAGGGAATTACGGCTCATCTCTTTT 1720
```


Primer VP1.5

Query: pCMV6-BCAT1(C335/8S)

Subject: serial cloner *in silico* pCMV6-BCAT1(WT)

```
Query 137 ACCGAGGAGATCTGCCGCCGCGATCGCCATGGATTGCAGTAACGGATGCTCCGCAGAGTG 196
          |||
Sbjct 1001 ACCGAGGAGATCTGCCGCCGCGATCGCCATGGATTGCAGTAACGGATGCTCCGCAGAGTG 1060

Query 197 TACCGGAGAAGGAGGATCAAAAGAGGTGGTGGGGACTTTTAAGGCTAAAGACCTAATAGT 256
          |||
Sbjct 1061 TACCGGAGAAGGAGGATCAAAAGAGGTGGTGGGGACTTTTAAGGCTAAAGACCTAATAGT 1120

Query 257 CACACCAGCTACCATTTTAAAGGAAAAACCAGACCCCAATAATCTGGTTTTTGGAACTGT 316
          |||
Sbjct 1121 CACACCAGCTACCATTTTAAAGGAAAAACCAGACCCCAATAATCTGGTTTTTGGAACTGT 1180

Query 317 GTTCACGGATCATATGCTGACGGTGGAGTGGTCCTCAGAGTTTGGATGGGAGAAACCTCA 376
          |||
Sbjct 1181 GTTCACGGATCATATGCTGACGGTGGAGTGGTCCTCAGAGTTTGGATGGGAGAAACCTCA 1240

Query 377 TATCAAGCCTCTTCAGAACCTGTCATTGCACCCTGGCTCATCAGCTTTCAGACTATGCAGT 436
          |||
Sbjct 1241 TATCAAGCCTCTTCAGAACCTGTCATTGCACCCTGGCTCATCAGCTTTCAGACTATGCAGT 1300

Query 437 GGAATTATTTGAAGGATTGAAGGCATTTTCGAGGAGTAGATAATAAAATTCGACTGTTTCA 496
          |||
Sbjct 1301 GGAATTATTTGAAGGATTGAAGGCATTTTCGAGGAGTAGATAATAAAATTCGACTGTTTCA 1360

Query 497 GCCAAACCTCAACATGGATAGAATGTATCGCTCTGCTGTGAGGGCAACTCTGCCGGTATT 556
          |||
Sbjct 1361 GCCAAACCTCAACATGGATAGAATGTATCGCTCTGCTGTGAGGGCAACTCTGCCGGTATT 1420

Query 557 TGACAAAGAAGAGCTCTTAGAGTGTATTCAACAGCTTGTGAAATTGGATCAAGAATGGGT 616
          |||
Sbjct 1421 TGACAAAGAAGAGCTCTTAGAGTGTATTCAACAGCTTGTGAAATTGGATCAAGAATGGGT 1480

Query 617 CCCATATTCAACATCTGCTAGTCTGTATATTTCGTCCTACATTATTGGAAGTGGAGCTTC 676
          |||
Sbjct 1481 CCCATATTCAACATCTGCTAGTCTGTATATTTCGTCCTACATTATTGGAAGTGGAGCTTC 1540

Query 677 TCTTGGAGTCAAGAAGCCTACCAAAGCCTGCTCTTTGTACTCTTGAGCCCAGTGGGACC 736
          |||
Sbjct 1541 TCTTGGAGTCAAGAAGCCTACCAAAGCCTGCTCTTTGTACTCTTGAGCCCAGTGGGACC 1600

Query 737 TTATTTTCAAGTGGAACTTTAATCCAGTGTCCCTGTGGGCCAATCCCAAGTATGTAAG 796
          |||
Sbjct 1601 TTATTTTCAAGTGGAACTTTAATCCAGTGTCCCTGTGGGCCAATCCCAAGTATGTAAG 1660

Query 797 AGCCTGGAAAGGTGGAAGTGGGGACTGCAAGATGGGAGGGAATTACGGCTCATCTCTTTT 856
          |||
Sbjct 1661 AGCCTGGAAAGGTGGAAGTGGGGACTGCAAGATGGGAGGGAATTACGGCTCATCTCTTTT 1720

Query 857 TGCCCAATGTGAAGCAGTAGATAATGGGTGTCAGCAGGTCCTGTGGCTCTATGGAGAGGA 916
          |||
Sbjct 1721 TGCCCAATGTGAAGCAGTAGATAATGGGTGTCAGCAGGTCCTGTGGCTCTATGGAGAGGA 1780
```

Primer FTAGR

Query: pCMV6-BCAT1(C335S)

Subject: serial cloner *in silico* pCMV6-BCAT1(WT)

Query	12	ATCCTCTTCTGAGATGAGTTTCTGCTCGAGCGGCCGCGTACGCGTGATAGCACAAATTGT	71
Sbjct	2228	ATCCTCTTCTGAGATGAGTTTCTGCTCGAGCGGCCGCGTACGCGTGATAGCACAAATTGT	2169
Query	72	CCAGTCGCTCTCTTCTCTTCCATACTGGATATCAGTTAATTTGCTCAAGATGCGGCTTGC	131
Sbjct	2168	CCAGTCGCTCTCTTCTCTTCCATACTGGATATCAGTTAATTTGCTCAAGATGCGGCTTGC	2109
Query	132	CAGCTTAGGACCATTCTCCATAGTTGGAATGTGTATTGTCTCGCCTTTGTACAGTATATC	191
Sbjct	2108	CAGCTTAGGACCATTCTCCATAGTTGGAATGTGTATTGTCTCGCCTTTGTACAGTATATC	2049
Query	192	AGAAACTGGGCTAACAACAGAGGCTGTACCAGAGCCAAACATCTCTCTCACTCTGTTCCC	251
Sbjct	2048	AGAAACTGGGCTAACAACAGAGGCTGTACCAGAGCCAAACATCTCTCTCACTCTGTTCCC	1989
Query	252	CTCCAGGGCTGTTGTCAAGTCATCCATGGTGAGGTATCTCTCTGACACCTTAAATTCACC	311
Sbjct	1988	CTCCAGGGCTGTTGTCAAGTCATCCATGGTGAGGTATCTCTCTGACACCTTAAATTCACC	1929
Query	312	CCACTGATGTGCCAGGTCCAGAATGCACCGCCTTGTCACTCCTGGAAGAATGATGCCATC	371
Sbjct	1928	CCACTGATGTGCCAGGTCCAGAATGCACCGCCTTGTCACTCCTGGAAGAATGATGCCATC	1869
Query	372	TAGTGGAGGAGTTGCCAGTTCTTCTTCTCCATCTTCATTTATCCAGTAAAGAAAAGATT	431
Sbjct	1868	TAGTGGAGGAGTTGCCAGTTCTTCTTCTCCATCTTCATTTATCCAGTAAAGAAAAGATT	1809
Query	432	CATAGTTCACACTTCAGTGATCTGATGGTCTCTCCATAGAGCCACAGGACCTGCTGACA	491
Sbjct	1808	CATAGTTCACACTTCAGTGATCTGATGGTCTCTCCATAGAGCCACAGGACCTGCTGACA	1749
Query	492	CCCATTATCTACTGCTTCACATTGGGCAAAAAGAGATGAGCCGTAATTCCTCCCATCTT	551
Sbjct	1748	CCCATTATCTACTGCTTCACATTGGGCAAAAAGAGATGAGCCGTAATTCCTCCCATCTT	1689
Query	552	GCAGTCCCCAGTTCCACCTTTCCAGGCTCTTACATACTTGGGATTGGCCCCACAGGGACAC	611
Sbjct	1688	GCAGTCCCCAGTTCCACCTTTCCAGGCTCTTACATACTTGGGATTGGCCCCACAGGGACAC	1629
Query	612	TGGATTAAAGGTTCCACTTGAAAAATAAGGTCCCACTGGGCTCAAGAGTACAAAGAGCAG	671
Sbjct	1628	TGGATTAAAGGTTCCACTTGAAAAATAAGGTCCCACTGGGCTCAAGAGTACAAAGAGCAG	1569
Query	672	GGCTTTGGTAGGCTTCTTGACTCCAAGAGAAGGCTCAGTTCCAATGAATGTAGGACGAAT	731
Sbjct	1568	GGCTTTGGTAGGCTTCTTGACTCCAAGAGAAGGCTCAGTTCCAATGAATGTAGGACGAAT	1509
Query	732	ATACAGACTAGCAGATGTTGAATATGGGACCCATTCCTTGATCCAATTTACAAGCTGTTG	791
Sbjct	1508	ATACAGACTAGCAGATGTTGAATATGGGACCCATTCCTTGATCCAATTTACAAGCTGTTG	1449
Query	792	AATACACTCTAAGAGCTCTTCTTTGTCAAATACCGGCAGAGTTGCCCTCACAGCAGAGCG	851
Sbjct	1448	AATACACTCTAAGAGCTCTTCTTTGTCAAATACCGGCAGAGTTGCCCTCACAGCAGAGCG	1389
Query	852	ATACATTCTATCCATGTTGAGGTTTGGCTGAAACAGTCGAATTT-ATTATCTACTCCTCG	910
Sbjct	1388	ATACATTCTATCCATGTTGAGGTTTGGCTGAAACAGTCGAATTTTATATCTACTCCTCG	1329

Primer T7F

Query: pET28-BCAT1(WT)

Subject: serial cloner *in silico* pET28-BCAT1(WT)

Query	134	ATGGATTGCAGTAACGGATGCTCCGCAGAGTGTACCGGAGAAGGAGGATCAAAAGAGGTG	193
Sbjct	1345	ATGGATTGCAGTAACGGATGCTCCGCAGAGTGTACCGGAGAAGGAGGATCAAAAGAGGTG	1286
Query	194	GTGGGGACTTTTAAGGCTAAAGACCTAATAGTCACACCAGCTACCATTTTAAAGGAAAAA	253
Sbjct	1285	GTGGGGACTTTTAAGGCTAAAGACCTAATAGTCACACCAGCTACCATTTTAAAGGAAAAA	1226
Query	254	CCAGACCCCAATAATCTGGTTTTTGGAACTGTGTTACGGATCATATGCTGACGGTGGAG	313
Sbjct	1225	CCAGACCCCAATAATCTGGTTTTTGGAACTGTGTTACGGATCATATGCTGACGGTGGAG	1166
Query	314	TGGTCCTCAGAGTTTGGATGGGAGAAACCTCATATCAAGCCTCTTCAGAACCTGTCATTG	373
Sbjct	1165	TGGTCCTCAGAGTTTGGATGGGAGAAACCTCATATCAAGCCTCTTCAGAACCTGTCATTG	1106
Query	374	CACCTGGCTCATCAGCTTTCAGCTATGCAGTGGAAATTTTGAAGGATTGAAGGCATTT	433
Sbjct	1105	CACCTGGCTCATCAGCTTTCAGCTATGCAGTGGAAATTTTGAAGGATTGAAGGCATTT	1046
Query	434	CGAGGAGTAGATAATAAAAATTCGACTGTTTCAGCCAAACCTCAACATGGATAGAATGTAT	493
Sbjct	1045	CGAGGAGTAGATAATAAAAATTCGACTGTTTCAGCCAAACCTCAACATGGATAGAATGTAT	986
Query	494	CGCTCTGCTGTGAGGGCAACTCTGCCGGTATTTGACAAAGAAGAGCTCTTAGAGTGTATT	553
Sbjct	985	CGCTCTGCTGTGAGGGCAACTCTGCCGGTATTTGACAAAGAAGAGCTCTTAGAGTGTATT	926
Query	554	CAACAGCTTGTGAAATTGGATCAAGAATGGGTCCCATATTC AACATCTGCTAGTCTGTAT	613
Sbjct	925	CAACAGCTTGTGAAATTGGATCAAGAATGGGTCCCATATTC AACATCTGCTAGTCTGTAT	866
Query	614	ATTCGTCTACATTCATTGGAAGTGGAGCTTCTCTTGGAGTCAAGAAGCCTACCAAAGCC	673
Sbjct	865	ATTCGTCTACATTCATTGGAAGTGGAGCTTCTCTTGGAGTCAAGAAGCCTACCAAAGCC	806
Query	674	CTGCTCTTTGTACTCTTGAGCCAGTGGGACCTTATTTTCAAGTGGAAACCTTTAATCCA	733
Sbjct	805	CTGCTCTTTGTACTCTTGAGCCAGTGGGACCTTATTTTCAAGTGGAAACCTTTAATCCA	746

Primer T7R

Query: pET28-BCAT1(WT)

Subject: serial cloner *in silico* pET28-BCAT1(WT)

```
Query 70 GCGGCCGCAAGCTTGTGCGACTGATCAGGATAGCACAAATGTCCAGTCGCTCTCTTCTCTT 129
          |||
Sbjct 165 GCGGCCGCAAGCTTGTGCGACTGATCAGGATAGCACAAATGTCCAGTCGCTCTCTTCTCTT 224

Query 130 CCATACTGGATATCAGTTAATTTGCTCAAGATGCGGCTTGCCAGCTTAGGACCATTCTCC 189
          |||
Sbjct 225 CCATACTGGATATCAGTTAATTTGCTCAAGATGCGGCTTGCCAGCTTAGGACCATTCTCC 284

Query 190 ATAGTTGGAATGTGTATTGTCTCGCCTTTGTACAGTATATCAGAACTGGGCAAACAACA 249
          |||
Sbjct 285 ATAGTTGGAATGTGTATTGTCTCGCCTTTGTACAGTATATCAGAACTGGGCAAACAACA 344

Query 250 CAGGCTGTACCAGAGCCAAACATCTCTCTCACTCTGTTCCTCCAGGGCTGTTGTCAAG 309
          |||
Sbjct 345 CAGGCTGTACCAGAGCCAAACATCTCTCTCACTCTGTTCCTCCAGGGCTGTTGTCAAG 404

Query 310 TCATCCATGGTGAGGTATCTCTCTGACACCTTAAATTCACCCCACTGATGTGCCAGGTCC 369
          |||
Sbjct 405 TCATCCATGGTGAGGTATCTCTCTGACACCTTAAATTCACCCCACTGATGTGCCAGGTCC 464

Query 370 AGAATGCACCGCCTTGTCACTCCTGGAAGAATGATGCCATCTAGTGGAGGAGTTGCCAGT 429
          |||
Sbjct 465 AGAATGCACCGCCTTGTCACTCCTGGAAGAATGATGCCATCTAGTGGAGGAGTTGCCAGT 524

Query 430 TCTTCTTCTCCATCTTCATTTATCCAGTAAAGAAAAAGATTCATAGTTCCTCACTTCAGTG 489
          |||
Sbjct 525 TCTTCTTCTCCATCTTCATTTATCCAGTAAAGAAAAAGATTCATAGTTCCTCACTTCAGTG 584

Query 490 ATCTGATGGTCCTCTCCATAGAGCCACAGGACCTGCTGACACCCATTATCTACTGCTTCA 549
          |||
Sbjct 585 ATCTGATGGTCCTCTCCATAGAGCCACAGGACCTGCTGACACCCATTATCTACTGCTTCA 644

Query 550 CATTGGGCAAAAAGAGATGAGCCGTAATTCCTCCCATCTTGCACTCCCAGTTCCACCT 609
          |||
Sbjct 645 CATTGGGCAAAAAGAGATGAGCCGTAATTCCTCCCATCTTGCACTCCCAGTTCCACCT 704

Query 610 TTCCAGGCTCTTACATACTTGGGATTGGCCACAGGGACACTGGATTAAAGGTTCCACTT 669
          |||
Sbjct 705 TTCCAGGCTCTTACATACTTGGGATTGGCCACAGGGACACTGGATTAAAGGTTCCACTT 764

Query 670 GAAAAATAAGGTCCCCTGGGCTCAAGAGTACAAAGAGCAGGGCTTTGGTAGGCTTCTTG 729
          |||
Sbjct 765 GAAAAATAAGGTCCCCTGGGCTCAAGAGTACAAAGAGCAGGGCTTTGGTAGGCTTCTTG 824

Query 730 ACTCCAAGAGAAGGCTCAGTTCCAATGAATGTAGGACGAATATACAGACTAGCAGATGTT 789
          |||
Sbjct 825 ACTCCAAGAGAAGGCTCAGTTCCAATGAATGTAGGACGAATATACAGACTAGCAGATGTT 884
```

Primer : T7 F
 Query: pET28-BCAT1(C335S)
 Subject: serial cloner *in silico* pET28-BCAT1(WT)

```

Query 92      TCATCACAGCAGCGGCCTGGTGCCGCGCGGCAGCCATATGGCTAGCATGGATTGCAGTAA 151
|
Sbjct 1391    TCATCACAGCAGCGGCCTGGTGCCGCGCGGCAGCCATATGGCTAGCATGGATTGCAGTAA 1332
|

Query 152     CGGATGCTCCGCAGAGTGTACCGGAGAAGGAGGATCAAAAAGAGGTGGTGGGGACTTTTAA 211
|
Sbjct 1331    CGGATGCTCCGCAGAGTGTACCGGAGAAGGAGGATCAAAAAGAGGTGGTGGGGACTTTTAA 1272
|

Query 212     GGCTAAAGACCTAATAGTCACACCAGCTACCATTTTAAAGGAAAAACCAGACCCCAATAA 271
|
Sbjct 1271    GGCTAAAGACCTAATAGTCACACCAGCTACCATTTTAAAGGAAAAACCAGACCCCAATAA 1212
|

Query 272     TCTGGTTTTTGGAACTGTGTTTCACGGATCATATGCTGACGGTGGAGTGGTCTCAGAGTT 331
|
Sbjct 1211    TCTGGTTTTTGGAACTGTGTTTCACGGATCATATGCTGACGGTGGAGTGGTCTCAGAGTT 1152
|

Query 332     TGGATGGGAGAAACCTCATATCAAGCCTCTTCAGAACCTGTCATTGCACCCTGGCTCATC 391
|
Sbjct 1151    TGGATGGGAGAAACCTCATATCAAGCCTCTTCAGAACCTGTCATTGCACCCTGGCTCATC 1092
|

Query 392     AGCTTTGCACTATGCAGTGAATTATTTGAAGGATTGAAGGCATTTTCGAGGAGTAGATAA 451
|
Sbjct 1091    AGCTTTGCACTATGCAGTGAATTATTTGAAGGATTGAAGGCATTTTCGAGGAGTAGATAA 1032
|

Query 452     TAAAATTCGACTGTTTCAGCCAAACCTCAACATGGATAGAATGTATCGCTCTGCTGTGAG 511
|
Sbjct 1031    TAAAATTCGACTGTTTCAGCCAAACCTCAACATGGATAGAATGTATCGCTCTGCTGTGAG 972
|

Query 512     GGCAACTCTGCCGGTATTTGACAAAGAAGAGCTCTTAGAGTGTATTCAACAGCTTGTGAA 571
|
Sbjct 971     GGCAACTCTGCCGGTATTTGACAAAGAAGAGCTCTTAGAGTGTATTCAACAGCTTGTGAA 912
|

Query 572     ATTGGATCAAGAATGGGTCCCATATTTCAACATCTGCTAGTCTGTATATTCGTCCTACATT 631
|
Sbjct 911     ATTGGATCAAGAATGGGTCCCATATTTCAACATCTGCTAGTCTGTATATTCGTCCTACATT 852
|

Query 632     CATTGGAAGTGAAGCTTCTCTTGGAGTCAAGAAGCCTACCAAAGCCCTGCTCTTTGTACT 691
|
Sbjct 851     CATTGGAAGTGAAGCTTCTCTTGGAGTCAAGAAGCCTACCAAAGCCCTGCTCTTTGTACT 792
|

```

Primer : T7 R

Query: pET28-BCAT1(C335S)

Subject: serial cloner *in silico* pET28-BCAT1(WT)

```
Query 92      TTGTCGACTGATCAGGATAGCACAATTGTCCAGTCGCTCTCTTCTCTTCCATACTGGATA 151
|
|
|
Sbjct 177     TTGTCGACTGATCAGGATAGCACAATTGTCCAGTCGCTCTCTTCTCTTCCATACTGGATA 236

Query 152     TCAGTTAATTTGCTCAAGATGCGGCTTGCCAGCTTAGGACCATTCTCCATAGTTGGAATG 211
|
|
|
Sbjct 237     TCAGTTAATTTGCTCAAGATGCGGCTTGCCAGCTTAGGACCATTCTCCATAGTTGGAATG 296

Query 212     TGTATTGTCTCGCCTTTGTACAGTATATCAGAAACTGGGCAAACAACAGAGGCTGTACCA 271
|
|
|
Sbjct 297     TGTATTGTCTCGCCTTTGTACAGTATATCAGAAACTGGGCAAACAACAGAGGCTGTACCA 356

Query 272     GAGCCAAACATCTCTCTCACTCTGTTCCTCCAGGGCTGTTGTCAAGTCATCCATGGTG 331
|
|
|
Sbjct 357     GAGCCAAACATCTCTCTCACTCTGTTCCTCCAGGGCTGTTGTCAAGTCATCCATGGTG 416

Query 332     AGGTATCTCTCTGACACCTTAAATTCACCCCACTGATGTGCCAGGTCCAGAATGCACCGC 391
|
|
|
Sbjct 417     AGGTATCTCTCTGACACCTTAAATTCACCCCACTGATGTGCCAGGTCCAGAATGCACCGC 476

Query 392     CTTGTCACTCCTGGAAGAATGATGCCATCTAGTGGAGGAGTTGCCAGTTCTTCTTCTCCA 451
|
|
|
Sbjct 477     CTTGTCACTCCTGGAAGAATGATGCCATCTAGTGGAGGAGTTGCCAGTTCTTCTTCTCCA 536

Query 452     TCTTCATTTATCCAGTAAAGAAAAAGATTTCATAGTTCCCACTTCAGTGATCTGATGGTCC 511
|
|
|
Sbjct 537     TCTTCATTTATCCAGTAAAGAAAAAGATTTCATAGTTCCCACTTCAGTGATCTGATGGTCC 596

Query 512     TCTCCATAGAGCCACAGGACCTGCTGACACCCATTATCTACTGCTTCACATTGGGCAAAA 571
|
|
|
Sbjct 597     TCTCCATAGAGCCACAGGACCTGCTGACACCCATTATCTACTGCTTCACATTGGGCAAAA 656

Query 572     AGAGATGAGCCGTAATTCCTCCCATCTTGCAGTCCCAGTTCCACCTTTCAGGCTCTT 631
|
|
|
Sbjct 657     AGAGATGAGCCGTAATTCCTCCCATCTTGCAGTCCCAGTTCCACCTTTCAGGCTCTT 716

Query 632     ACATACTTGGGATTGGCCACAGGGACACTGGATTAAGGTTCCACTTGAAAAATAAGGT 691
|
|
|
Sbjct 717     ACATACTTGGGATTGGCCACAGGGACACTGGATTAAGGTTCCACTTGAAAAATAAGGT 776

Query 692     CCCACTGGGCTCAAGAGTACAAAGAGCAGGGCTTTGGTAGGCTTCTTGACTCCAAGAGAA 751
|
|
|
Sbjct 777     CCCACTGGGCTCAAGAGTACAAAGAGCAGGGCTTTGGTAGGCTTCTTGACTCCAAGAGAA 836
```

Primer : T7 F
 Query: pET28-BCAT1(C338S)
 Subject: serial cloner *in silico* pET28-BCAT1(WT)

```

Query 79      atcatcmtcatcatcaCAGCAGCGGCCTGGTGCCGCGCGGCAGCCATATGGCTAGCATGG 138
            |||
Sbjct 1401    ATCATCATCATCATCACAGCAGCGCCTGGTGCCGCGCGGCAGCCATATGGCTAGCATGG 1342
            |||

Query 139     ATTGCAGTAACGGATGCTCCGCAGAGTGTACCGGAGAAGGAGGATCAAAAGAGGTGGTGG 198
            |||
Sbjct 1341    ATTGCAGTAACGGATGCTCCGCAGAGTGTACCGGAGAAGGAGGATCAAAAGAGGTGGTGG 1282
            |||

Query 199     GGACTTTTAAGGCTAAAGACCTAATAGTCACACCAGCTACCATTTTAAAGGAAAACCAG 258
            |||
Sbjct 1281    GGACTTTTAAGGCTAAAGACCTAATAGTCACACCAGCTACCATTTTAAAGGAAAACCAG 1222
            |||

Query 259     ACCCCAATAATCTGGTTTTTGGAACTGTGTTACGGATCATATGCTGACGGTGGAGTGGT 318
            |||
Sbjct 1221    ACCCCAATAATCTGGTTTTTGGAACTGTGTTACGGATCATATGCTGACGGTGGAGTGGT 1162
            |||

Query 319     CCTCAGAGTTTGGATGGGAGAAACCTCATATCAAGCCTCTTCAGAACCTGTCATTGCACC 378
            |||
Sbjct 1161    CCTCAGAGTTTGGATGGGAGAAACCTCATATCAAGCCTCTTCAGAACCTGTCATTGCACC 1102
            |||

Query 379     CTGGCTCATCAGCTTTCAGCTATGCAGTGAATTATTTGAAGGATTGAAGGCATTTTCGAG 438
            |||
Sbjct 1101    CTGGCTCATCAGCTTTCAGCTATGCAGTGAATTATTTGAAGGATTGAAGGCATTTTCGAG 1042
            |||

Query 439     GAGTAGATAATAAAAATTCGACTGTTTCAGCCAAACCTCAACATGGATAGAATGTATCGCT 498
            |||
Sbjct 1041    GAGTAGATAATAAAAATTCGACTGTTTCAGCCAAACCTCAACATGGATAGAATGTATCGCT 982
            |||

Query 499     CTGCTGTGAGGGCAACTCTGCCGGTATTTGACAAAGAAGAGCTCTTAGAGTGTATTCAAC 558
            |||
Sbjct 981     CTGCTGTGAGGGCAACTCTGCCGGTATTTGACAAAGAAGAGCTCTTAGAGTGTATTCAAC 922
            |||

Query 559     AGCTTGTGAAATTGGATCAAGAATGGGTCCCATATTCAACATCTGCTAGTCTGTATATTC 618
            |||
Sbjct 921     AGCTTGTGAAATTGGATCAAGAATGGGTCCCATATTCAACATCTGCTAGTCTGTATATTC 862
            |||

Query 619     GTCCTACATTCATTGGAAGTGGAGCTTCTCTTGGAGTCAAGAAGCCTACCAAAGCCCTGC 678
            |||
Sbjct 861     GTCCTACATTCATTGGAAGTGGAGCTTCTCTTGGAGTCAAGAAGCCTACCAAAGCCCTGC 802
            |||

Query 679     TCTTTGTACTCTTGAGCCAGTGGGACCTTATTTTTCAAGTGAACCTTTAATCCAGTGT 738
            |||
Sbjct 801     TCTTTGTACTCTTGAGCCAGTGGGACCTTATTTTTCAAGTGAACCTTTAATCCAGTGT 742
            |||

```

Primer : T7 R
 Query: pET28-BCAT1(C338S)
 Subject: serial cloner *in silico* pET28-BCAT1(WT)

```

Query 72      GCGGCCCAAGCTTGTTCGACTGATCAGGATAGCACAAATTGTCCAGTCGCTCTCTTCTCTT 131
                |||
Sbjct 165      GCGGCCCAAGCTTGTTCGACTGATCAGGATAGCACAAATTGTCCAGTCGCTCTCTTCTCTT 224

Query 132     CCATACTGGATATCAGTTAATTTGCTCAAGATGCGGCTTGCCAGCTTAGGACCATTCTCC 191
                |||
Sbjct 225     CCATACTGGATATCAGTTAATTTGCTCAAGATGCGGCTTGCCAGCTTAGGACCATTCTCC 284

Query 192     ATAGTTGGAATGTGTATTGTCTCGCCTTTGTACAGTATATCAGAAACTGGGCTAACAACA 251
                |||
Sbjct 285     ATAGTTGGAATGTGTATTGTCTCGCCTTTGTACAGTATATCAGAAACTGGGCTAACAACA 344

Query 252     CAGGCTGTACCAGAGCCAAACATCTCTCTCACTCTGTTCCCTCCAGGGCTGTTGTCAAG 311
                |||
Sbjct 345     CAGGCTGTACCAGAGCCAAACATCTCTCTCACTCTGTTCCCTCCAGGGCTGTTGTCAAG 404

Query 312     TCATCCATGGTGAGGTATCTCTCTGACACCTTAAATTCACCCCACTGATGTGCCAGGTCC 371
                |||
Sbjct 405     TCATCCATGGTGAGGTATCTCTCTGACACCTTAAATTCACCCCACTGATGTGCCAGGTCC 464

Query 372     AGAATGCACCGCCTTGTCACTCCTGGAAGAATGATGCCATCTAGTGGAGGAGTTGCCAGT 431
                |||
Sbjct 465     AGAATGCACCGCCTTGTCACTCCTGGAAGAATGATGCCATCTAGTGGAGGAGTTGCCAGT 524

Query 432     TCTTCTTCTCCATCTTCATTTATCCAGTAAAGAAAAAGATTCATAGTTCCTCACTTCAGTG 491
                |||
Sbjct 525     TCTTCTTCTCCATCTTCATTTATCCAGTAAAGAAAAAGATTCATAGTTCCTCACTTCAGTG 584

Query 492     ATCTGATGGTCCTCTCCATAGAGCCACAGGACCTGCTGACACCCATTATCTACTGCTTCA 551
                |||
Sbjct 585     ATCTGATGGTCCTCTCCATAGAGCCACAGGACCTGCTGACACCCATTATCTACTGCTTCA 644

Query 552     CATTGGGCAAAAAGAGATGAGCCGTAATTCCTCCCATCTTGAGTCCCAGTTCCACCT 611
                |||
Sbjct 645     CATTGGGCAAAAAGAGATGAGCCGTAATTCCTCCCATCTTGAGTCCCAGTTCCACCT 704

Query 612     TTCCAGGCTCTTACATACTTGGGATTGGCCACAGGGACACTGGATTAAAGGTTCCACTT 671
                |||
Sbjct 705     TTCCAGGCTCTTACATACTTGGGATTGGCCACAGGGACACTGGATTAAAGGTTCCACTT 764

Query 672     GAAAAATAAGGTCCCCTGGGCTCAAGAGTACAAAGAGCAGGGCTTTGGTAGGCTTCTTG 731
                |||
Sbjct 765     GAAAAATAAGGTCCCCTGGGCTCAAGAGTACAAAGAGCAGGGCTTTGGTAGGCTTCTTG 824

Query 732     ACTCCAAGAGAAGGCTCAGTTCCAATGAATGTAGGACGAATATACAGACTAGCAGATGTT 791
                |||
Sbjct 825     ACTCCAAGAGAAGGCTCAGTTCCAATGAATGTAGGACGAATATACAGACTAGCAGATGTT 884

Query 792     GAATATGGGACCCATTCTTGATCCAATTTACAAGCTGTTGAATACACTCTAAGAGCTCT 851
                |||
Sbjct 885     GAATATGGGACCCATTCTTGATCCAATTTACAAGCTGTTGAATACACTCTAAGAGCTCT 944

```


Primer : T7 R

Query: pET28-BCAT1(C335/8S)

Subject: serial cloner *in silico* pET28-BCAT1(WT)

```
Query 75      GGCCSCAAGCTTGTCTGACTGATCAGGATAGCACAATTGTCCAGTCGCTCTCTTCTCTTCC 134
          |||||
Sbjct 167      GGCCGCAAGCTTGTCTGACTGATCAGGATAGCACAATTGTCCAGTCGCTCTCTTCTCTTCC 226

Query 135     ATACTGGATATCAGTTAATTTGCTCAAGATGCGGCTTGCCAGCTTAGGACCATTCTCCAT 194
          |||||
Sbjct 227     ATACTGGATATCAGTTAATTTGCTCAAGATGCGGCTTGCCAGCTTAGGACCATTCTCCAT 286

Query 195     AGTTGGAATGTGTATTGTCTCGCCTTTGTACAGTATATCAGAAACTGGGCTAAACAACAGA 254
          |||||
Sbjct 287     AGTTGGAATGTGTATTGTCTCGCCTTTGTACAGTATATCAGAAACTGGGCAACAACACA 346

Query 255     GGCTGTACCAGAGCCAAACATCTCTCTCACTCTGTTCCTCCAGGGCTGTTGTCAAGTC 314
          |||||
Sbjct 347     GGCTGTACCAGAGCCAAACATCTCTCTCACTCTGTTCCTCCAGGGCTGTTGTCAAGTC 406

Query 315     ATCCATGGTGAGGTATCTCTCTGACACCTTAAATTCACCCCACTGATGTGCCAGGTCCAR 374
          |||||
Sbjct 407     ATCCATGGTGAGGTATCTCTCTGACACCTTAAATTCACCCCACTGATGTGCCAGGTCCAG 466

Query 375     AATGCACCGCCTTGTCACTCCTGGAAGAATGATGCCATCTAGTGGAGGAGTTGCCAGTTC 434
          |||||
Sbjct 467     AATGCACCGCCTTGTCACTCCTGGAAGAATGATGCCATCTAGTGGAGGAGTTGCCAGTTC 526

Query 435     TTCTTCTCCATCTTCATTTATCCAGTAAAGAAAAAGATTCATAGTTCCTCCACTTCAGTGAT 494
          |||||
Sbjct 527     TTCTTCTCCATCTTCATTTATCCAGTAAAGAAAAAGATTCATAGTTCCTCCACTTCAGTGAT 586

Query 495     CTGATGGTCCTCTCCATAGAGCCACAGGACCTGCTGACACCCATTATCTACTGCTTCACA 554
          |||||
Sbjct 587     CTGATGGTCCTCTCCATAGAGCCACAGGACCTGCTGACACCCATTATCTACTGCTTCACA 646

Query 555     TTGGGCAAAAAGAGATGAGCCGTAATTCCTCCCATCTTGCACTCCCAGTTCACACCTTT 614
          |||||
Sbjct 647     TTGGGCAAAAAGAGATGAGCCGTAATTCCTCCCATCTTGCACTCCCAGTTCACACCTTT 706

Query 615     CCAGGCTCTTACATACTTGGGATTGGCCACAGGGACACTGGATTAAAGGTTCCACTTGA 674
          |||||
Sbjct 707     CCAGGCTCTTACATACTTGGGATTGGCCACAGGGACACTGGATTAAAGGTTCCACTTGA 766

Query 675     AAAATAAGGTCCCCTGAGGCTCAAGAGTACAAAGAGCAGGGCTTTGGTAGGCTTCTTGAC 734
          |||||
Sbjct 767     AAAATAAGGTCCCCTGAGGCTCAAGAGTACAAAGAGCAGGGCTTTGGTAGGCTTCTTGAC 826

Query 735     TCCAAGAGAAGGCTCAGTTCCAATGAATGTAGGACGAATATACAGACTAGCAGATGTTGA 794
          |||||
Sbjct 827     TCCAAGAGAAGGCTCAGTTCCAATGAATGTAGGACGAATATACAGACTAGCAGATGTTGA 886

Query 795     ATATGGGACCCATTCTTGATCCAATTTACAAGCTGTTGAATACACTCTAAGAGCTCTTC 854
          |||||
Sbjct 887     ATATGGGACCCATTCTTGATCCAATTTACAAGCTGTTGAATACACTCTAAGAGCTCTTC 946

Query 855     TTTGTCAAATACCGGCAGAGTTGCCCTCACAGCAGAGCGATACATTCTATCCATGTTGAG 914
          |||||
Sbjct 947     TTTGTCAAATACCGGCAGAGTTGCCCTCACAGCAGAGCGATACATTCTATCCATGTTGAG 1006
```

Primer V2

Query: pLenti-BCAT1(WT)

Subject: serial cloner *in silico* pLenti-BCAT1(WT)

Query	77	TCSCCATGGATTGCAGTAACGGATGCTCCGCAGAGTGTACCGGAGAAGGAGGATCAAAAAG	136
Sbjct	7552	TCGCCATGGATTGCAGTAACGGATGCTCCGCAGAGTGTACCGGAGAAGGAGGATCAAAAAG	7611
Query	137	AGGTGGTGGGGACTTTTAAGGCTAAAGACCTAATAGTCACACCAGCTACCATTTTAAAGG	196
Sbjct	7612	AGGTGGTGGGGACTTTTAAGGCTAAAGACCTAATAGTCACACCAGCTACCATTTTAAAGG	7671
Query	197	AAAAACCAGACCCCAATAATCTGGTTTTTGGAACTGTGTTACGGATCATATGCTGACGG	256
Sbjct	7672	AAAAACCAGACCCCAATAATCTGGTTTTTGGAACTGTGTTACGGATCATATGCTGACGG	7731
Query	257	TGGAGTGGTCCCTCAGAGTTTGGATGGGAGAAACCTCATATCAAGCCTCTTCAGAACCTGT	316
Sbjct	7732	TGGAGTGGTCCCTCAGAGTTTGGATGGGAGAAACCTCATATCAAGCCTCTTCAGAACCTGT	7791
Query	317	CATTGCACCCTGGCTCATCAGCTTTGCACTATGCAGTGAATTATTTGAAGGATTGAAGG	376
Sbjct	7792	CATTGCACCCTGGCTCATCAGCTTTGCACTATGCAGTGAATTATTTGAAGGATTGAAGG	7851
Query	377	CATTTTCGAGGAGTAGATAATAAAATTCGACTGTTTTTCAGCCAAACCTCAACATGGATAGAA	436
Sbjct	7852	CATTTTCGAGGAGTAGATAATAAAATTCGACTGTTTTTCAGCCAAACCTCAACATGGATAGAA	7911
Query	437	TGTATCGCTCTGCTGTGAGGGCAACTCTGCCGGTATTTGACAAAGAAGAGCTCTTAGAGT	496
Sbjct	7912	TGTATCGCTCTGCTGTGAGGGCAACTCTGCCGGTATTTGACAAAGAAGAGCTCTTAGAGT	7971
Query	497	GTATTCAACAGCTTGTGAAATTGGATCAAGAATGGGTCCCATATTCAACATCTGCTAGTC	556
Sbjct	7972	GTATTCAACAGCTTGTGAAATTGGATCAAGAATGGGTCCCATATTCAACATCTGCTAGTC	8031
Query	557	TGTATATTCGTCCCTACATTCATTGGAAGTGGACCTTCTCTTGGAGTCAAGAAGCCTACCA	616
Sbjct	8032	TGTATATTCGTCCCTACATTCATTGGAAGTGGACCTTCTCTTGGAGTCAAGAAGCCTACCA	8091
Query	617	AAGCCCTGCTCTTTGTACTCTTGAGCCAGTGGGACCTTATTTTTCAAGTGGAAACCTTTA	676
Sbjct	8092	AAGCCCTGCTCTTTGTACTCTTGAGCCAGTGGGACCTTATTTTTCAAGTGGAAACCTTTA	8151
Query	677	ATCCAGTGTCCCTGTGGGCAATCCCAAGTATGTAAGAGCCTGGAAAGGTGGAAGTGGGG	736
Sbjct	8152	ATCCAGTGTCCCTGTGGGCAATCCCAAGTATGTAAGAGCCTGGAAAGGTGGAAGTGGGG	8211
Query	737	ACTGCAAGATGGGAGGAATTACGGCTCATCTCTTTTTGCCCAATGTGAAGCAGTAGATA	796
Sbjct	8212	ACTGCAAGATGGGAGGAATTACGGCTCATCTCTTTTTGCCCAATGTGAAGCAGTAGATA	8271
Query	797	ATGGGTGTCAGCAGGTCTGTGGCTCTATGGAGAGGACCATCAGATCACTGAAGTGGGAA	856
Sbjct	8272	ATGGGTGTCAGCAGGTCTGTGGCTCTATGGAGAGGACCATCAGATCACTGAAGTGGGAA	8331

Primer FTAGR

Query: pLenti-BCAT1(WT)

Subject: serial cloner *in silico* pLenti-BCAT1(WT)

```
Query 53      CGCGTGGATAGCACAAATTGTCCAGTCGCTCTCTTCTCTCCATACTGGATATCAGTTAAT 112
          |||
Sbjct 8716    CGCGTGGATAGCACAAATTGTCCAGTCGCTCTCTTCTCTCCATACTGGATATCAGTTAAT 8657

Query 113     TTGCTCAAGATGCGGCTTGCCAGCTTAGGACCATTCTCCATAGTTGGAATGTGTATTGTC 172
          |||
Sbjct 8656    TTGCTCAAGATGCGGCTTGCCAGCTTAGGACCATTCTCCATAGTTGGAATGTGTATTGTC 8597

Query 173     TCGCCTTTGTACAGTATATCAGAAACTGGGCAAACAACACAGGCTGTACCAGAGCCAAAC 232
          |||
Sbjct 8596    TCGCCTTTGTACAGTATATCAGAAACTGGGCAAACAACACAGGCTGTACCAGAGCCAAAC 8537

Query 233     ATCTCTCTCACTCTGTTCCCCTCCAGGGCTGTTGTCAAGTCATCCATGGTGAGGTATCTC 292
          |||
Sbjct 8536    ATCTCTCTCACTCTGTTCCCCTCCAGGGCTGTTGTCAAGTCATCCATGGTGAGGTATCTC 8477

Query 293     TCTGACACCTTAAATTCACCCCACTGATGTGCCAGGTCAGAATGCACCGCCTTGTCACT 352
          |||
Sbjct 8476    TCTGACACCTTAAATTCACCCCACTGATGTGCCAGGTCAGAATGCACCGCCTTGTCACT 8417

Query 353     CCTGGAAGAATGATGCCATCTAGTGGAGGAGTTGCCAGTCTTCTTCTCCATCTTCATTT 412
          |||
Sbjct 8416    CCTGGAAGAATGATGCCATCTAGTGGAGGAGTTGCCAGTCTTCTTCTCCATCTTCATTT 8357

Query 413     ATCCAGTAAAGAAAAAGATTTCATAGTTCCCACTTCAGTGATCTGATGGTCTCTCCATAG 472
          |||
Sbjct 8356    ATCCAGTAAAGAAAAAGATTTCATAGTTCCCACTTCAGTGATCTGATGGTCTCTCCATAG 8297

Query 473     AGCCACAGGACCTGCTGACACCCATTATCTACTGCTTCACATTGGGCAAAAAGAGATGAG 532
          |||
Sbjct 8296    AGCCACAGGACCTGCTGACACCCATTATCTACTGCTTCACATTGGGCAAAAAGAGATGAG 8237

Query 533     CCGTAATTCCTCCCATCTTGCAGTCCCAGTTCACCTTTCCAGGCTCTTACATACTTG 592
          |||
Sbjct 8236    CCGTAATTCCTCCCATCTTGCAGTCCCAGTTCACCTTTCCAGGCTCTTACATACTTG 8177

Query 593     GGATTGGCCACAGGGCACTGGATTAAAGGTTCCACTTGAAAAATAAGGTCCCACTGGG 652
          |||
Sbjct 8176    GGATTGGCCACAGGGCACTGGATTAAAGGTTCCACTTGAAAAATAAGGTCCCACTGGG 8117

Query 653     CTCAAGAGTACAAAGAGCAGGGCTTTGGTAGGCTTCTTGACTCCAAGAGAAGGCTCAGTT 712
          |||
Sbjct 8116    CTCAAGAGTACAAAGAGCAGGGCTTTGGTAGGCTTCTTGACTCCAAGAGAAGGCTCAGTT 8057

Query 713     CCAATGAATGTAGGACGAATATACAGACTAGCAGATGTTGAATATGGGACCCATTCTTGA 772
          |||
Sbjct 8056    CCAATGAATGTAGGACGAATATACAGACTAGCAGATGTTGAATATGGGACCCATTCTTGA 7997

Query 773     TCCAATTCACAAGCTGTTGAATACACTCTAAGAGCTCTCTTTGTCAAATACCGGCAGA 832
          |||
Sbjct 7996    TCCAATTCACAAGCTGTTGAATACACTCTAAGAGCTCTCTTTGTCAAATACCGGCAGA 7937
```

Primer V2

Query: pLenti-BCAT1(C338S)

Subject: serial cloner *in silico* pLenti-BCAT1(WT)

```
Query 80 ATCGCCATGGATTGCAGTAACGGATGCTCCGCAGAGTGTAACGGAGAAGGAGGATCAAAA 139
|
Sbjct 7551 ATCGCCATGGATTGCAGTAACGGATGCTCCGCAGAGTGTAACGGAGAAGGAGGATCAAAA 7610

Query 140 GAGGTGGTGGGGACTTTTAAGGCTAAAGACCTAATAGTCACACCAGCTACCATTTTAAAG 199
|
Sbjct 7611 GAGGTGGTGGGGACTTTTAAGGCTAAAGACCTAATAGTCACACCAGCTACCATTTTAAAG 7670

Query 200 GAAAAACAGACCCCAATAATCTGGTTTTTGGAACTGTGTTTCACGGATCATATGCTGACG 259
|
Sbjct 7671 GAAAAACAGACCCCAATAATCTGGTTTTTGGAACTGTGTTTCACGGATCATATGCTGACG 7730

Query 260 GTGGAGTGGTCCTCAGAGTTTGGATGGGAGAAACCTCATATCAAGCCTCTTCAGAACCTG 319
|
Sbjct 7731 GTGGAGTGGTCCTCAGAGTTTGGATGGGAGAAACCTCATATCAAGCCTCTTCAGAACCTG 7790

Query 320 TCATTGCACCCTGGCTCATCAGCTTTGCACTATGCAGTGAATTATTTGAAGGATTGAAG 379
|
Sbjct 7791 TCATTGCACCCTGGCTCATCAGCTTTGCACTATGCAGTGAATTATTTGAAGGATTGAAG 7850

Query 380 GCATTTTCGAGGAGTAGATAATAAAATTCGACTGTTTCAGCCAAACCTCAACATGGATAGA 439
|
Sbjct 7851 GCATTTTCGAGGAGTAGATAATAAAATTCGACTGTTTCAGCCAAACCTCAACATGGATAGA 7910

Query 440 ATGTATCGCTCTGCTGTGAGGGCAACTCTGCCGGTATTTGACAAAGAAGAGCTCTTAGAG 499
|
Sbjct 7911 ATGTATCGCTCTGCTGTGAGGGCAACTCTGCCGGTATTTGACAAAGAAGAGCTCTTAGAG 7970

Query 500 TGTATTCAACAGCTTGTGAAATTGGATCAAGAATGGGTCCCATATTCAACATCTGCTAGT 559
|
Sbjct 7971 TGTATTCAACAGCTTGTGAAATTGGATCAAGAATGGGTCCCATATTCAACATCTGCTAGT 8030

Query 560 CTGTATATTCGTCCACATTCATTGGAAGTGGAGCCTTCTCTTGGAGTCAAGAAGCCTACC 619
|
Sbjct 8031 CTGTATATTCGTCCACATTCATTGGAAGTGGAGCCTTCTCTTGGAGTCAAGAAGCCTACC 8090

Query 620 AAAGCCCTGCTCTTTGTACTCTTGAGCCAGTGGGACCTTATTTTTCAAGTGAACCTTT 679
|
Sbjct 8091 AAAGCCCTGCTCTTTGTACTCTTGAGCCAGTGGGACCTTATTTTTCAAGTGAACCTTT 8150

Query 680 AATCCAGTGTCCCTGTGGCCAATCCCAAGTATGTAAGAGCCTGGAAAGGTGGAAGTGGG 739
|
Sbjct 8151 AATCCAGTGTCCCTGTGGCCAATCCCAAGTATGTAAGAGCCTGGAAAGGTGGAAGTGGG 8210

Query 740 GACTGCAAGATGGGAGGGAATTACGGCTCATCTCTTTTTGCCCAATGTGAAGCAGTAGAT 799
|
Sbjct 8211 GACTGCAAGATGGGAGGGAATTACGGCTCATCTCTTTTTGCCCAATGTGAAGCAGTAGAT 8270

Query 800 AATGGGTGTCAGCAGGTCCTGTGGCTCTATGGAGAGGACCATCAGATCACTGAAGTGGGA 859
|
Sbjct 8271 AATGGGTGTCAGCAGGTCCTGTGGCTCTATGGAGAGGACCATCAGATCACTGAAGTGGGA 8330

Query 860 ACTATGAATCTTTTTCTTTACTGGATAAATGAAGATGGAGAAGAAGAACTGGCAACTCCT 919
|
Sbjct 8331 ACTATGAATCTTTTTCTTTACTGGATAAATGAAGATGGAGAAGAAGAACTGGCAACTCCT 8390

Query 920 CCACTAGATGGCATCATTCTTCCAGGAGTGACAAGGCGGTGCATTCTGGACCTGGCACAT 979
|
Sbjct 8391 CCACTAGATGGCATCATTCTTCCAGGAGTGACAAGGCGGTGCATTCTGGACCTGGCACAT 8450
```


Primer FTAGR

Query: pLenti-BCAT1(C335/8S)

Subject: serial cloner *in silico* pLenti-BCAT1(WT)

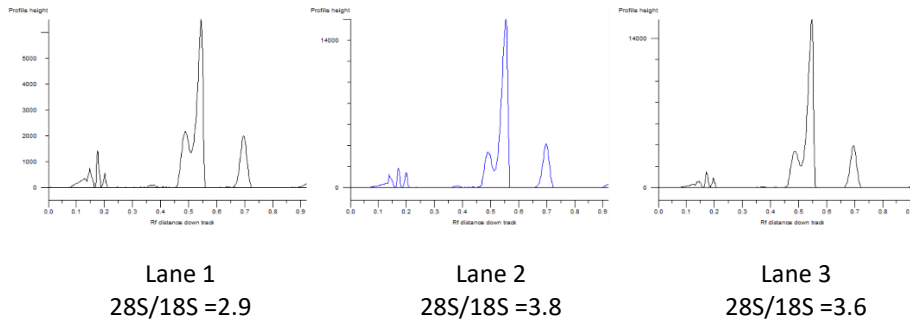
Query	55	CGCGTGGATAGCACAATTGTCCAGTCGCTCTCTTCTCTCCATACTGGATATCAGTTAAT	114
Sbjct	8716	CGCGTGGATAGCACAATTGTCCAGTCGCTCTCTTCTCTCCATACTGGATATCAGTTAAT	8657
Query	115	TTGCTCAAGATGCGGCTTGCCAGCTTAGGACCATTCTCCATAGTTGGAATGTGTATTGTC	174
Sbjct	8656	TTGCTCAAGATGCGGCTTGCCAGCTTAGGACCATTCTCCATAGTTGGAATGTGTATTGTC	8597
Query	175	TCGCCTTTGTACAGTATATCAGAACTGGGCTAACAACAGAGGCTGTACCAGAGCCAAAC	234
Sbjct	8596	TCGCCTTTGTACAGTATATCAGAACTGGGCAACAACACAGGCTGTACCAGAGCCAAAC	8537
Query	235	ATCTCTCTCACTCTGTTCCCTCCAGGGCTGTTGTCAAGTCATCCATGGTGAGGTATCTC	294
Sbjct	8536	ATCTCTCTCACTCTGTTCCCTCCAGGGCTGTTGTCAAGTCATCCATGGTGAGGTATCTC	8477
Query	295	TCTGACACCTTAAATTCACCCCACTGATGTGCCAGGTCAGAATGCACCGCCTTGTCACT	354
Sbjct	8476	TCTGACACCTTAAATTCACCCCACTGATGTGCCAGGTCAGAATGCACCGCCTTGTCACT	8417
Query	355	CCTGGAAGAATGATGCCATCTAGTGGAGGAGTTGCCAGTTCTTCTTCTCCATCTTCATTT	414
Sbjct	8416	CCTGGAAGAATGATGCCATCTAGTGGAGGAGTTGCCAGTTCTTCTTCTCCATCTTCATTT	8357
Query	415	ATCCAGTAAAGAAAAAGATTATAGTTCACACTTCAGTGATCTGATGGTCTCTCCATAG	474
Sbjct	8356	ATCCAGTAAAGAAAAAGATTATAGTTCACACTTCAGTGATCTGATGGTCTCTCCATAG	8297
Query	475	AGCCACAGGACCTGCTGACACCCATTATCTACTGCTTCACATTGGGCAAAAAGAGATGAG	534
Sbjct	8296	AGCCACAGGACCTGCTGACACCCATTATCTACTGCTTCACATTGGGCAAAAAGAGATGAG	8237
Query	535	CCGTAATTCCTCCCATCTTGCAGTCCCAGTTCCACCTTTCAGGCTCTTACATACTTG	594
Sbjct	8236	CCGTAATTCCTCCCATCTTGCAGTCCCAGTTCCACCTTTCAGGCTCTTACATACTTG	8177
Query	595	GGATTGGCCACAGGGACACTGGATTAAGGTTCCACTTGAAAAATAAGGTCCCCTGGG	654
Sbjct	8176	GGATTGGCCACAGGGACACTGGATTAAGGTTCCACTTGAAAAATAAGGTCCCCTGGG	8117
Query	655	CTCAAGAGTACAAAGAGCAGGGCTTTGGTAGGCTTCTTGACTCCAAGAGAAGGCTCAGTT	714
Sbjct	8116	CTCAAGAGTACAAAGAGCAGGGCTTTGGTAGGCTTCTTGACTCCAAGAGAAGGCTCAGTT	8057
Query	715	CCAATGAATGTAGGACGAATATACAGACTAGCAGATGTTGAATATGGGACCCATTCTTGA	774
Sbjct	8056	CCAATGAATGTAGGACGAATATACAGACTAGCAGATGTTGAATATGGGACCCATTCTTGA	7997
Query	775	TCCAATTCACAAGCTGTTGAATACACTCTAAGAGCTCTTCTTTGTCAAATACCGGCAGA	834
Sbjct	7996	TCCAATTCACAAGCTGTTGAATACACTCTAAGAGCTCTTCTTTGTCAAATACCGGCAGA	7937
Query	835	GTTGCCCTCACAGCAGAGCGATAACATTCTATCCATGTTGAGGTTTGGCTGAAACAGTCGA	894
Sbjct	7936	GTTGCCCTCACAGCAGAGCGATAACATTCTATCCATGTTGAGGTTTGGCTGAAACAGTCGA	7877
Query	895	ATTTTATTATCTACTCTCGAAATGCCTTCAATCCTTCAAATAATTCCACTGCATAGTGC	954
Sbjct	7876	ATTTTATTATCTACTCTCGAAATGCCTTCAATCCTTCAAATAATTCCACTGCATAGTGC	7817

Query 955 AAAGCTGATGAGCCAGGGTGCAATGACAGGTTCTGAAGAGGCTTGATATGAGGTTTCTCC 1014
|||||
Sbjct 7816 AAAGCTGATGAGCCAGGGTGCAATGACAGGTTCTGAAGAGGCTTGATATGAGGTTTCTCC 7757

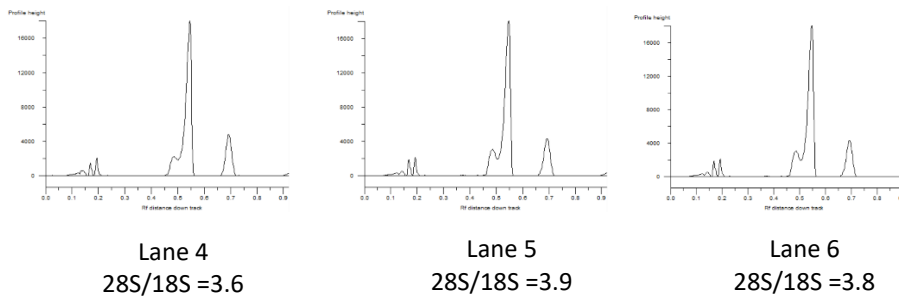
Appendix B. Densitometric analysis of RNA agarose gels. 28S:18S rRNA ratio ≥ 2

indicates intact RNA suitable for downstream analysis

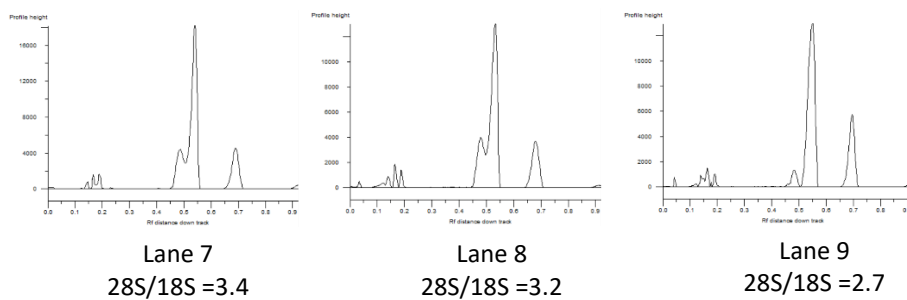
U937-Control(EV)



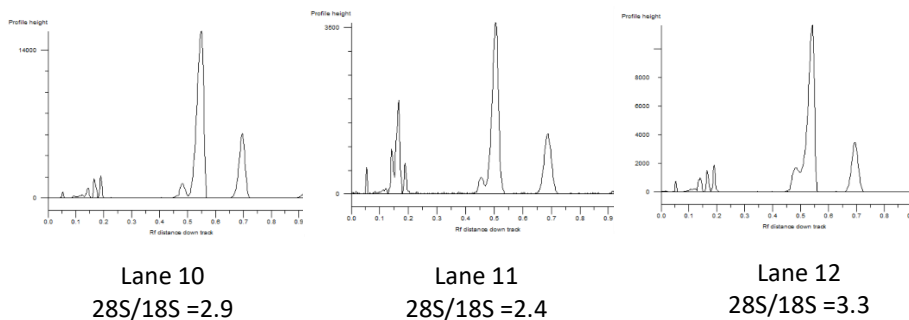
U937-BCAT1(WT)



U937-BCAT1(C338S) RNA

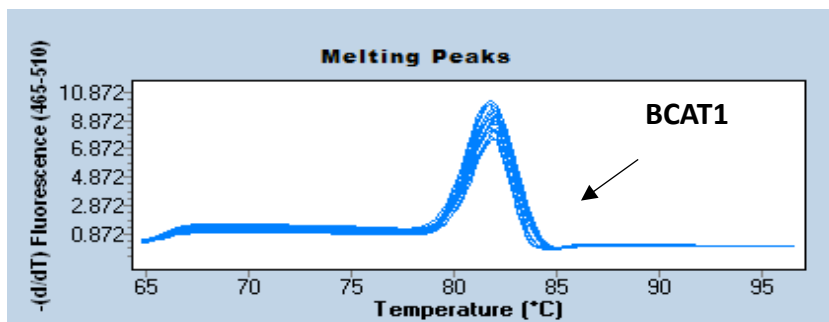


U937-BCAT1(C335/8S) RNA

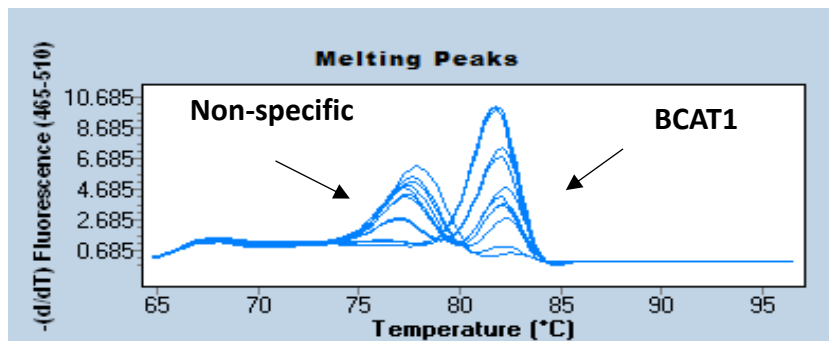


Appendix C. Melt-curve analysis of qPCR calibration curves. Profile of **A)** BCAT1 product amplified from pCMV6-BCAT1 template and **B)**BCAT1 product amplified from U937-Control(EV), non-specific amplification of primer dimer seen after x1000 dilution of template. **C)** β 2M product amplified from U937-Control(EV) template. multiple curves represent 1/10 template serial dilution of template.

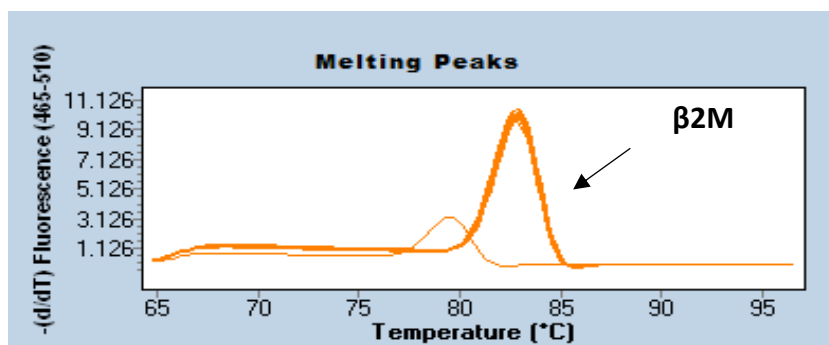
A) PCMV6-BCAT(WT)

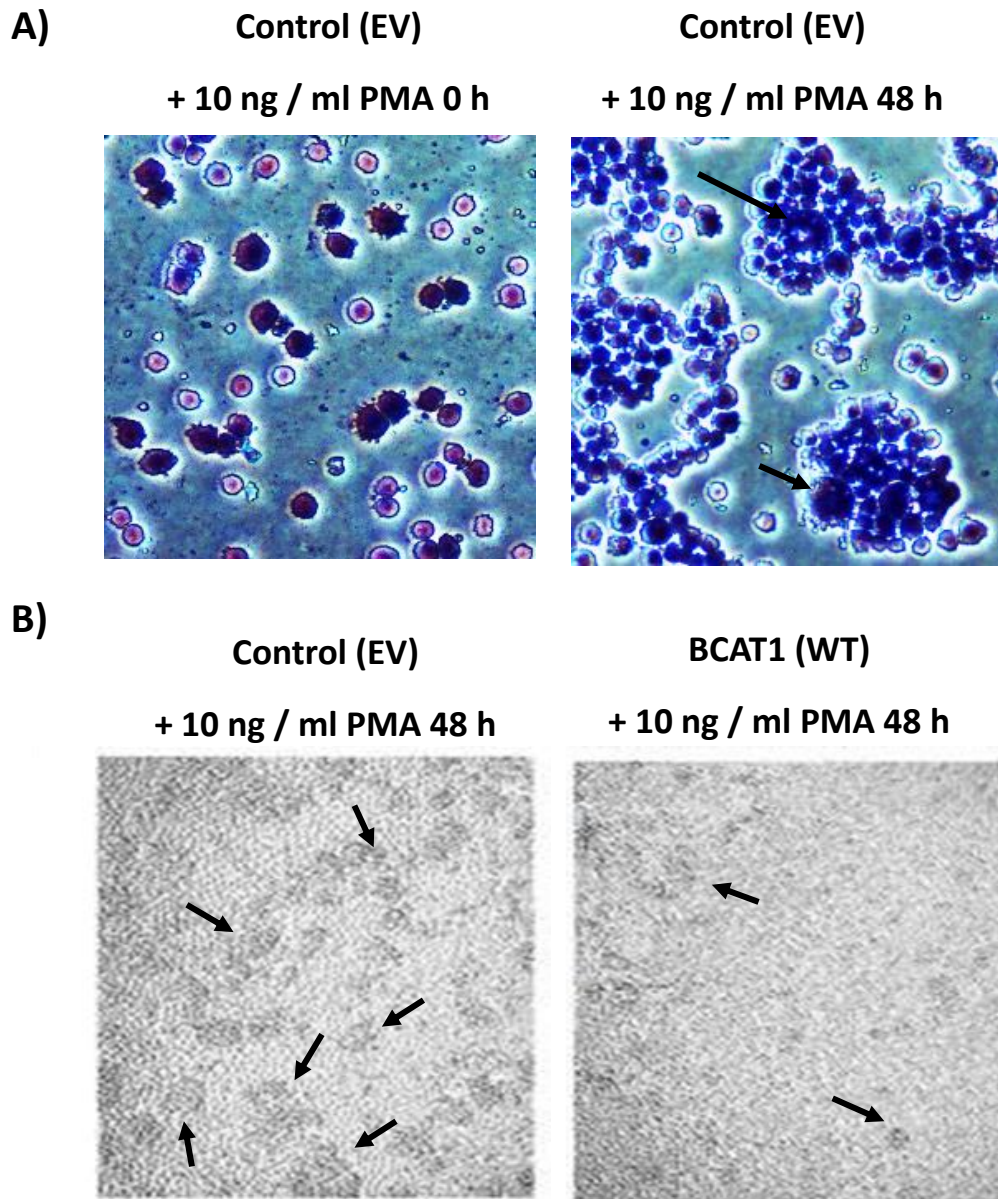


B) U937-Control(EV)



C) U937-Control(EV)





Appendix D Differential aggregation of U937 transgenic cells following addition of PMA. Light microscope images displaying U937 cells following incubation with ± 10 ng/mL PMA 48h. **A)** Giemsa stained U937-Control(EV) cells display aggregation and monocyte to macrophage differentiation (indicated by arrows) following addition of PMA. **B)** U937-BCAT1(WT) cells display visibly reduced aggregation (dark patches indicated by arrows) compared to U937-Control(EV).